New insights on Thermal Coding in the Rodent Brain using Functional Ultrasound Imaging

Haritha Koorliyil

PSL
UNIVERSITÉ PARIS

THÈSE DE DOCTORAT
DE L'UNIVERSITÉ PSL

Préparée à ESPCI Paris

New Insights on Thermal Coding in the Rodent Brain using Functional Ultrasound Imaging

Étude des aires cérébrales impliquées dans l'encodage de la sensation thermique chez le rongeur par imagerie ultrasonore ultrarapide

Soutenue par
Haritha KOORLIYIL
Le 23 mars 2022

Ecole doctorale n° 158
CERVEAU, COGNITION, COMPORTEMENT (ED3C)

Spécialité
NEUROSCIENCES

Composition du jury :

M. Jacobo D, SITT	*Président*
Mme. Ipek, YALCIN	*Rapporteur*
M. Fabien, MARCHAND	*Rapporteur*
M. Gary, LEWIN	*Examinateur*
M. Mickael, TANTER	*Examinateur*
Mme. Sophie, PEZET	*Directeur de thèse*

ESPCI PARIS

Acknowledgement

I am grateful for the opportunity to be a part of a reputed institution such as ESPCI and work alongside some of the greatest scientific minds during my PhD. My journey so far, from a small town on the other side of the world to this point would have been impossible without the love and support of people I keep close to my heart.

Thank you, Sophie. For being by my side from beginning to end, as not only my supervisor, but as a mentor, as a friend. For your kindness and good spirit. For constantly motivating me to do my best, for showing me that every day and everything can be phenomenal in science. For sharing your knowledge, for thought-provoking conversations and most importantly for shaping my mind to think like I have never done before.

Thank you, Mickael. For choosing me, for giving me this chance to be a part of your laboratory to learn fUS imaging. For being a strong pillar throughout my scientific journey. For your intriguing questions that light up my brain. For your perspectives that are unique. For always leaving me with something to think about. For leading by example.

Thank you, Nathalie. For your kindness and patience. For teaching me surgical skills. For supporting me throughout my PhD. For making me believe that language is not a barrier to make a connection.

Thank you, Hicham. For your humor on good and bad days. For your curiosity. For your positivity. For building the Peltier device from scratch to help me in my project. Lastly, for being a good friend.

Thank you, Haleh. For your friendship and support. For doing experiments with me, for keeping up the positive spirit, for helping me with the figures. For contributing your valuable time and effort.

Thank you, each and every one at PhysMed. For inspiring me in your own unique ways. For good friendships and conversations.

Thank you Papa, Amma, Namitha and Harshitha. For always being my cheerleaders.

Thank you, Abin. For encouraging and supporting me with all your heart.

Résumé

Les mécanismes centraux du codage thermique sont très complexes et impliquent principalement le thalamus, le cortex somatosensoriel, le cortex insulaire, le cortex cingulaire et l'hypothalamus. L'objectif de ce travail de thèse était d'étudier le rôle des circuits supra-spinaux dans le codage thermique chez les rongeurs, grâce à l'imagerie fonctionnelle ultrasonore (fUS). L'imagerie fUS est basée sur le couplage neurovasculaire, phénomène physiologique qui lie l'activité neuronale et les changements du volume sanguin cérébral (CBV).

Notre première étude visait à cartographier la matrice des zones activées par des stimulations thermiques cutanées nociceptives ou non chez le rat anesthésié. Le résultat de cette étude a malheureusement été essentiellement négatif. Nous avons conclu que les stimuli non douloureux n'induisaient aucun changement du CBV. A l'inverse, les stimulations thermiques nociceptives induisaient une augmentation locale du CBV, mais de manière non reproductible, en raison de facteurs physiologiques tels que l'augmentation de la pression artérielle qui entraîne de fortes fluctuations du CBV.

La deuxième étude visait à déchiffrer l'interaction entre les régions somato-motrices, cingulaires et hypothalamus dans le traitement de la sensation thermique. Nous avons choisi d'aborder cette question en utilisant l'imagerie fUS sur des souris éveillées et libres de leurs mouvements. L'imagerie fUS transcrânienne fut réalisée pendant que les souris étaient exposées à une température fixe (neutre 25°C, chaude 35°C et froide 15°C) ou à une température variable à un rythme rapide et lent. L'étude de la connectivité fonctionnelle, une mesure indirecte de la fonction et de la force des réseaux cérébraux, a révélé une dichotomie de fonction entre le réseau somato-moteur (SM)-cingulaire et le réseau SM-hypothalamique dans la détection du froid. L'étude des états dynamiques du cerveau a révélé i) des modes spécifiques pour cette dichotomie, ii) un mode dans lequel, pendant l'exposition statique à une température froide (15°C), où le cortex cingulaire était connecté différemment aux autres réseaux et enfin iii) un mode "état de repos", qui est le plus fréquent de tous et est significativement plus présent à la température de repos.

Ces résultats apportent des informations clef sur la dynamique des réseaux impliqués dans la sensibilité au froid.

Summary

The underlying central mechanisms of thermal coding are very complex and involves mainly the thalamus, somatosensory cortex, insular cortex, cingulate cortex and hypothalamus. The functional dependency of these brain regions in thermal sensation, thermal perception and thermal regulation has been of interest for researchers for decades. The aim of the thesis was to investigate the role of supraspinal circuitry in thermal coding in rodents using a new imaging modality named, functional ultrasound (fUS) imaging. fUS imaging is based on neurovascular coupling i.e., the phenomenon that links neural activity and changes in cerebral blood volume (CBV).

Our first study aimed at mapping the matrix of areas activated by innocuous and noxious thermal skin stimulations in anesthetized rats. The outcome of this study was mostly negative. We concluded that innocuous stimuli did not induce any change of CBV. On the contrary, noxious thermal stimulations induced local increase of CBV, but in a non-reproducible manner, due to the physiological factors such as increased arterial blood pressure that leads to high fluctuations in CBV.

The second study aimed at deciphering the interplay between the somato-motor, cingulate and hypothalamus regions in thermal processing. We chose to address this question, using fUS imaging on awake and freely moving mice, which allows recording of natural and innate brain responses without the bias of anesthesia. Transcranial fUS imaging was performed while the mice were exposed to either a fixed temperature (neutral 25°C, warm 35°Cand cold 15°C) or varying temperature at a fast and slow pace. Study of the functional connectivity, an indirect measure of brain network's function and strength, revealed a dichotomy of function between the somato-motor (SM)-cingulate network and the SM-hypothalamic network in cold sensing. Study of the dynamic brain states revealed: i) specific modes for this dichotomy, ii) a mode in which, during static exposure to cold temperature (15°C) the cingulate cortices is differently connected to the other networks studies and finally iii) a 'resting state' mode, which is the most frequent of all as is more frequently present at the resting temperature. These results provide key information on the dynamic of networks in cold sensing.

Table of Contents

List of Figures

CHAPTER 1:

INTRODUCTION

1. Thermosensation: An evolutionary perspective

The four-billion-year-old planet Earth encountered its hottest thermal environment in its early forming years. Scott Wing and Brian Huber, a paleo botanist and paleontologist, respectively have described this temperature roller coaster in their studies (VOOSEN, 2019). It took tens of millions of years for Earth to cool down, but even then the thermal environment would have been impossible to survive. Evidence also suggests of an ice age after the scorching heat, hundreds of millions of years. *Figure 1* illustrates the global temperature curve of the planet from 500 million years ago until now and it suggests that temperature in our plant is ever-changing. Since the beginning of life on Earth, the omnipresent thermal cues have shaped the evolutionary thermal responses of all the species.

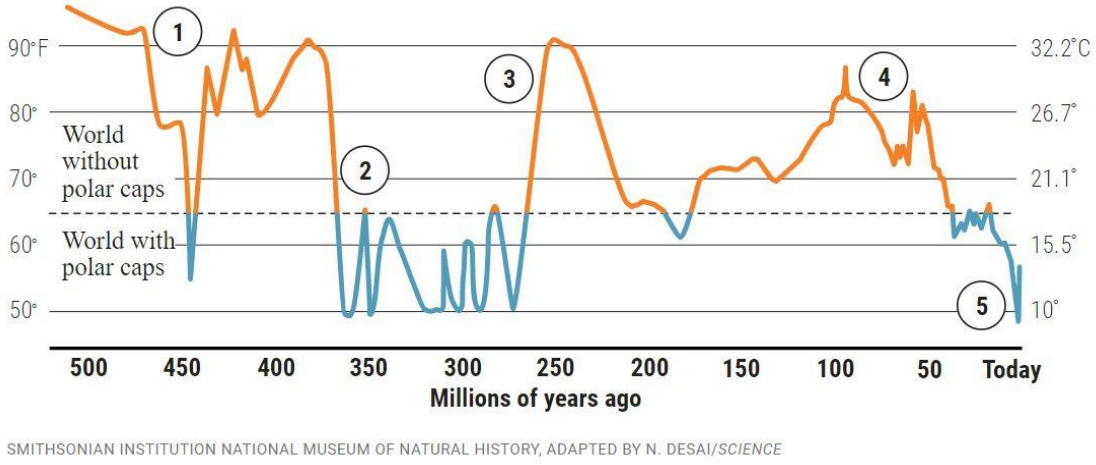

Figure 1: Global temperature curve showing the variation in temperature in the last 500 million years*. (1) Heat before plants absorbed CO2, (2) formation of polar ice caps, (3) volcanic eruptions increases temperature, (4) evolution of mammals in the warm temperature, (5) climate change and increasing temperature as of today. Graphic: Smithsonian institution national museum of natural history, adapted by n. Desai/science. (VOOSEN, 2019)*

Environmental and core body temperature influence the biological mechanisms required for survival such as physiology, growth, reproduction and even circannual rhythms. Different species develop complex coping mechanisms to their ever-changing thermal environment. The exposure to such fluctuations could be for short or long durations. Nevertheless, it results in sudden metabolic adjustments

such as breathing rate, sweating, shivering etc. While some of these adjustments are common, some are species-specific.

The molecular strategies used of thermosensititivity in fish, amphibians, reptiles, birds and mammals are diverse and has been well explained in (Gracheva and Bagriantsev, 2015). To begin with, the remarkable ability of fish to survive in extreme geographic and climate zones ranging from African deserts to Antarctic ice caps, greatly depends on the fact that they do not have the cold activated TRPM8 channels. Thermo-TRP channels are cationic channels that act as thermal sensors. (Detailed explanation on TRP channels in 3.2 Neurophysiology of thermal sensation). Despite their tolerance level for cold, they are highly sensitive to warm and hot climates. Many fish species do not thrive well in temperatures above 32°C. Amphibians tolerate extreme cold by hibernating, but they go onto estivation which is a state of dormancy due to hot and dry weather. The South African clawed frog (*Figure 2*) responds to cold sensations only at 15-10°C in contrast to mammalian cold threshold of 26°C. On the other hand, molecular adaptions in amphibians did not modify heat sensors extensively, keeping the TRPV1 activation threshold at 40°C and TRPA1 at 38°C. Reptiles can sense increasing temperature (warm and heat) by the activation of TRPV1 synergistically with TRPA1 whereas its cold receptors are still not known (*Figure 2*).

Birds are homeothermic creatures, with a high core body temperature between 40-44°C. Thermal receptors of birds are adapted to fly for long duration and in different climate zones ranging from tropical to polar, while maintaining the high internal temperature. Heat sensors in chicken (*Figure 2*) are only activated at 46-48°C, in strong contrast with the mammalian threshold of 42°C. Its cold receptors, however, are activated at 29°C. The evolutionary adaptations in thermal sensing strongly points in the direction of the irreplaceable link between somatosensory system, the surrounding environment and the physiological and behavioral needs of the organism.

Mammals are complex homeothermic animals which keep their internal body temperature in a very narrow range between 36-38°C. Some desert species such as squirrels and camels have the ability to withstand up to 46°C and when the ambient temperature is 32°C they can raise their core body temperature to 43°C. They show great adaptability but the molecular components of these processes in the thermosensory and thermoregulatory circuits are still a mystery.

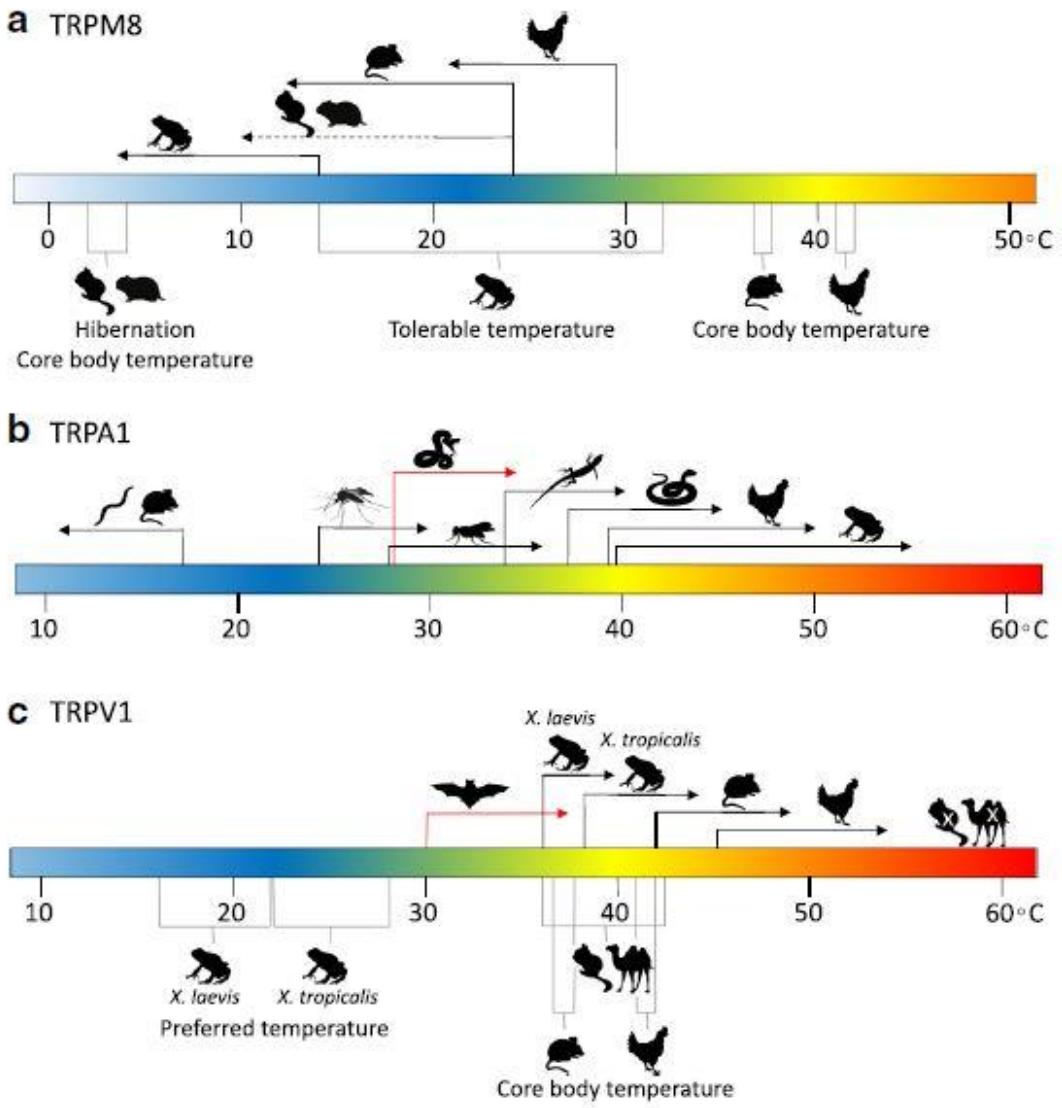

Figure 2: Temperature ranges for the thermo-TRP channels - TRPM8, TRPA1, TRPV1 in different species*. (Hoffstaetter et al., 2018). a. TRPM8 (cold sensor) activation threshold for chicken (29.4 °C), rat (24 °C), and frogs (13.9 °C). Core body temperature of squirrel and hamster drops to 2-4°C and have reduced TRPM8 sensitivity. b. TRPA1 in mouse is activated at < 17 °C where as in insects and reptiles between 24°C and 37°C and for chicken and frog at 39.4 °C and 39.7 °C respectively. The red arrow means that TRPA1 is used as a special heat sensor in snake pit organs. c. TRPV1 is activated at 36°C and 38°C in two different species of frogs, 38 °C), and for mouse and chicken at >42 °C and > 45 °C. Squirrels and camels can tolerate higher temperatures as theirs TRPV1 is not sensitive to heat. The red arrow shows the use of TRPV1 as a heat sensor by vampire bats.*

Mammals such as vampire bats rely on their thermal sensitivity to support their feeding behavior. Vampire bats detect its preys using TRPV1 using it as a special heat sensor (*Figure 2*). To avoid harsh temperatures, certain primates and rodents hibernate. They follow a similar physiological phenotype- extreme cold tolerance, lower metabolic rates and drastic drop in core body temperature. Some arctic (-20°C) hibernators can lower their internal body temperature to unbelievable levels in the order of -2.9°C. Despite the recent advancements, the molecular strategies and adaptations in these extreme thermoregulatory pathways is still unresolved.

What lies ahead for researchers is a long quest to unravel evolutionary aspects of thermal reception and perception in the wide array of species on Earth.

2. Psychophysics of thermal sensation

The average skin temperature of humans spans from 20-40°C based on day-to-day activities, but mostly stays at 30-36°C. Warming >42°C and cooling <15°C can produce painful thermal sensations. (Gagge and Gonzalez, 1996; Gagge and Nishi, 1977) summarized how skin temperature can be associated with a sensory state (*Figure 3*).

TABLE 1. *General Relation of Skin Temperature (T_{sk}) to Various Physiological and Sensory States*

T_{sk}	State
Above 45°	Rapid tissue damage
43°–41°	Threshold of burning pain
41°–39°	Threshold of transient pain
39°–35°	Sense of hot
37°–35°	Initial sense of warm
34°–33°	Neutral temperature sense at rest; comfortable
33°–32°	Neutral temperature sense at 2–4 mets exercise
32°–30°	Neutral temperature sense at 3–6 mets exercise
36°–30°	*Range where $T_{sk} \sim T_o$ and is independent of M*
31°–29°	Uncomfortable cold while sedentary
25° (local)	Numbing of skin sensation
20° (hand)	Uncomfortable, cold
15° (hand)	Extremely uncomfortable, cold
5° (hand)	Painful, cold

Met, metabolic rate (for sedentary human beings 1 met = 58.2 $W \cdot m^{-2}$); M, rate of metabolic energy production; T_o, operative temperature.

***Figure 3: Association of a skin temperature with a sensory state**. Skin temperature (Tsk) drives our judgement of thermal comfort and helps us differentiate between heat, cold and pain. It can be seen that 30-36°C is the comfortable range. As per (Gagge and Nishi, 1977), operative temperature (To) is a temperature index of the physical heat stress caused by the environment on human beings and is independent of the temperature of the skin surface and insulation of clothing worn.*

(Filingeri, 2016; Jones and Berris, 2002) points out that the psychophysics underlying thermal sensations mainly depends on: (i) absolute skin temperature; (ii) rate of change of temperature; (iii) stimulus area; and (iv) region of stimulation.

2.1. Absolute skin temperature

When the skin temperature is 30-34°C , it is said to be adapted and the subject feels neither cold nor warm sensations. An increase or decrease of temperature from these adaptive temperature results in warm and cold sensing, respectively. When the skin adapts to a temperature outside the 30-34°C range, a much larger change in skin temperature is required for the thermal sensation to be perceived. When the initial skin temperature is less than ~30◦C , for instance at 27°C, and adaptation has not been reached, a cool sensation is experienced. Now if we increase the temperature from 27°C, it will first reduce the strength of the cool sensation first, and then followed by the subject experiencing warmth. Vice-versa, if the temperature is initially above 34°C without adaptation (at 38°C, for instance), warm sensation is felt. But decreasing the temperature will first reduce the intensity of the warmth before the subject feels cold. See *Figure 4* A showing the absolute thresholds and

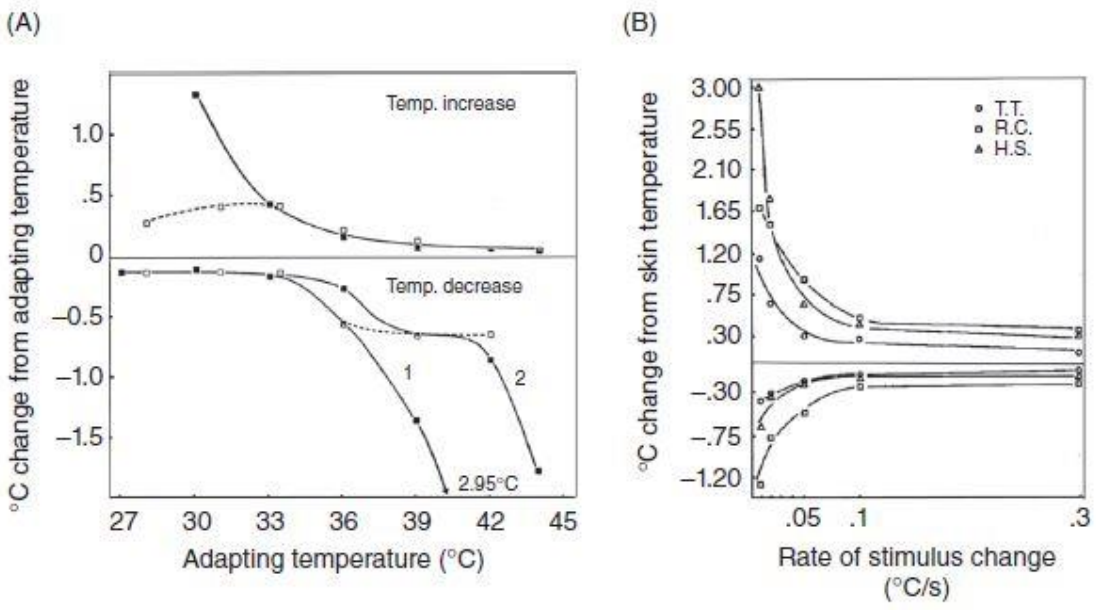

Figure 4: Effect of absolute skin temperature and rate of change of temperature*. A. Shows change from adapting temperatures (absolute temperature threshold) required for thermosensation (solid line and squares) according to different adapting temperatures. Broken lines and open squares indicate noticeable difference threshold (Filingeri, 2016). B shows rates of changes in temperature and how much change from normal skin temperature is required to produce warm or cool temperatures*

2.2. Rate of change of temperature

Rate of increase or decrease of temperature greatly influences the way we perceive a temperature. Faster the rate of change from adapted temperature at 34°C, a smaller change can induce a thermal sensation. On the other hand, slower the rate of change of temperature much larger change is needed to induce a thermal sensation.(Kenshalo et al., 1968) explained this in a study where the skin temperature of forearm was increased or decreased at rates of change: 0.3, 0.1, 0.05, 0.02, and 0.01◦C/s. The participants experienced different thresholds for cool and warm depending of the rate of change. At slower rates, the thermal threshold was higher *Figure 4*.

In our daily life, when we touch a cold or hot object, there is a sudden change in temperature happens. This is due to the heat exchanges between the skin and the object in contact. The magnitude of this exchange decides the intensity of the sensation.

2.3. Area under stimulation

By exposing a larger area for thermal stimulation, the temperature threshold needed to produce a thermal sensation is decreased. It also projects the importance of the interaction of the stimulus area and spatial summation can significantly increase the magnitude of the sensory stimuli experienced. The spatial summation of thermal perception makes it different from other sensations such as visual and audio. Thermal stimulation greatly depend on the quantity of stimulation, meaning the more area stimulated spatially, there is a change in the intensity experienced. *Figure 5* shows the effect of area of thermal stimulation on temperature thresholds (Filingeri, 2016; Jones and Berris, 2002; Kenshalo et al., 1967).

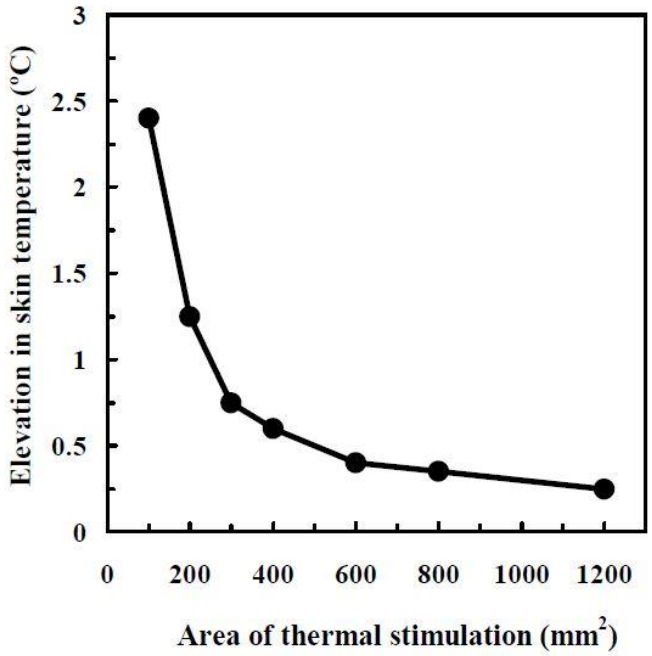

Figure 5: Less area of thermal stimulation requires higher temperature threshold *(200mm2). Decrease in threshold as the area of thermal stimulation increases (1200mm2). (Filingeri, 2016; Jones and Berris, 2002; Kenshalo et al., 1967)*

2.4. Region of body stimulated

Finally, the regions in the body could decide how and with what intensity we sense heat or cold. These regional differences were first studied by mapping warm and cold spots in the body in (Donaldson, 1885; Norrsell et al., 1999) and it was found that the overall density of cold spots is more than that of warm spots.

Head and face exhibit high sensitivity to warmth. On the contrary, cool sensitivity is high in torso (abdomen) *Figure 6* (C. Stevens Kenneth K. Choo, 1998; Gerrett et al., 2014). Thermal sensitivity is seen to vary between hairy regions and glabrous (palm) skin regions.

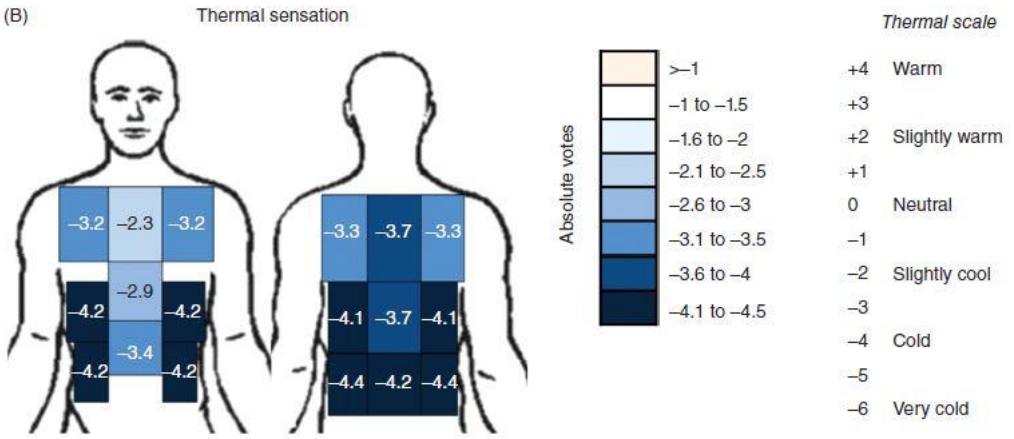

Figure 6: Regional differences in thermal sensations in response to skin cooling. *(Filingeri, 2016). The same cold stimulation produces more intense sensations when applied to lower back and sides of chest and abdomen.*

In conclusion, the psychophysical aspects of thermosensation in humans largely depends on the changes in skin temperature and other parameters such as area and region of stimulation. Although this is an important principle in thermosensation, it also makes us wonder how these changes are manifested at the molecular level and how these peripheral mechanisms are transduced to higher levels in the system.

3. Neurobiology of thermal sensation

3.1. Primary Afferent Fibers

Environmental temperature is a highly dynamic stimuli that invokes both voluntary and involuntary responses. They are constantly being detected and responded to. The skin, being our primary sensory organ, is the first point of interface with the immediate environment. In 1880s, it was discovered that human skin has warm and cold spots that are sensitive to specific stimuli (Green, 2004; Norrsell et al., 1999). Soon after, electrophysiological studies revealed that painful and non-painful thermal sensations felt on skin are encoded and transmitted to the central nervous system by primary afferents. Simply put, they are axons or nerve fibers in the peripheral nervous system (Gebhart and Schmidt, 2013; Green, 2004; Schepers and Ringkamp, 2010). The terminals of these afferent fibers acts as free nerve endings on the skin.

Myelinated Aβ mechanoreceptors (Duclaux and Kenshalo, 1972a), thinly myelinated Aδ fibers and unmyelinated polymodal C fibers (Bautista et al., 2007; Campero et al., 2001a; Schepers and Ringkamp, 2010) are some of the main primary afferents found at the periphery. Among them, non-myelinated polymodal C fibres and thinly myelinated Aδ fibres are the main cutaneous sensory neurons involved in the molecular transmission of thermal information. Since its discovery, numerous research groups characterized A-fibers and C-fibers (Bessou and Perl, 1969; Brown and Iggo, 1967; Campero et al., 2009, 2001a, 2001b, 1996; Darian-Smith et al., 1973; Duclaux and Kenshalo, 1972a, 1972b; Hensel and Boman, 1960; Iggo, 1959; Kenshalo and Duclaux, 1977; Simone and Kajander, 1997). *Figure 7* , an illustration from (Ma, 2010) summarized the findings of human studies (Campero et al., 2009) focused on: Aδ-cold fibers (myelinated, activated by innocuous cold temperature, inactivated by nociceptive cold) and thermosensitive polymodal C-fibers (CH, C-fibers responding only to noxious heat; CMH, C-fibers responding to noxious mechanical stimuli and heat; C2, C-fibers responding cold and warmth/heat; CMHC, C-fibers responding to noxious mechanical stimuli, heat, and noxious cold; Aδ-cold, A-fibers responding to innocuous cold; C-warm, C-

fibers responding to warm temperatures; Aδ-MH, A-type fibers responding to mechanical stimuli and heat (Campero et al., 2009; Ma, 2010)).

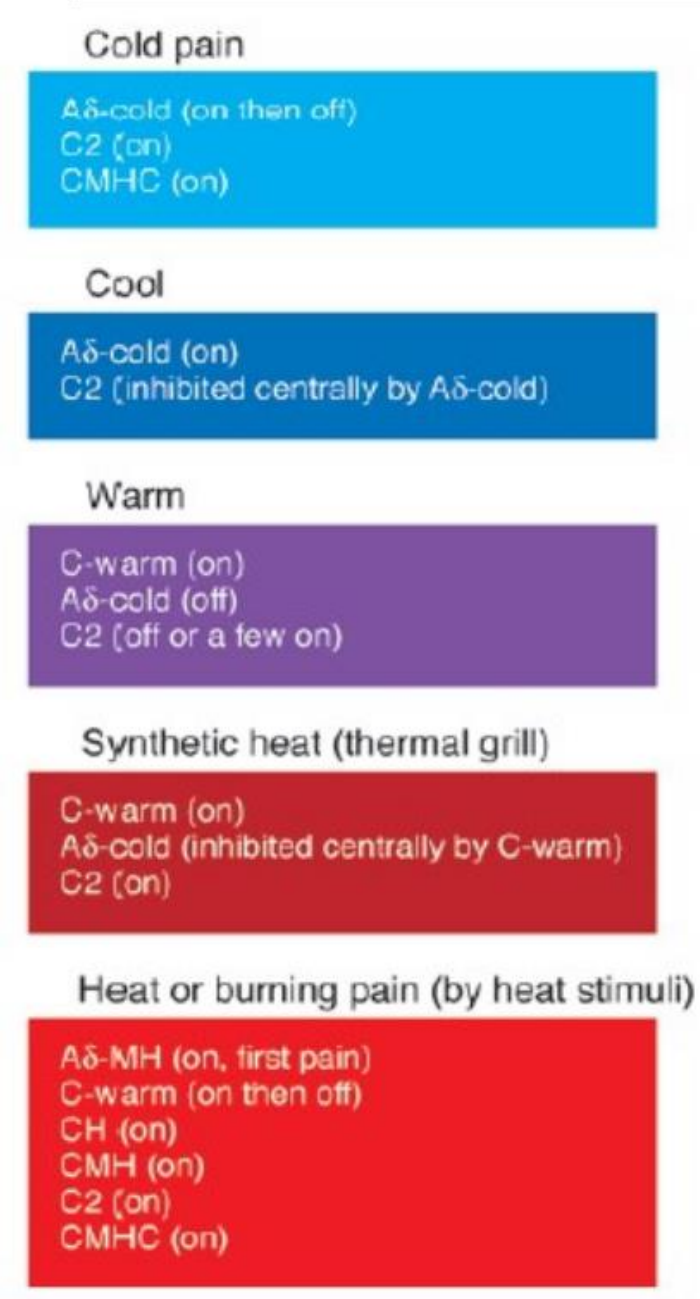

Figure 7: Specific thermal sensations and the fibers associated with them. *CH, C-fibers responding only to noxious heat; CMH, C-fibers responding to noxious mechanical stimuli and heat; C2, C-fibers responding cold and warmth/heat; CMHC, C-fibers responding to noxious mechanical stimuli, heat, and noxious cold; Aδ-cold, A-fibers responding to innocuous cold; C-warm, C-fibers responding to warm temperatures; Aδ-MH, A-type fibers responding to mechanical stimuli and heat. Adapted from* (Ma, 2010).

Mammals take advantage of the afferent neurons of the somatosensory system to form their thermal perception. Cell bodies of the sensory neurons which innervate the head and face are located in the trigeminal ganglia (TG) whereas the ones that innervate the rest of the body is are localized in the dorsal root ganglia (DRG) (Gracheva and Bagriantsev, 2015; Ran and Chen, 2019; Vriens et al., 2014). They are calibrated to convert specific thermal, mechanical, and chemical stimuli to electrical signals, which are transmitted from the skin to the central nervous system as action potentials. *Figure 8* shows a representation of the transmission of cutaneous thermal sensations to the cell bodies of afferent fibers in the DRG which synapses with the dorsal horn neurons in the spinal cord.

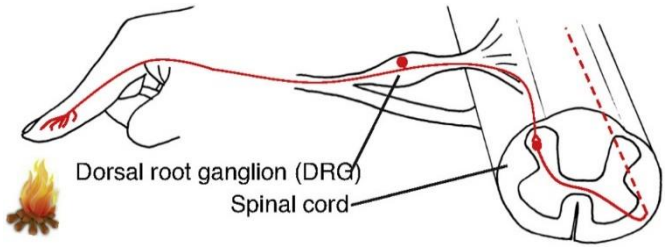

Figure 8: Transmission of cutaneous thermal sensations. *Temperature is detected at the periphery by the afferent fibers whose cell bodies are located in the dorsal root ganglia (DRG). They synapse on to the dorsal horn neurons in the spinal cord for processing and further transmission to brain (Ran and Chen, 2019).*

3.2. TRP Channels

Specialized thermal sensors known as the transient receptor potential (TRP) ion channels are expressed in the terminals of the aforementioned afferent fibers. They are polymodal cation channels which respond to multiple sensory stimuli (Hoffstaetter et al., 2018; Venkatachalam and Montell, 2007; Xiao and Xu, 2021; Yue and Xu, 2021). For example, a TRP channel can be activated by temperature changes and chemicals such as capsaicin (Julius, 2013; Patapoutian et al., 2003). However, subsets of the TRP channels are designed to specifically detect particular temperature ranges in heat and cold. The activation of these channels are closely linked to their environmental temperature (Voets et al., 2004).

(Clapham and Miller, 2011; Vriens et al., 2014)explains how can the temperature sensitivity of channel opening be so high to be able to detect even the subtle changes in thermal cues. According to the laws of thermodynamics, all biochemical reactions have a thermal dependance. The degree of this this dependance can be quantified using Q10. It denotes the relative change in the current when there is a 10 degree temperature rise (Hoffstaetter et al., 2018).

$$Q10=\alpha\_(T+10)/\alpha\_T$$

where αT and αT + 10 are reaction rates at two temperatures 10 degrees apart.

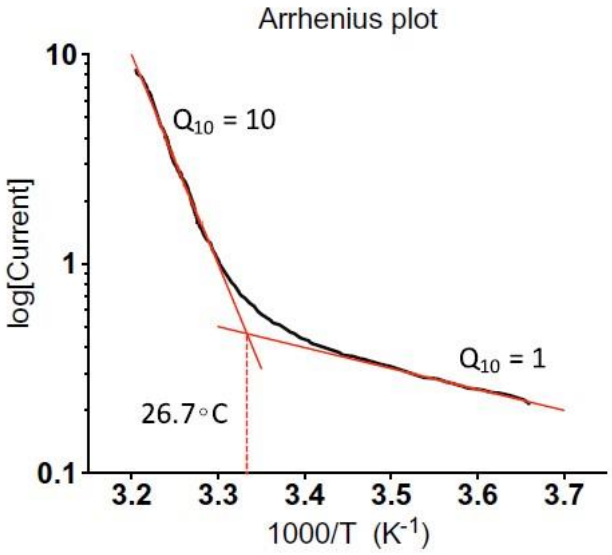

Figure 9: Finding Q10 of a thermo-TRP channel using Arrhenius plot. *The x-axis is logarithm of current and y axis inverse of temperature (Kelvin). The slope of the resulting curve is used to calculate Q10. The intersection of the tangents corresponds to the approximate threshold for thermal sensing (Hoffstaetter et al., 2018)*

The Q10 value of most bio-enzymatic reactions and ion channel gating, which are independent of temperature have a lower value in the range of 1-3 (Hille, 2001). Remarkably, the thermo-sensitive ion channels exhibit a much increased Q10 value. Therefore it is safe to define thermo-TRP ion channels as highly sensitive molecular 'thermometers' with Q10 value much greater than 3. *Figure 9* shows the calculation of activation threshold of a hypothetical thermo-TRP channel using Arrhenius plot (Hoffstaetter et al., 2018). The intersection of the tangents of the

curve (logarithm of current verses inverse of temperature (Kelvin), corresponds to the approximate activation threshold (26.7°C).

3.2.1. TRP Subfamilies

The fundamental principle of thermosensation lies in the TRP family of channels. Currently, 28 TRP channels from the TRP superfamily have been identified and classified into 6 subfamilies namely, TRPC, TRPV, TRPM, TRPA, TRPML and TRPP with respect to their functionalities (Caterina et al., 1997). Among these TRPA, TRPV, TRPM and TRPC are the mammalian thermo-TRPs (*Figure 10*).

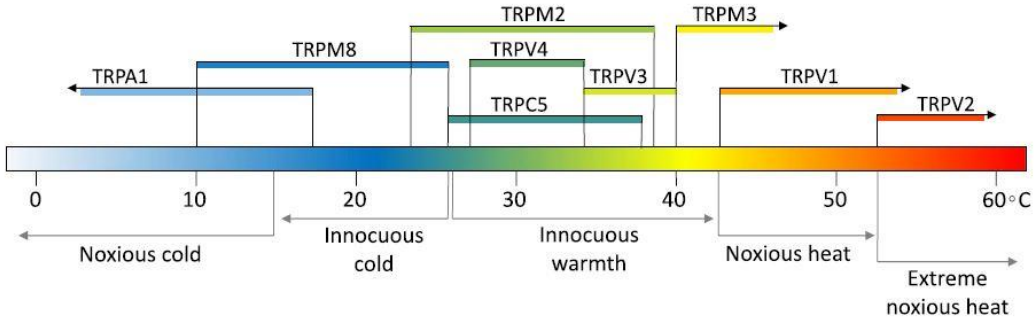

Figure 10: Mammalian thermo TRPs in the range of 0-60°C . *(As illustrated in (Hoffstaetter et al., 2018)).*

3.2.2. Innocuous and Noxious Heat Sensors

Numerous TRP channels have been identified for their role in warm and hot temperature sensing (*Figure 10*). TRPV1 is the most well characterized ion channel that detects noxious heat >42°C (*Figure 11*). It is polymodal as it is activated by capsaicin and heat (Caterina et al., 1997). Noticeably, 42-45°C is the threshold of thermal pain in humans (Defrin et al., 2002; Yarnitsky et al., 1994)and it supports the theory that TRPV1 is a multimodal sensor which mediates temperature sensation and pain. Apart from TRPV1, TRPM3 and TRPA1 also take part in redundant noxious heat sensing (Vandewauw et al., 2018). Although Trpv1 KO mice only exhibits slight deficits in temperature discrimination, surprisingly, TRPV1-TRPM3-TRPA1 triple knockout mice completely lack motor reflex to noxious heat. It can thus be acknowledged that, noxious heat presents itself as a

dangerous stimuli and clearly multiple channels participate in protecting us from any damage or injury.

In the case of innocuous warm sensors, several thermo-TRP channels have shown to be activated in the warm range in-vitro. But, physiological basis of warm sensation presents itself differently. Although TRPV3 and TRPV4 responds to warm temperature ranges of 32–39°C and 26-34°C respectively, TRPV3 and TRPV4 double KO mice did not exhibit any serious thermal detection deficits (Huang et al., 2011).

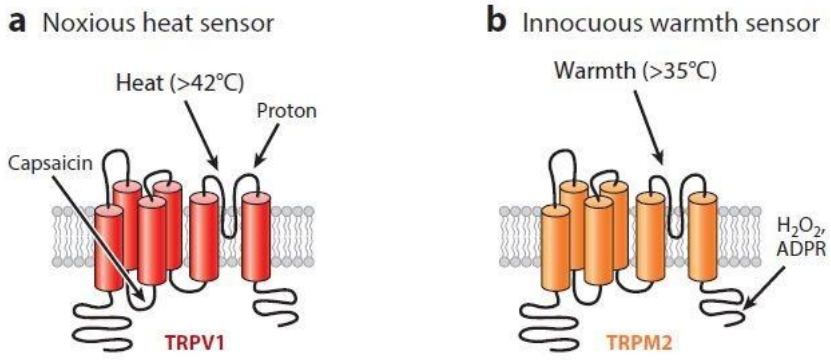

Figure 11: Noxious and innocuous heat sensors *(Xiao and Xu, 2021).*

TRPM2 channel activates at approximately at 35°C (*Figure 11*) by sensing environmental temperatures (Song et al., 2016; Tan and McNaughton, 2018). TRPM2 is also expressed in DRG neuron subsets whereas the other TRP channels such as TRPV 1-4 and TRPM3 are not. TRPM2 KO mice exhibit no avoidance at 38°C during the thermal preference test indicating that TRPM2 is a key component in sensing warm temperatures. There are promising studies pointing in the direction of the presence of other warm sensors as TRPM2 KO mice showed some DRG neurons responded to warming.

While TRPM2 is clearly a warm sensor, its role in sensing noxious heat is open to discussion (Vilar et al., 2020). Deletion of TRPM2 affects the warm sensing but it still can detect the noxious temperature higher than 42°C (Haraguchi et al., 2012;

Tan and McNaughton, 2018, 2016) (Haraguchi et al., 2012). While the TRPV1-TRPM3-TRPA1 triple KO mice (Vandewauw et al., 2018) eliminates the ability to sense noxious heat, TRPM2 KO responds to 30°C to 40°C range in-vivo. Until recently, TRPM2 was not in the spotlight unlike many of its TRP counterparts, but its role in not only thermosensation, but also in immune system, insulin secretion, neuropathic and inflammatory pain is becoming more and more evident (Tan and McNaughton, 2018).

See *Figure 12* for a list of known heat sensors identified in the mouse thermal system and their corresponding activation temperature.

Table 1 Summary of molecular heat sensors in different model systems

Heat sensors	Species	T_{act}	Q_{10}	Remarks
TRPV1	Mouse	~42°C	>15	Mediate noxious heat sensation and pain and warmth sensation
TRPM3	Mouse	~40°C	~7	Mediate noxious heat sensation and pain
TRPA1	Mouse	variable	~10	Mediate noxious heat sensation and pain
ANO1	Mouse	~44°C	20	May play a redundant role in noxious heat sensation
TRPV2	Mouse	~52°C	~100	Heat sensitive in vitro No notable thermal phenotype in KO mice
TRPM2	Mouse	~35°C	~15.6	Mediate warmth sensation, also a redox sensor
STIM1	Mouse	~35°C	6.8	Act in skin keratinocytes to mediate warmth sensation
TRPV3	Mouse	~32°C	33	Heat sensitive in vitro No notable thermal phenotype in KO mice
TRPV4	Mouse	~27°C	~10	Heat sensitive in vitro No notable thermal phenotype in KO mice
TRPM4	Mouse	~15°C	~8	Heat sensitive in vitro
TRPM5	Mouse	~15°C	~10	Contribute to the temperature effect on perceived sweet taste

Figure 12: List of heat sensors *identified in mice with their corresponding Q10 values and activation temperatures (Xiao and Xu, 2021).*

3.2.3. Innocuous and Noxious Cold Sensors

There is one TRP channel best-known as an innocuous cold sensor- the TRPM8. It is also known as a menthol receptor (McKemy et al., 2002; Peier et al., 2002). Heterologous expression of TRPM8 showed that it is activated between 23-27°C. TRPM8 KO mice present significant deficiencies with respect to cold detection. But they are sensitive enough to avoid surfaces below 10 °C proving that TRPM8 is the

essentially a cool sensor (Bautista et al., 2007). However (Dhaka et al., 2007), discusses that TRPM8 deficient mice respond normally to a cold plate at -1°C whereas when acetone is applied to the surface of the paw, the TRPM8 deficient mice exhibit significantly reduced response of paw withdrawal and licking. Wet-dog shakes after an injection of icilin, is almost absent in TRPM8 deficient mice. Taken together, TRPM8 might be involved in sensing unpleasant or noxious cold but it also points to the presence of other noxious cold receptors (*Figure 13*).

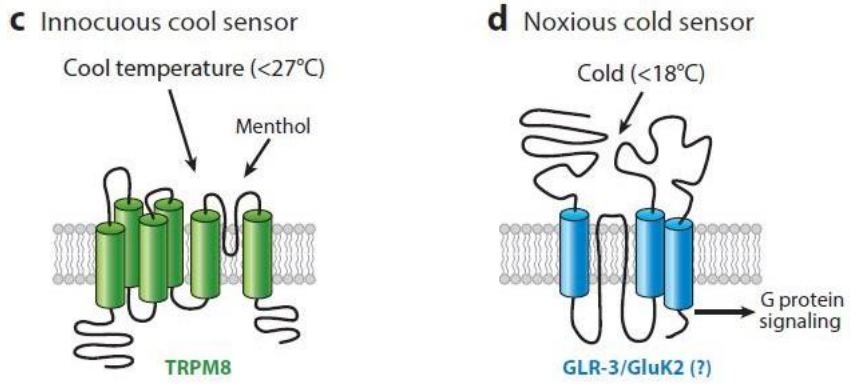

Figure 13: Noxious and innocuous cold sensors *(Xiao and Xu, 2021).*

Efforts to identify noxious cold sensors is still ongoing. TRPA1 was one of the first candidates proposed as a noxious cold sensor with an activation threshold of approximately 17°C (Story et al., 2003). But TRPA1 KO mice do not exhibit deficits in avoiding noxious cold temperatures (Bautista et al., 2006; Kwan et al., 2006). Additionally, evidence emerged stating that TRPA1 is a major contributor in noxious heat sensing (Vandewauw et al., 2018). Altogether, it is reasonable to conclude that TRPA1 is not noxious cold detection in mammals.

Although candidate gene approaches have been fruitful in identifying heat sensors, it has not been very helpful in identifying cold sensors. Hence, the cold sensors other than TRP channels were undetected until recently. (Gong et al., 2019) conducted an unbiased genetic screen to identify cold receptors in C. elegans. This led to the discovery of GLR-3,a kainite-type glutamate receptor homolog, as a cold receptor. GLR-3 present in the peripheral nervous system of C. elegans senses the cold

temperatures and exhibits avoidance behavior. GLR-3 is mostly activated at noxious cold rather than cool temperatures with an activation threshold well below 20°C.

Heterologous expression of vertebrate homologue of GLR-3, GluK2 from fish, mouse and humans, strongly advocates for GLR-3 and GluK2 cold sensors, in vitro. Interestingly mouse GLuK2 can function as a substitute for GLR-3 when expressed as a transgene in ASER neuron (Gong et al., 2019) in vivo, indicating that GluK2 in mouse can be a prospective cold receptor. Undisputedly, GLR-3 and GluK2 are promising candidates, but further investigations are required to identify its functions in vitro and in vivo (Xiao and Xu, 2021) (*Figure 13*).

See *Figure 14* for a list of known cold sensors identified in the mouse thermal system and their corresponding activation temperature.

Table 2 Summary of molecular cold sensors in different model systems

Cold sensors	Species	T_{act}	Q_{10}	Remarks
TRPM8	Mouse	~27°C	24	Cool sensor mediating cool sensation
TRPC5	Mouse	~25°C	~10	Cool sensitive in vitro No notable thermal phenotype in KO mice
GC-G	Mouse	Over 30°C	ND	Cool sensing in Grueneberg ganglion
TRPA1	Mouse, human	Variable	~10	Heat sensitive under physiological conditions, but cold sensitive under oxidative stress conditions
GluK2	Mouse	~18°C	ND	Cold sensitive in vitro Knockdown of GluK2 suppresses noxious cold, but not cool, sensation in DRG neurons

Figure 14: List of cold sensors *identified in mice with their corresponding Q10 values and activation temperatures (Xiao and Xu, 2021).*

3.2.4. TRP channel activation mechanisms

TRP channels are capable of detecting and transmit specific sensory stimuli through molecular mechanisms of ion channels and pumps. *Figure 15* A illustrates the main components in that process. When primary sensory neurons encounter a sensory stimuli, they undergo graded depolarization. The volage-dependent sodium channels (Nav1.7 and Nav1.8) generate an action potential due to the inward current. At the same time, voltage-gated potassium channels (Kv's) act to stop the depolarization, thereby limiting the excitability. Excitation is only achieved, if the depolarization reaches a specific threshold. Therefore, if the threshold is close to the resting

membrane potential, it aids in firing a response to the sensory stimuli. This resting potential can be regulated by Nav1.9. Na+/K+-ATPase responsible for membrane gradients and thermosensitive leak potassium channels (TREK-1, TREK-2, and TRAAK) which limits the excitation, also regulate resting potential (Hoffstaetter et al., 2018). *Figure 15* B shows the main components of an action potential.

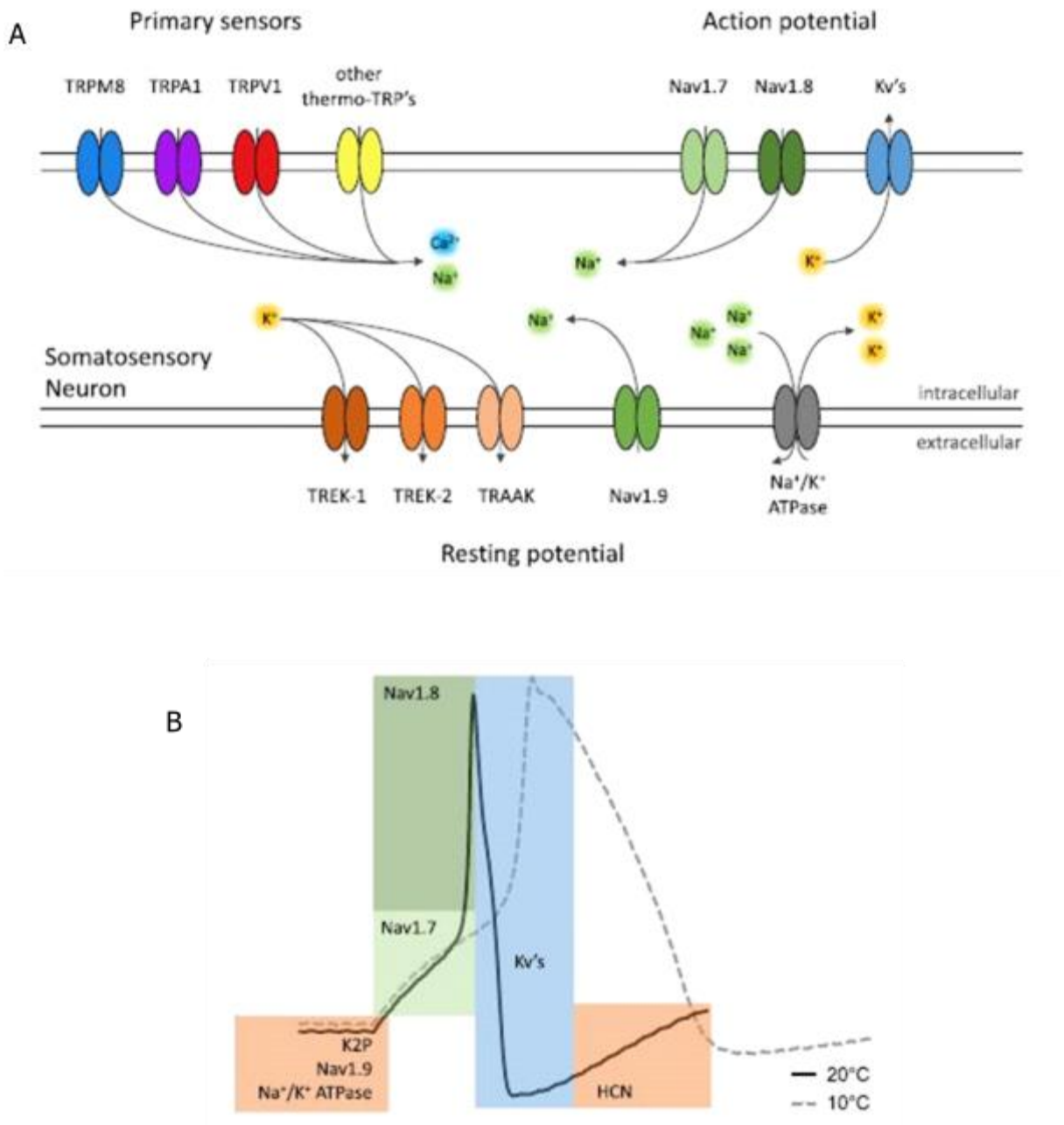

Figure 15: TRP channel excitation and components of action potential.. *A. Nav1.7 and Nav1.8 are voltage gated sodium channels that generate an action potential (inward flux of Na+)l. Kv's counter act to limit this excitability(outward flux of K+). Resting potential is regulated by Nav1.9, Na+/K+-ATPase and thermosensitive leak potassium channels (TREK-1, TREK-2, and TRAAK) (Hoffstaetter et al., 2018). B. Typical shape of an action potential. Colored region represents channel activity. K2P's, Nav1.9, and Na+/K+-ATPase maintain the resting potential and Nav1.7 is responsible for initial depolarization (upstroke) whereas Nav1.8*

contributes to the rapid upstroke. Kv's repolarizes the cell (falling phase). HCN channels regulate the hyperpolarization back to resting potential. Curve at cold temperature is broader because. Voltage-gated sodium channels (Nav1.7 and Nav1.8), Voltage gated potassium channels (Kv's) Hyperpolarization-activated, cyclic nucleotide-gated (HCN).

Temperature has been found to activate TRPV, TRPC, TRPM and TRPA channels with high Q10 values (Refer 3.2 TRP Channels). Fundamentally, temperature induces conformational changes in TRP channel proteins contributing to activation and de-activation. However (Voets et al., 2004) suggested that temperature changes induces a voltage-dependent gating process. (Matta and Ahern, 2007) later show that voltage, temperature and ligands take part in the thermal sensitivity of TRP channels. Certain chemicals such as capsaicin can activate the heat sensor TRPV1 (Caterina et al., 1997) and recently pungent compounds including cinnamaldehyde and mustard oil were found to activate TRPA1 (Bandell et al., 2004). The complex bio-physical aspect of how temperature activates TRP channels is a vast arena. Experiments by mutagenesis and chimeric protein analysis, have shed light into how these channels respond to cold and heat.

4. Thermosensory circuits

After activation, thermo-TRP channels convert the thermal information into electrical signals, which is transmitted from the periphery to central nervous system. The thermosensory circuit can be divided into 2: primary afferents to spinal cord and supraspinal circuitry consisting of spino-thalamic or thalamo-cortical pathways.

Figure 16 illustrates the pathways in thermal processing (Vriens et al., 2014). To summarize what was explained in the aforementioned section (*See Primary Afferent Fibers 3.1*), sensory neurons in the skin, myelinated Aδ fibres and non-myelinated C fibers (green, yellow), have their cell bodies are in the dorsal root ganglia (DRGs). Their axons have 2 branches: one extending towards the skin with free nerve endings; the other synapses in the layers of dorsal horn. Thermal information in encoded as action potential at the periphery and transmitted to the dorsal horn. This gives rise to 3 possible outcomes: a) rapid withdrawal or motor reflex as a result of noxious temperatures/pain; b) the thermal information is transmitted across the spinothalamic tract to several thalamic regions and then to the somatosensory cortex; c) initiation of thermoregulatory processes (Vriens et al., 2014).

This section will describe the thermosensory pathways in two parts. Section 4.1 will explain the thermal processing at the level of spinal cord. Furthermore, Section 4.2 will explain the supraspinal circuitry involving thalamic regions, somatosensory cortex, insular cortex and hypothalamus and their respective roles in integrating the thermal information to form a thermal perception or initiate thermoregulation.

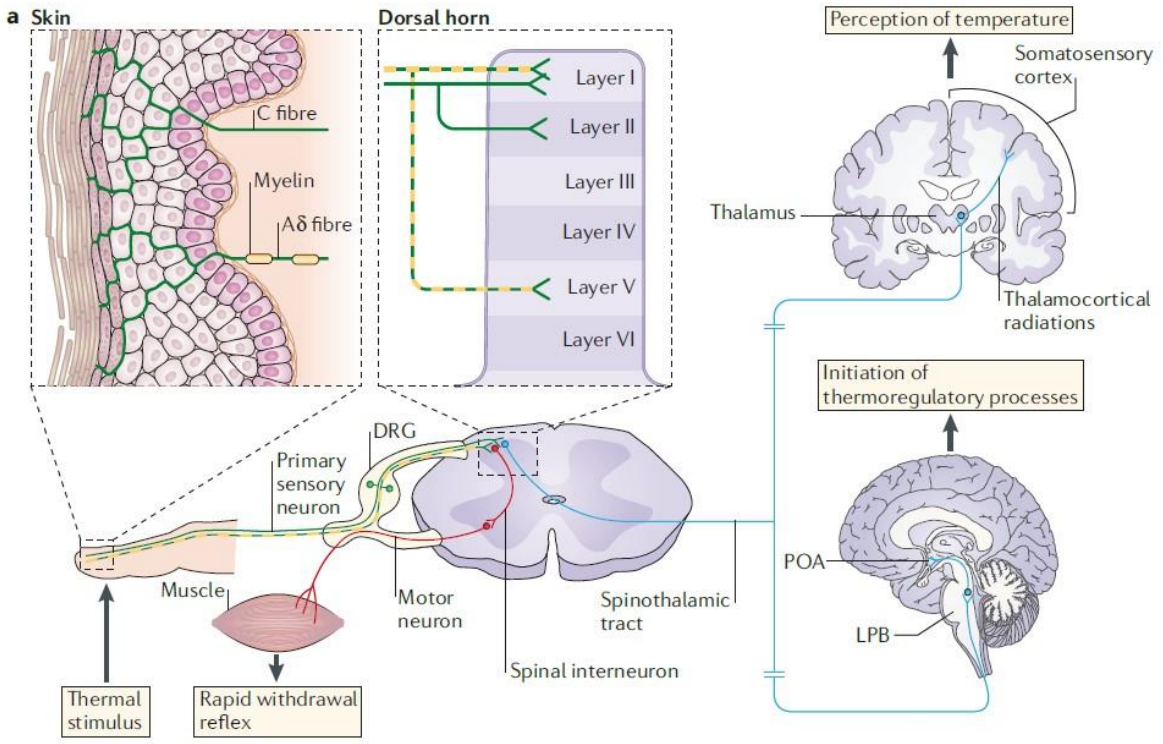

Figure 16: Thermosensory pathways. *Sensory neurons in the skin, myelinated Aδ fibres and non-myelinated C fibers (green, yellow), whose cell bodies are in the dorsal root ganglia (DRGs). Their axons have 2 branches: one extending towards the skin with free nerve endings; the other synapses in the layers of dorsal horn. Thermal information in encoded as action potential at the periphery and transmitted to the dorsal horn. This gives rise to 3 possible outcomes: a) rapid withdrawal or motor reflex as a result of noxious temperatures; b) the thermal information is transmitted across the spinothalamic tract to several thalamic regions and then to the somatosensory cortex; c) initiation of thermoregulatory processes. (Vriens et al., 2014).*

4.1. Spinal Integration and Transmission

The dorsal horn of spinal cord receives somatosensory signals from the body and is critical in processing them. Out of the six layers (or Laminae), Lamina I/II, the most superficial layers of the dorsal horn has incoming Aδ and C primary afferent fibers (*Figure 16*). It is also the source of the main outgoing projections from spinal cord to brain stem and thalamus (Craig, 2002).

In an experiment conducted in rats exposed to scrotal skin temperature variations, (Hellon and Misra, 1973) reports that neurons were excited by both cooling and warming. Later on, (Andrew and Craig, 2001; Craig et al., 2001), thoroughly evaluated the thermo-responsive spinothalamic tract neurons in cats and classified them as: i) nociceptive-specific (NS), ii) innocuous thermo-receptive-specific (COOL or WARM), and iii) polymodal nociceptive (HPC) sensitive to noxious **h**eat, **p**inch, and noxious **c**old (Andrew and Craig, 2001; Craig et al., 2001). Warm

neurons have a threshold range of 35-37°C. Cool neurons respond for temperatures going down from 34°C to 15°C. The nociceptive specific and HPC neurons responded to between 45 and 53°C. HPC neurons also exhibit accelerating response to cold below 24°C and until 9°C (Andrew and Craig, 2001; Craig et al., 2001).

In summary, first order neurons which are responsive to temperature changes, projecting to the dorsal horn of spinal cord, synapse with second-order neurons in lamina I/II. These neurons then projects to thalamic regions via anterolateral column of spinal cord. Thus the spino-thalamic tract is the first hub of the central integration of thermal processing.

4.2. Supraspinal Circuitry

The supraspinal pathway for thermal processing mainly consists of thalamic nuclei such as Ventral posterolateral (VPL), posterior medial (POm), and the caudally positioned triangular posterior thalamic (PoT) nuclei projecting to somatosensory cortex (primary and secondary somatosensory cortex (S1 and S2), Insular Cortex (IC) *Figure 17* (Bokiniec et al., 2018).

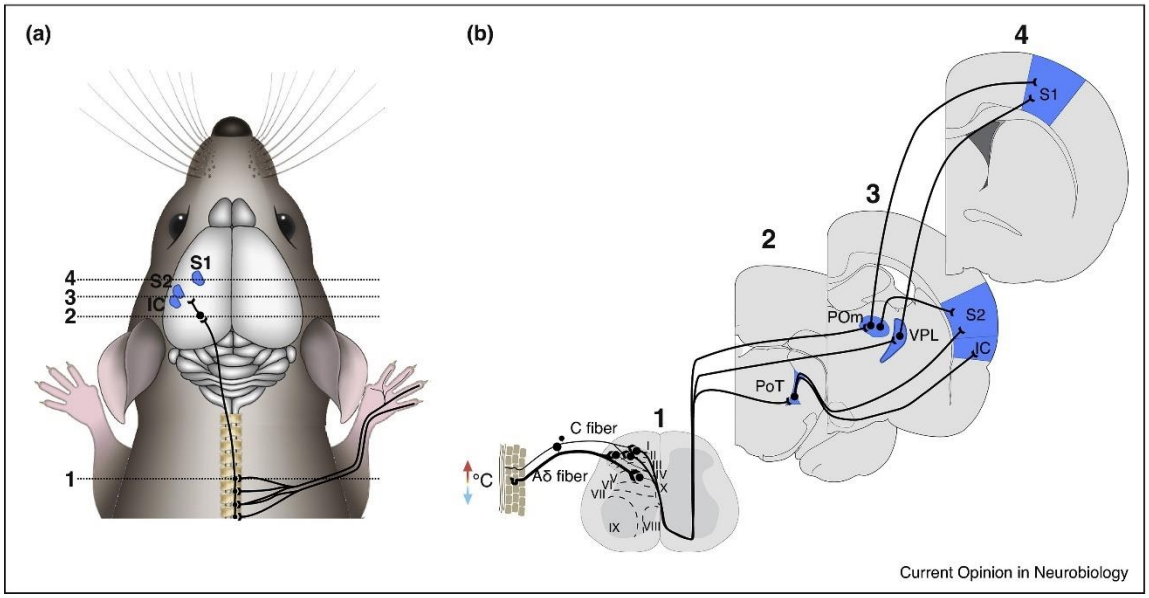

Figure 17: Thermal pathways of supraspinal circuitry in the mouse thermal system. *(Bokiniec et al., 2018) 1-afferent to spinal cord, 2-spino-thalamic tract to thalamic nuclei (PoT, Pom, VPL), 3-thalamo-cortical pathway to S1, S2, IC, 4-cortical processing. Ventral posterolateral (VPL), posterior medial (POm), and the caudally positioned triangular posterior thalamic (PoT) nuclei, primary somatosensory cortex and secondary somatosensory cortex (S1 and S2), Insular Cortex (IC) (Bokiniec et al., 2018).*

4.2.1. Thalamic Nuclei

The spino-thalamic tract can be seen as a spinal route, as well as the primary contact with the central nervous system and its mechanisms. It is the synergistic integration that give rise to a thermal sensation and perception. Thalamus being the second hub after spinal cord, it has been shown in several studies that the second order neurons project to the contralateral ventral posterolateral (VPL), posterior medial (POm), and the caudally positioned triangular posterior thalamic (PoT) nuclei (Egan et al., 2005; Gauriau and Bernard, 2004; Hellon and Misra, 1973; Schingnitz and Werner, 1980; Zhang, 2006).

The responsiveness of thalamic neurons to thermal stimuli have been interrogated in humans, cats, and primates (Auen et al., 1980; Bushnell et al., 1993; Craig et al., 1994a; Davis et al., 1999a; Duncan et al., 1993; Egan et al., 2005; Landgren, 1960). Selective lesion studies of thalamic nuclei such as ventral medial nucleus (Finger and Frommer, 1970; Norrsell and Craig, 1999) only induced mild loss of thermosensory discrimination, suggesting a partial role in discrimination of temperature. From the thalamic nuclei, the thermosensory information is further transmitted to the somatosensory cortex.

4.2.2. Somatosensory Cortex

The cortical processing of temperature to form a sensation or a perception is evident in the primary somatosensory cortex and secondary somatosensory cortex (S1 and S2) via thalamo-cortical pathway (Becerra et al., 1999; Chatt and Kenshalo, 1977; Egan et al., 2005; Hellon et al., 1973a; Landgren, 1957a; Milenkovic et al., 2014; Moulton et al., 2012; Tsuboi et al., 1993).

At this point, all evidence points in the direction that the somatosensory cortex is absolutely necessary to encode thermal cues. One of the first findings (Landgren, 1957a) was that the somatosensory cortex of a cat responded to thermal stimulations on the tongue. Cortical neurons in the rat somatosensory cortex are also activated by the temperature changes in the scrotal skin and hind paw (Hellon et al., 1973a). Rats with S1 and S2 lesions (Finger and Frommer, 1970) were reported to have failed temperature discrimination tasks. Similarly cortex ablation in rats (Porter et al., 1993) proved to induce thermosensory deficits. Much more recently, (Milenkovic et al., 2014) found that the cortical

neurons in the mouse somatosensory cortex responded to cooling of glabrous skin and interestingly also to touch. (Milenkovic et al., 2014) also showed that the silencing of these multimodal cortical neurons resulted in significant behavioral thermal discrimination. An early study (Chatt and Kenshalo, 1977) in humans, suggested that somatosensory cortex is a key player in thermal processing by measuring evoked potentials recorded from scalp. Neuroimaging study (Becerra et al., 1999) in humans shed light on the involvement of frontal gyri, anterior and posterior cingulate gyrus, thalamus, motor cortex, somatosensory cortex (SI and SII), supplementary motor area, insula, and cerebellum when the skin was stimulated by heat (46°C) stimuli.

4.2.3. Insular Cortex

Though it is tempting to conclude somatosensory cortex to be the most crucial and exclusive contestant in thermal integration, an alternate theory proposes posterior insular cortex to be equally important.

The insular cortex and its role in thermosensation has been studied by several groups (Becerra et al., 2011; Birklein et al., 2005; Corradi-Dell'Acqua et al., 2011; Craig et al., 2000; Gogolla et al., 2014; Nagashima et al., 2018; Peltz et al., 2011; Penfield and Faulk, 1955; Rodgers et al., 2008; Wager et al., 2013). Activity of insula has been correlated with perceived temperature in (Craig et al., 2000; Hua et al., 2005; Olausson et al., 2005). In addition to the discriminative component of thermal sensation, there is a hedonic component, i.e., thermal comfort or the pleasantness/unpleasantness associated with any particular temperature. (Nagashima et al., 2018) suggests that thermal comfort or discomfort is determined by central mechanisms rather than peripheral mechanisms and that insular cortex and cingulate cortex could be the brain regions driving the behavioral responses that aid thermoregulation.

The response of insula to pain and temperature was studied in patients with lesions in: anterior insula, posterior insula, retro insula, and parietal operculum and found that anterior and posterior insular regions contribute significantly to these responses (Greenspan et al., 1999). Parietal and insular cortical lesions resulted in hypoesthesia in patients (Veldhuijzen et al., 2010a), reaffirming the role of insula in thermosensory discrimination. All evidence at this point

confirms that the insular cortex might be equally essential in thermal sensation and perception.

4.2.4. Cingulate Cortex

The role of cingulate cortex in the mechanism of pain and emotion has been known for a long time. Although it is not directly a part of the established thermosensory circuit, the affective component of thermal stimulations always pointed towards cingulate cortex (Becerra et al., 1999; Brooks et al., 2002; Craig et al., 1996; Derbyshire et al., 2002; Gelnar et al., 1999). (Vogt, 2005) explained that the midline and intralaminar nuclei (MITN) projects to limbic cortex, amygdala and anterior cingulate cortex (ACC). Several studies have studies the role of ACC in pain responses (Barthas et al., 2015; Gasquoine, 2013; Hutchison et al., 1999; Iwata et al., 2005; Vogt et al., 1996, 1993; Xiao et al., 2021; Xiao and Zhang, 2018). Interestingly, there are no nociceptive labelled lines that projects from L1 neurons to cingulate cortex. Since thalamic projections to cingulate are not focused on one specific region, there is no particular nociceptive region in cingulate. The subgenual part of ACC is more involved in autonomic control and emotion than the posterior cingulate (PCC). (Büchel et al., 2002) showed the dorsal posterior ACC were part of sensory discrimination activations rathen than pain processing. (Vogt et al., 1996) reported cerebral blood flow increases associated with application of noxious stimulation on human hands in posterior ACC and mid cingulate. This could be due to the dense projection of nociceptive inputs from MITN to the anterior mid cingulate than ACC and posterior mid cingulate as proposed by (Vogt, 2005). Cingulate lesions studies have found to impair pain and avoidance behavior (Donahue et al., 2001, 2001; Fuchs et al., 2014).

In summary, cingulate cortex and its subparts play a major in processing nociceptive stimuli and can guide autonomic responses arising from thermal comfort or discomfort.

4.2.5. Hypothalamus

Hypothalamus is known to be the thermo-regulative center of the brain. The preoptic anterior hypothalamus (POAH) has been linked to thermoregulatory behavior in numerous studies (Berk and Finkelstein, 1981; Blatteis and Banet, 1986; DiMicco and Zaretsky, 2007; Ishiwata et al., 2002; Rothhaas and Chung, 2021; Van Tienhoven et al., 1979; Wang et al., 2019a).

Interestingly, a recent study (Yahiro et al., 2017a) proposes another thermosensory pathway from dorsal horn to the lateral parabrachial nucleus (LPB) and then to the preoptic area (POA) of the hypothalamus. In this study, lesions in ventral posteromedial and ventral posterolateral thalamic nuclei (VPL/VPM) in the rats did not show impairment in their behavior. On the other hand, lesions in the LPB eliminated the heat/cold avoidance behavior(Yahiro et al., 2017a). It demonstrated that the heat/cold avoidance is not governed by the thalamocortical pathway and it is the lateral parabrachial nucleus (LPB) that mediates the thermosensory signals that drive behavioral thermoregulation.

Taken together, we can agree that there are integrated peripheral and central mechanisms that encode thermal sensations. Probing the interplay between the brain regions involved would strengthen our overall understanding of cortical and thalamic integration of thermal cues.

5. Principles of thermal coding

Even with big leaps in understanding thermosensation, we still lack a finite answers to several fundamental questions. In this section, we will discuss how temperature is encoded at the afferent level, spinal and supraspinal level. There are several concepts of thermal coding which can shed light on this matter.

5.1. Specificity and Pattern Theory

The integration of peripheral thermal information in the brain has given rise to two major theories: Specificity theory and Pattern theory. Specificity theory arises from the point of view that dedicated channels encode heat and cold (Ma, 2010). This means that the thermosensory information follows a specific and dedicated neural circuit or pathway from skin to brain (Ma, 2010). For instance, (Mishra and Hoon, 2010) concluded that by using RTX -a TrpV1 agonist that can destroy cells that express TRPV1, heat sensation is affected, but cold sensation remains intact. Their model claims that TRPV1 mediates heat processing and mechanical nociception. Similarly, (Knowlton et al., 2013) explains how TRPM8 is necessary to encode cool and noxious cold. By ablating TRPM8-expressing neurons in adult mice, (Knowlton et al., 2013) showed that the cold sensitivity is severely compromised but heat sensitivity is untouched. Also the polymodality of the afferent fibres mean that a particular stimuli can activate multiple labelled lines and that a labelled line might receive different somatosensory stimuli (Ma, 2010).

As opposed to the specificity theory, pattern theory claims that the final perception of sensory stimuli is the culmination of inputs from multiple sensory afferents and that their interplay or cross-talk at different stages of thermal transmission leads to the final perception. A popular example of pattern theory is when simultaneous heat and cold is misinterpreted as a burning pain (*Figure 18*).

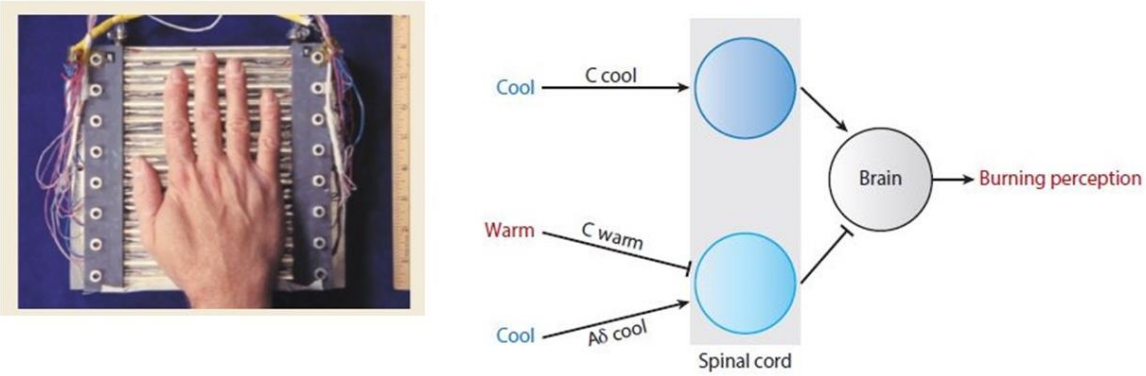

Figure 18: Pattern theory and thermal grill illusion. *When humas touched interlaced bars of innocuous warm (40°C) and cold (20°C) temperatures, they reported a burning hot pain. A cold labelled line or innocuous cold-sensitive Aδ-fibers are necessary for cold sensation. This activation normally masks the cold-sensitive C-fibers which is labeled line for heat or pain. The simultaneous activation of warm fibers on adjacent spots on skin will result in the blocking of cold-sensitive Aδ-fibers and thereby activating the cold-sensitive C-fibers (Craig, 2002; Xiao and Xu, 2021).*

This phenomenon was first discovered by Thunberg and Alrutz (Craig, 2002; Craig and Bushnell, 1994). When humas touched interlaced bars of innocuous warm (40°C) and cold (20°C) temperatures, they reported a burning hot pain, even though the temperatures were well within the non-noxious limit. A cold labelled line or innocuous cold-sensitive Aδ-fibers are necessary for cold sensation. This activation normally masks the cold-sensitive C-fibers which is labeled line for heat or pain. The simultaneous activation of warm fibers on adjacent spots on skin will result in the blocking of cold-sensitive Aδ-fibers and thereby activating the cold-sensitive C-fibers (*Figure 18*). This is a 'nociceptive' pain-labeled line and create paradoxical burning sensation (Ma, 2010).

5.2. Graded and Combinatory Coding

DRG neurons are the primary afferent neurons that encode thermal sensations at the peripheral level. In a recent study, (Wang et al., 2018), performed Ca2+imaging of DRG neurons and showed that neurons that encode heat and cold use very different strategies. Earlier, (Prescott et al., 2014; Prescott and Ratté, 2012) showed that it is possible to have one stimuli to activate a specific pathway and the sensation depends on the pathway activated. At the same time, each sensory stimuli could activate more than one neuron. The distinct combinations could form a particular sensation.

(Wang et al., 2018) explored how various somatosensory (mechanical and thermal (noxious and innocuous) inputs are encoded by population of mouse DRG neurons (*Figure 19* A) using Ca2+ imaging. Interestingly, there were two main findings: a) half of the neurons in the study were polymodal and b) different strategies were used to encode heat and cold.

Figure 19 B-D shows the polymodal nature of the sensory neurons. (Wang et al., 2018) looked into the overlap between mechano-sensitive and thermosensitive neurons. 21% of 522 neurons are sensitive to both [pinch and heating] and [pinch and 50°C] (*Figure 19* B,C marked in yellow). Majority of cooling sensitive neurons responded to pinching (*Figure 19* D marked in yellow). Depending on the size of the neurons, the medium and large neurons responded to mechanic stimuli whereas most of the small neurons exhibited polymodality and were seen to respond to both mechanic and thermal stimuli.

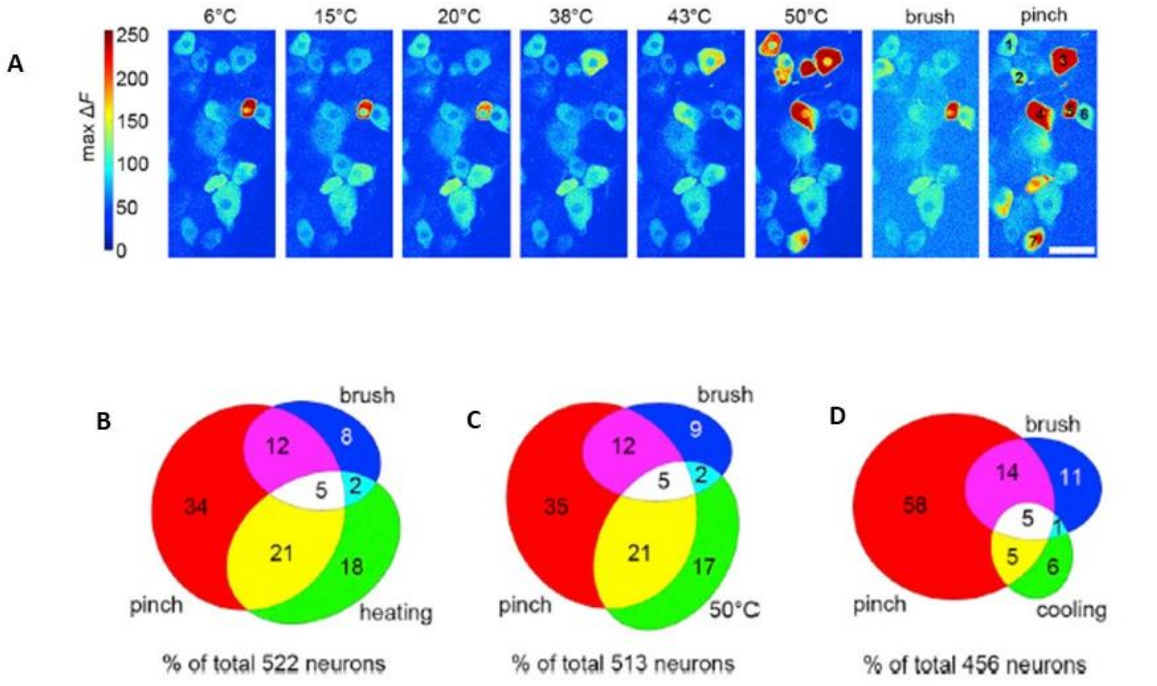

Figure 19: In-Vivo two photon imaging of DRG neurons. *A. Ca2+ imaging field showing how DRG neurons respond to noxious and innocuous thermal and mechanical stimuli. B-D shows the polymodal nature of the sensory neurons by looking at the overlap between mechano-sensitive and thermosensitive neurons using Euler diagram. 21% of 522 neurons are sensitive to both [pinch and heating] and [pinch and 50°C]. Majority of cooling sensitive neurons responded to pinching. Image adapted from (Wang et al., 2018).*

The second major finding was the encoding in the heating and cooling range. Among the thermoceptive neurons, (Wang et al., 2018) studied the responses for cool/cold (6°C, 15°C, or20°C) and warm/heat (38°C, 43°C, and 50°C). *Figure 20* A and B shows the overlap in the response for warm or heat and cool or cold. 8% of 548 neurons responded to all warm/when heat temperatures and 28% of 183 neurons responded to all cool/cold temperatures. Notably, only 3% is activated only by 38°C and 4% by 43°C and quite drastically, 63% of the neurons respond to 50°C (*Figure 20* A). At the same time, 16%, 17% and 20% of the cold-sensitive neurons respond to 20°C, 15°C and 6°C respectively (*Figure 20* B). This proves that as the temperature increases from 38 to 50°C, more number of neurons are activated, indicating a graded coding in the warm/heat range. On the contrary this is not true for the cool/cold temperatures and suggests combinatorial coding.

(Wang et al., 2018) studied the response of neurons that responded to all heating stimuli and cooling stimuli (white part in the Euler diagrams). The Ca2+ responses from different neurons prove that, as temperature goes up, more neurons are activated and each neuron's response gets stronger with the temperature (*Figure 20* C). Unlike the heat sensitive neurons, the Ca2+ traces does not support a graded coding strategy in the cold sensitive neurons. Decreasing temperature does not recruit more neurons or exhibit higher response, reaffirming a combinatory coding strategy in the cooling range (*Figure 20* D).

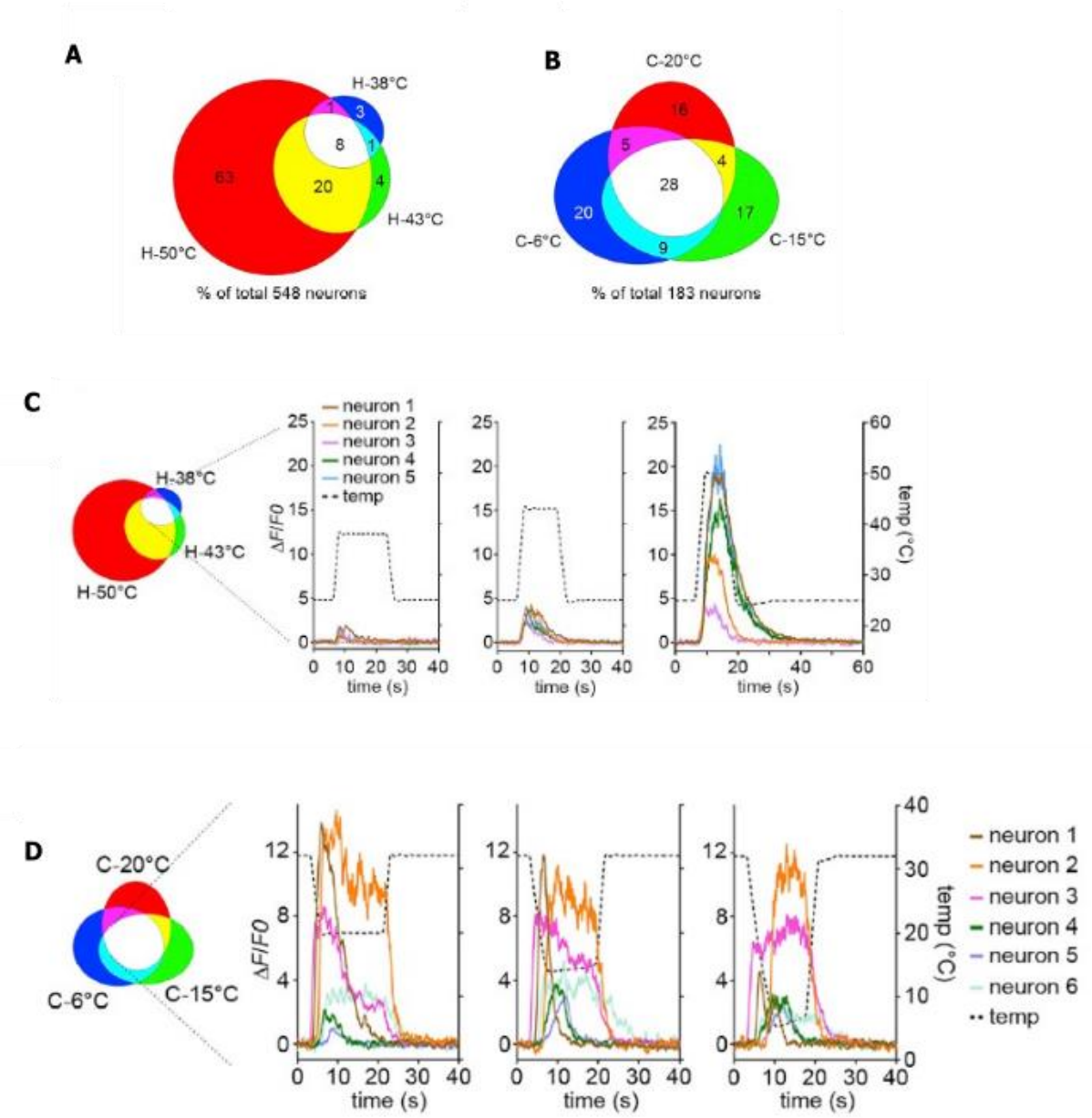

Figure 20: Overlapping thermoceptive neurons and their coding strategies. *A). 8% of 548 neurons responded to all warm/when heat temperatures. Notably, only 3% is activated only by 38°C and 4% by 43°C and quite drastically, 63% of the neurons respond to 50°C. B). In the cooling range, 28% of 183 neurons responded to all cool/cold temperatures. 16%, 17% and 20% of the cold-sensitive neurons respond to 20°C, 15°C and 6°C respectively. C). The Ca2+ responses from different neurons prove that, as temperature goes up, more neurons are activated and each neuron's response gets stronger with the temperature. D) Ca2+ traces suggests that decreasing temperature does not recruit more neurons or exhibit higher response, reaffirming a combinatory coding strategy in the cooling range. Image adapted from (Wang et al., 2018)*

5.3. Encoding of absolute temperature and temperature changes

(Ran et al., 2016) examined how thermal information is characterized in the spinal cord of mouse and how this characterization is different for heat and cold using two-photon calcium imaging of spinal cord. By stimulating hind paw of anesthetized mice using a stimulation chamber superfused with water at different (*Figure 21* A) temperatures (5-50°C)

A 10°C cooling from 32-22°C showed maximum response during the cooling process than the stable stage when the temperature is maintained (*Figure 21* B, left top and bottom). Interestingly, it was observed that cooling rate has no noticeable effect on the responsiveness of cold sensitive neurons (*Figure 21* C). Taken together, the results concluded that cold-sensitive neurons are more sensitive temperature changes (ΔT) and they quickly adapt to a constant cold temperature (Ran et al., 2016).

In the same study, (Ran et al., 2016) observed drastic differences in the encoding of heat in the spinal cord neurons. Heating the skin to higher temperature activated more neurons. When heated from 32°C to 45°C, heat-responsive neurons did not display adaptation and the response was constantly high during the stable temperature (*Figure 21* B, right top and bottom). Similarly to the cooling rate, heating rate did not affect the percentage or peak response amplitudes of neurons that respond to heat (*Figure 21* C). It was concluded that heat sensitive neurons code absolute temperature and therefore, higher the heat : stronger the neuronal response (Ran et al., 2016).

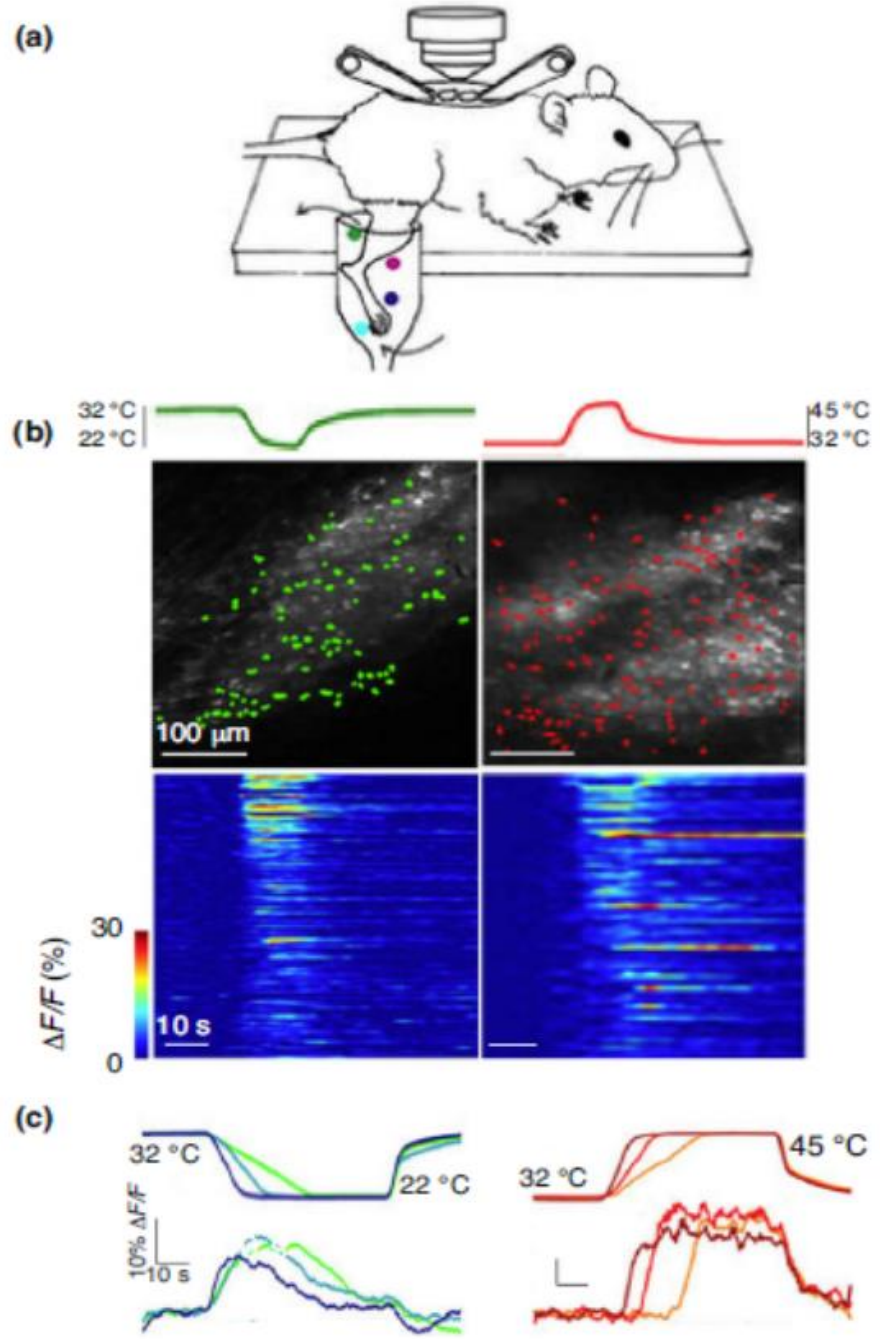

Figure 21: Spinal Encoding of Absolute Temperature and Temperature Changes. *A) Ca2+ imaging of LI/LII of spinal cord during stimulation of hind paw of anesthetized mice using a stimulation chamber superfused with water at different temperatures (5-50°C). B). Top: In-vivo images of responsive neurons (green and red), Bottom: Ca2+ response during cooling and heating. The cold-sensitive neurons are more sensitive temperature changes (ΔT) and they quickly adapt to a constant cold temperature. The heat sensitive neurons code absolute temperature and therefore, stronger the neuronal response when the temperature is high. C). Top: stimulation temperature during cooling and heating. Bottom: Ca2+ responses for different cooling and heating rates. Cooling and heating rate has no noticeable effect on the responsiveness of neurons (Ran et al., 2016). Image adapted from (Bokiniec et al., 2018).*

6. Functional Ultrasound Imaging

Ultrasound imaging is a widely used imaging modality, acclaimed for its portability, real-time imaging, sensitivity and cost effectiveness. Although it was not already widely used in clinical neuroimaging, it was applied in neonatal neuroimaging or a as a neurosurgical tool, where in both cases skull was not an obstacle. Transcranial Color Doppler Ultrasound (TSSD) used to measure blood flow velocities was another very popular early application of ultrasound (Aaslid et al., 1982). However, at that point, ultrasound lacked sensitivity factor and was used mainly to image large vessels. It was not until the introduction of ultrafast imaging in the last two decades (Tanter and Fink, 2014) that the ultrasound *neuroimaging* technique gained momentum. As of now, ultrafast Doppler imaging is one of the most sought after imaging technique in virtue of its sensitivity, spatial (~100 μm) and temporal resolution (tens of milliseconds) and portability (Deffieux et al., 2021).

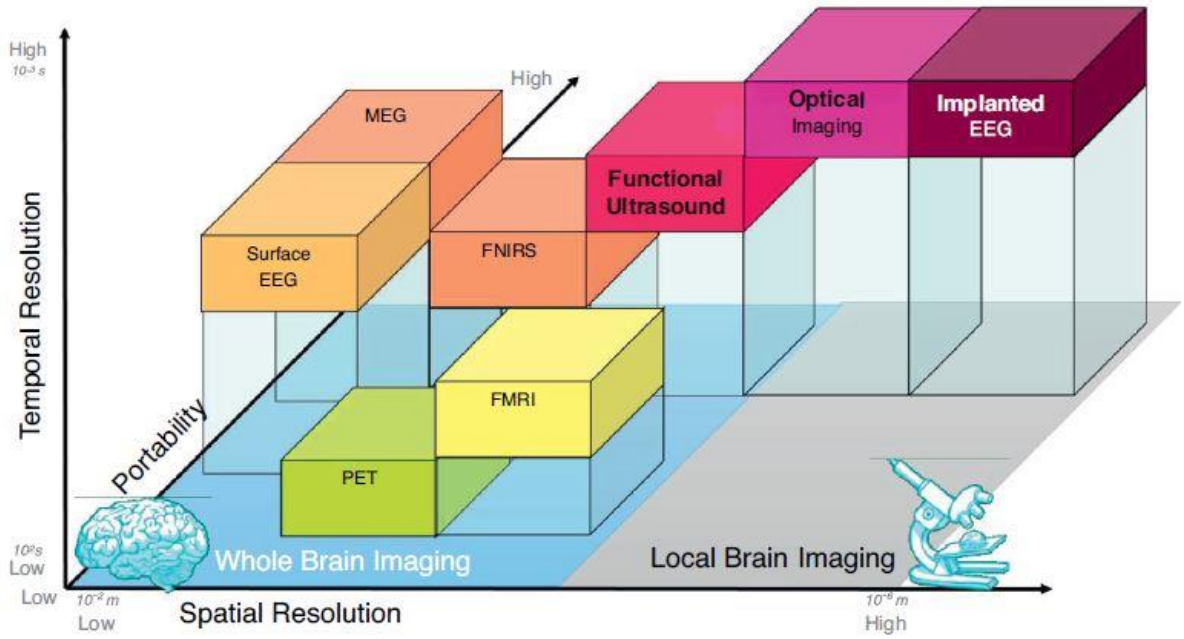

Figure 22: Comparison between different functional neuroimaging techniques *(Deffieux et al., 2018). FMRI has limitations in terms of temporal resolution, huge operational and maintenance cost and has limited portability. PET imaging uses radioactive tracers to image the uptake of glucose in the brain. It is a highly sensitive imaging technique but has poor spatial resolution has to be combined with MRI or CT. EEG and MEG measures brain's electrical and magnetic fields respectively and has higher temporal resolution. Localized brain imaging techniques or optical imaging has the highest spatial and temporal resolution so far, but mostly used in animal studies and are usually limited to the surface of the cortex (Pais-Roldán et al., 2021)*

In today's scientific world of functional neuroimaging, currently used non-invasive techniques include electroencephalography (EEG), magnetoencephalography (MEG), functional magnetic resonance imaging (fMRI), or positron emission tomography (PET) (Deffieux et al., 2018). However, all these techniques have their own limiting factors with respect to spatial and temporal resolution, possibility to image whole brain and specificity (*Figure 22*). Although fMRI is considered the benchmark of functional neuroimaging because of its clinical and preclinical use, whole brain imaging, non-invasiveness, it is burdened by huge operational and maintenance cost and has limited portability. PET imaging uses radioactive tracers to image the uptake of glucose in the brain. It is a highly sensitive imaging technique but has poor spatial resolution has to be combined with MRI or CT to get the desired results. EEG and MEG measures brain's electrical and magnetic fields respectively and has higher temporal resolution. Localized brain imaging techniques or optical imaging has the highest spatial and temporal resolution so far. But its use is mostly confined to animal studies and are usually limited to the surface of the cortex (Pais-Roldán et al., 2021) (*Figure 22*).

Functional Ultrasound (fUS), on the other hand, has high spatial and temporal resolution and sensitivity compared to the widely used fMRI and PET (Boido et al., 2019; Macé et al., 2011; Tanter and Fink, 2014). It can definitely bridge the gap between fMRI and optical imaging techniques. Unlike the other established techniques, fUS imaging offers a wide range of possibilities in pre-clinical and clinical research. It has a large field of view and can be used alongside behavioral studies and super-resolution ultrasound localization microscopy. Although it is primarily used to image animal models in awake and anesthetized states and to study brain connectomics, fUS has been proven to be useful during intra-operative procedures in awake patients (Imbault et al., 2017; Soloukey et al., 2020) and also in neonatal neuroimaging (Baranger et al., 2021; Demene et al., 2017) (*Figure 23*).

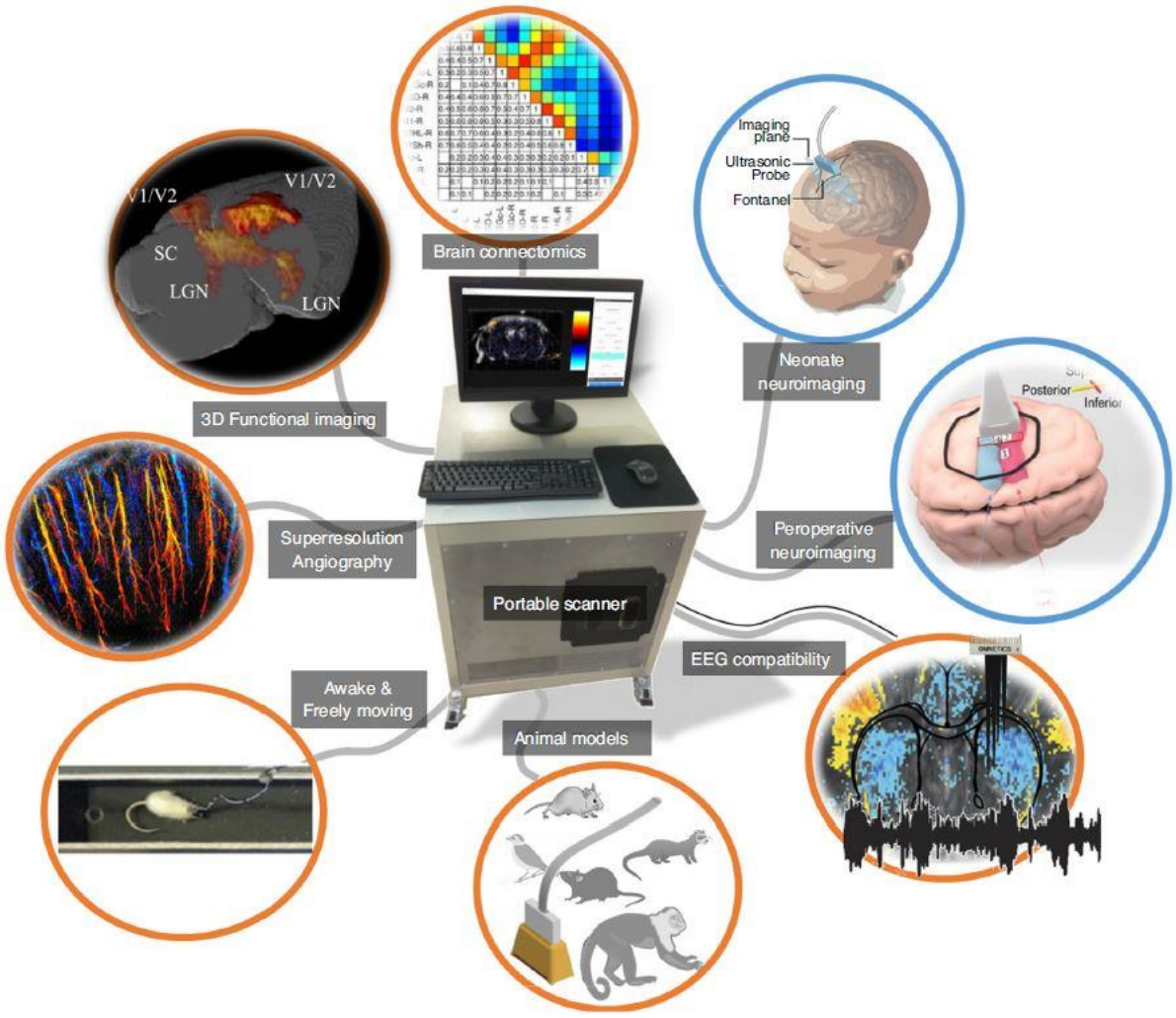

Figure 23: Wide range of possibilities in pre-clinical and clinical research offered by fUS. *It can be used alongside behavioral studies and super-resolution ultrasound localization microscopy. Although it is primarily used to image animal models in awake and anesthetized states and to study brain connectomics, fUS has been proven to be useful during intra-operative procedures in awake patients (Deffieux et al., 2018).*

6.1. Physics behind fUS

The inception of ultrasound has played an important role in the medical diagnostics history. In the 1970s, it was introduced as a way to image the abdomen and pelvis. Fast forward to 2021, it has major applications in obstetrics, gynecology, cardiology, abdominal imaging and even neuroimaging. Ultrasound imaging stands out from other imaging techniques by its non-ionizing nature, portability and real-time imaging capability.

In terms of acoustic physics, ultrasound refers to high frequency sound waves that are inaudible to the human acoustic range i.e., greater than 20 kHz. But the frequency used in medical imaging is much greater and usually between typically 2 to 10 megahertz (MHz) (Powles et al., 2018). The body part to be imaged receives pulsed ultrasound waves which in turn give rise to ultrasonic echoes that are backscattered by tissues or fluids (Aldrich, 2007; Campbell, 2013; Jensen, 2007; Macé et al., 2011). Traditional ultrasound uses focused beam to image line by line. In other words, one focused beam permits acquisition of one image line. This means, generally, in order to acquire a full image we may need a few imaging lines in the order of 64-512(*Figure 24*) (Bercoff, 2011).

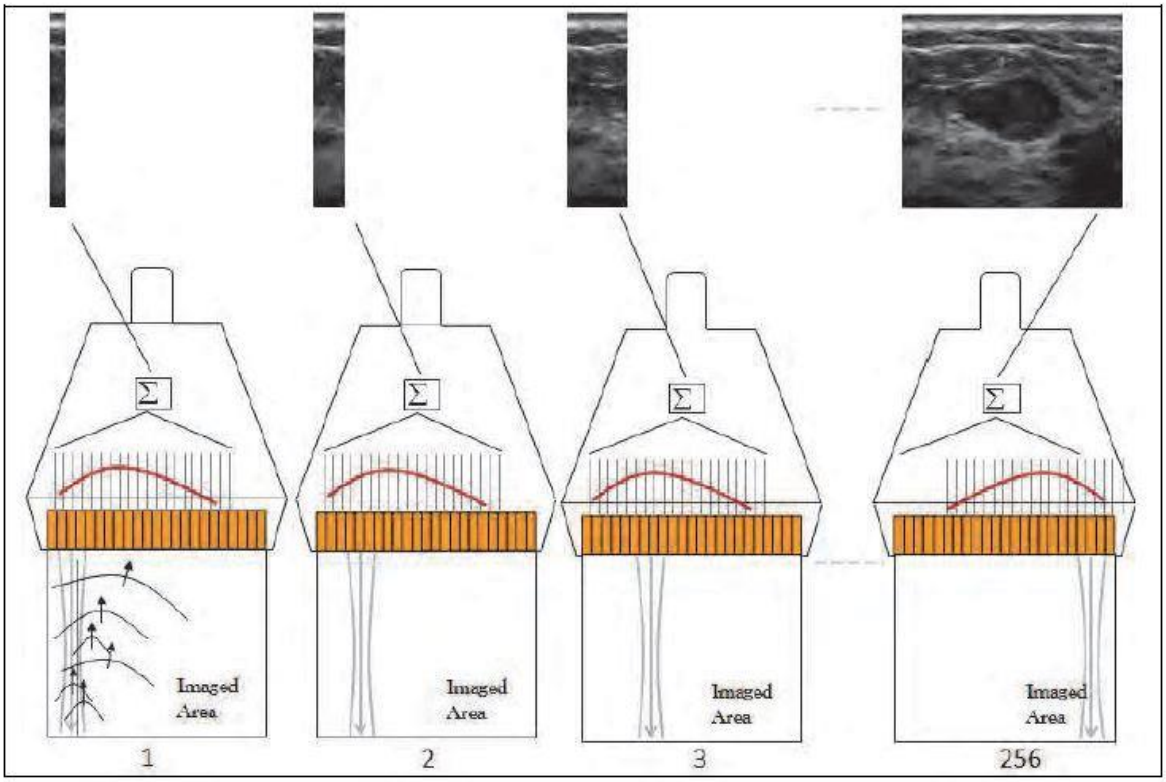

Figure 24: Conventional US imaging. *Traditional ultrasound uses focused beam to image line by line. In other words, one focused beam permits acquisition of one image line. This means, generally, in order to acquire a full image we may need a few imaging lines in the order of 64-512. (Bercoff, 2011)*

For instance, following the conventional way, to obtain an image at 5cm depth and 256 lines width, the frame rate would be 60Hz. Scanning line by line can be slow to acquire large images at kilohertz frame rate. Imaging blood dynamics using this technique demands to split the large imaging field to smaller parts that are to be

imaged one after the other. This limits the sensitivity of the technique as it has low sampling rate (Mace et al., 2013; Macé et al., 2011).

fUS was envisioned as a better technique to measure changes in blood volume in brain at a higher spatial-temporal resolution than the conventional technique (Macé et al., 2011; Tanter and Fink, 2014). It employs plane wave transmission as opposed to the focused beam to obtain a large field of view. The single plane wave can acquire larger number of samples per pixel than a focused beam, which improves the sensitivity. Furthermore, by using multiple tilted planar waves (Montaldo et al., 2009; Tanter et al., 2002; Tiran et al., 2015), the resulting images are summed to produce the final coherently compounded ultrasound image. This technique not only maintained the high frame rate (thousands of frames per second), but improved the quality of the image in terms of resolution and noise (Bercoff et al., 2011).

To elucidate the fundamental principles of fUS imaging see *Figure 25*. (Macé et al., 2011) illustrates the emission of tilted planar ultrasonic waves (17 waves tilted at angles from -8° to 8° by steps of 1°) which forms 17 images with a field of view 2cmx2cm. These 17 images are summed together to produce a compounded image obtained in 1ms. This process results in 200 compounded images in 200ms. The hemodynamic signal can be extracted from the temporal changes in the amplitude of backscattered ultrasound echoes for each pixel by implementing a high pass filter. From the frequency spectrum of the blood signal, axial blood velocity and intensity of power Doppler can be determined (Mace et al., 2013) and therefore we can obtain an axial velocity image or a power Doppler image (*Figure 25*). The cut-off frequency to avoid tissue motion, allows the detection of blood signals with typical axial velocity >4mm/s. The power Doppler values are directly proportional to cerebral blood volume and it is well suited for imaging vascular hemodynamics. Using the phenomenon of neurovascular coupling (changes the local cerebral blood volume due to transitory neural activity), fUS can be an indicator for brain activity patterns.

(Mace et al., 2013) explained how the high pass filter can remove echoes from tissues but it might lose the blood signal from capillaries where axial blood velocity is low (2-4mm/s) depending on the cut-off frequency. The much advanced spatiotemporal clutter filtering (Demene et al., 2015) was introduced to separate

tissue and blood signals in a more efficient manner. Moving blood scatterers have low covariance when compared to the static or slowly moving tissue scatterers with high covariance. This method was successful in removing clutter signals by using Singular Value Decomposition (SVD) and blood velocity as low as 0.5 mm/s could be now detected and included in the filtered signal.

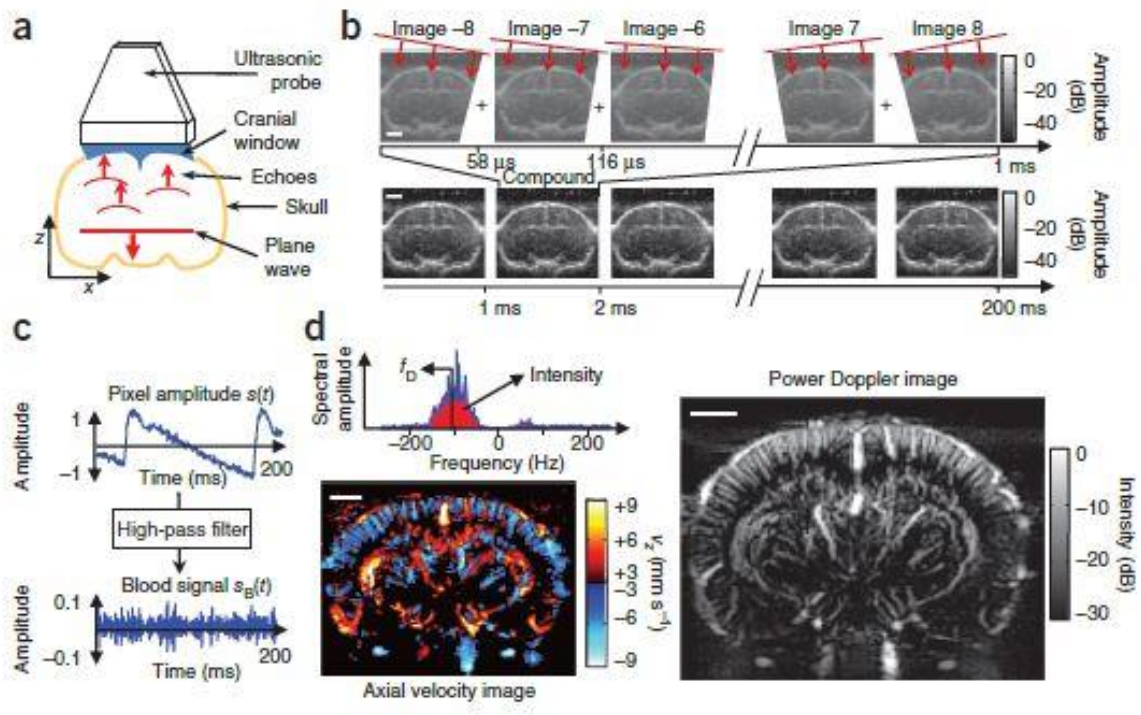

Figure 25: Fundamental principles of fUS Imaging. *a-b) Emission of tilted planar ultrasonic waves (17 waves tilted at angles from -8° to 8° by steps of 1°) which forms 17 images with a field of view 2cmx2cm, summed together to produce a compounded image obtained in 1ms. This process results in 200 compounded images in 200ms. c) The hemodynamic signal sB(t) can be extracted from the temporal changes in the amplitude of backscattered ultrasound echoes s(t) for each pixel by implementing a high pass filter. d) From the frequency spectrum of the blood signal, axial blood velocity and intensity of power Doppler can be determined and an axial velocity image or a power Doppler image can be obtained. The concept of fUS is based on power doppler images (Macé et al., 2011).*

6.2. Functional Neuroimaging

The high spatial resolution offered by fUS imaging makes it a perfect candidate for functional neuroimaging; also referred to as task based neuroimaging. In one of first studies, (Macé et al., 2011), fUS was used to image brain activation evoked by whisker stimulation. Using neurovascular coupling, fUS detects brain areas that are activated based on localized increase in CBV. (Macé et al., 2011) captured activation of the barrel cortex during whisker stimulation in anesthetized rats (*Figure 26*).

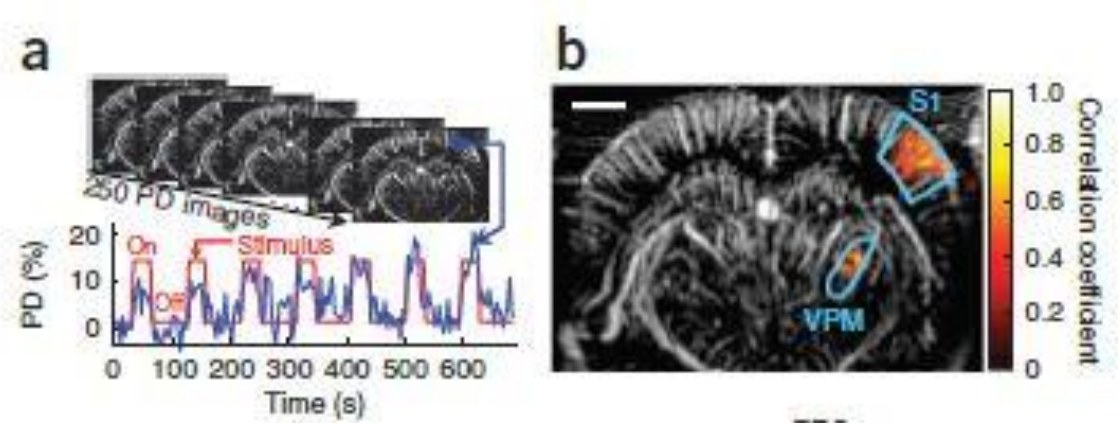

Figure 26 : Activation of S1BF in response to whisker stimulation. *a) The whisker stimulation was performed in a total of 10 trials (7 trials shown in figure), each trial consisted of 32s ON and 64sec OFF. b) Activation of right S1BF by stimulating left whiskers. S1BF: primary somatosensory barrel cortex; VPM: ventral posterior medial nucleus (Macé et al., 2011).*

Left whiskers were stimulated 10 times (only 7 shown in *Figure 26*) and each stimulation consisted of a 32s ON and 64s OFF time. Power Doppler is represented relative to the baseline. By computing the correlation co-efficient between the power Doppler and stimulus pattern, the activation map was obtained (*Figure 26* b), indicating activation in S1BF (primary somatosensory barrel cortex) and VPM, ventral posterior medial nucleus of the thalamus. A strong increase in cerebral blood volume (10-20%) can be observed in the S1BF during the stimuli (ON). The activated pixels correspond to a correlation coefficient value (Macé et al., 2011).

Later on fUS, was shown to detect activation corresponding to visual stimulation (Gesnik et al., 2017), electrical stimulation (Osmanski et al., 2014) and auditory stimulation (Bimbard et al., 2018).

Even though a craniotomy was performed for acute imaging of the rat brain in (Macé et al., 2011), a thinned skull method was later introduced in rats (Urban et

al., 2014) which allowed for chronic functional neuroimaging and the acquisition of high resolution doppler images. In (Sieu et al., 2015), fUS went a step further, by combining electroencephalography (EEG) recordings of neuronal activity along with the imaging in awake and mobile rats. After excising the skull bone in the desired window, electrodes were implanted and a biopolymer polymethyl pentene (PMP) film was sealed in place of the removed skull. The ultrasound probe used in (Sieu et al., 2015) was miniaturized to be lightweight and the cable was made more flexible for ease of movement, which did not interfere with its sensitivity. These improvements enables researchers to perform fUS imaging in freely moving animals for behavioral studies (Bergel et al., 2020). Moving forward, fUS was also combined with optogenetics and two-photon microscopic imaging in (Rungta et al., 2017) in anesthetized mice to study photo-activation and its effect on cerebral blood flow.

Taken together, skull bone poses as an obstacle in fUS imaging. Direct imaging through skull of rat's brain is not possible as it induces attenuation and irregularities of the ultrasonic waves. Other than the very invasive craniotomy procedure, thinned skull could be a feasible choice for chronic imaging, but the image quality deteriorates over time due to the natural revival of bone. In (Errico et al., 2016), a non-invasive fUS imaging approach by using a contrast agent was proposed. This method not only allowed imaging through the skull in rats, but also facilitates chronic and longitudinal studies.

6.3. Awake fUS imaging

Imaging studies make use of anesthetics to prevent animal movements and motion artefacts. Conducting behavioral or cognitive studies or perceptual tasks is not possible under anesthesia and it can interfere with the metabolic activity of the central nervous system and affect cerebral blood flow (Lahti et al., 1999). Due to these reasons, there was a need to develop a transcranial and minimally invasive technique to image awake and freely moving mice.

The first proof of concept of transcranial fUS imaging in awake and freely moving mice were published in (Tiran et al., 2017). It was accomplished using an ultralight ultrasound probe (*Figure 27*). Compared to the probe used awake and mobile rats

(Sieu et al., 2015), the thickness and weight was reduced and the cable was made even more flexible.

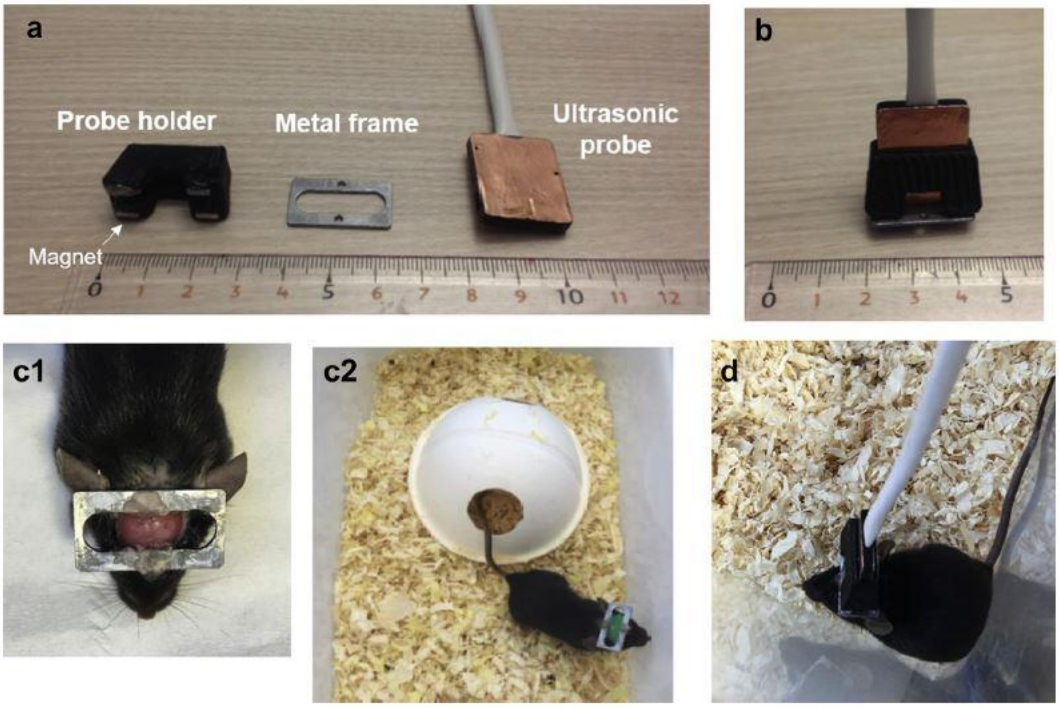

Figure 27: Experimental setup of transcranial imaging in freely moving mice *(Tiran et al., 2017). Setup consists of a metal frame, probe holder and ultralight probe. Metal frame is surgically implanted to the skull using dental cement and screws. Layer of Kwik-cast protects the skull. Four small magnets are attached on the probe holder for easy magnetic clip-on attachment of the probe holder to the metal frame. (Tiran et al., 2017).*

Figure 27 illustrates the experimental setup used in the transcranial fUS imaging. The metal frame (12x23 mm) is attached to the mouse skull using dental cement and screws under anesthesia. Four small magnets are attached on the probe holder for easy magnetic clip-on attachment of the probe holder to the metal frame. The exposed skull is always protected by a Kwik-cast layer (in green color), which is removed under light isoflurane anesthesia before imaging and then re-applied afterwards.

(Tiran et al., 2017) also investigated task evoked activation of brain regions using transcranial awake fUS imaging. It was accomplished by placing the mouse in an empty cage and the whiskers were manually stimulated using a cotton swab. The changes in the cerebral blood volume was correlated to the stimulus pattern and resulted in the activation of S1BF (*Figure 28*).

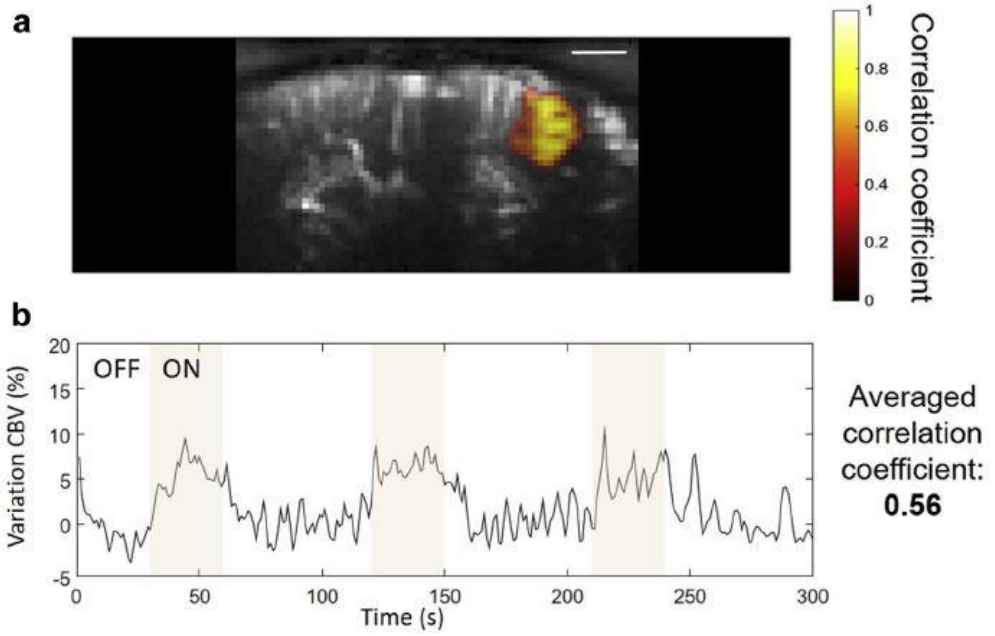

Figure 28: Transcranial fUS imaging of task evoked brain activity in freely moving mice. *Changes in cerebral blood flow in the S1 barrel cortex in response to whisker stimulation. The increase in CBV corresponds to the stimulus pattern (Tiran et al., 2017).*

This was an important milestone in the advancement of non-invasive fUS imaging technique and was reliable in reporting hemodynamic variations through the skull without the requirement of thinning or contrast agents. It was further adopted in pharmacological studies in (Rabut et al., 2020). This same technique has been adapted to be used in Study 2 of this thesis.

Recently (Macé et al., 2018), put forward a whole brain fUS imaging approach using the head fixed approach in awake mice, making it another choice to conduct awake behavioral studies (*Figure 29*).

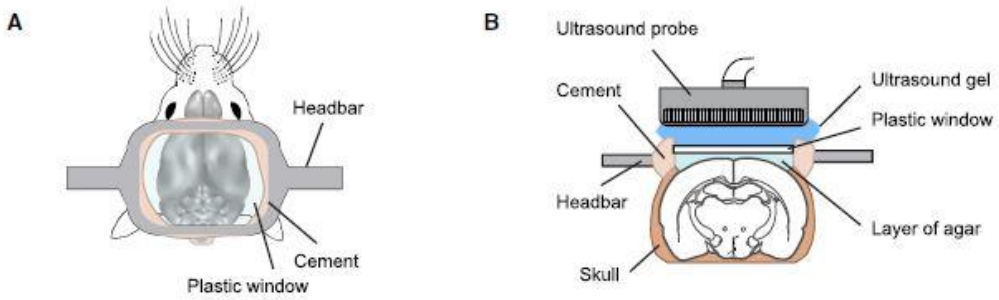

Figure 29: Whole brain fUS imaging of head fixed awake mouse. *A) Chronic craniotomy window. Dental cement secures the head bar on to the skull and plastic window transparent to US. B) Positioning of the US probe with respect to the window. (Macé et al., 2018).*

7. Functional Connectivity

7.1. Basis of functional connectivity

Human brain comprises of complex structural and functional connections between regions and therefore mapping human brain function or studying brain connectomics is essential to understand the nuances of the underlying mechanics that allow us to think, feel and behave. Functional Connectivity (FC) fundamentally refers to the functional relationship between anatomically or spatially separate brain regions.

Although the existence of intrinsic brain activity can be traced back to when German psychiatrist, Hans Berger introduced electroencephalography in 1929 (Gloor, 1969; İnce et al., 2021), the functional imagining perspective was only discovered in 1995. The existence of coherent activity between distant brain regions was first reported in (Biswal et al., 1995) using echo-planar MRI. The "noise" they observed in the spontaneous fMRI blood oxygen level dependent (BOLD) signal was coherent with the sensorimotor regions. Interestingly, the high correlation of the low frequency (<0.1 Hz) fluctuations in the resting brain with the motor cortex, could be considered as the first proof of resting-state (rs) functional connectivity (FC) in brain. Numerous research groups replicated and probed into rs FC between brain regions since then (Biswal et al., 2010, 1997; Cordes et al., 2000; Damoiseaux et al., 2006; De Luca et al., 2005; Fox et al., 2005; Fox and Raichle, 2007; Grandjean et al., 2020; Greicius et al., 2003; Margulies et al., 2007; Smith et al., 2009).

In simple terms, functional connectivity between brain regions is thought to be established when temporal signals from anatomically separate brain regions are correlated. It could be defined as a measure of similarity between the temporal activity in different brain regions (*Figure 30*). These patterns may occur at resting state and vary among tasks or during different pathophysiological conditions.

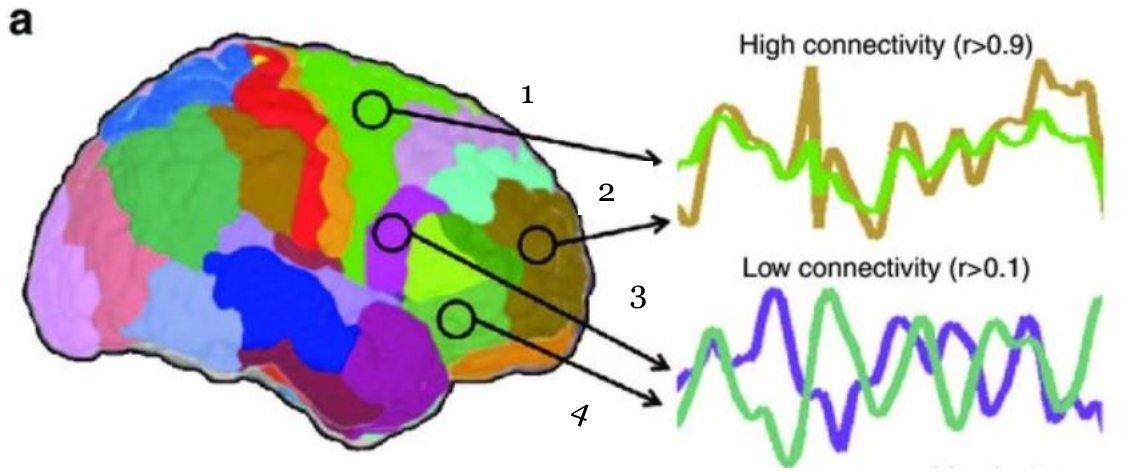

Figure 30: A representation of FC. Consider regions 1, 2 3, and 4. *The temporal signals from 1 and 2 regions are coherent and indicates high functional connectivity (correlation coefficient >0.9) whereas the temporal signals from 3 and 4 are incoherent and therefore shows low connectivity (correlation coefficient >0.9) (Scheinost et al., 2017).*

Later on the Marcus E. Raichle, American neurologist, observed that the brain is constantly active even when the subject is not engaged in a task. He put forward the term "default mode network" (DMN) (Raichle, 2015, 2011, 2010; Raichle et al., 2001; Raichle and Snyder, 2007) referring to the brain's networks at rest. The idea that, DMN activity increases when the subject is in resting state or non-task state, became an important branch of neuroscience as it varies in health and disease (Baliki et al., 2008; Bathelt and Geurts, 2021; Buckner et al., 2008a; Dennis and Thompson, 2014a; Garrity et al., 2007; Gonen et al., 2020; Greicius et al., 2003, 2004; Jenkins, 2019; Li et al., 2021; Mohan et al., n.d.; Parsons et al., 2020; Satpute and Lindquist, 2019; Scheinost et al., 2017; Zhao et al., 2007).

7.2. Stationary and Dynamic FC Approaches

7.2.1. Stationary FC

Classic resting state functional connectivity studies use averaged temporal resting-state signals from regions of interest. They are usually assessed using the following techniques:

a. Seed -Based connectivity analysis

A predefined seed region is defined by the user and the average time course of the signal is extracted. This signal is then correlated to the average temporal signals from other regions of interest. It summarizes how coherent the ROIs are with the seed. An example of seed-based correlation analysis is shown in *Figure 31* (Rahal et al., 2020)

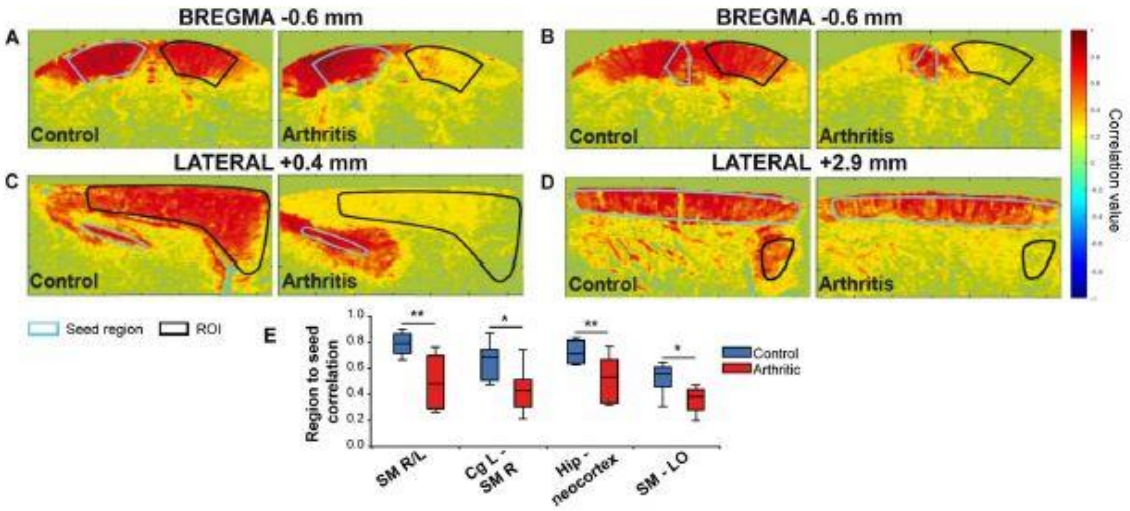

Figure 31: Seed based correlation matrix analysis. *A-D) shows a seed region (cyan) and region of interest in black. Pearson correlation was then computed in the ROI (delineated in black). E) Boxplots of the correlation coefficients between (SM = Somato Motor cortex, Cg = Cingulate cortex, Hipp = Hippocampus, LO = Lateral orbital cortex) (Rahal et al., 2020).*

b. Correlation Matrix analysis

A more generalized version of seed-based connectivity analysis, correlation matrix in which each ROI (defined based on an atlas), is correlated to every other ROI. For instance, if we have ROIs 1-4, average temporal signal of ROI 1 is compared to that of ROI 2, 3 and 4 and so on. It is then possible to evaluate whether two regions are functionally connected and how strongly so by computing a Pearson correlation co-

efficient matrix. *Figure 32* shows the correlation matrix analysis of FC (Rahal et al., 2020).

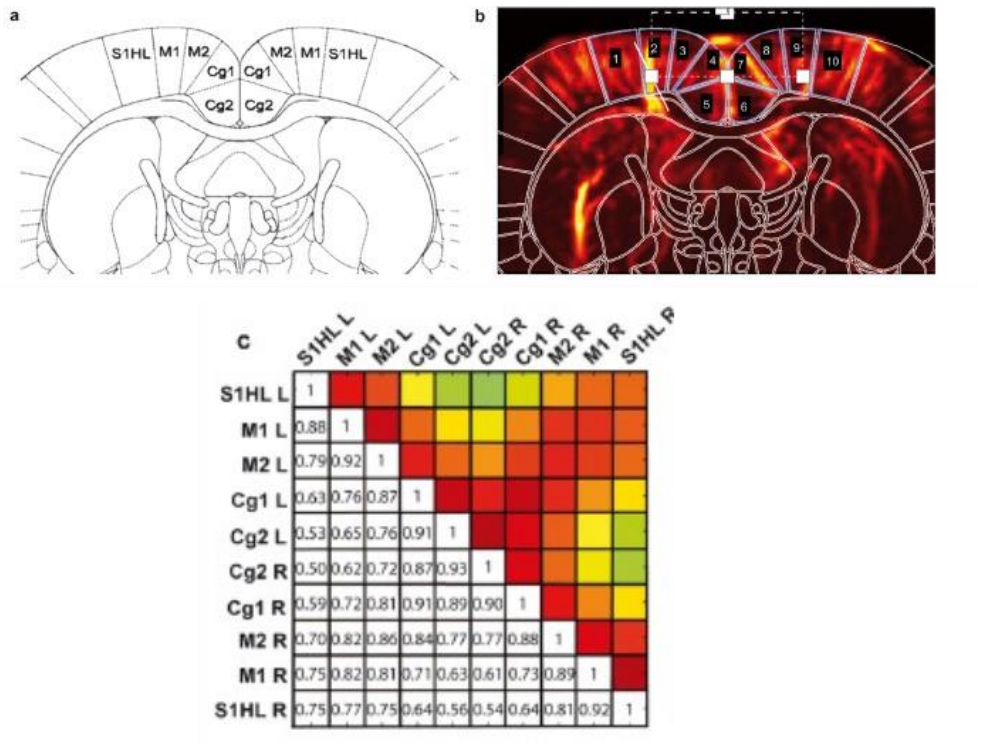

Figure 32: Correlation matrix analysis of the FC. *A) Imaging plane from rat atlas. (b) Doppler image of the plane indicating the region of interests (1-10). (c) Averaged Pearson correlation matrix showing the correlation coefficient of one ROI with all the other ROIs resulting in a 10x10 matrix. S1HL (Primary sensory cortex, Hind Limb part), M1 (Primary motor cortex), M2 (Secondary motor cortex), Cg1 (Primary cingulate cortex),Cg2 (Secondary cingulate cortex) (Rahal et al., 2020)*

c. <u>Independent Components Analysis (ICA)</u>

   ICA is a data-driven modelling technique that decomposes the resulting imaging data into different spatial nodes or networks which can be compared to study resting state-FC.

Taken together, stationary FC is definitely indicative of the overall strength of connections between brain regions but the properties of static connectivity matrices may vary among subjects and physiological conditions. Moreover, the dynamic aspects of intrinsic brain activity cannot be overlooked.

7.2.2. Dynamic FC

While stationary FC studies assume temporal stationarity and has been widely used, recent findings suggested that resting-state activity is more dynamic and can change in a matter of seconds. Later on dynamic functional connectivity (dFC) expanded as a separate body of research (See Reviews (Cohen, 2018; Hutchison et al., 2013; Park and Friston, 2013; Preti et al., 2017)). dFC is found to be altered in autism (Li et al., 2021), schizophrenia (Zou and Yang, 2019), Alzheimer's disease (Gu et al., 2020), aging (Tian et al., 2018) and in task related approaches (Gonzalez-Castillo and Bandettini, 2018; Kieliba et al., 2019). Although the brain is structurally defined like any other organ in our body, its functional versatility is perplexing and challenging at the same time.

To understand the dynamic characteristics of brain networks, an unsupervised data grouping technique, such as k-means clustering can be used. When we set k=3, the input data is grouped into 3 clusters. *Figure 33* is a schematic showing unclustered and clustered data using k-means. First of all, 3 centroids are randomly assigned. Distance of each input data point to the clusters is calculated and the one with minimal distance between them are grouped together. In the next step, 3 new centroids (mean of each group) are calculated. This iterative process is continued until it converges and data are grouped into 3 and the data points are distributed around its centroid.

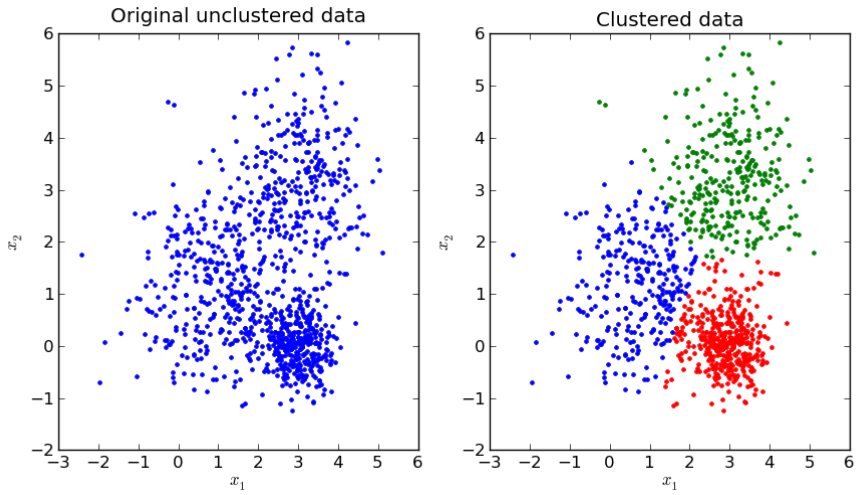

Figure 33: Schematic of K-means Clustering technique for K=3 clusters. *The input data (blue) is grouped into 3 (green, blue and red). First of all, 3 centroids are randomly assigned. Distance of each input data point to the clusters is calculated and the one with minimal distance between them are grouped together. In the next step, 3 new centroids (mean of each group) are calculated. This iterative process is continued until it converges and data are grouped into 3 and the data points are distributed around it's centroid (Viswarupan, 2017).*

fMRI studies in monkeys (Barttfeld et al., 2015) and humans (Demertzi et al., 2019a) have revealed brain state patterns that can be indicative of consciousness, using clustering techniques. An example of using clustering of brain states is shown in (*Figure 34*) from (Barttfeld et al., 2015). They observed the dynamics of rs networks to study its vigilance level. The clustering revealed 7 brain state matrices, sorted by their similarity to the structural matrix. States 1-4 have strong coupling with the presence of correlations (red) and anticorrelations (blue) which can be a characteristic of a conscious brain or wakefulness. On the other hand, weakly coupled, low correlation states are similar to an unconscious brain state pattern commonly seen in sedative states (Barttfeld et al., 2015).

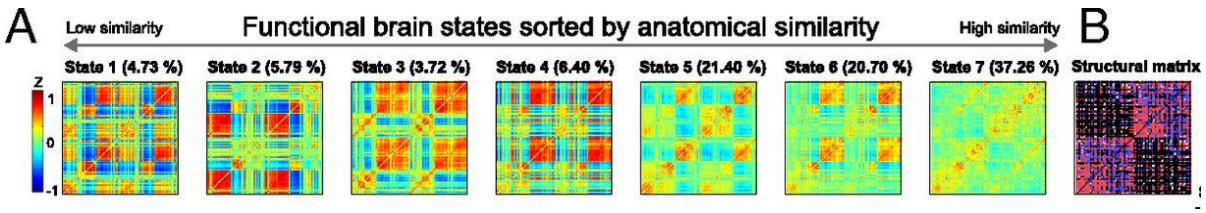

Figure 34: Brain states clustering of resting state networks. *(A) Seven brain states, obtained by unsupervised clustering, sorted according to their similarity to the structural connectivity matrix. (B) Structural matrix derived from the CoCoMac atlas of anatomical macaque.(Barttfeld et al., 2015). The states with positive and negative correlations (1-5) are indicative of conscious state. The weakly coupled low correlation state (6-7), is a characteristic of unconsciousness. (Barttfeld et al., 2015).*

7.3. Study of FC using fUS imaging

Compared to popular techniques such as fMRI and PET, fUS offers a larger field of view of the brain and has better spatial and temporal characteristics. It can also be done in awake or head-fixed rodents which facilitates behavioral studies coupled with fUS imaging. In recent developments, it has been shown numerous times that fUS is capable of identifying intrinsic activity and that it is a powerful tool to study brain connectomics.

The first functional connectivity study using fUS was done in (Osmanski et al., 2014) in anesthetized rats through thinned skull. It was able to identify spontaneous low frequency fluctuations in cerebral blood flow which were highly correlated in the sensorimotor networks (*Figure 35*).

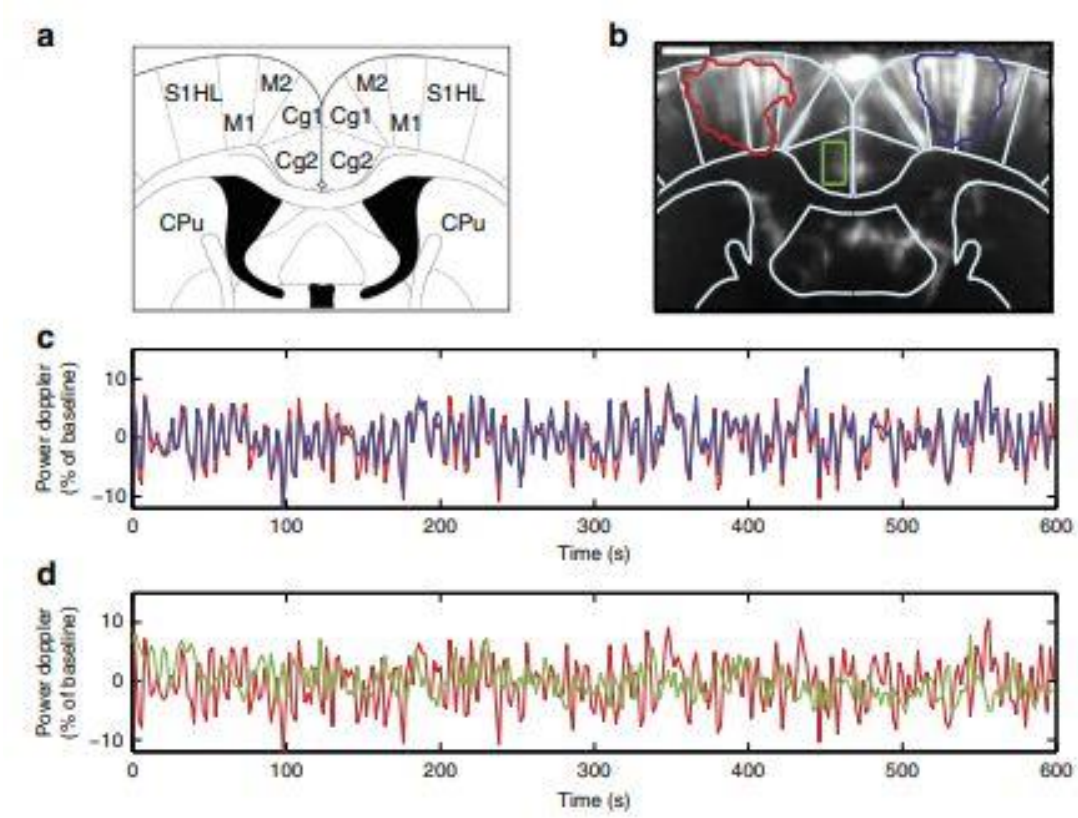

Figure 35: fUS imaging of FC. *a-b) Atlas of imaging plane and regions blue and red denoting S1HL+M1 and green denoting ipsilateral secondary cingular cortex. c) Power Doppler signal from S1HL and M1 on contralateral sides (red and blue outline) are highly correlated, indicative of functional connectivity. d) It also shows the weak correlation of S1HL+M1 with the secondary cingulate cortex Cg2 on the ipsilateral side (red and green) (Osmanski et al., 2014).*

To further advance the technique, functional connectivity studies in awake rodents has been done using fUS in pharmacological studies. Using the transcranial imaging approach in mice, first introduced in (Tiran et al., 2017), time and dose dependent changes in functional connectivity were studied after the injection of a psychoactive drug called scopolamine in (Rabut et al., 2020). The modulations in functional connectivity due to the drug was identified and thus can be a promising way to study the effects of drugs in brain connectivity. Similarly, (Rahal et al., 2020) shows that arthritic pain alters FC in anesthetized rats in the somato-motor network. Nevertheless, using fUS to study connectomics could enhance our understanding of pathologies in preclinical models.

Recently, (Ferrier et al., 2020) developed a protocol for activation and functional connectivity studies by introducing a light sedation protocol to avoid locomotion induced artefacts in FC. *Figure 36* shows discrete FC patterns in awake and lightly

sedated mice. They also reported the task related default mode network deactivation in mouse brain.

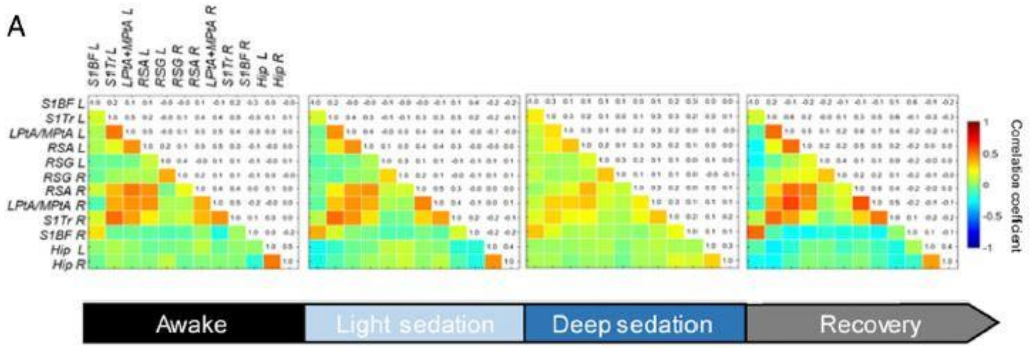

Figure 36: Correlation Matrices at different level of sedation. *Light sedation protocol to avoid movement induced artefacts in FC. Low-dose medetomidine sedation fully preserving the FC patterns observed in awake resting mice (Ferrier et al., 2020).*

The transient properties of functional connectivity was first studied using fUS in (Rahal et al., 2020). Dynamical FC analysis was performed using unsupervised k-means clustering algorithm. Seven brain states were extracted and their occurrence probability in healthy and arthritic rats were calculated (*Figure 37*). It was found that three out of seven states were more prominent in arthritic rats. Notable difference was that (Rahal et al., 2020) used a phase -difference matric rather than the usual correlation matric. The result of dynamic connectivity analysis is very promising even in anesthetized conditions.

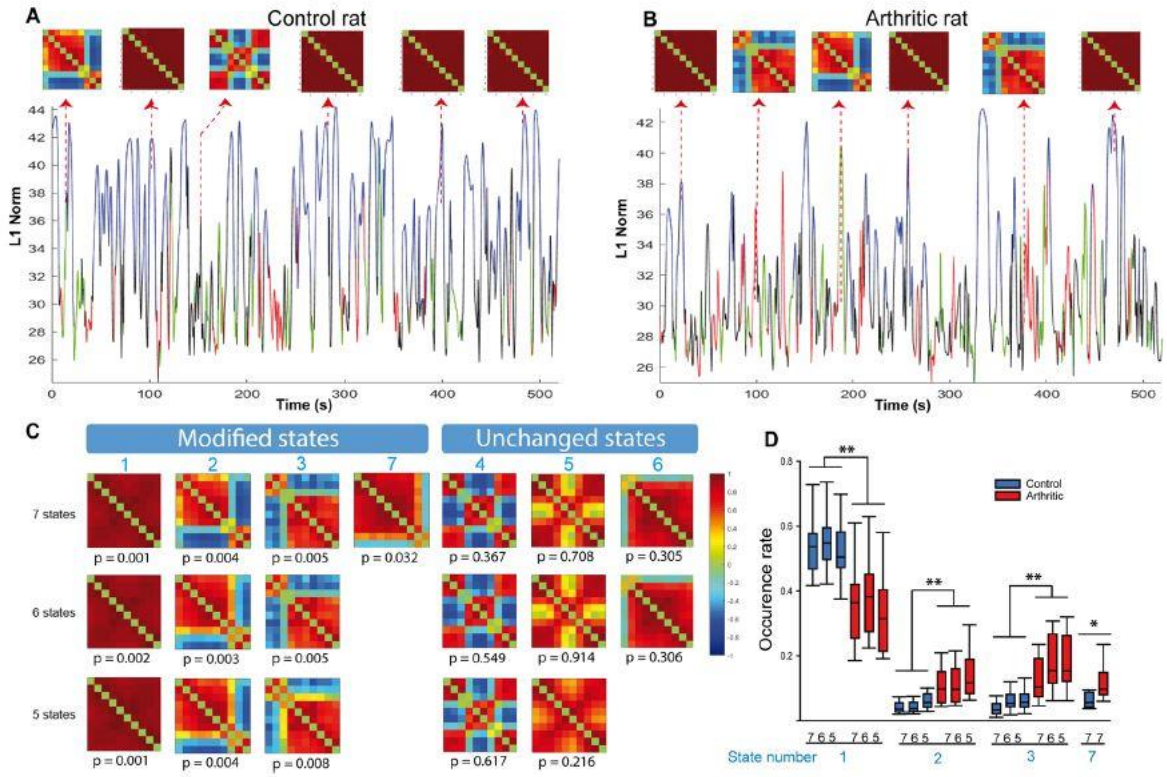

Figure 37: Dynamic FC Analysis in control and arthritic by fUS imaging in anesthetized rats. *A-B) Time course of the L1 norm of the phase-locked matrix of a control and an arthritic rat, indicating brain state patterns at particular points. C) Decomposition into brain states 5, 6 and 7 obtained by unsupervised k-means clustering of the phase matrices., show significant alterations in 4 states (1,2,3,7) D) Box plots presenting the occurrence rate of each of the four different states for control and arthritic groups (Rahal et al., 2020).*

Brain dynamics were linked to consciousness signatures using fMRI (Demertzi et al., 2019a). Very recently, (Baranger et al., 2021) used fUS imaging to study dynamic resting state connectivity patterns in sleeping preterm neonates and term neonates (*Figure 38*). By monitoring intrinsic functional connectivity using fUS imaging, the goal was to identify markers of cerebral activity to compare term and preterm neonates.

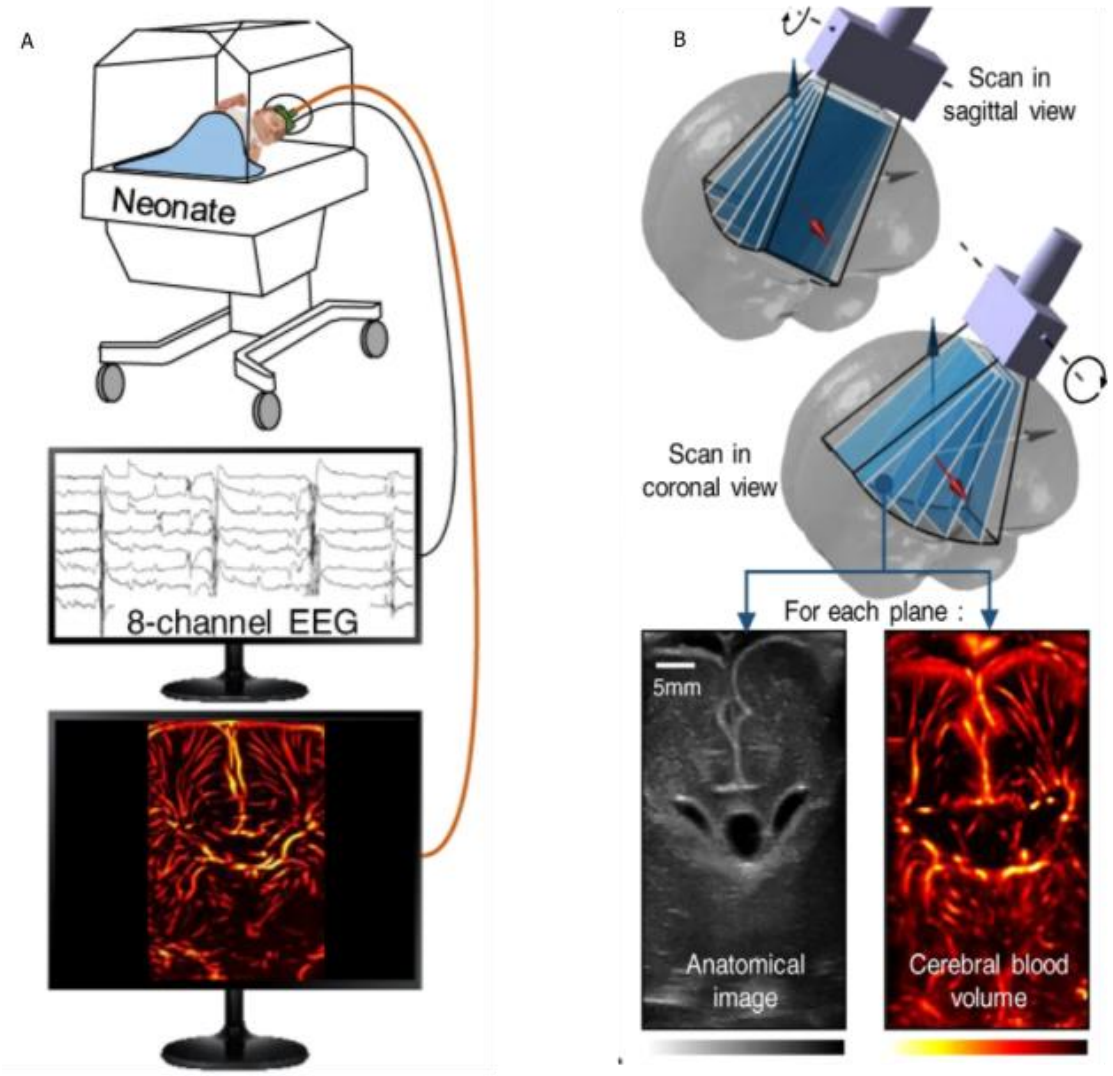

Figure 38: Neonatal fUS imaging. *A) EEG and fUS recorded simultaneously in incubated neonates. B) Coronal and sagittal scan of neonatal brain scans generates anatomic B-mode image and vascular doppler image for each plane (Baranger et al., 2021)*

Dynamic FC analysis of neonatal brain proves that there are markers of brain impairments and developments that are intertwined with transient FC patterns and fUS is a promising new tool in this aspect (*Figure 39*).

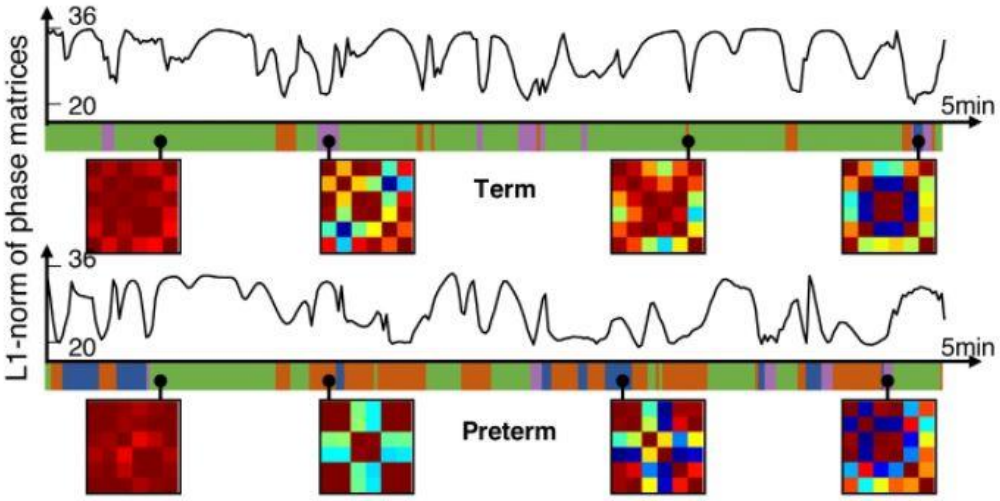

Figure 39: Dynamic FC in sleeping neonatal brain. *rsFC connectivity patterns are different in sleeping preterm neonates and term neonates. fUS can be used to detect markers of impairment by dynamic FC analysis (Baranger et al., 2021)*

In conclusion, fUS can be used to measure FC in anesthetized (Osmanski et al., 2014; Rahal et al., 2020) and awake animals (Ferrier et al., 2020; Rabut et al., 2020; Tiran et al., 2017) and in neonates (Baranger et al., 2021). Stationary and dynamic analysis of FC can be performed to extract the characteristics of intrinsic brain activity.

CHAPTER 2:

OBJECTIVES

Decrypting thermal sensory coding at the level of the brain networks using Functional Ultrasound Imaging was the goal of the thesis. The specific advantages offered by fUS imaging such as its excellent spatial and temporal resolutions, possibility to image in awake and anesthetized conditions in a large field of view and portability, makes it a frontrunner for sensory studies in rodents. fUS can also be used to image intrinsic brain activity and thereby facilitate functional connectivity studies to understand how different brain regions interact during thermal sensing process.

In the first study, we wanted to start by imaging the brain regions that are known to be key players in thermal sensation and perception in anesthetized rats. The second study was designed to investigate the interplay between brain regions during thermosensation in awake mouse brain.

1. Study 1: fUS imaging of brain areas involved in thermal processing in anesthetized rats

The current knowledge of the thermosensory organization elucidate the mechanism of supraspinal integration of thermal sensory inputs. The main regions that are commonly associated and studied are thalamus, somatosensory cortex, insular cortex and cingulate cortex. Keeping this in mind, this study was conducted in anesthetized rats using innocuous and noxious thermal stimulations imaging 2 different sagittal planes that contains the aforementioned brain regions. As fUS imaging allows functional activation mapping by capturing changes in cerebral blood volume, we postulated that when thermal stimulations are applied to the glabrous skin of hind paw, there will be an increase in neuronal activity thereby inducing CBV changes in these brain regions that take part in thermal sensing.

2. Study 2: Awake fUS imaging of thermal coding in mouse brain

Study 2 was designed to overcome the challenges and bias due to anesthesia in Study 1. To record the most natural brain responses to thermal input, it was decided that awake transcranial fUS imaging in mice posed as a better technique. It was minimally invasive and allowed longitudinal studies. We wanted to answer the questions: How do different brain regions interact during thermosensation? Are their activities temporally correlated or anti-correlated with each other? What is the strength of their correlation? We set out to answer this by looking at the inter-regional functional connectivity (static and dynamic) between somato-motor, cingulate and hypothalamic brain regions in awake mice. fUS imaging of awake mouse brain was performed during the application of thermal stimuli.

CHAPTER 3:

fUS IMAGING OF BRAIN AREAS INVOLVED IN THERMAL PROCESSING IN ANESTHETIZED RATS

1. INTRODUCTION

A large number of studies have been conducted to understand thermosensation at the molecular, spinal and supraspinal level in rodents. The goal of this study was to understand how thermosensation is processed in the rat brain and which areas are involved in the process, using fUS imaging. Compared to contemporary imaging techniques, such as fMRI and PET, fUS offers various advantages. It has high spatial-temporal resolution and is highly sensitive to brain activity thereby making fUS, an effective tool to study functional activation of brain areas.

By using the capability of functional activation mapping in fUS imaging, we postulated that thermally activated brain areas could be identified in the thalamo-cortical circuits. As established earlier, fUS imaging uses plane wave imaging. This means, we can image a 2-dimensional plane at a time. These planes of imaging can be either coronal and sagittal planes (or any other non-orthogonal plane) by changing its orientation using 3-dimensional motors. In this study we leveraged this property to do sagittal plane imaging.

It has been shown in humans and animals that the ventral posterolateral and posteromedial thalamic nuclei (VPL-VPM) are responsive to thermal stimuli (Bowsher, 1961; Burton et al., 1970; Bushnell et al., 1993; Craig et al., 1994b; Davis et al., 1999b; Duncan et al., 1993; Egan et al., 2005; Norrsell and Craig, 1999; Poulos and Benjamin, 1968). From the thalamus, thermal information is passed on to the next processing centers the somatosensory cortex: primary and secondary somatosensory cortex (S1, S2), insular cortex (Birklein et al., 2005; Downer and Zubek, 1954; Egan et al., 2005; Finger et al., 1970; Finger and Frommer, 1970; Gogolla et al., 2014; Greenspan et al., 1999; Hellon et al., 1973b; Landgren, 1957b; Peltz et al., 2011; Penfield and Faulk, 1955; Porter et al., 1993; Rodgers et al., 2008; Singh et al., 2020; Tsuboi et al., 1993; Veldhuijzen et al., 2010b, 2010a). The cingulate cortex consisting of anterior, medial and posterior parts plays a major role in the emotional aspect of nociception and can be associated to thermal discomfort (Derbyshire et al., 1997; Devinsky et al., 1995; Fuchs et al., 2014; Hutchison et al., 1999; Kwan et al., 2000a; Vogt et al., 1993; Xiao et al., 2021; Xiao and Zhang, 2018).

In virtue of these regions of interest, we chose 2 sagittal planes : i) lateral at 3 mm (somatosensory cortex, thalamic nuclei, insular cortex) ii) lateral at 0.5 mm (anterior, medial, posterior cingulate cortex). We anticipated that when thermal stimulations are applied to the hind paw of an anesthetized rat, there will be an increase in neuronal activation and a corresponding CBV change in these aforementioned brain regions. To test this hypothesis, we performed fUS imaging in anesthetized rats using a thinned skull window.

2. MATERIAL AND METHODS

2.1. ANIMALS

This study was conducted using male Sprague Dawley rats: N = 24 (Janvier Labs). They weighed 250–350g at the beginning of the experiments. All experiments were performed in agreement with the European Community Council Directive of 22nd September 2010 (010/63/UE) and the local ethics committee (Comité d'éthique en matière d'expérimentation animale n°59, C2EA –59, 'Paris Centre et Sud', project agreement # 2014-14). Rats were pre-ordered to arrive one week prior to the experiments and two were housed in one cage. They were given utmost care and were housed at a constant temperature of 22°C with an alternating 12-hour light/dark cycle. They received food and water ad libitum.

2.2. SURGICAL PREPARATION OF THINNED SKULL WINDOWS

The rat skull bone attenuates acoustic waves which can deteriorate the quality of the fUS images. Therefore, fUS imaging in rats requires a full craniotomy or preparation of a thinned skull window. In our study, we chose to image via a thinned skull window as it is comparatively less invasive. This procedure was done 3 days before the experiments.

A mixture of Ketamine (40mg/kg) and Domitor (0.3mg/kg), used to induce the anesthesia was injected intraperitonially. After making sure that paw withdrawal reflex was absent, the head of the rat was placed on the stereotaxic frame. The cranial window from 5mm anterior to Bregma until Lambda was prepared as shown in *Figure 40*. Using a micro drill steel burr (Fine Science Tools, cat. no. 19007-07), three layers of skull bone was removed by slow drilling. To avoid the heating effect

of drilling, the skull was often cooled using saline. At the end of the procedure, skin was sutured back using 5.0 non-absorbable Ethicon thread. A subcutaneous injection of atipamezole (Antisedan®, 1 mg/kg) was used to reverse the anesthesia along with an analgesic for post-surgical pain (Metacam®, 0.2 mg/kg).

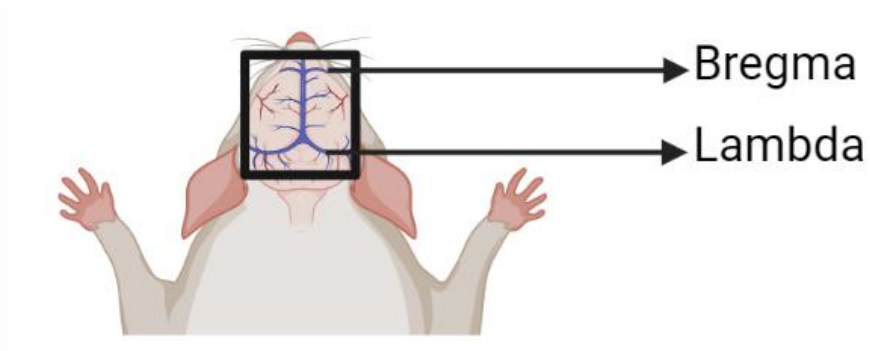

Figure 40: Thinned skull window preparation in rats. *Window begins at 5mm anterior to Bregma until Lambda, prepared by slow drilling and removing three layers of skull bone. Skin is sutured back at the end of the procedure.*

2.3. CHOICE OF IMAGING PLANES

fUS is capable of measuring cerebral blood volume with high sensitivity and spatial-temporal resolution using multiple plane wave insonification. fUS also allows us to image coronal or sagittal planes by placing the ultrasound probes in the desired manner with respect to the brain. We chose to perform fUS imaging in 2D sagittal planes with our regions of interest.

The planes chosen for this study with their corresponding regions of interests are listed below:

i. Sagittal Plane 1: lateral +3.0 mm

In this plane we aimed at imaging mainly the somatosensory cortex of hind limb, fore limb, trunk, motor cortex (S1HL, S1FL, S1Tr, M1). This plane also contained insular cortex, lateral parietal association cortex- secondary visual cortex mediolateral area (LPtA-V2ML), ventral posterolateral thalamic nucleus-ventral posteromedial nucleus (VPM-VPL), Globus Pallidus (GP), Caudate Putamen (CPu) (*Figure 41* A-B).

ii. Sagittal Plane 2: lateral +0.5 mm

This plane was chosen primarily to visualize the cingulate cortex consisting of anterior, medial and posterior parts. It also contains secondary motor cortex (M2), retrosplenial dysgranular cortex-retrosplenial granular cortex (RSD-RSG), Hippocampus, ventral posterolateral thalamic nucleus (VPL) - ventral posteromedial thalamic nucleus (VPM) (*Figure 41* C-D).

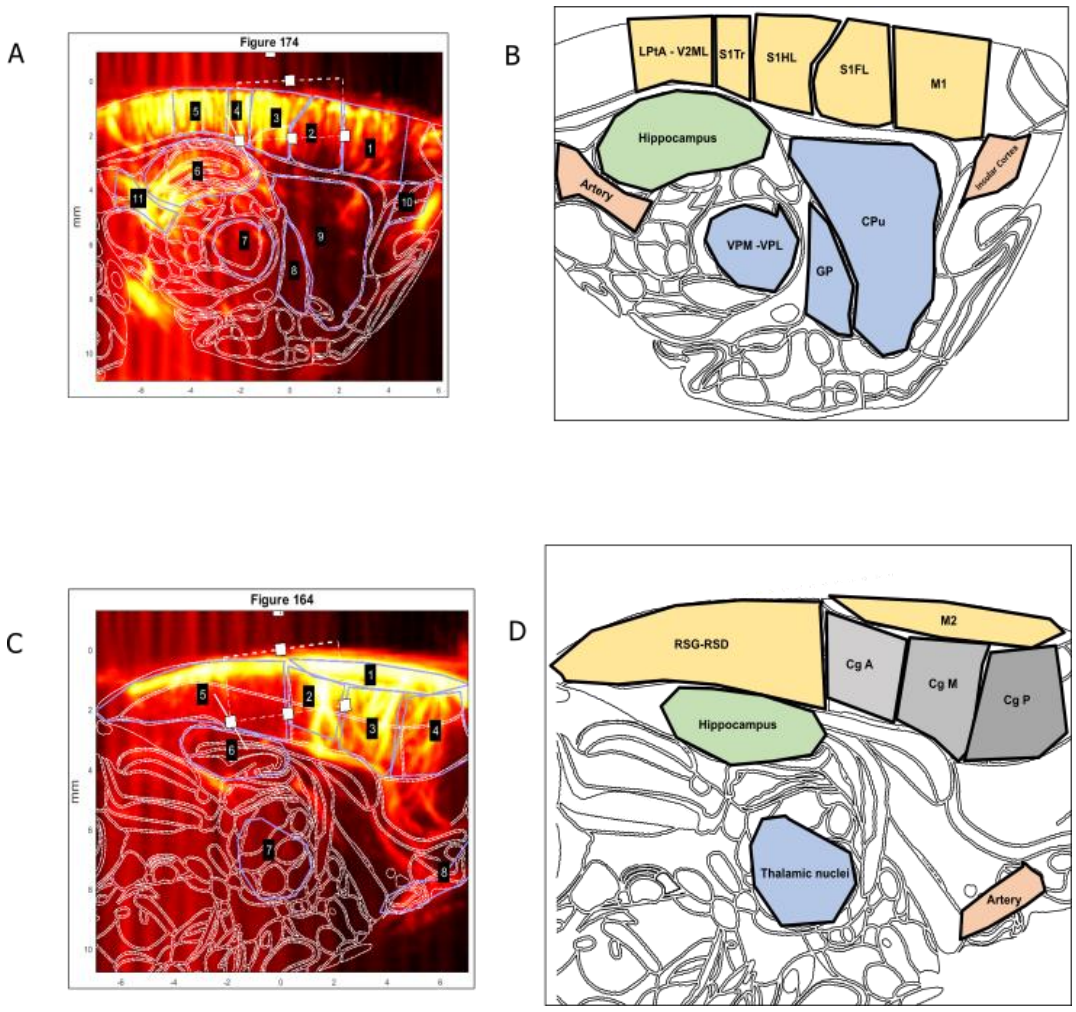

Figure 41: Planes chosen for fUS imaging. *A-B) Doppler image of the sagittal plane lateral at 3mm of rat brain with the corresponding mask of regions of interest delineated and the schematic of the same plane based on Paxinos atlas (Paxinos and Watson, 1997) respectively. C-D) Doppler image of the sagittal plane lateral at 0.5mm of rat brain with the corresponding mask of regions of interest delineated and the schematic of the same plane based on Paxinos atlas (Paxinos and Watson, 1997) respectively. The artery in both planes is also marked.*

S1HL: Primary Somatosensory Cortex, Hind Limb part, S1FL: Primary Somatosensory Cortex Fore Limb part, S1Tr: Primary Somatosensory Cortex, Trunk part, M1: Primary Motor Cortex, IC: Insular Cortex, LPtA-V2M: Lateral parietal association cortex- Secondary visual cortex, mediolateral area, VPM-VPL: Ventral Posterolateral Thalamic Nucleus-Ventral Posteromedial Nucleus, GP: Globus Pallidus , CPu: Caudate Putamen . Cg A: Anterior Cingulate cortex, Cg M: Medial Cingulate cortex, Cg P: Posterior Cingulate cortex, M2 : Secondary Motor Cortex, RSD-RSG: Retrosplenial Dysgranular Cortex- Retrosplenial Granular Cortex, Hippocampus, (Ventral Posterolateral thalamic Nucleus (VPL) - Ventral Posteromedial thalamic Nucleus (VPM)).

2.4. fUS IMAGING

To perform fUS imaging, the rats were anesthetized using a bolus of intraperitoneal injection of Ketamine (40 mg/kg) - Domitor (0.3 mg/kg), at first. The anesthesia was later maintained by subcutaneous perfusion of medetomidine (0.1 mg/kg/h) and ketamine (12.5 mg/kg/h). Due to challenges encountered in the experiment, we also performed the imaging under isoflurane anesthesia. Isoflurane was used at concentrations of 2–4% for induction and 1-1.5% for maintenance, while maintaining an air-oxygen ratio of 1:2. Rat are placed on to the stereotaxic frame, when they were under stable level of anesthesia. The body temperature was maintained using a heating blanket and heart rate and respiration rates were measured (STARR Life Science, Oakmont, USA).

The thinned skull window is was exposed by opening the sutured skin, followed by gentle cleaning using saline solution. Centrifuged echographic gel was applied on the window before imaging. A linear ultrasound probe (128 elements, 15 MHz central frequency, 100µm spatial pitch and 8 mm elevation focus, Vermon, Tours, France) was used for imaging. Multiple tilted plane waves angled from −10° to +10° which are 2° apart were used for insonification of the rat brain (Macé et al., 2011) at a pulse repetition frequency of 5.5 kHz. By coherently compounding the sum of these11 tilted plane waves, we obtained a Doppler image in every 2ms. Repeating this sequence 200 times at a sampling rate of 500 Hz, meant that 200 coherently compounded doppler images were acquired in 400ms. Tissue signal was isolated from the cerebral blood volume (CBV) signal by using a SVD clutter filter (Demené et al., 2015) and by averaging the CBV in each pixel every 400ms, we obtained a Power Doppler image.

2.5. EXPERIMENTAL SETUP

To accomplish the goal of this study i.e., to better understand the brain regions involved in thermal coding in rats, we performed mechanical brush stimulation as a positive control and then used 3 different approaches to induce the thermal stimulations as explained below.

2.5.1. Mechanical Brush Stimulation

fUS imaging of mechanical brush stimulation was performed at the beginning of each imaging session. It serves as a positive control to make sure we are at the optimal level of anesthesia and right conditions and have a good hemodynamic response, specific to the brush stimulation. Under the right condition, stimulating the hind paw specifically activates the somatosensory cortex of hind limb (S1HL). Absence of activation can happen due to several biological reasons, such as deep level of anesthesia, or any physiological reasons for a low neurovascular coupling. Therefore, in the case of absence of specific hemodynamic response in this test, the animal was excluded.

Four successive brush stimulations were applied on the glabrous skin of the hind paw, as shown in *Figure 42*. Each stimulation consisted of 60s baseline followed by 20 seconds brush stimulation (ON) and 60s without stimulation (OFF). The total duration of the fUS imaging session was 380s.

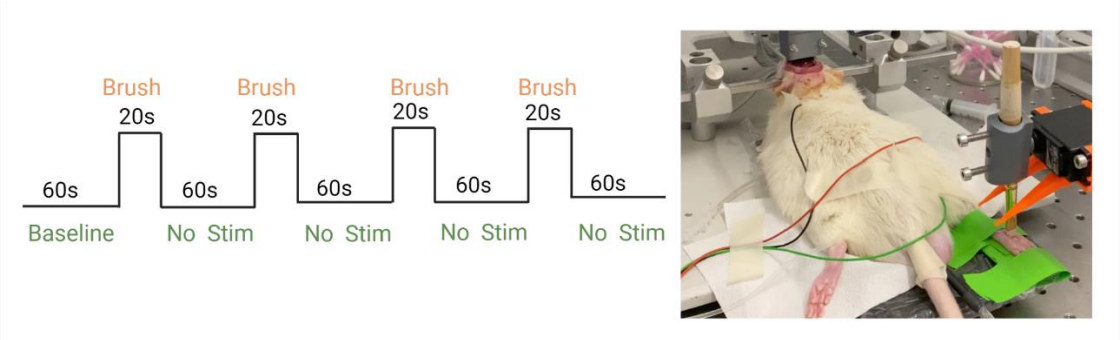

Figure 42: Mechanical Brush Stimulation in rats. *Four successive brush stimulations were applied to the hind paw. Each stimulation consisted of 60s OFF without any stimulations followed by 20 seconds brush stimulation (ON).*

2.5.2. Warm Water

A beaker of warm water (39°C) was used to apply innocuous thermal stimulations by immersion of the hind paw. Two successive stimulations were applied as shown in *Figure 43*. Paw temperature was at 30°C at the beginning of the experiment during a 60s baseline. The hind paw was immersed in the warm water at 39°C for a duration of 10s. During the 60s OFF time, stimulations were not applied. The total duration of the fUS imaging session was 200s.

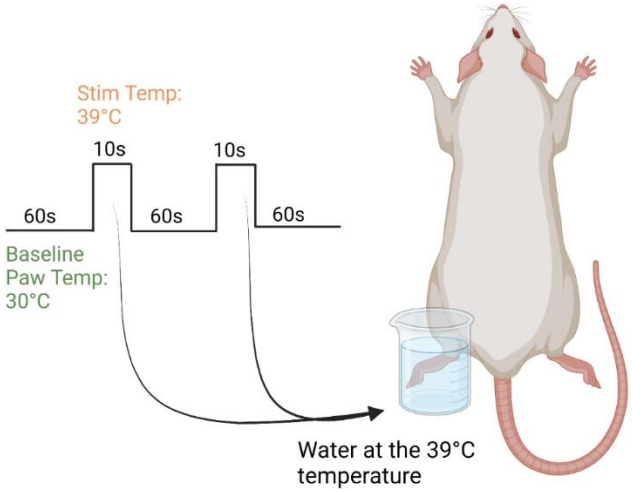

Figure 43: Innocuous thermal stimulation using warm water. *Paw temperature is at 30°C at the beginning of each trial. Two successive stimulations in which the paw is immersed in the warm water at 39°C for a duration of 10s.*

2.5.3. Peltier Module

A custom-made Peltier device was developed by one of our research engineers at the Physics for Medicine Laboratory (*Figure 44*). This Peltier device is a thermoelectric module (Module Peltier 12 Vcc TEC1-12706 40 x 40 mm - 51,4 W) that can be cooled or heated . By modulating the electric current through the module, it is possible to change the temperature or maintain it at a target temperature. The pace of change can also be modulated which allows for a fast or slow rate.

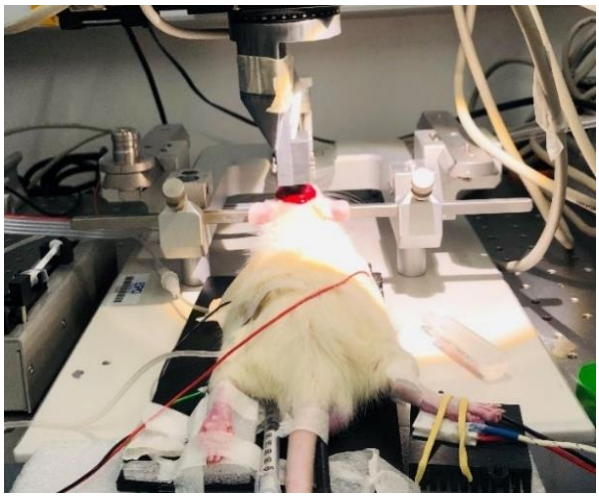

Figure 44: Custom-made Peltier device *used to apply thermal stimulations to the right hind paw in the experimental setup. It consisted of a Peltier element and TEC controller that is the heart of the device, regulating the current supplied. Heat sink below the Peltier element dissipated the heat to the surrounding air.*

We applied both innocuous and noxious stimulations using the device. During the noxious heat stimulations, the Peltier element was held at a baseline temperature of 27°C for 105s and a noxious stimulation of 49°C was applied for 15s (*Figure 45* A). Similarly, during the warm stimulations, the Peltier element was held at a baseline temperature of 30°C for 240s and a warming stimulation of 39°C was applied for 10s (*Figure 45* B).

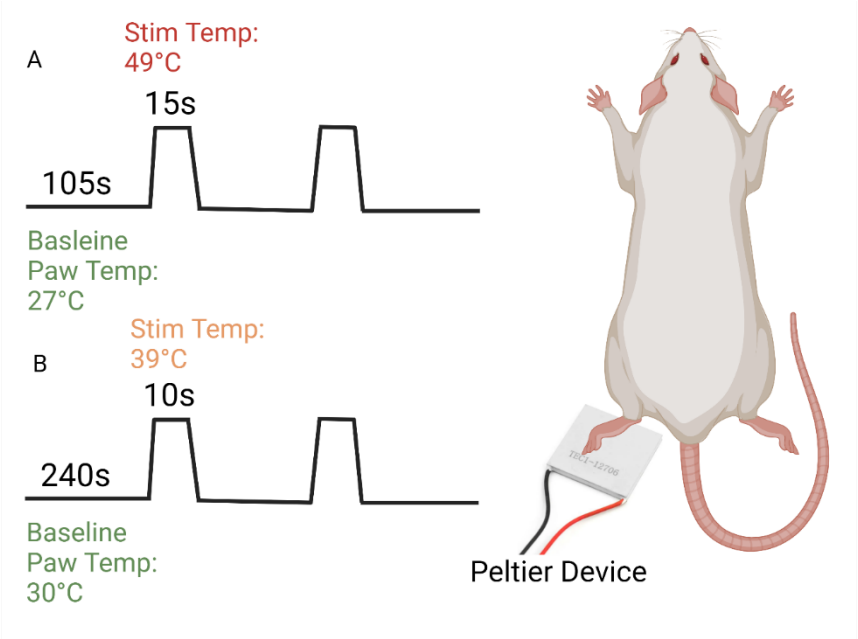

Figure 45: Peltier device capable of delivering innocuous and noxious thermal stimuli. *A) Peltier element was held at a baseline temperature of 27 and 30°C for 105s and 240s respectively and either noxious (49°C) or innocuous (39°C) stimulation of were applied for 15s or 10s, respectively.*

2.5.4. Bioseb HC plate

The Bioseb HC plate can be used to apply thermal stimulations using its metallic floor. It can be held at a particular temperature or can be programmed to go from one temperature to another at a particular rate of change.

We used it to apply a slow ramp over 1380s at 1.6°C/min going from innocuous to noxious temperature 32-46° after a baseline of 120s at 32°C (*Figure 46* A). In order to apply short term stimulation, we first pre-heated the metallic floor to 50°C. Paw was at a baseline temperature of 30°C for 60S after which the hind paw was carefully placed on the floor for 30s (*Figure 46* B).

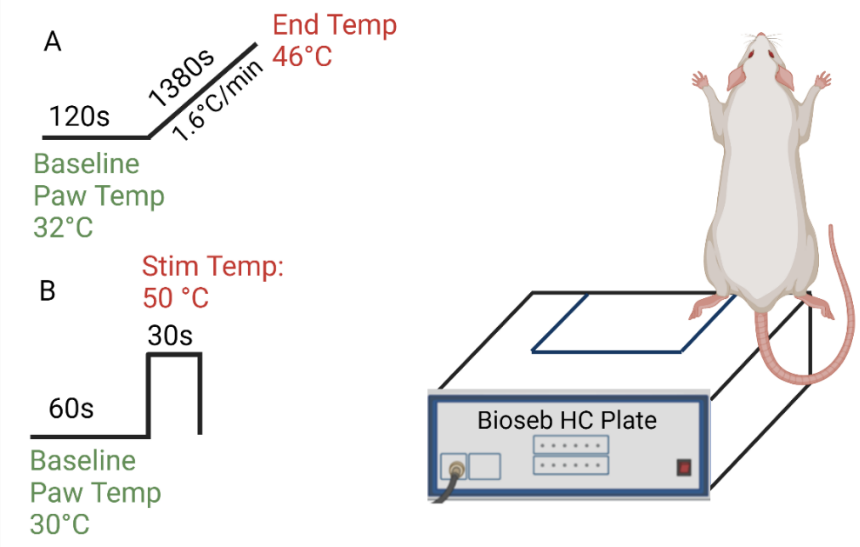

Figure 46: Application of innocuous to noxious ramp and short sustained noxious stimulations using Bioseb HC plate. *A) After a baseline of 120s at 32°C, a slow ramp over 1380s at 1.6°C/min was applied from innocuous to noxious temperatures (32-46°). B) Sustained noxious stimulation at 50°C applied for 30s after a 60s baseline at 30°C.*

2.6. DOPPLER SIGNAL ANALYSIS

Activation Maps were obtained by implementing a generalized linear model (GLM) approach in which the stimulus is convolved with a default hemodynamic response function (HRF). This is done because the response in the brain does not follow a binary pattern like the stimulus. Z-score maps were computed between temporal signal from each pixel and the stimulus pattern. Multiple comparison correction was performed with the Bonferroni method by dividing the conventional p value (0.05) by the total number of pixels, resulting in a stricter final threshold for each individual pixel activation. The color-coded Z-score maps with the significantly activated pixels are superimposed on the power Doppler image, thus forming an activation map. By looking at the activation map, we can find out which pixels or group of pixels from a brain region are activated.

ΔrCBV Maps are indicative of the changes in cerebral blood volume (CBV) relative to the baseline (color coded and expressed as percentage change) in the significantly activated pixels.

Time course of CBV variations (percentage change from baseline) were obtained from the pre-defined mask of regions of interest (ROIs) delineated based on Paxinos atlas (Paxinos and Watson, 1997).

3. RESULTS

In this study, we investigated the brain regions involved in thermal sensing in two sagittal planes: lateral at 0.5 mm and 3 mm using fUS imaging in anesthetized rats. Two types of anesthesia were used: low dose of Ketamine-Domitor (KD) and Isoflurane.

3.1. fUS IMAGING AT LOW DOSE OF KETAMINE DOMITOR ANESTHESIA

3.1.1. Mechanical brush stimulation of hind paw

As fUS allows to measurement of localized changes in blood volume during a sensory stimulation, we established a mechanical brush stimulation as a positive control that made sure that we are at the optimal level of anesthesia to perform the experiments.

The activation map over all trials show a statistically significant activation of somatosensory cortex of hind paw (ROI1-S1HL) in response to the brush stimulation and it's corresponding CBV changes are shown in *Figure 47* (A and B). The activated pixels in the S1HL region showed up to 20% increase in CBV. Analysis of the time course of the relative changes in CBV in S1HL and M1 respectively confirms a selective activation in the S1HL and lack of changes the primary motor cortex M1 (*Figure 47* C-D).

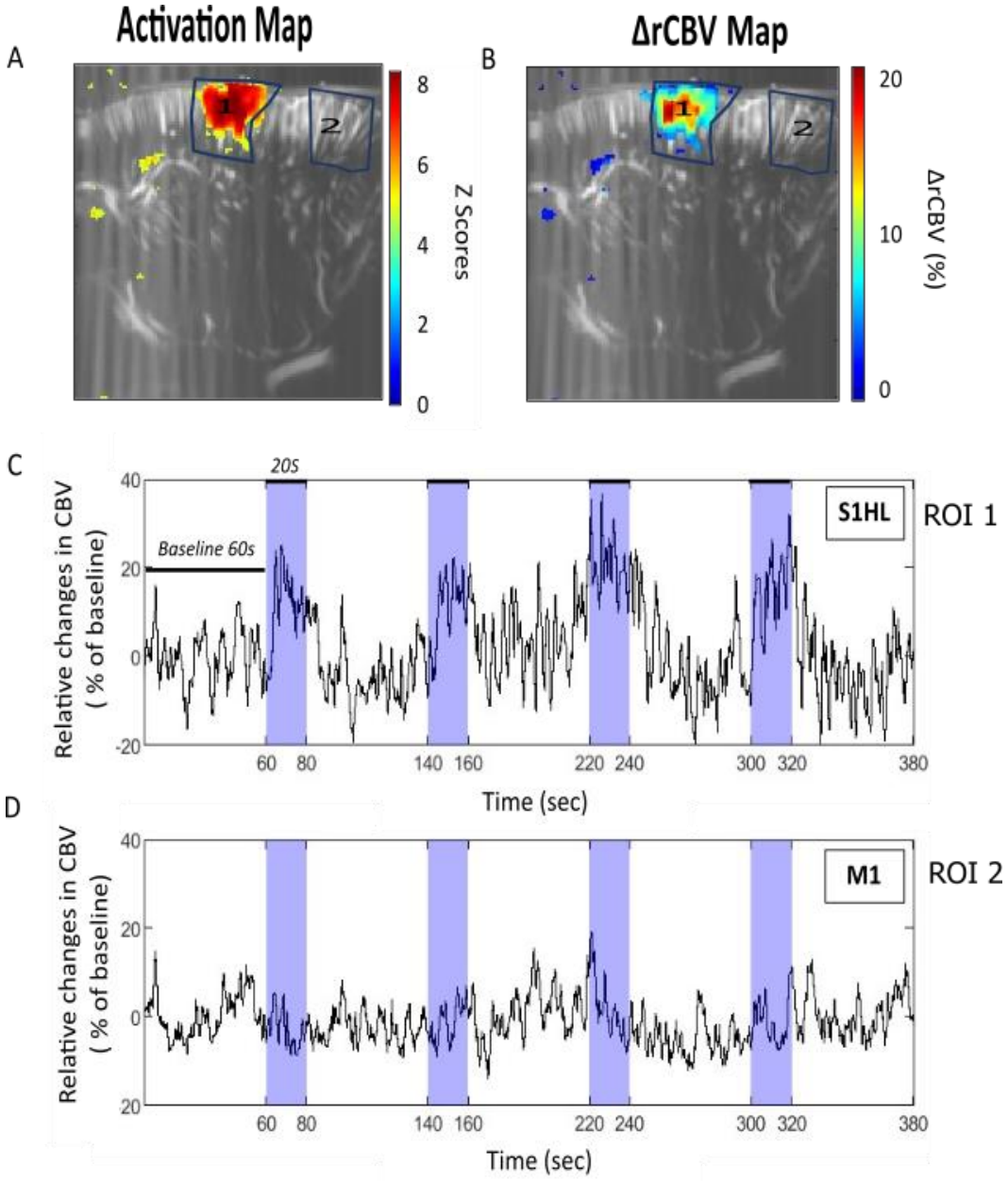

Figure 47: Example of hemodynamic responses in the primary somatosensory cortex of hind limb part (S1HL) induced by hind paw stimulations. *(A) Activation map is showing significantly activated pixels following mechanical stimulation of the right hind paw (20 s ON, 60 s OFF, 4 times) in an anesthetized rat, using a sagittal plane of imaging at lateral 3 mm. Z-scores (color coded) is superimposed on Doppler image. Activated pixels are well located inside the S1HL cortex. B) ΔrCBV map is shown over activated pixels during 4 stimulation trials. (C) Time course changes of CBV as a percentage of baseline in the S1HL cortex during four stimulation trials (20 s ON - 60 s OFF). (D) Changes in CBV in the same experiment, but from the primary motor cortex (M1) show a lack of change in correlation with the stimulation pattern.*

3.1.2. Innocuous warm stimulation

Warm temperature at 39°C was applied twice to the hind paw held at a baseline of 30°C using the 3 setups: Peltier, Bioseb HC plate and water for different duration of stimulations from 10s to 30s while fUS imaging was performed on sagittal plane at 3 mm. We observed a lack of activation in regions that are associated to thermal processing. An example of the lack of activation obtained using Peltier module is shown in *Figure 48*. Doppler image of the sagittal plane with the corresponding mask of regions of interest delineated based on Paxinos atlas (Paxinos and Watson, 1997) is shown in *Figure 48* A. The regions of interests and their corresponding changes in CBV are shown in *Figure 48* B. During the stimulation, the ROIs (1-11) did not show significant changes in CBV. Taken together, warm stimulation applied using water, Peltier and Bioseb HC plate did not induce a statistically significant change in CBV in regions implicated in thermosensation.

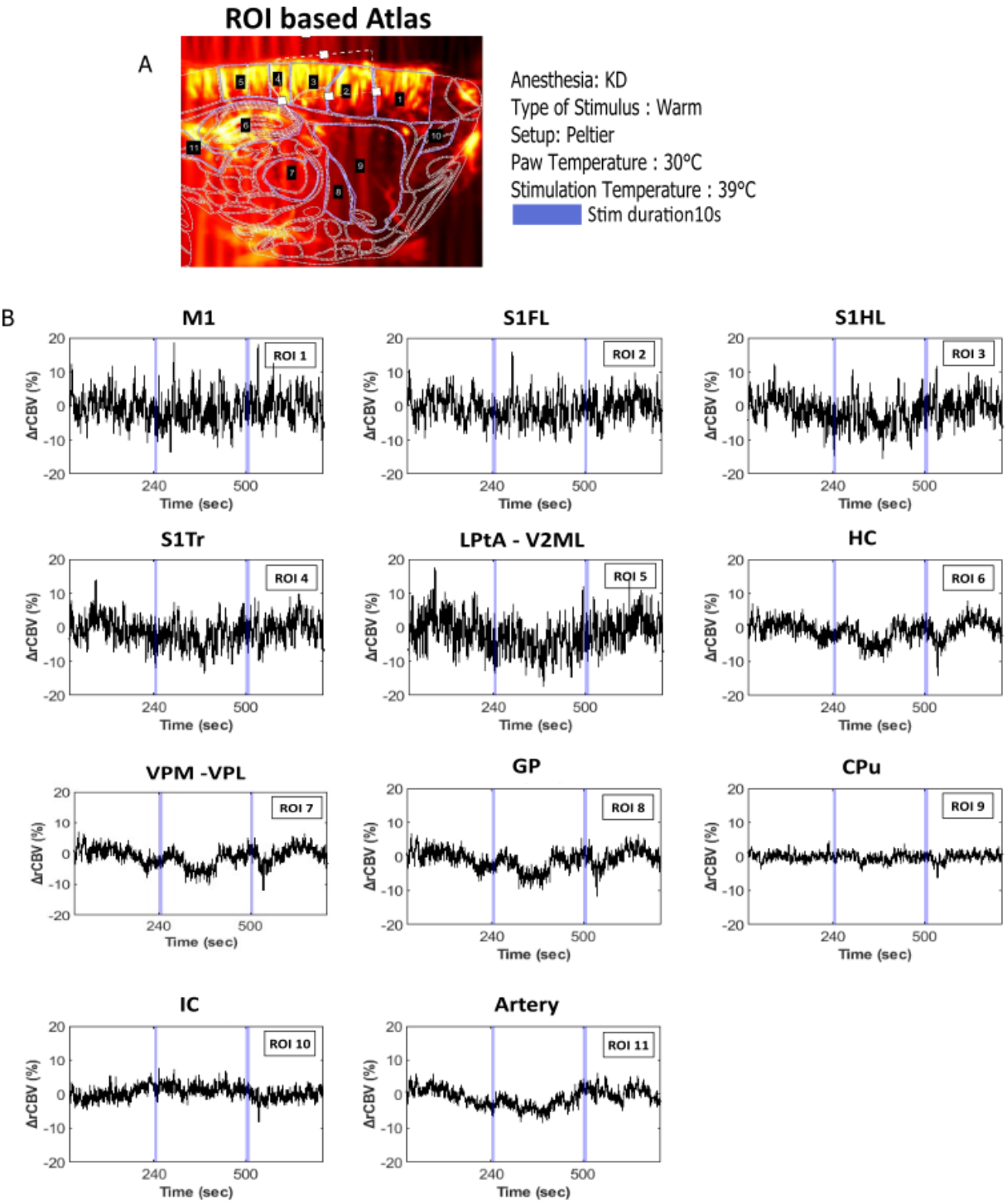

Figure 48: Representative example of lack of activation obtained during warm stimulation using Peltier module*. A) Doppler image of the sagittal plane lateral at 3mm with the corresponding mask of regions of interest delineated based on Paxinos atlas (Paxinos and Watson, 1997). B) The regions of interests and their corresponding changes in CBV. Blue window indicates the stimulation duration. S1HL: Primary Somatosensory Cortex Hind Limb part, S1FL: Primary Somatosensory Cortex Fore Limb part, S1Tr: Primary Somatosensory Cortex Trunk part, M1: Primary Motor Cortex, IC: Insular Cortex, LPtA-V2ML: Lateral parietal association cortex- Secondary visual cortex, mediolateral area, VPM-VPL: Ventral Posterolateral Thalamic Nucleus-Ventral Posteromedial Nucleus, GP: Globus Pallidus , CPu: Caudate Putamen.*

3.1.3. Noxious heat stimulation

The puzzling absence of activation in the warm range led us to expand the experiments to the noxious range. Noxious thermal stimulations at 49°C was applied twice to the hind paw held at a baseline of 27°C using the Peltier setup for a duration of 15s. fUS imaging of the sagittal plane at 3mm, revealed no activation in our regions of interest. An example of our observation is illustrated in *Figure 49*. Doppler image of the sagittal plane with the corresponding mask of regions of interest delineated based on Paxinos atlas (Paxinos and Watson, 1997) is shown in *Figure 49* A. The regions of interests and their corresponding changes in CBV are shown in *Figure 49* B. During the stimulation, the ROIs (1-11) did not show significant changes in CBV. We also applied noxious stimulation with water, but it did not induce any significant activation due to changes in CBV.

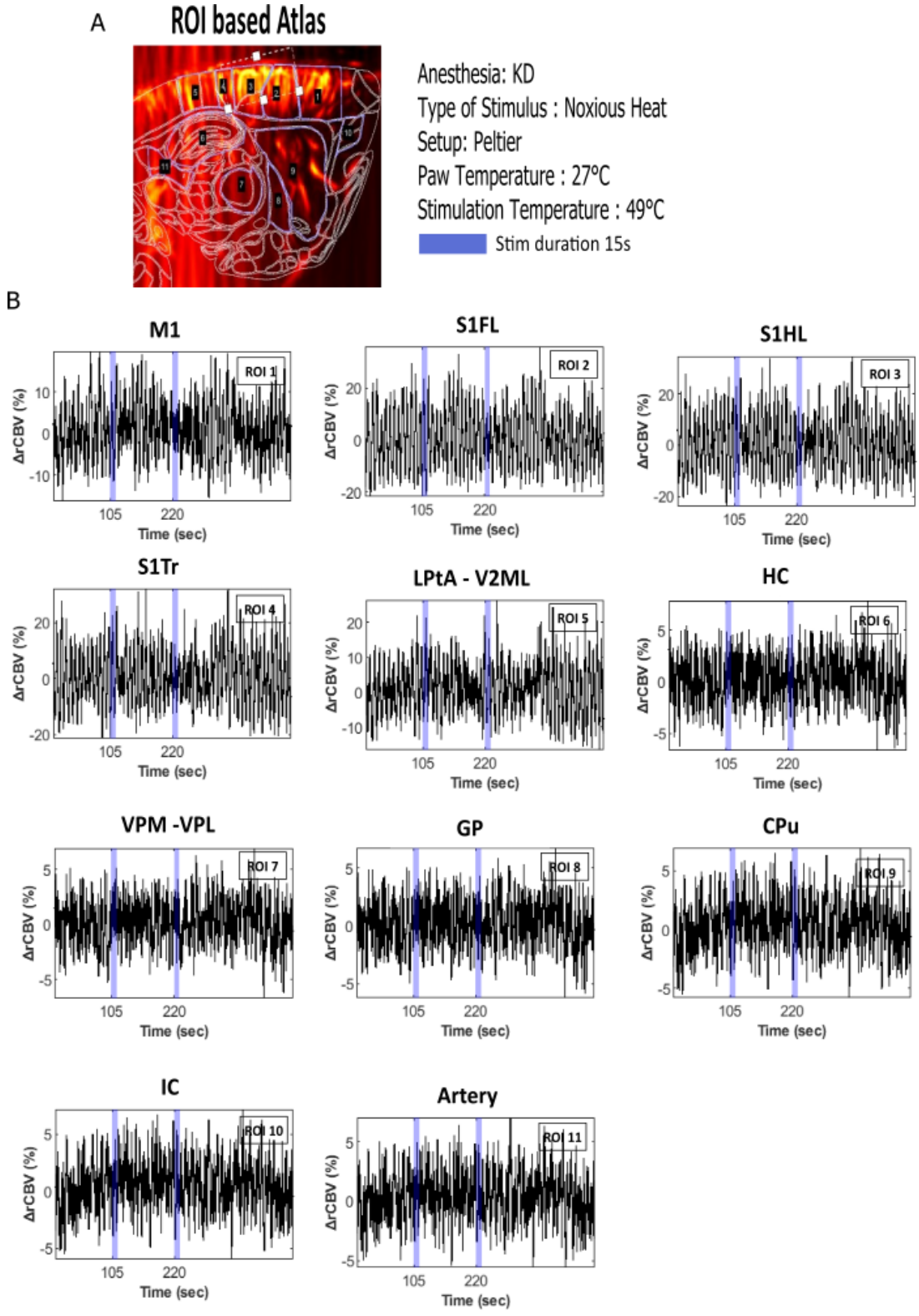

Figure 49: Absence of significant activation during noxious heat stimulation using Peltier module. *A) Doppler image of the sagittal plane lateral at 3mm with the corresponding mask of regions of interest delineated based on Paxinos atlas (Paxinos and Watson, 1997). B) The regions of interests (1-11) and their corresponding changes in CBV. Blue window indicates the stimulation duration. S1HL: Primary Somatosensory Cortex Hind Limb part, S1FL: Primary Somatosensory Cortex Fore Limb part, S1Tr: Primary Somatosensory Cortex Trunk part, M1: Primary Motor Cortex, IC: Insular Cortex, LPtA-V2ML: Lateral parietal association cortex- Secondary visual cortex, mediolateral area, VPM-VPL: Ventral Posterolateral Thalamic Nucleus-Ventral Posteromedial Nucleus, GP: Globus Pallidus, CPu: Caudate Putamen.*

3.1.4. Innocuous to noxious ramp using Bioseb HC plate

Using the Bioseb hot-cold plate, we designed a ramp stimulation that starts at 32°C and ends at 46°C at the rate of 1.6°C/minute after a 120s baseline. fUS imaging was performed at the sagittal plane at 3mm. During the whole ramp 32°C-46°C, we observed strong activation in the cortical (motor, hind limb, fore limb, trunk) regions (*Figure 50* A) but ΔrCBV map only showed modest (5-10%) increased CBV in the activated pixels (*Figure 50* B). The activation maps computed for signals taken between 32-40°C and 40-43°C, it was seen that there was a decrease in activated pixels (*Figure 50* D and G). ΔrCBV map did not show changes in CBV in the activated pixels (*Figure 50* E and H). The time course of the changes in CBV during the ramp did not follow an increasing trend with respect to an increasing ramp but it was observed that there is a slight increasing trend in the beginning and decreasing trend towards the end (*Figure 50* C, F, I).

The experiment was conducted in several trials and at different rates but the results were negative. It is complex to analyze a ramp stimulus using a square stimulus pattern as the stimuli is not constant during the ON time.

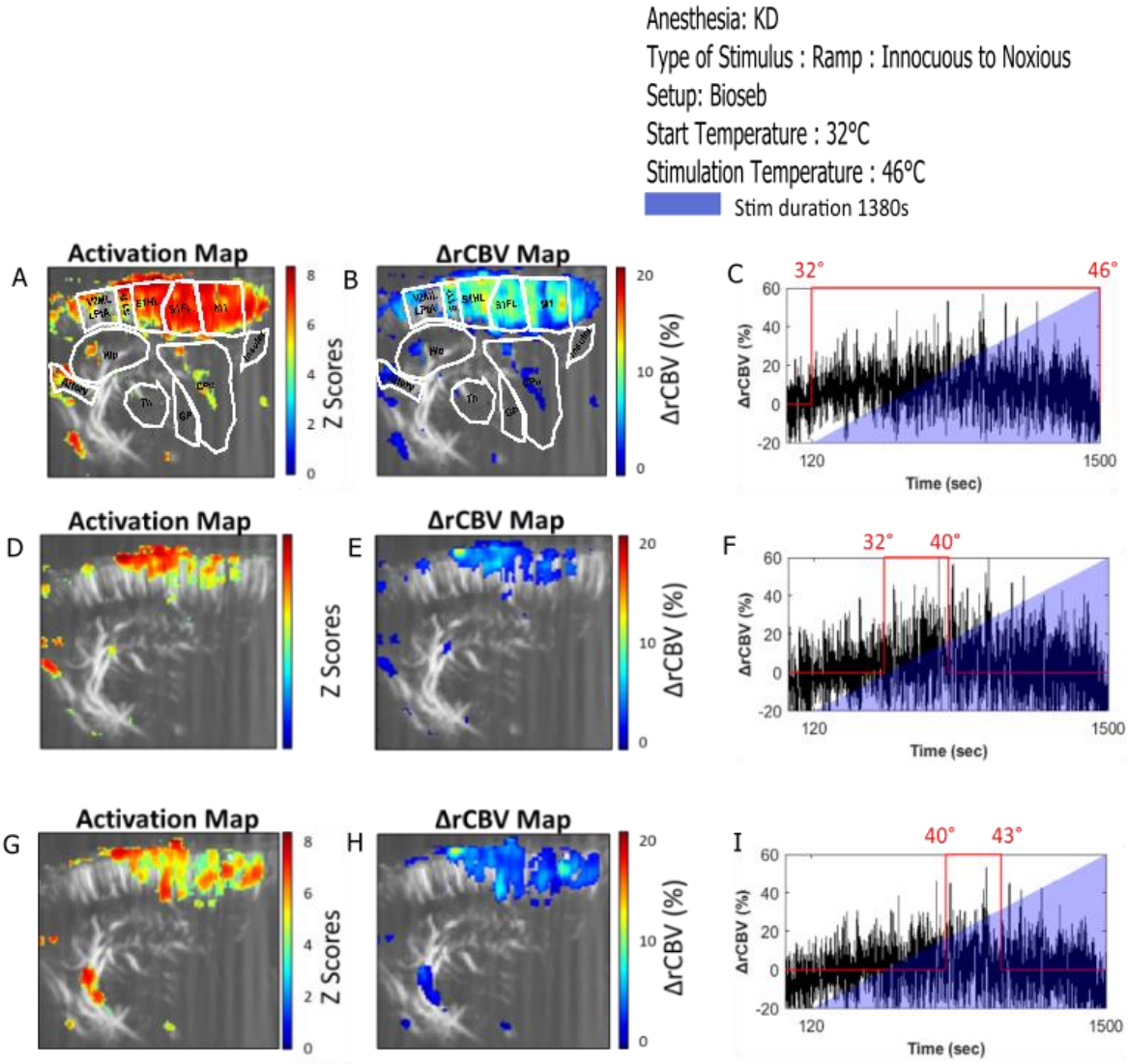

Figure 50: Innocuous to noxious ramp stimulation using Bioseb HC plate show inconsistent CBV changes. *A-C) The activation map and ΔrCBV map, corresponding to the whole duration of the ramp i.e. from 32-46°C. D-F) The activation map and ΔrCBV map, corresponding to a part of the ramp i.e. from 32-40°C. G-I) The activation map and ΔrCBV map, corresponding to a part of the ramp i.e. from 40-43°C. Activation map show significant activation in the cortical regions during the whole ramp (A) and it decreases when part of the ramp is chosen (D, G). ΔrCBV map (B, E, H) did not show a n increase in CBV. The time course of CBV changes show a slight increase in the beginning but a decreasing tendency towards the end. (C, F, I). S1HL: Primary Somatosensory Cortex Hind Limb part, S1FL: Primary Somatosensory Cortex Fore Limb part, S1Tr: Primary Somatosensory Cortex Trunk part, M1: Primary Motor Cortex, IC: Insular Cortex, LPtA-V2ML: Lateral parietal association cortex-Secondary visual cortex, mediolateral area, VPM-VPL: Ventral Posterolateral Thalamic Nucleus-Ventral Posteromedial Nucleus, GP: Globus Pallidus, CPu: Caudate Putamen.*

3.1.5. Short sustained noxious stimulation using Bioseb HC plate

To remove the complexity of ramp stimulations, noxious stimulations were applied by manually placing the hind paw on the Bioseb floor at 50°C. fUS imaging was conducted on the sagittal plane lateral at 3mm. *Figure 51* A is the Doppler image of this plane with the corresponding mask of regions of interest delineated based on Paxinos atlas (Paxinos and Watson, 1997). *Figure 51* B and C show an example of activation in the somatosensory regions of hind limb, trunk S1HL, S1Tr and LPtA-V2ML. ΔrCBV map show significantly activated pixels, with mild CBV changes in (*Figure 51* D).

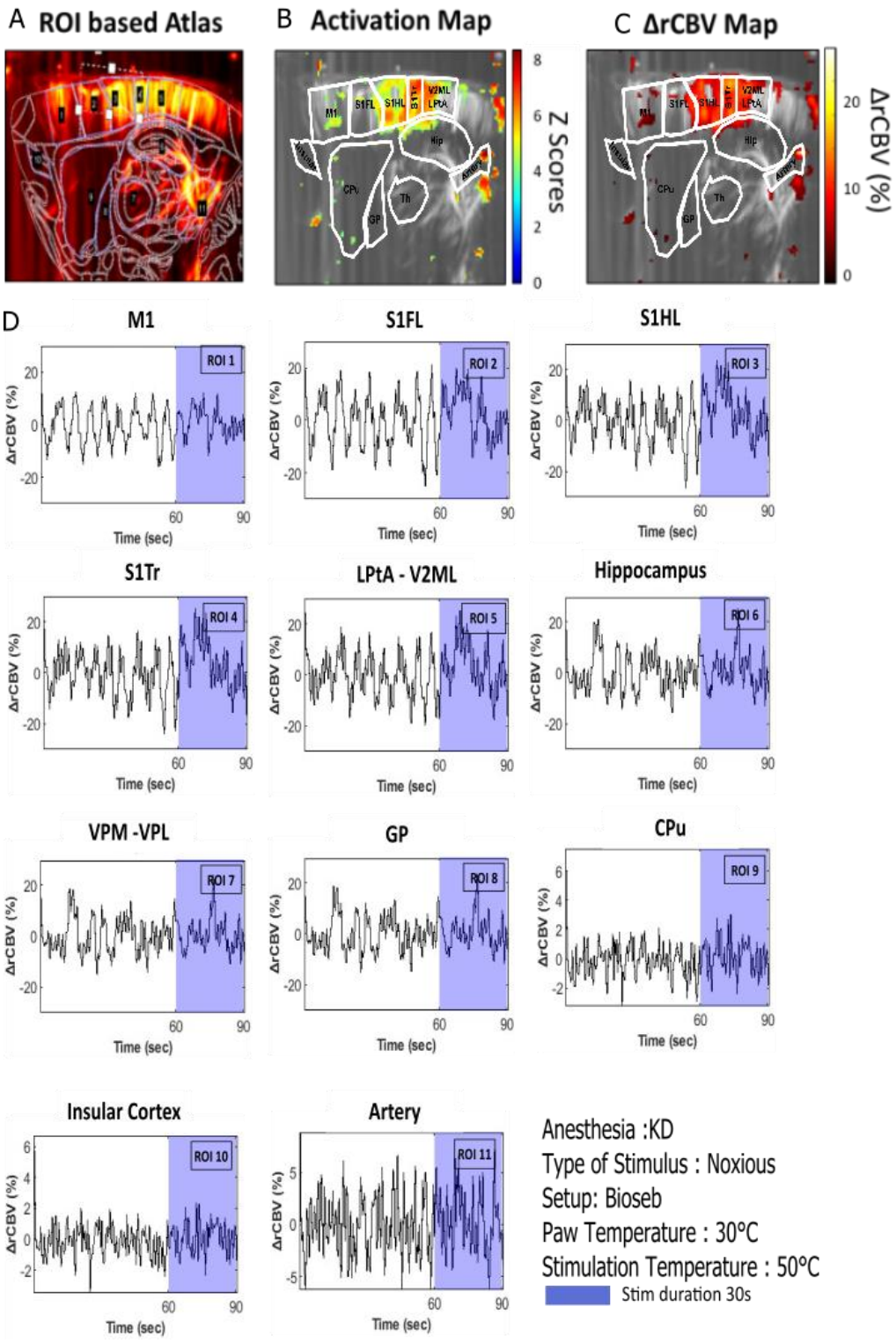

Figure 51: Short and sustained noxious stimulation applied using Bioseb HC plate induced mild CBV changes. *A) Doppler image of the sagittal plane lateral at 3 mm with the corresponding mask of regions of interest delineated based on Paxinos atlas (Paxinos and Watson, 1997). B-C) Pixels that are significantly activated and the changes in CBV in the activated pixels represented by activation map and ΔrCBV map respectively. D) The regions of interests (1-11) and their corresponding changes in CBV. Blue window indicates the duration of stimulation. S1HL: Primary Somatosensory Cortex of the Hind Limb, S1FL: Primary Somatosensory Cortex of the Fore Limb, S1Tr: Primary Somatosensory Cortex of the Trunk, M1: Primary Motor Cortex, IC: Insular Cortex, LPtA-V2ML: Lateral parietal association cortex- Secondary visual cortex, mediolateral area, VPM-VPL: Ventral Posterolateral Thalamic Nucleus-Ventral Posteromedial Nucleus, GP: Globus Pallidus, CPu: Caudate Putamen.*

Summary of results obtained using Ketamine-Domitor anesthesia

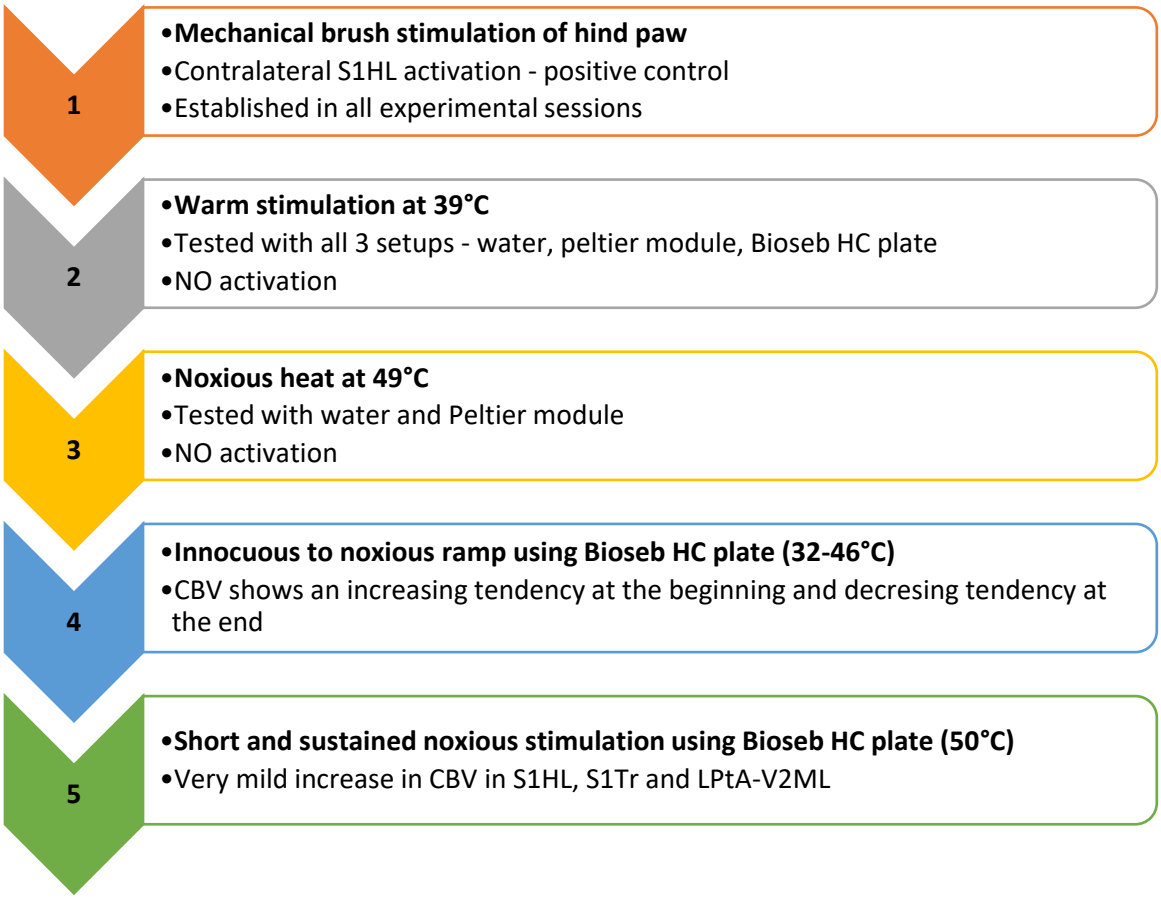

By using Ketamine-Domitor anesthesia, we were unable to observe activation of brain regions involved in thermal stimulation. Despite the low level of anesthesia, the analgesic properties of ketamine (through its antagonism of the N-methyl-d-aspartate (NMDA) receptors), is likely to have dampened the hemodynamics we wanted to investigate. To avoid such interference, we switched to another anesthetic: isoflurane, which does not have any analgesic properties.

3.2. fUS IMAGING UNDER ISOFLURANE ANESTHESIA

Under isoflurane, *only noxious heat* stimulations were applied. fUS imaging was conducted on 2 sagittal plates: lateral at 3 mm and lateral at 0.5 mm. Three types of hemodynamic responses were observed, as described below.

3.2.1. Sharp and transient response

Imaging on sagittal plane that contains the S1HL (lateral at 3mm) and with noxious thermal stimulations of 46°C was applied twice to the hind paw, induced a sharp (rise time: 4.4 sec) and transient (duration: 23.2 sec) hemodynamic response in the somatosensory regions with an increase in CBV (*Figure 52* A-C). Analysis of the time course of the CBV changes in the ROIs 1-11 (*Figure 52* D) shows a strong increase (35%) in M1, S1FL, S1HL, S1Tr and LPtA-V2ML (ROIS 1-5), while a more modest increase (~15%) in the hippocampus, thalamic nuclei: VPL and VPM and GP regions. Finally, changes in the CPu, insula and artery regions were even weaker (~5%).

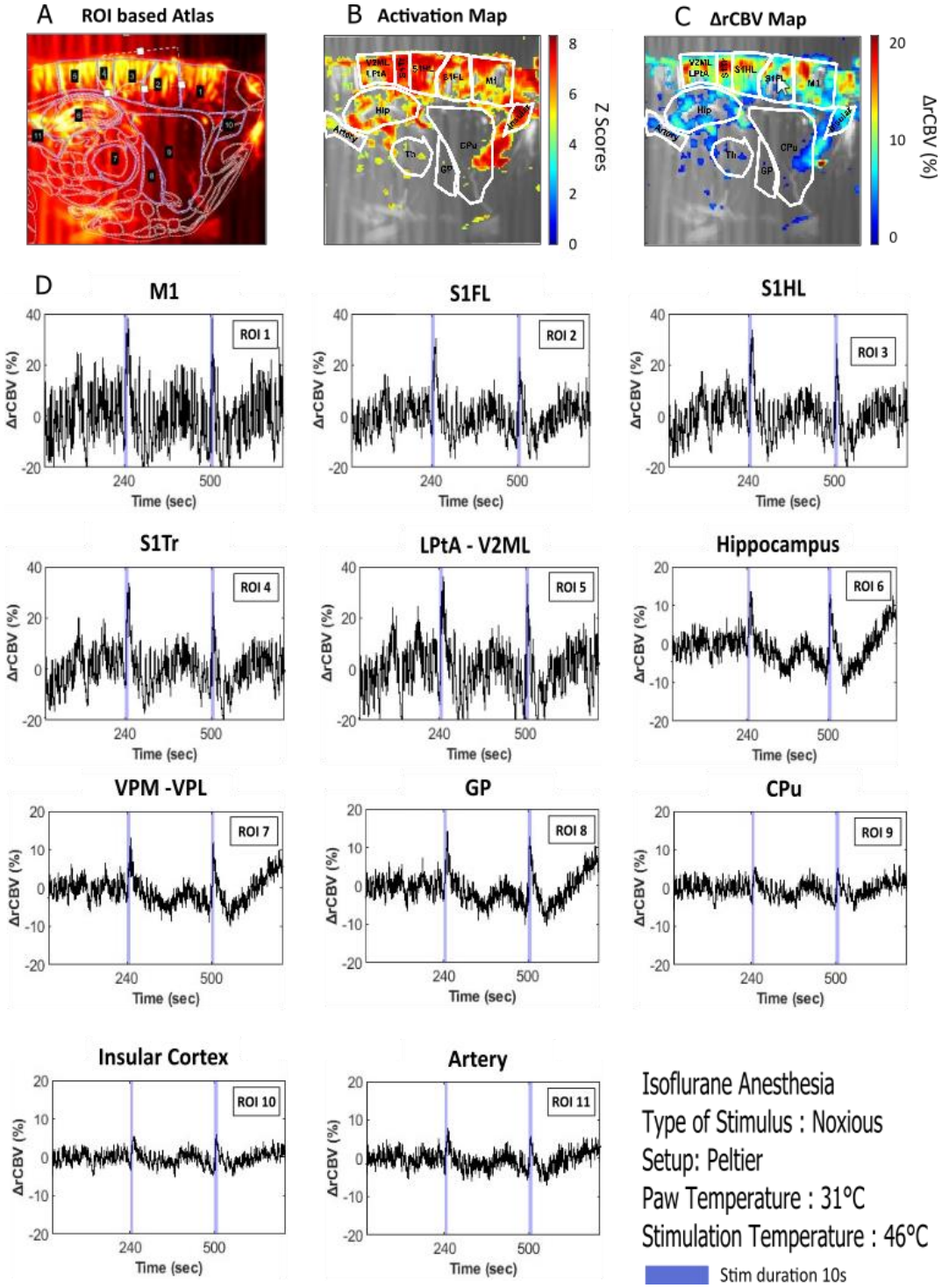

Figure 52: Strong increase in CBV during noxious stimulation with Peltier. *(A) Doppler image of the sagittal plane lateral at 3mm with the corresponding mask of regions of interest delineated based on Paxinos atlas (Paxinos and Watson, 1997). (B-C) Pixels that are significantly activated and the changes in CBV in the activated pixels represented by activation map and ΔrCBV map respectively. (D) The regions of interests (1-11) and their corresponding changes in CBV. Blue window indicates the duration of stimulation. Somato-motor regions (ROIs 1-5) have ~35% CBV increase in response to the stimulations. Hippocampus, thalamic nuclei VPL and VPM and GP regions have~15% increase in CBV, whereas CPu, insula and artery regions have ~5% increase in CBV. S1HL: Primary Somatosensory Cortex Hind Limb part, S1FL: Primary Somatosensory Cortex of Fore Limb part, S1Tr: Primary Somatosensory Cortex of Trunk part, M1: Primary Motor Cortex, IC: Insular Cortex, LPtA-V2ML: Lateral parietal association cortex- Secondary visual cortex, mediolateral area, VPM-VPL: Ventral Posterolateral Thalamic Nucleus-Ventral Posteromedial Nucleus, GP: Globus Pallidus, CPu: Caudate Putamen.*

3.2.2. Long-lasting non-specific CBV increase

In another trial using noxious thermal stimulations at 46°C for 10s using the Peltier setup (with the hind paw held at a baseline of 30°C), we imaged the plane that contains S1HL (lateral 3mm). This induced strong, but inconsistent CBV increases, as shown in *Figure 53* (A-C). The Z-score map indicates that the regions with statistical changes are in the M1, S1HL, hippocampus, thalamus and dorsal CPu.

However, close analysis of the variations of CBV over time (*Figure 53* D) reveals large and long-lasting (rise time: 8.4 sec and duration: 243.2 sec) variations of hemodynamic response between trials (from 100% for first stimulation to 50% for the subsequent stimulations in the S1HL in the example showed in *Figure 53*). In addition, these changes were observed in all ROI analyzed, but with various amplitudes, suggesting a non-specific hemodynamic response induced by noxious stimulations. Among all ROIs, the strongest effects were observed in all cortical areas (M1, S1HL, S1FL, S1Tr and LPtA-V2ML).

Due to the relative strong increased CBV in the artery (>50%), it is likely that the strong long-lasting CBV increased could be attributed to an increased arterial pressure in this experiment; therefore, could not have been a direct result from the noxious stimulations.

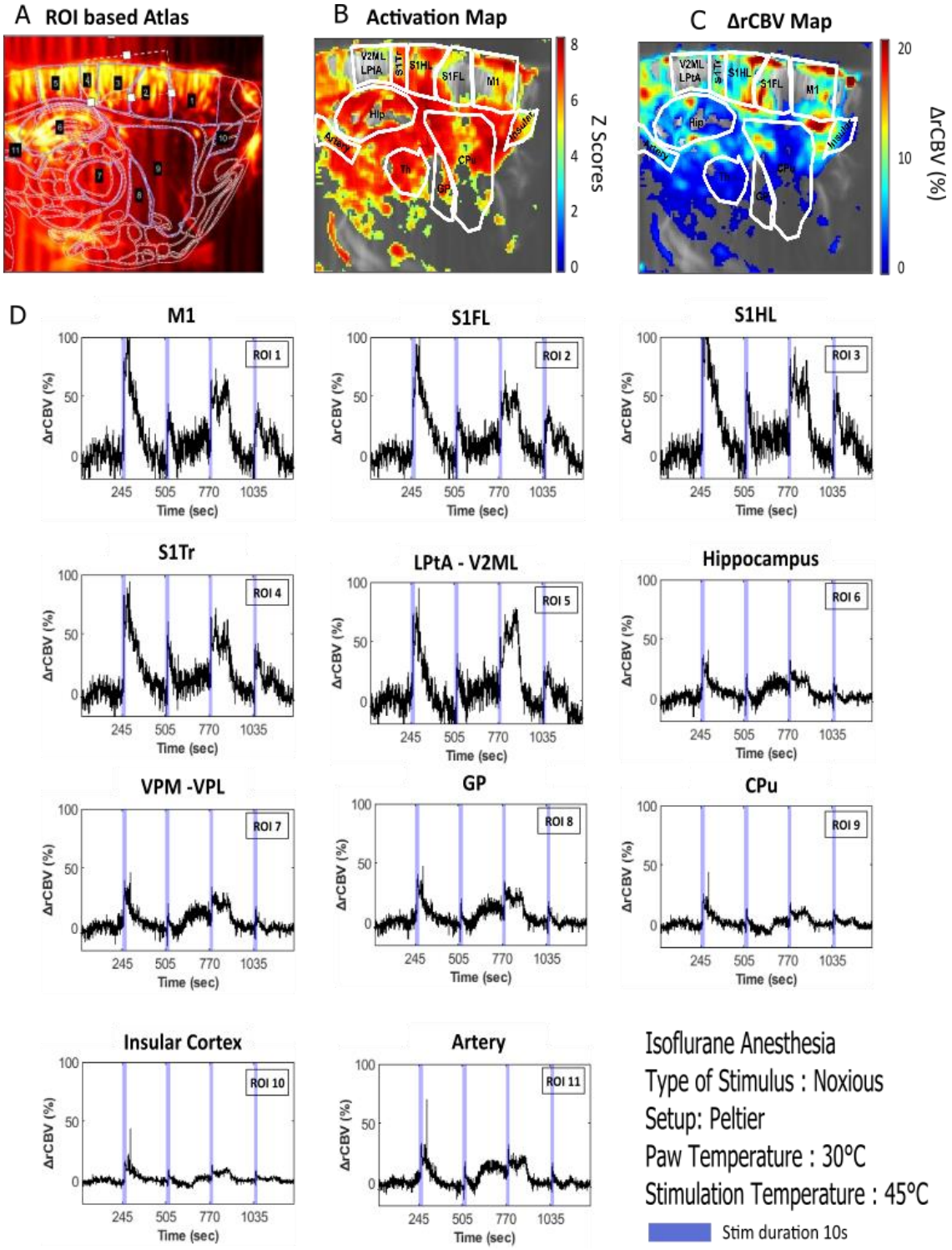

Figure 53: Long-lasting high CBV changes in ROIs could be an indirect consequence of increased arterial pressure induced by noxious stimulations. *A) Doppler image of the sagittal plane lateral at 3 mm with the corresponding mask of regions of interest delineated based on Paxinos atlas (Paxinos and Watson, 1997). B-C) Pixels that are significantly activated and the changes in CBV in the activated pixels represented by activation map and ΔrCBV map respectively. D) The regions of interests (1-11) and their corresponding changes in CBV. Blue window indicates the duration of stimulation. ROIs 1-5 have exceptionally high CBV increases especially during the first stimulation but decreases during subsequent stimulations. In the artery just after the first stimulation, there is a spike in CBV (>50%) and this could have contributed to the CBV changes in the other ROIs. S1HL: Primary Somatosensory Cortex Hind Limb part, S1FL: Primary Somatosensory Cortex Fore Limb part, S1Tr: Primary Somatosensory Cortex Trunk part, M1: Primary Motor Cortex, IC: Insular Cortex, LPtA-V2ML: Lateral parietal association cortex- Secondary visual cortex, mediolateral area, VPM-VPL: Ventral Posterolateral Thalamic Nucleus-Ventral Posteromedial Nucleus, GP: Globus Pallidus, CPu: Caudate Putamen.*

3.2.3. Biphasic response observed in the cingulate cortex

By applying two stimulations of 45°C with a duration of 10s using the Peltier while imaging on the sagittal plane lateral 0.5mm, mainly aiming to visualize the cingulate cortex, we observed a dual temporal response:

i. A fast and sharp immediate response (onset time: 2.4 sec, duration: 11.2 sec), but of high amplitude (50% CBV)
ii. A secondary delayed, but long-lasting hemodynamic response (onset time: 62 sec, duration: 109.6 sec), of very high amplitude (between 50% and 100% depending on the ROI)

The Z-sore map indicated that these changes are statistically significant in all regions analyzed, including the artery (*Figure 54* A-C). However, comparison on the amplitude of CBV changes over time (*Figure 54* D) indicates that the mid-cingulate cortex has the strongest response (100%), while the response of all other regions is approximately 40%. Because the response of these regions is of the same amplitude as the artery, we conclude that, as observed previously, the hemodynamic response is likely to be non-specific and is likely due to unspecific increased arterial pressure. We can conclude however, that a part of the mid-cingulate response is due to a specific hemodynamic response induced by noxious stimulations.

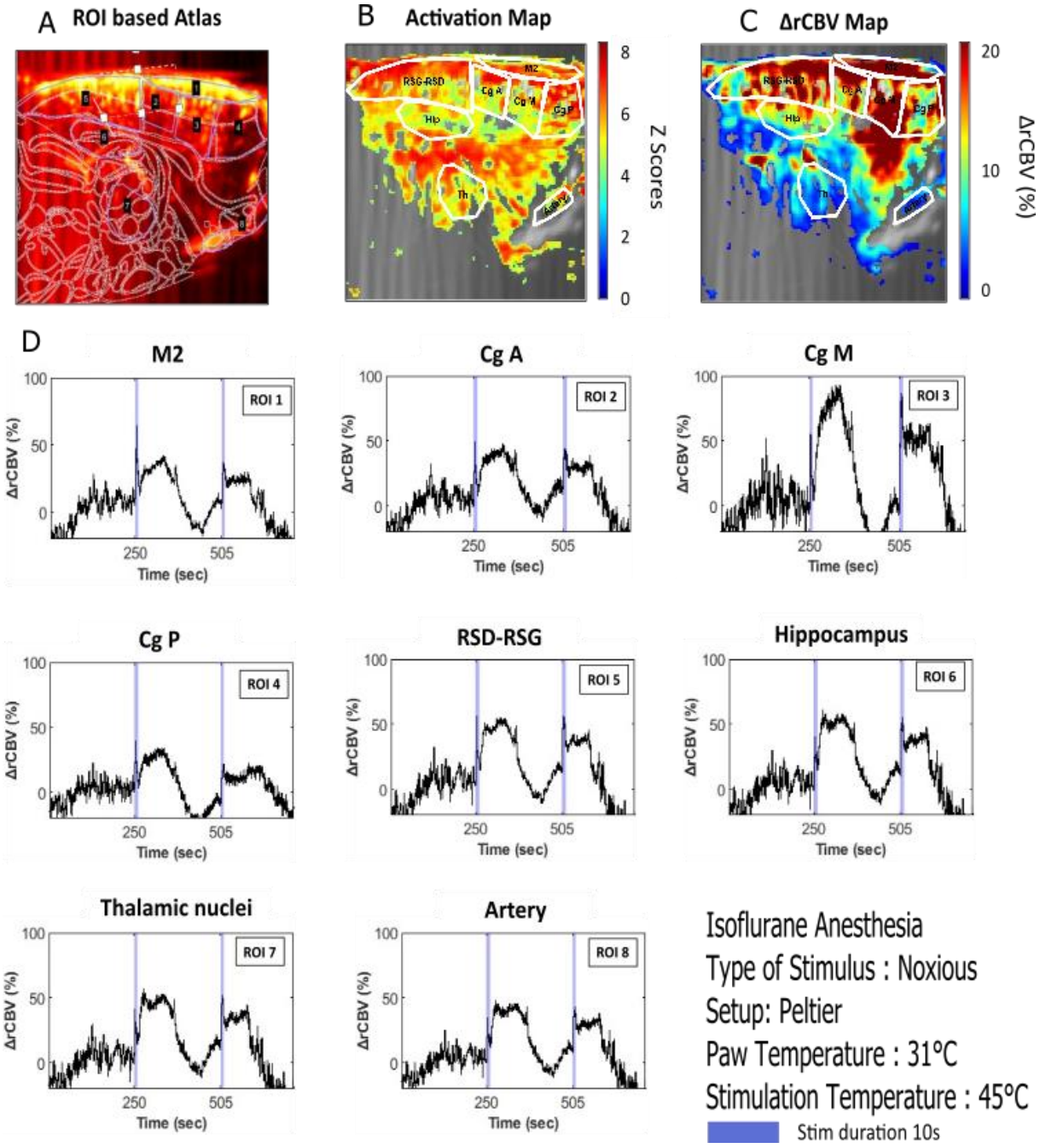

Figure 54: Dual response in cingulate cortex during noxious stimulation at 49°C using Peltier. *A-C) Doppler image of this plane with the corresponding mask of regions of interest delineated based on Paxinos atlas (Paxinos and Watson, 1997) and significantly activated pixels and the changes in CBV in them represented by activation map and ΔrCBV map respectively. It can be seen that there is a strong response and significantly activated regions show 20% increase in CBV in the activation map and ΔrCBV map respectively. D) Temporal CBV changes in ROIs. The stimulation (blue window) induced in all the ROIS a biphasic hemodynamic response: a sharp increase in the CBV at first, followed by another long-lasting peak. Medial cingulate has a much higher response (90%), than the anterior and posterior cingulate cortices. The amplitude of CBV increase observed in the artery is also observed in all other the ROIs, except mid cingulate. A: Anterior Cingulate, Cg M: Medial Cingulate, Cg P: Posterior Cingulate, M2: Secondary Motor Cortex, RSD-RSG: Retrosplenial Dysgranular Cortex-Retrosplenial Granular Cortex , Hippocampus , (Ventral Posterolateral thalamic Nucleus (VPL) - Ventral Posteromedial thalamic Nucleus (VPM).*

3.2.4. Noxious stimulation strongly activates S1HL and Cg

As a final step, we compared the promising results obtained under isoflurane anesthesia in the 2 sagittal planes: lateral at 0.5mm and 3mm. From the results of sagittal plane lateral at 3mm, we chose to compare 2 regions: S1HL (primary somatosensory cortex of hind limb, which is a brain region involved in thermal sensing) and CPu (caudate putamen, which is not known to be a part of thermal sensory circuit and therefore considered as control region).

Two stimulations (42° or 46°C ± 1°C) were compared at 2 different paw baseline temperatures 28°C and 31°C.

In the plane lateral 3mm, 46± 1°C produced a statistically significant higher CBV response in the S1HL and the CPu than 42± 1°C, indicating that the higher the temperature, higher the response. This effect was of higher amplitude in the S1HL than the CPu, substantiating that S1HL is more involved in thermal processing than the CPu.

Using a 2-way Anova with Bonferroni multiple comparisons test (in which p-values were adjusted as required), we tested the initial baseline paw temperature as a possible confounding effect of the magnitude of the noxious heat stimulation. For both S1HL and CPu, when the paw baseline temperature was at 28°C, the increase in the CBV response at 46°C vs 42°C was stronger than at 31°C (*Figure 55* A-B).

Using the plane imaging the cingulate cortex, we compared the responses of its three subdivisions: (anterior, medial and posterior) induced by stimulations at 42°C and 46°C, for baseline paw temperature at 31°C (*Figure 55* C). To understand the effect of stimulation temperatures and the differences of it among three subdivisions of cingulate cortex, we performed a 2-way Anova with Bonferroni multiple comparisons test (adjusted p-values), which concluded that stimulation at 46°C elicit a stronger CBV response in all 3 parts: anterior, posterior and medial cingulate cortex. The CBV responses between anterior, medial and posterior parts did not reveal any statistically significant difference. However, there is a tendency of a higher response in the mid cingulate during 46°C. This results strongly point in the direction of involvement of the cingulate cortex in thermal circuitry.

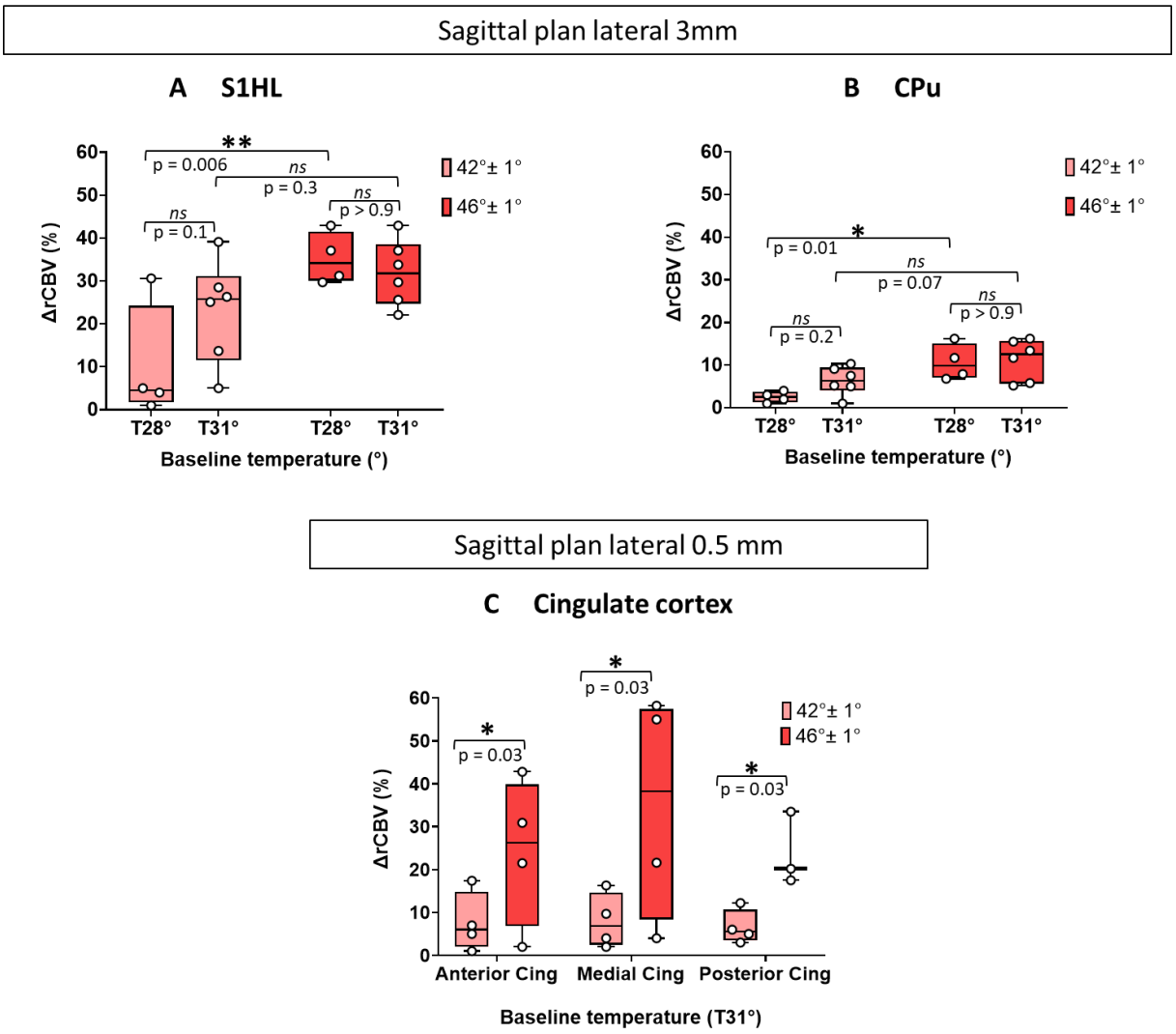

Figure 55: Quantification of the CBV changes induced by innocuous and noxious thermal stimulations. *A-B) Changes in the CBV in the S1HL and CPu at 2 different baseline temperatures. Higher CBV response was observed at 46°C ± 1°C than 42°C ± 1°C in both S1HL and CPu. The baseline paw temperature does not significantly modify the amplitude of evoked response (C) Changes in CBV in the anterior, medial, posterior cingulate cortex in the sagittal plane lateral at 0.5 mm. Significant changes in CBV are observed in all three subdivisions during the 46°C ± 1°C stimulation. 2-way Anova with Bonferroni multiple comparisons test in which p-values are adjusted as required.*

4. DISCUSSION

The quest for decrypting the underlying processes in thermal sensing started decades ago. Although there are a lot of studies explaining the role of supraspinal regions using fMRI and PET imaging, using fUS offered many advantages. In virtue of its high spatial and temporal resolution, functional activations could be precisely mapped. Its high sensitivity gave us the opportunity to map even the slightest hemodynamic responses.

Therefore, this study aimed at looking into the brain regions that are known to be involved in thermal processing (thalamic nuclei, S1, insula, cingulate) using fUS imaging. We were able to visualize the sagittal plane at 3mm that contains thalamic nuclei, S1 and insula and sagittal plane at 0.5mm that has the cingulate cortex.

4.1. Lack of activation induced by innocuous stimulation

Innocuous stimulation (39°C) did not induce hemodynamic response in all brain regions studied. Human thermal psychophysical studies have shown that between 30-34°C, neither cold nor warm sensations are felt. When temperature increases from the adaptive temperature, one starts feeling the warmth (Filingeri, 2016; Jones and Berris, 2002). From the perspective of our study, even though 39°C met the activation threshold for warm sensors (TRPM2, TRPV4, TRPV3), it did not elicit changes in the CBV. (Ran et al., 2016; Wang et al., 2018) previously showed that warmth and heat are coded in a graded strategy, implying, a much higher temperature produces a higher neuronal activation leading to CBV changes. Taken together, we drew the inference that, the neuronal activation induced by innocuous warm stimulations is not strong enough to induce an increased CBV that was detectable using fUS.

This observation agrees with previous studies that showed the hemodynamic response induced by either noxious or innocuous stimuli are much milder in the primary sensory cortex than the spinal cord, the relay of these information (He et al., 2015).

4.2. Effect of Ketamine-Domitor anesthesia

In our study, noxious heat stimulations (46°C) were shown to induce higher CBV response under isoflurane anesthesia in S1HL and the cingulate cortex. But interestingly we did not observe this effect under ketamine-domitor anesthesia. It has been shown that ketamine has NMDA (N-methyl-d-aspartate) antagonist properties and can have analgesic effects (Bennett, 2000; Franceschini et al., 2010; Franks and Lieb, 1994; Masamoto and Kanno, 2012; Yamamoto and Yaksh, 1992; You et al., 2021). The NMDA receptor is an ionotropic glutamate receptor that modulate most of the excitatory transmission in the CNS and is responsible for central and peripheral sensitization during pain states (Petrenko et al., 2003). Structures that are associated to nociception such as supraspinal circuitry, dorsal horn of the spinal cord and primary afferents have a strong presence of NMDA receptors and its subtypes: commonly called GluN1, GluN2A, GluN2B, GluN2C, and GluN2D but also called NR1, NR2A, B, C, D (Sleigh, 2014). Ketamine induces the blockade of the GluN2B/NR2B NMDA receptors in the supraspinal circuitry could lead to the analgesic effects and could explain the lack of activation observed during noxious stimulations.

It is also worthwhile to notice that glutamate receptor is a major neuronal contributor in the neurovascular coupling. Indeed, cortical excitatory pyramidal neurons or interneurons release vasodilator substances (such as prostaglandin (pyramidal neurons) and Nitric Oxide – Vasoactive Intestinal Peptide (in the case of interneurons)) in an NMDA-receptor dependent mechanism (Cauli, 2010). Blockade of glutamate receptors by ketamine thereby implies a disruption of these mechanisms and a reduction in the neurovascular coupling leading to diminished activations patterns observed using fUS imaging.

4.3. Brain areas activated by noxious heat

The sharp and transient response in S1 during noxious stimulations reaffirms its role in thermal sensing which has been widely studied in thermal processing. The primary somatosensory cortex is crucial to form a thermal perception (Becerra et al., 1999; Chatt and Kenshalo, 1977; Egan et al., 2005; Hellon et al., 1973b; Landgren, 1957b; Milenkovic et al., 2014; Moulton et al., 2012; Tsuboi et al., 1993). Rats with S1 and S2 lesions (Finger and Frommer, 1970; Porter et al., 1993) were reported to have failed temperature discrimination tasks. S1 also processes nociceptive signals that are

transmitted along ascending pathways. (Singh et al., 2020) recently suggested that there could be a S1 → ACC projection to integrate the sensory and affective nociceptive signal.

The cingulate cortex: anterior, mid, posterior parts are typically activated during nociceptive processing and are responsible for affective responses (Devinsky et al., 1995; Gasquoine, 2013; Hoffman et al., 2004; Hutchison et al., 1999; Iwata et al., 2005; Nevian, 2017; Ploner et al., 2002; Vogt et al., 1993, 1996; Vogt, n.d.; Xiao et al., 2021; Xiao and Zhang, 2018). Among the subparts, the anterior cingulate is widely studied in regard to pain processing and emotion. The subgenual part of ACC is more responsible for autonomic control and can be designated as the region that processes emotions (Vogt, 2005).The posterior part of ACC has been shown to be activated due to pain in a MEG study and is often associated to the 'suffering' component in nociceptive experiences. (Craig et al., 1996) studied activation in brain using PET under 5 conditions: cool (20°C), warm (40°C), noxious cold (5°C), and noxious hot (47°C) stimuli and thermal grill. Anterior cingulate cortex and insular cortex are very responsive to noxious heat and cold. (Vogt et al., 1996) observed that the cerebral blood flow increased when noxious heat was applied to back of the hand of human subjects especially in posterior ACC and mid cingulate cortex. It has been suggested that these regions encode the intensity of nociceptive inputs(Coghill et al., 1999; Derbyshire et al., 1997). Furthermore, (Vogt, 2005) reinstates that ACC (anterior cingulate cortex) and MCC (mid cingulate cortex) are activated during acute noxious stimulation and suggests that the highest density of nociceptive afferents is to the aMCC (anterior midcingulate cortex). In our study, the increase in CBV in the mid cingulate cortex during noxious stimulation is in agreement with previous studies.

A large body of studies have showed that insular cortex is crucial for thermal discrimination, as well as pain perception (Becerra et al., 2011; Birklein et al., 2005; Craig et al., 2000; Gogolla et al., 2014; Lu et al., 2016; Nagashima et al., 2018; Peltz et al., 2011; Penfield and Faulk, 1955; Rodgers et al., 2008; Wager et al., 2013). While the anterior IC has been commonly associated with emotional aspects, posterior IC is associated with sensory discriminative aspects. In our study, we identified that there were no significant CBV responses that were specific to the activation of insular cortex, but there were non-specific CBV increase due to increase in blood pressure. The lack

of activation contrasts with the observations with previous studies. One possible explanation for such discrepancies, is the fact that we only imaged a part of the insula and as the somatotopy of the insula has not been characterized in rodents, we may have not imaged the part dedicated to the hind paw.

Anatomical and topographical integration of S1 and M1 has been of interest in sensorimotor studies. (Nandakumar et al., 2021) recently investigated how the S1HL plays a role in trunk stabilization using electrophysiological mapping and strongly advocated that there are significant interactions and somatosensory integration between trunk and hindlimb. They observed that the S1Tr and M1Tr (primary somatosensory and motor cortex of trunk) receives incoming information, especially from hindlimb. This integration is often stronger between the hindlimb and trunk rather than forelimb and trunk. In this study, we observed co-activation of S1HL and S1Tr during noxious stimulation of hind paw, which could be a consequence the integration of the thermal input between these regions and the overlap between S1Tr and S1HL (*Figure 56*).

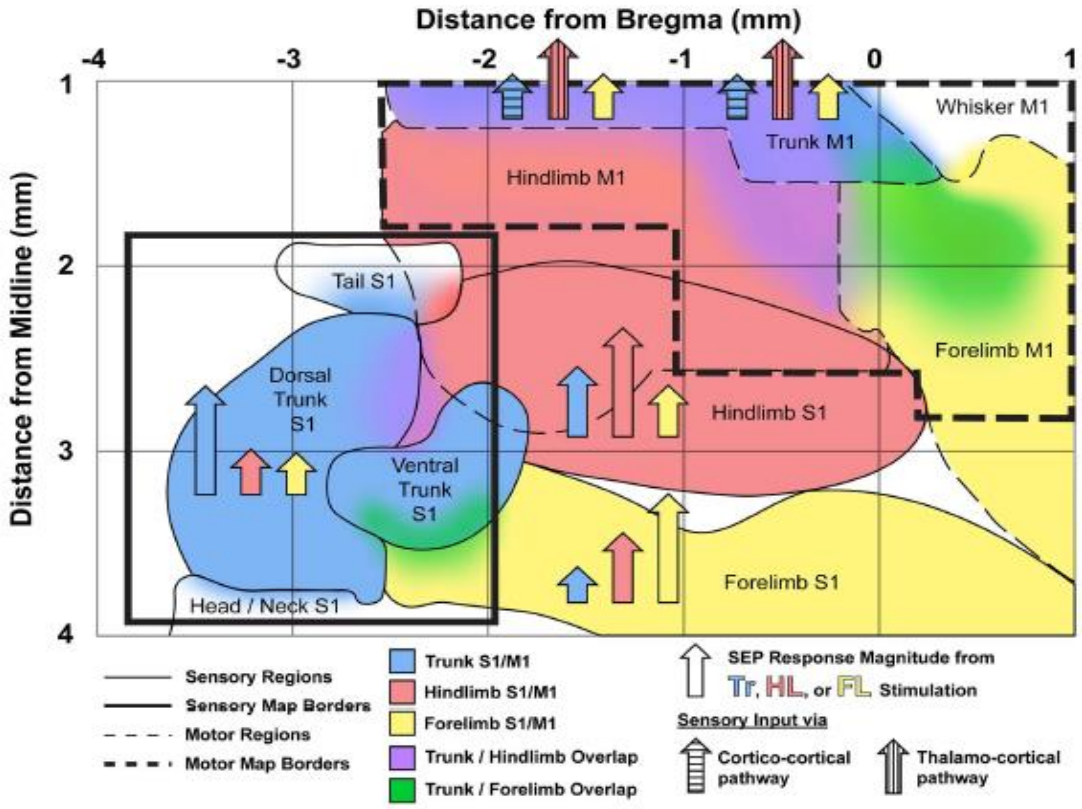

Figure 56: Summary of somatosensory overlap. *Illustration shown by (Nandakumar et al., 2021) indicates that the trunk has a greater overlap with hindlimb (violet) than forelimb (green).*

4.4. Blood Pressure Increase: A confounding factor in fUS imaging of peripheral noxious challenges

During the noxious stimulations under isoflurane, in some recordings, we observed large CBV increase in many brain areas. Interestingly, the team of Mathieu Piche previously showed that while neurovascular induced by peripheral noxious stimulation is tightly coupled in the spinal cord (Piché et al., 2017), it is not the case at the level of the primary sensory cortex (Jeffrey-Gauthier et al., 2013; Paquette et al., 2019b, 2019a). Indeed, (Jeffrey-Gauthier et al., 2013) performed electrical stimulation of hind paw of rats and measurement of cortical (S1) blood flow and local field potential (LFP) recordings. They monitored simultaneously the mean arterial pressure (MAP) changes using a cannula inserted into the right axillary artery and connected to a pressure transducer. The CBF intensity progressively increased with the stimulation intensity, although LFP recordings did not follow this pattern. MAP was significantly increased by these stimulations (*Figure 57*). These findings suggest that noxious stimulations and the evoked blood pressure changes may alter neurovascular coupling.

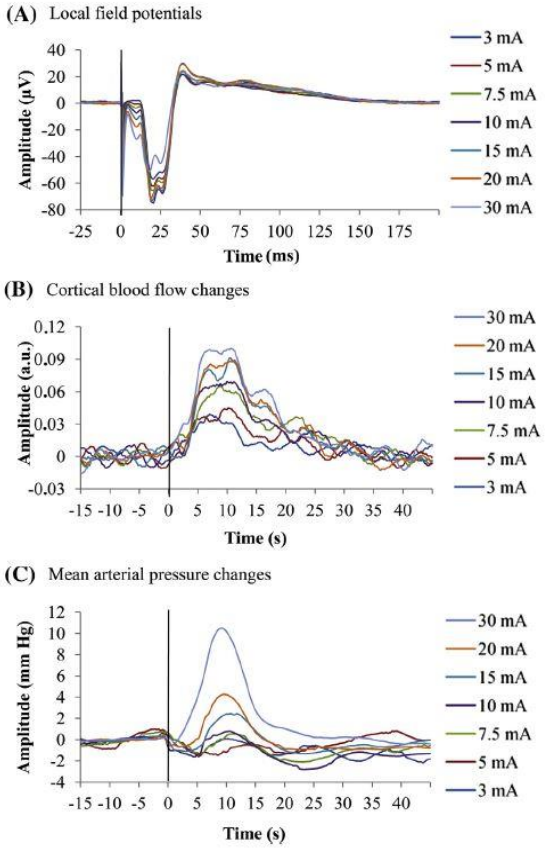

Figure 57: MAP changes during electrical stimulation of hind paw of a rat using intensities from 3mA to 30m. *(A) LFP recordings, (B) CBF changes, and (C) MAP changes. The line at 0 is the starting of the stimulation(10s) (Jeffrey-Gauthier et al., 2013).*

Following these observations, and due to the large changes of CBV induced by noxious stimulations in our experiments, we wondered if a part of this response might be due to the autonomous effect described by M. Piche's team. We measured the variation of CBV in an artery present on our imaging plane and observed a >50% increase, suggesting an increase in the arterial blood pressure induced by the noxious stimulation. This quantification was generalized to all our acquisitions and this helped us to quantify the proportion of CBV changes that is only due to the increased MAP. In the cingulate cortex, the stimulation specific CBV increase was limited to the mid cingulate, whereas all the other regions have an unspecific CBV increase due to the increased arterial blood pressure. On the other hand, in the primary somatosensory and motor cortices, we observed that only 50% increase was contributed by the high arterial blood pressure.

5. CONCLUSION

The investigation of thermal coding in rats concluded that the type of anesthesia used in thermal experiments is critical. The first approach using ketamine-domitor anesthesia posed significant challenges. The interference from blood pressure changes in the artery during nociceptive stimulations also posed a problem. Under isoflurane anesthesia, we were able to identify and quantify the specific activation of S1 and mid cingulate in response to noxious heat stimulations. Although insular cortex is a crucial part of thermosensation circuitry, due to the limitation in imaging the laterally situated insular cortex, we imaged only a part of insula. Therefore, at this point, in our study, it can be concluded that S1 and mid cingulate are major players in noxious heat sensing.

The above-mentioned findings inspired us to re-evaluate our goals which led us to design a fUS imaging study in awake animals, as explained in the next chapter (Chapter 4).

CHAPTER 4:

AWAKE fUS IMAGING OF THERMAL CODING IN MOUSE BRAIN

1. INTRODUCTION

In order to overcome the limitations encountered in the investigation of thermal coding in anesthetized rats (see Chapter 3), the goal was redirected to study thermal coding in a refined experimental design. To avoid the adverse effect of anesthesia, it was imperative to choose awake fUS imaging. However, conducting a longitudinal study using rats has disadvantages. Preparing the rat skull for chronic imaging is an invasive procedure and the image quality deteriorates over time due to bone regeneration. Therefore, due to ethical and effectiveness reasons, choosing to investigate the mouse thermal system was a reasonable choice. Furthermore, there has been successful previous studies from our laboratory that showed the effectiveness feasibility of transcranial fUS imaging in mice for several weeks (Rabut et al., 2020; Tiran et al., 2017). Therefore, we decided to investigate non-noxious or innocuous thermal coding in awake and freely moving mice, using minimally invasive transcranial fUS imaging.

The overall goal, from a functional connectivity point of view, was to understand the interplay between different brain regions during thermosensation using fUS imaging. In simpler words, we set out to find which brain regions take part in the thermal sensory process and how strongly they are connected or disconnected with each other.

As extensively discussed in chapter 1, the thermosensory circuit can be classified into two: periphery to spinal cord and spinal cord to brain. From existing findings, we can conclude that the spinal cord forms the primary contact with the thalamus via the spino-thalamic tract which is then projected to the cortical regions via the thalamo-cortical pathway (*Figure 58*). The symbiosis of both these pathways gives rise to thermal perception. Additionally, there is another pathway for thermoregulation that extends to the lateral parabrachial nucleus (LPB) and then to the preoptic area (POA) of the hypothalamus.

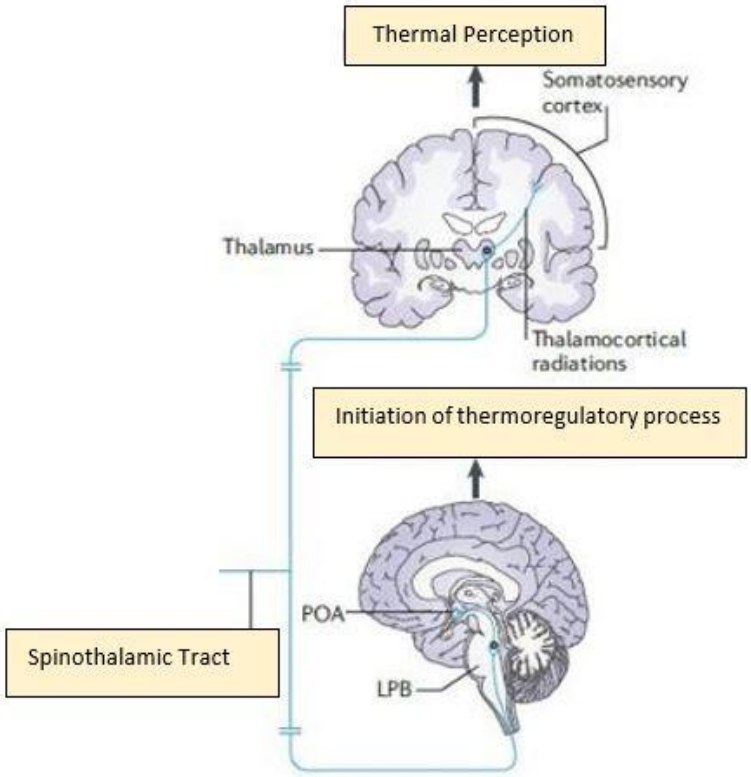

Figure 58: Supraspinal thermosensory circuit. *Spinothalamic tract projects to thalamus, thalamocortical projections to somatosensory and insular cortices. Thermoregulatory circuit involving lateral parabrachial nucleus (LPB) and preoptic area (POA) (Vriens et al., 2014)*

Our main focus was to study the supraspinal thermosensory regions. Here is a short summary of our current knowledge on the brain regions involved in thermal sensory processes:

i. The primary and secondary somatosensory cortex is essential for thermosensation and this has been shown in humans and other models. The integration of the thermal signals take place at the cortical circuitry.
ii. Insular cortex and cingulate cortex have been found to drive the behavioral response to thermal pleasantness/unpleasantness.
iii. Lateral parabrachial nucleus (LPB) and preoptic area (POA) of the hypothalamus plays a major role in thermoregulation.

Therefore, our choice of brain regions in this study included: primary somatosensory cortex of hind limb (S1HL), primary and secondary motor cortex (M1 and M2), cingulate cortex (Cg) and hypothalamus (HyTh).

The capability of fUS imaging in awake and freely moving mouse enabled us to image the aforementioned brain regions in a single plane, while the mouse spends time on a metal surface at warm, neutral or cold temperatures and temperature ramps. It allowed the measurement of cerebral blood volume with unmatchable spatial (200µm) and temporal (20ms) resolution with high sensitivity. Thermal stimulations are bound to increase neuronal activations in the region of interests and by the phenomenon of neurovascular coupling, cerebral blood volume changes can be measured and forms the fUS image. By measuring FC using fUS imaging, we investigated how somato-motor, cingulate and hypothalamic regions are involved in thermal processing.

2. QUESTIONS TO BE ADDRESSED

Probing thermosensation in awake and freely moving mouse brain, using fUS imaging, is expected to break new grounds. The first and basic question we wanted to address was how FC is changing during sustained application of constant temperatures. We then moved on to address if FC is different during temperature ramps in the heat and cold. To go into more depth, we also wanted to find out:

- How does the rate of change of temperature influence thermal coding?
- How different is the coding of fast and slow ramps from the fixed temperature?
- How are the transient properties of dynamic FC varying during the thermal conditions ?

3. MATERIAL AND METHODS

3.1. ANIMALS

The experiments were conducted in compliance with the European Community Council Directive of 22 September 2010 (010/63/UE) and the local ethics committee (Comité d'éthique en matière d'expérimentation animale number 59, "Paris Centre et Sud," project 2018-05). C57Bl/6 male mice from Janvier Labs were used for all the experiments.

The fixed temperature experiments and the temperature ramp experiments were conducted in different sets of mice. Two batches of N=6 (total N=12) mice were used in which, the first batch (N=6) was used to apply the fixed temperature and second set was used for the fast or slow ramp experiments. Mice were 7 weeks old when they arrived in the laboratory and the experiments typically lasted for 4-6 weeks. Animals were given utmost care and were housed at a constant temperature of 22°C with an alternating 12-hour light/dark cycle. They received food and water ad libitum. The number of animals in this project was kept to the necessary minimum by reimaging and reusing them. This was achieved the use of the minimally invasive transcranial fUS imaging.

3.2. SURGICAL IMPLANTATION OF METAL PLATE

Approximately one week after their arrival (*Figure 59* A) the mice underwent surgery for the implantation of the metal plate (Tiran et al., 2017). A mixture of ketamine (100 mg/kg) and medetomidine (1 mg/kg) was administered intraperitoneally and then the mouse was placed on a stereotaxic frame. Importantly, paw withdrawal reflex was checked to make sure of the anesthesia. The skull bone was then exposed after removing the skin and periosteum. The metal plate was fixed on the skull using Superbond C&B (Sun Medical, USA) and small screws, minimally drilled in the skull. The field of interest was approximately 5mm between the Bregma and Lambda points.

The surgery took 45 minutes to 1 hour to complete. Subcutaneous injection of atipamezole (1 mg/kg, Antisedan) and Metacam (5 mg/kg/day) were administered to reverse the anesthesia and prevent postsurgical pain, respectively. A protective cap was mounted on the metal plate using the magnets to guard the skull and to keep the field of imaging intact for 4-6 weeks (Bertolo et al., 2021). Altogether, the metal plate and the cap did not interfere with the daily normal activity of the mice. After a recovery period of 3 days, the mice proceeded towards the habituation phase.

3.3. HABITUATION

After recovering from the metal plate implantation, the mice were subjected to an extensive handling and habituation protocol (*Figure 59* A). To make sure that the mice were not under any stress during the experiment, it was crucial that they are at ease with the user and the setup. They were initially handled by the user and then exposed to the Bioseb HC Plate. Their interaction time in the Bioseb apparatus was gradually increased in the order of 15 minutes, 30 minutes, 1 hour, 1 hour 30 minutes up to 2 hours. Depending on the level of habituation of each mouse, the user practiced the removal of protective cap, cleaning of skull using saline and application of echographic gel without anesthesia by gently restricting the head movement. After each session, they received a reward. The process lasted 10-12 days and depending upon the comfort level of the mice, we then proceeded to the imaging phase.

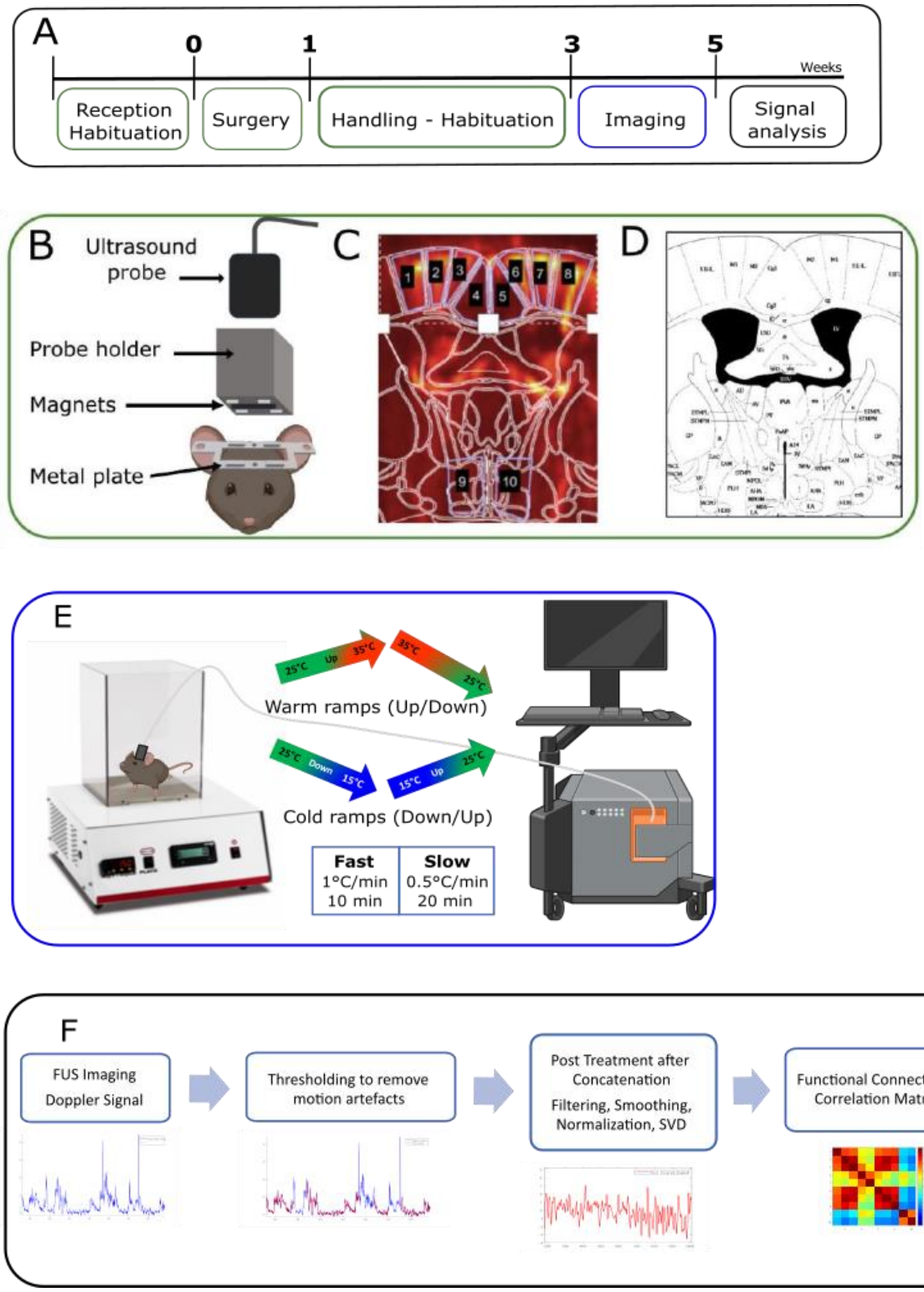

Figure 59: Experimental Timeline, Design and Analysis. *(A) The total duration of the experiments lasted 5-6 weeks. One week after the arrival in the lab, mice underwent surgery to implant the metal plates. After recovery, user followed an extensive handling and habituation protocol for 2 weeks. Imaging was then performed for the next 2 weeks or more depending on the quality of the skull and well-being of the mice. (B) Schematic showing the metal plate, probe holder and fUS probe. (C) Doppler image of the plane of interest Bregma -0.34 mm. (D) Paxinos atlas corresponding to the same plane (Paxinos and Franklin, 2011). (E. Experimental setup with Bioseb and fUS Imaging (Iconeus). Mice were subjected to fixed and ramp temperatures in the warm and cold range at fast and slow pace. (F) The doppler signal obtained from imaging underwent thresholding to remove motion artefacts and was subjected to filtering, smoothing, normalization and SVD. The clean doppler was then used for functional connectivity analysis.*

3.4. EXPERIMENTAL PARADIGM

The global aim was to understand the interplay between different regions in the mouse brain during innocuous thermosensation using awake fUS imaging. As intrinsic functional connectivity was shown to measure the activity and functionality of the brain networks, we postulated that FC could differ during exposure to cold, warm and neutral temperature range and during changes of temperature. Therefore, the experimental design revolved around a few core ideas. We wanted to incorporate both fixed and ramp temperature in the study. In the ramp temperatures, we wanted to study a fast and slow rate of temperature change.

Subjecting the awake mice to thermal stimulations pose certain challenges. Motion artifacts from free movement of mice can alter the quality of the ultrasound signals and in the initial phase, we made efforts to prevent these artifacts. In preliminary experiments, we established the range of temperatures in which did not cause discomfort for the animals. Combining the observations of the animal's natural behavior (grooming, exploration, urination and freezing) and measurements of naturally emitted ultrasound vocalizations, we observed that the range of temperature 15°C to 35°C was optimal. Even though the temperature is comfortable, motion artefacts due to head movements, grooming, licking etc. have to be later removed during the post processing (Detailed explanation in Section 4.1).

We used the Bioseb 'Hot-Cold Plate' to conduct the experiments (*Figure 59* E). The metal floor of the BioSeb equipment can be kept at a fixed temperature or the temperature can be increased or decreased at different rates. The standard range of temperature for the Hot-Cold plate is -2°C to 55°C. It has a transparent enclosure, a real time temperature display and a timer.

i. Fixed Temperature

A constant temperature of either **15°C** or **25°C** or **35°C** was applied for 20 minutes. Experiments at these temperatures were performed on separate days as shown below and was repeated once (*Figure 60*). At the beginning of every session the floor is held at 25°C. The Bioseb can change to 15 or 35°C, from 25°C within seconds.

D1	D2	D3	D4	D5	D6
25°C	15°C	35°C	25°C	15°C	35°C

Figure 60: Fixed Temperatures in the cold, neutral and warm range. *The mice are exposed to one temperature per day and only repeated once.*

ii. Varying Temperature at fast or slow pace

Varying Temperature at fast or slow pace – Temperature ramps were either going in the warm (UP: 25°C to 35°C) and DOWN (35°C to 25°C); or in the cold going: DOWN (25°C to 15 °C) and UP (15°C to 25°C) (*Figure 59* E). In order to determine the effect of speed of temperature change, these ramps were performed at 2 different paces: either a slow rate of 0.5°C per minute (each ramp lasted 20 minutes) and a fast ramp at the rate of 1°C per minute (10 minutes/ ramp) were chosen. The ramps were designed to start and end at 25°C. The mice were reimaged at least 3 times. In order to avoid any bias due to the order of these ramps, the order of ramps was randomized (*Figure 61*). The nomenclature chosen is the following:

Cold Ramps:

- **FCD**: Fast Cool Down: 25°C to 15 °C (- 1°C per minute)
- **FCU**: Fast Cool Up: 15°C to 25° (+ 1°C per minute)

- **SCD**: Slow Cool Down: 25°C to 15 °C (+ 0.5°C per minute)
- **SCU**: Slow Cool Up: 15°C to 25°C (- 0.5°C per minute)

Warm Ramps

- **FWU**: Fast Warm Up: 25°C to 35°C (+1°C per minute)
- **FWD**: Fast Warm Down: 35°C to 25°C (-1°C per minute)

- **SWU**: Slow Warm Up: 25°C to 35°C (+0.5°C per minute)
- **SWD**: Slow Warm Down: 35°C to 25°C (- 0.5°C per minute)

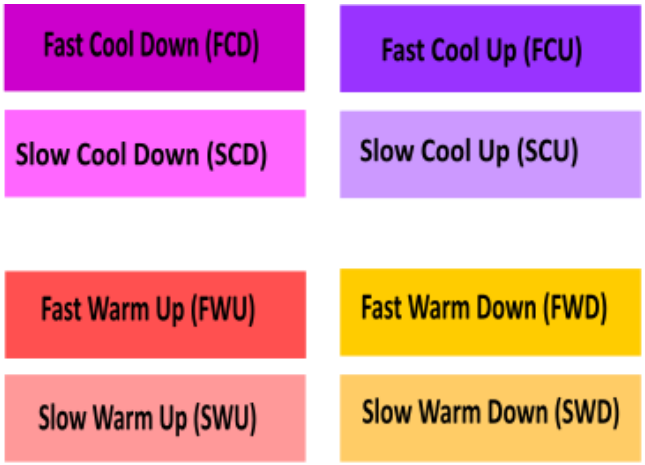

D1	D2	D3	D4	D5	D6
WU, WD, CD, CU	WU, WD, CD, CU	CD, CU, WU, WD	WU, WD, CD, CU	CD, CU, WU, WD	WU, WD, CD, CU

Figure 61: Cold and warm ramps at fast and slow pace. *Each day one mouse underwent fUS imaging during 4 ramps in the order [WU, WD, CD, CU] or [CD,CU,WU,WD] either in the fast or slow pace. WU/WD: Warm Up/ Warm Down, CC/CU: Cool Down/ Cool Up*

3.5. TRANSCRANIAL AWAKE fUS IMAGING

Three days prior to the first imaging session, the mice were anesthetized with isoflurane (1.5%). The respective probe holders were magnetically clipped to the metal plate (*Figure 59* B). Real time transcranial doppler images were acquired using NeuroScan and the position of the probe was adjusted to select the Bregma -0.34 mm plane. The skull is then thoroughly inspected and cleaned to avoid any infections. The mice are put back in their cages and are imaged only after 3 days to avoid any interference from the isoflurane anesthesia.

Unlike the previous awake imaging protocols explained in (Tiran et al., 2017), mice were not anaesthetized to prepare the skull during the imaging phase (See Section 3.3). They were trained and habituated for detaching the protective cap, cleaning the skill with saline and application of echographic gel with minimal force. They were then gently introduced into the Bioseb apparatus and the probe holder was attached to the implanted metal frame using the magnets on both pieces. Experiments began shortly after.

Real time vascular images were obtained by ultrafast compound doppler imaging technique (Mace E. et al., 2011; Deffieux et al., 2018). 11 successive tilted plane waves (-10° to +10 °) which are 2° apart were used for insonification. Each image was obtained from 200 compounded frames acquired at the rate of 500Hz frame rate at a 5.5 kHz pulse repetition frequency. Tissue signal was isolated from the cerebral blood volume signal by using a SVD clutter filter (Demené et al., 2015) to obtain a Power Doppler image.

3.6. DOPPLER SIGNAL ANALYSIS

3.6.1. Removal of motion artefacts

Imaging in awake mice meant that it was necessary to remove motion artefacts due to head movements and behavioral movements such as grooming. We followed the same analysis as previously described in (Rabut et al., 2020) by first using a singular value decomposition (SVD) clutter filter to separate blood motion from tissue motion and then by thresholding tissue motion and doppler signal to find the frames with motion artefacts. The thresholds are chosen by carefully examining the tissue motion signal and the threshold that removes most of the motion artefacts is chosen. An example of two different thresholding values are shown in (*Figure 62*). While keeping the clean frames, we made sure they are successive bits of at least 50 time points.

The concatenated clean frames were treated using a low pass filter at 0.1 Hz to extract the resting state frequencies. A polynomial fit of order 3 was applied to detrend the signal and finally a singular value decomposition of the data was performed before connectivity analysis (*Figure 59* F).

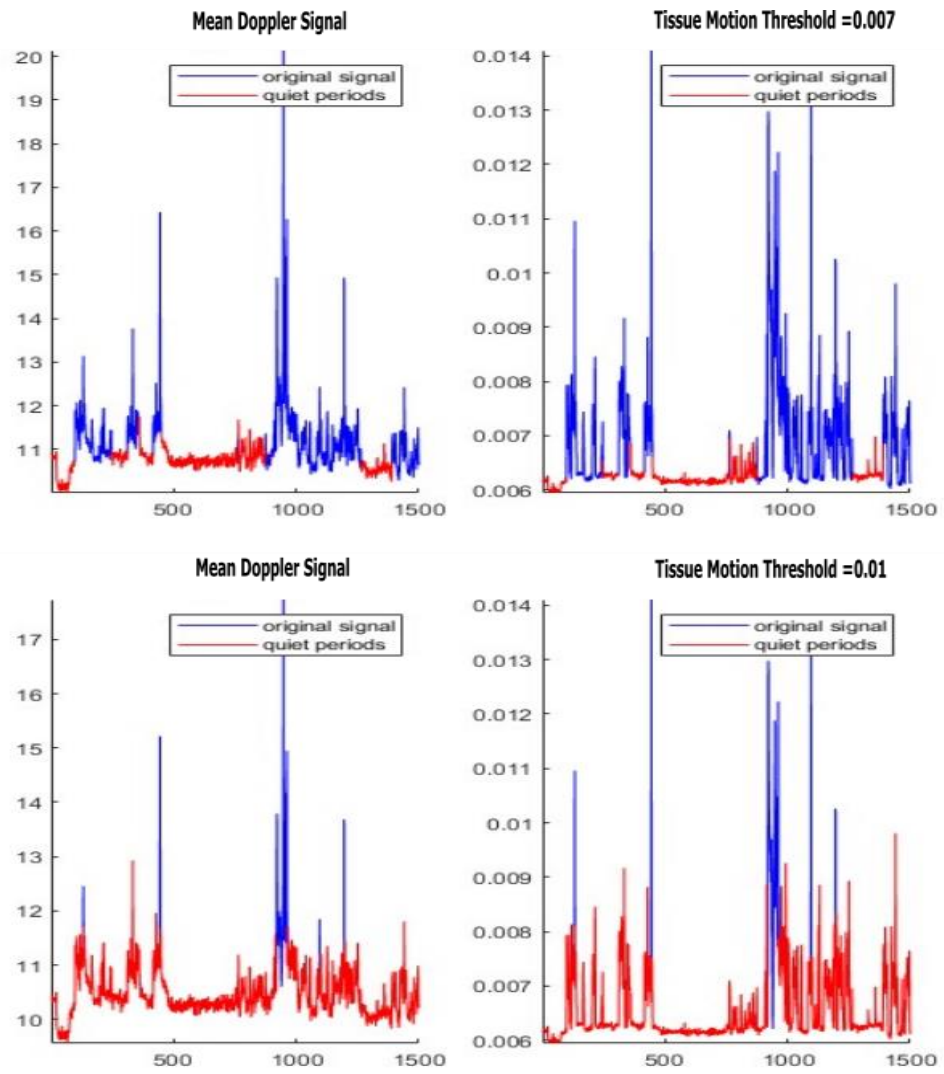

Figure 62: Tissue motion thresholds to remove motion artefacts. *An example of two different thresholds:0.007 and 0.01 resulting in a different number of clean timepoints.*

3.6.2. Stationary FC analysis

To understand the interaction between the brain regions during the temperature coding, we first did the stationary FC analysis. The functional connectivity of the following brain regions present in the imaging plane were first studied: Primary Somatosensory Hind Limb part, Primary and Secondary Motor, Cingulate and Hypothalamus (*Figure 59* B). This plane of imaging was chosen by the role of some of these regions in thermosensation and thermoregulation. The ROIs were defined based on the Paxinos Atlas (Paxinos, G and Franklin, 2012).

In order to study static functional connectivity during the thermal conditions, the post-treated time course of the CBV signal from the 10 ROIs (Fig 1B) were extracted. In simpler words, from each region of interest the temporal signal during the calm periods (without motion artefacts) is extracted. The Pearson correlation was computed between each ROIs, resulting in a 10 x10 matrix with the respective correlation coefficients. We then estimated the averaged correlation matrix for each thermal condition.

To compare different thermal conditions, the correlation coefficients were Fisher Transformed to normalize the distribution. In cases of normal distribution, Welch's test was performed; otherwise, the non-parametric Wilcoxon rank-sum test was performed. Finally, Benjamini–Hochberg false discovery rate correction for multiple comparisons was also done between the groups with $p < 0.05$.

3.6.3. Dynamic FC analysis

To understand the dynamic characteristics of brain networks as a response to thermal input, we utilized an unsupervised data grouping technique: k-means clustering algorithm using the L1 distance function as implemented in MATLAB. For instance, when we set k=4, the input data is grouped into 4 clusters. First of all, 4 centroids are randomly assigned. Distance of each input data point to the clusters is calculated and the one with minimal distance between them are grouped together. In the next step, 4 new centroids (mean of each group) are calculated. This iterative process is continued until it converges and data are grouped into 4 and the data points are distributed around its centroid.

From 92 fUS imaging sessions, the post-treated doppler timeseries for each ROIs (1-10) were extracted after the removal of artefacts, filtering, smoothing, normalization and SVD. This comprised of N=8 for 15°C, N=8 for 25°C, N=8 for 35°C, N=10 for FCD, N=10 for FCU, N=8 for SCD, N=6 for SCU, N=9 for FWU, N=9 for FWD, N=8 for SWU and N=8 for SWD. The time series data from all the 92 acquisitions were concatenated together to form one single time series

(10x 84499, where 10 is the number of ROIs and 84499 is the number of time points). To obtain a time resolved correlation matrix, Pearson correlation was computed at each timepoint between any two ROIs, yielding a 45 x 84499 matrix where 45 is the number of possible pairwise interactions.

The time resolved correlation matrix then undergoes an unsupervised learning of brain states for k=5,6,7 clusters. The clustering algorithm was repeated 500 times to avoid local-minima, with random initialization of centroid positions. Finally, each time point was assigned a cluster or a brain state resulting in a dynamic characterization of connectivity patterns.

The occurrence rate of each brain state was calculated for all conditions and the k=7, k=6 and k=5. Finally, in order to quantify the difference of occurrence rates between conditions, we performed a one-way ANOVA along with Benjamini–Hochberg false discovery rate correction for multiple comparisons with $p < 0.05$.

4. RESULTS

In order to decipher the FC alterations in brain networks, which is an indicator of dynamic changes in the brain, we developed an experimental setup, based on previously established protocol on awake and freely moving mice (Rabut et al., 2020). We adapted the protocol to apply plantar temperatures using the BioSeb HC plate during the imaging session (See Material and Methods, 3.4). From test experiments, it was concluded that the range from 25 to 35°C was most suitable for awake imaging and they did not cause any discomfort or aversive behavior. Therefore, the Bregma -0.34 mm plane was imaged for 20 minutes at 15°C, 25°C and 35°C. The experiments were designed in such a way that each mouse underwent only one of these temperature on a particular day.

After the acquisition of doppler images, motion artefacts were removed as described in Section 3.6.1 Removal Of Motion Artefacts. The clean doppler signal was then concatenated and underwent post treatment (filtering, smoothing, normalization and SVD). The time course of the final doppler signal is subjected to stationary FC analysis which is time-averaged of all the imaging sessions.

4.1. STATIONARY FC ANALYSIS

4.1.1. Fixed Temperatures: Cold and Warm Vs Neutral

The warm (35°C) and cold (15°C) temperatures were compared to neutral temperature (25°C) which also happens to be the mid-point of the temperature range.

First, we compared the cold to neutral temperature i.e., 15°C to 25°C. *Figure 63*(A-C) shows the stationary functional connectivity comparison between 25°C and 15°C and the significance matrix showing the ROI pairs that are significantly different between the groups. Strong and statistically significant changes in FC between these conditions were observed, with the largest number of changes for the cold temperature, where the FC of 19 pairs of ROI were statistically different (*Figure 63*D). Twelve of these couples of ROI concerned

areas of the somato-motor network (SMN), which showed to have a stronger connectivity at 15°C, than at 25°(*Figure 63* D).

The six other couples of ROI are areas between one ROI of the SMN and the hypothalamus (*Figure 63*D). Interestingly, in these couples, the FC was altered in the opposite direction: the FC was significantly decreased. One ROI pair shows the interaction between cingulate and hypothalamus: stronger connectivity at 15°C than 25°C.

Next, we compared the warm to neutral temperature i.e., 35°C to 25°C as shown in *Figure 64*(A-C). Even though there is a +/- 10°C difference in both warm and cold conditions, warm induced only mild changes in functional connectivity. A mere 6 ROI pairs showed statistically significant changes in FC. Two of these were pairs of the SMN, which displayed an increased FC when the animals were subjected to 35°C (*Figure 64*D). The five other pairs of ROI were areas between the SMN and the hypothalamus. There ROI pairs, on the other hand, showed the opposite effect: an increased FC when the animals experienced warm temperature compared to neutral (*Figure 64*D). Interestingly, unlike in the cold, there were no ROI pairs involving the cingulate region.

The stationary FC analysis of fixed temperatures led to the conclusion that cold invokes more FC alterations than warm by a stronger connectivity among the somato-motor and weakened connectivity between hypothalamus-somato-motor.

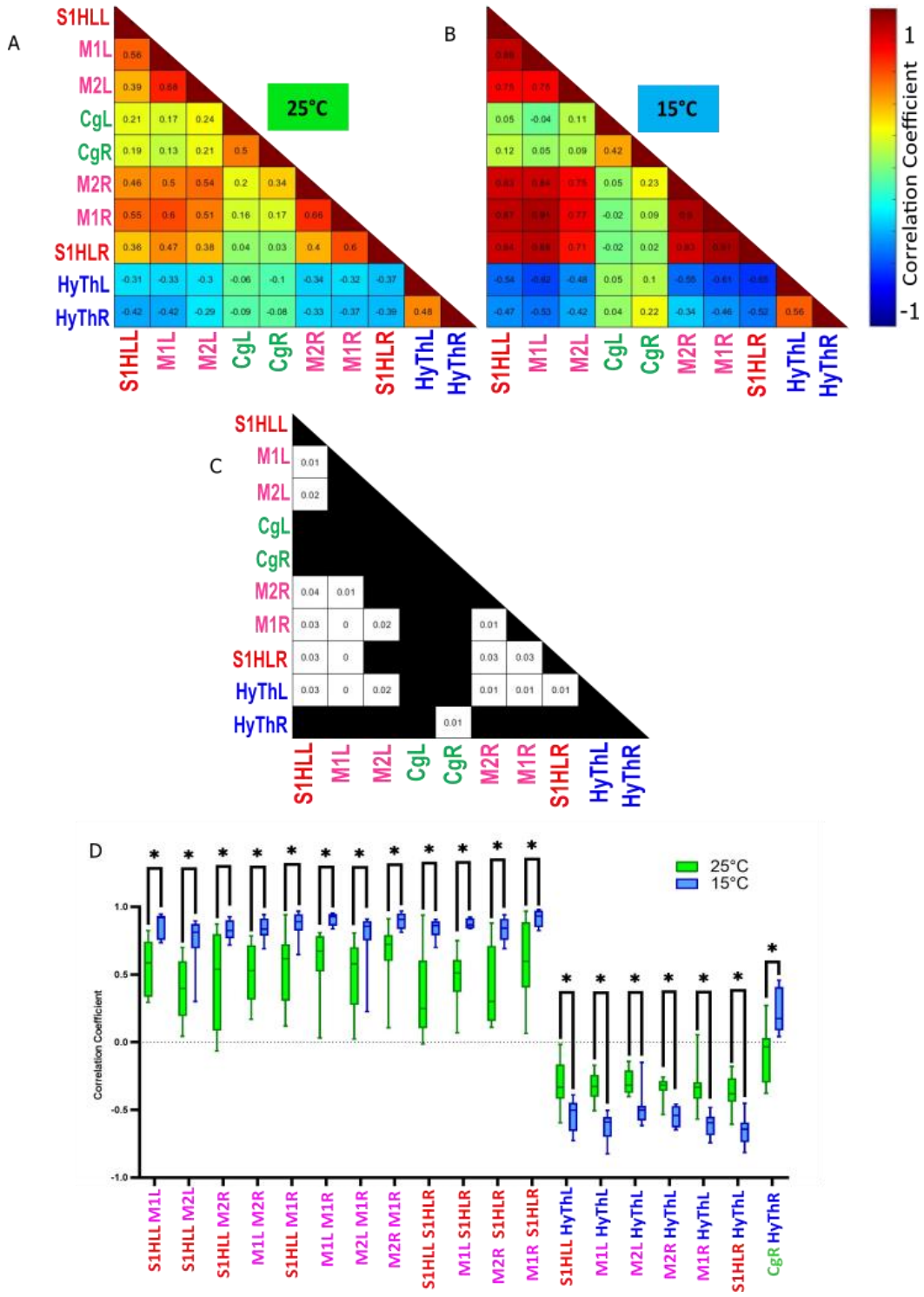

Figure 63: Functional connectivity comparison using correlation matrices between 15°C and 25°C show striking differences in cold (15°C). *(A) Averaged Pearson correlation matrix of N=8 imaging sessions at 25 °C. (B) Averaged Pearson correlation matrix of N=8 imaging sessions at 15°C. (C) Matrix indicating the ROI pairs with significant differences of 25°C with 15°C. The correlation coefficients of ROI pairs were Fisher transformed. In case of a normal distribution, a parametric Welsh test was performed and otherwise Wilcoxon rank-sum test was performed. Benjamini-Hochberg's correction for multiple comparisons was applied with a false discovery rate of 0.05. Pairs of ROIs with significant alterations between the two groups is indicated by the white squares with its corresponding p-values. (D) Boxplot representation of each ROI pair with a significant FC alteration between the groups 25°C (blue) Vs 15°C (green). *p < 0.05, **p < 0.01 and ***p < 0.001*

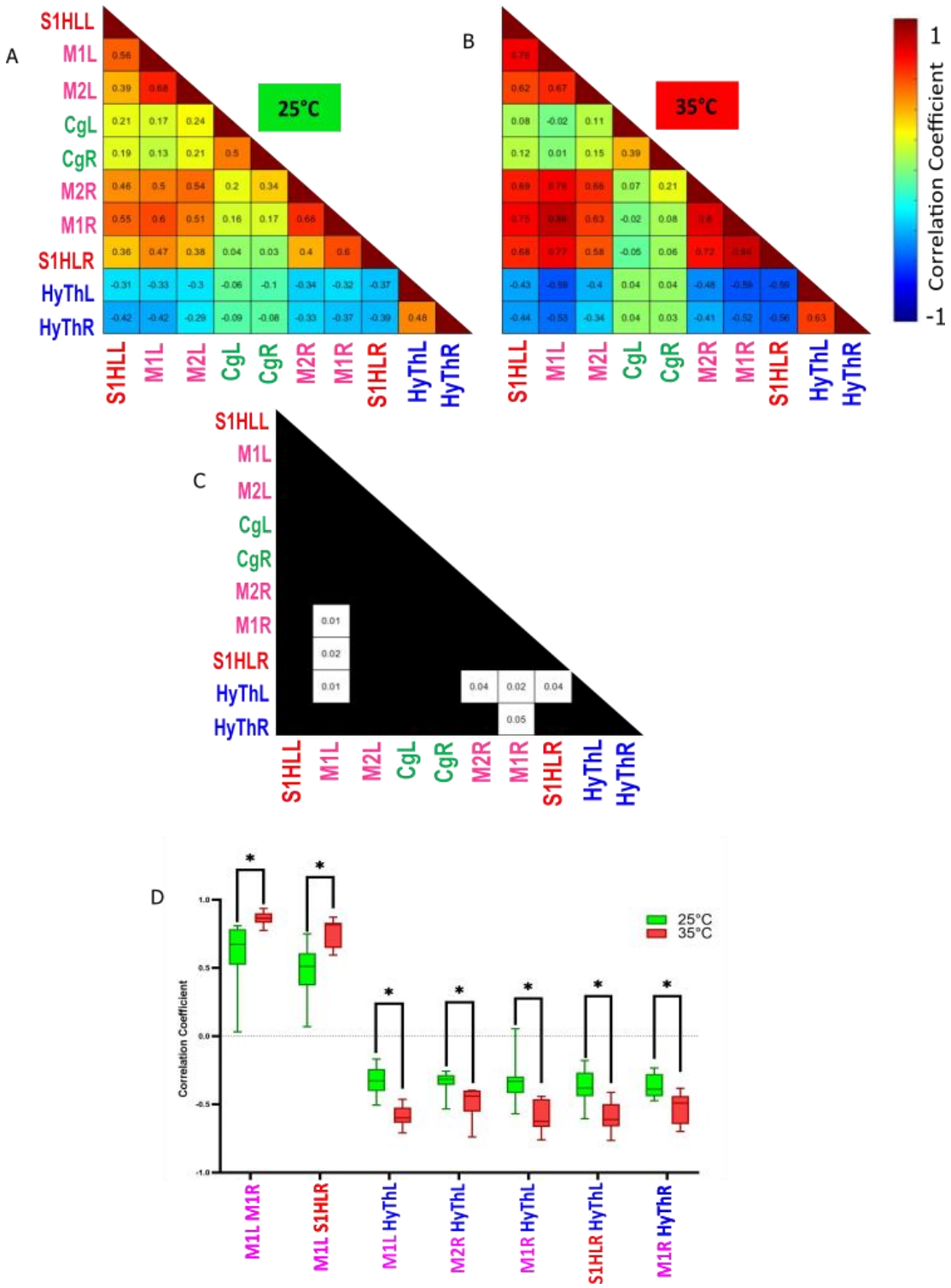

Figure 64: Functional connectivity comparison using correlation matrices between 35°C and 25°C show modest differences in warm (35°C). *(A) Averaged Pearson correlation matrix of N=8 imaging sessions at 25 °C. (B) Averaged Pearson correlation matrix of N=8 imaging sessions at 35 °C. (C) Matrix indicating the pairs of ROI with significant differences between 25°C and 35°C. The correlation coefficient of each pair of ROI was Fisher transformed. In case of a normal distribution, a parametric Welsh test was performed and otherwise Wilcoxon rank-sum test was performed. Benjamini-Hochberg's correction for multiple comparisons was applied with a false discovery rate of 0.05. Pairs of ROIs with significant alterations between any two groups is indicated by the white squares with its corresponding p-values. (D) Boxplot representation of each ROI pair with a significant FC alteration between the groups 25°C (green) Vs 35°C (red). *p < 0.05, **p < 0.01 and ***p < 0.001*

4.1.2. Cold Ramps Vs Fixed Cold and Neutral Temperature

To decipher the neural mechanisms underlying thermal encoding of temperature ramps, we compared each ramp to its corresponding fixed temperature. For instance, temperature ramps cold ramps up and down (CU: 25°C to 15 °C and CD: 15°C to 25 °C) were compared to both 25°C and 15°C. Stationary FC analysis was performed, as explained in Section 3.6.2 Stationary FC analysis.

a. Alterations in FC during fast rate of change of temperature

We first compared the stationary FC in fast cold ramps with sessions, where the animals were exposed to a Fast Cool Down (25°C to 15 °C decreasing 1°C per minute) or Fast Cool Up (15°C to 25 °C increasing 1°C per minute) *Figure 65* (A-E).

The Fast Cold Down ramp showed the most noticeable difference when compared to 25°C with 33 ROI pairs (*Figure 65* F) that are significantly different between the two groups. Out of the 33 ROI pairs, there were 10 pairs involving cingulate and somato-motor, 11 pairs among somato-motor and 11 pairs involving hypothalamus and somato-motor and just one pair involving cingulate and hypothalamus.

There was an increase in FC in the cingulate-somato-motor and somato-motor-somato-motor pairs during the ramps i.e., as the temperature is going down from 25°C to 15 °C compared to the condition where temperature stays at 25°C. At the same time, the ROI pairs involving hypothalamus which is already anti-correlated at 25°C shows even stronger anti-correlation during 25°C to 15 °C ramp.

When the Fast Cool Down ramp was compared to 15°C, 16 ROI duos with significant FC alterations were revealed (*Figure 65* G). The 8 motor-cingulate and a single S1HL-cingulate pairs show an increase in FC during the ramps, as the temperature is getting colder. Interestingly, 3 ROI pairs (1 motor-motor and 2 motor-S1HL), displayed the opposite behavior i.e., slightly decreased FC during the ramps. Finally, hypothalamus and cingulate regions, showed anti-correlations during the ramp.

Overall, these results suggest that a fast decrease in temperature is associated with a strengthening in the correlation of the somato-motor network and a weakening in the link between the hypothalamus and the somato-motor network.

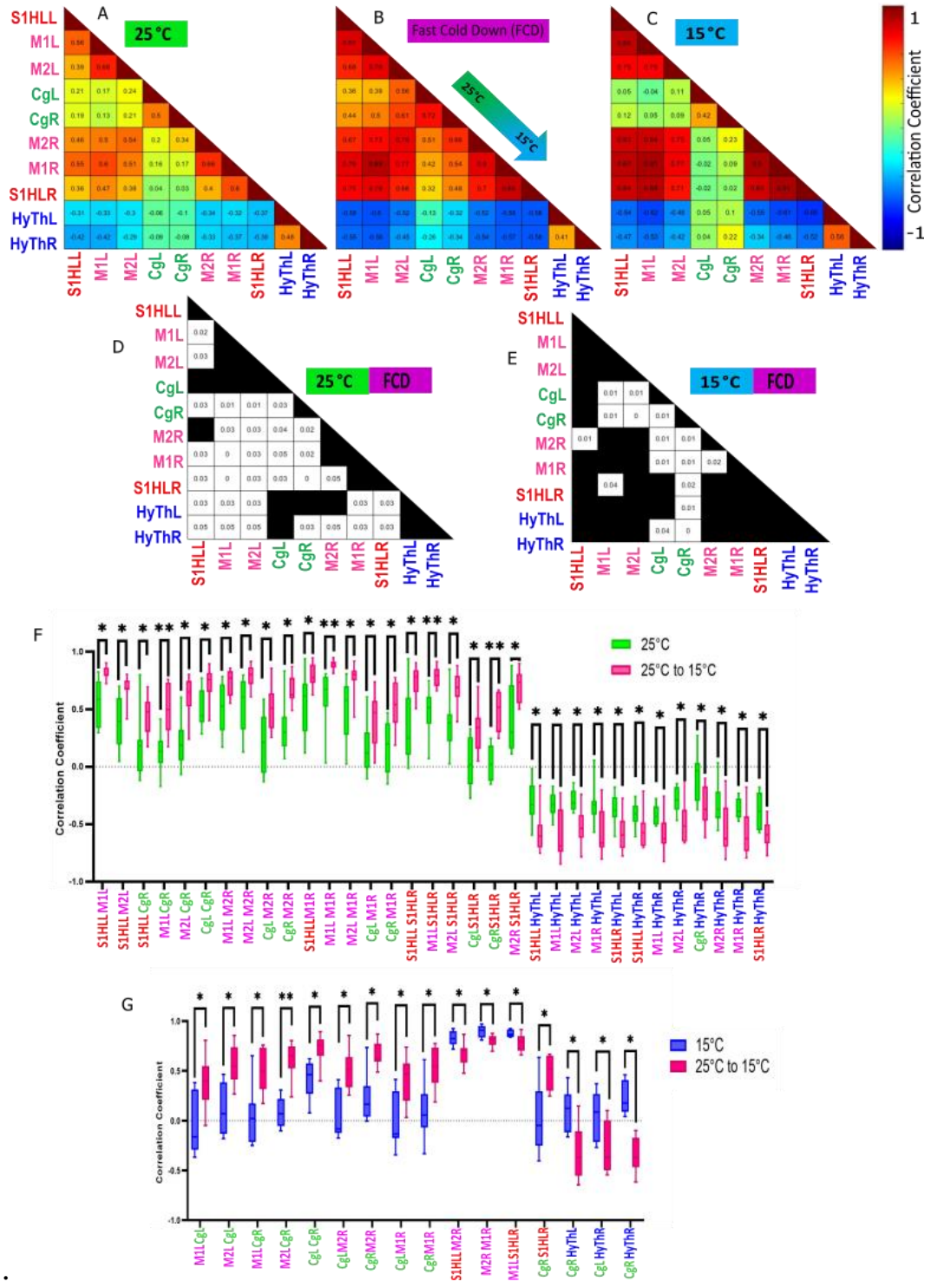

Figure 65: Functional connectivity comparison using correlation matrices of Fast Cool Down ramp (FCD) with 15°C and 25°C show strong differences*, characterized by an increase in connectivity in the somato-motor-cingulate ROI pairs and an anti-correlation in the hypothalamic ROI pairs during the FCD ramps. (A-C) Averaged Pearson correlation matrix of N=8 imaging sessions at 25°C, N=10 imaging sessions during FCD, and N=8 imaging sessions at 15°C respectively. (D, E) Matrix indicating the ROI pairs with significant differences between FCD Vs 25°C and FCD Vs 15°C respectively. The correlation coefficients of ROI pairs were Fisher transformed. In case of a normal distribution, a parametric Welsh test was performed and otherwise Wilcoxon rank-sum test was performed. Benjamini-Hochberg's correction for multiple comparisons was applied with a false discovery rate of 0.05. Pairs of ROIs with significant alterations between any two groups is indicated by the white squares with its corresponding p-values. (F,G) Boxplot representation of each ROI pair with a significant FC alteration between the groups between FCD (dark pink) Vs 25°C (green) and FCD Vs 15°C (blue). *p < 0.05, **p < 0.01 and ***p < 0.001*

Fast Cool Up ramp was compared to 25°C and 15°C in the stationary FC analysis. The average Pearson correlation matrices were compared to find the significant FC alterations *Figure 66* (A-E). The Fast Cool Up ramp showed similar pattern of results as Fast Cool Down, but with fewer FC alterations. Fast Cool Up ramp compared to 25°C, revealed 20 ROI couples that are significantly different *Figure 66*(F). Among them, 10 were with the somato-motor network and they showed an increase in FC during the ramp than at 25°C. The other 10 ROI pairs comprising the hypothalamus and somato-motor areas displayed a stronger anti-correlation during the ramps.

Comparison of Fast Cool Up ramps with 15°C uncovered only 6 pairs of regions that are significantly different *Figure 66*(G). When the cingulate-motor ROI pair showed an increase in FC during the ramp, the other ROI pairs showed a decrease in FC during the ramp.

Within these two Fast cold ramps, the striking difference is the largest number of subnetworks within the somato-motor-cingulate networks in which the functional connectivity was reinforced. In both cases, the hypothalamus-somato-motor-cingulate networks which are slightly anti-correlated in fixed temperature conditions, display a much stronger anti-correlation during these ramps.

These results highlight the complex inter-regional functional connectivity between the cingulate, somatosensory and motor cortices and hypothalamus when subjected to cold temperature ramps. They suggest a dichotomy between the somato-motor-cingulate and the hypothalamus-somato-motor networks.

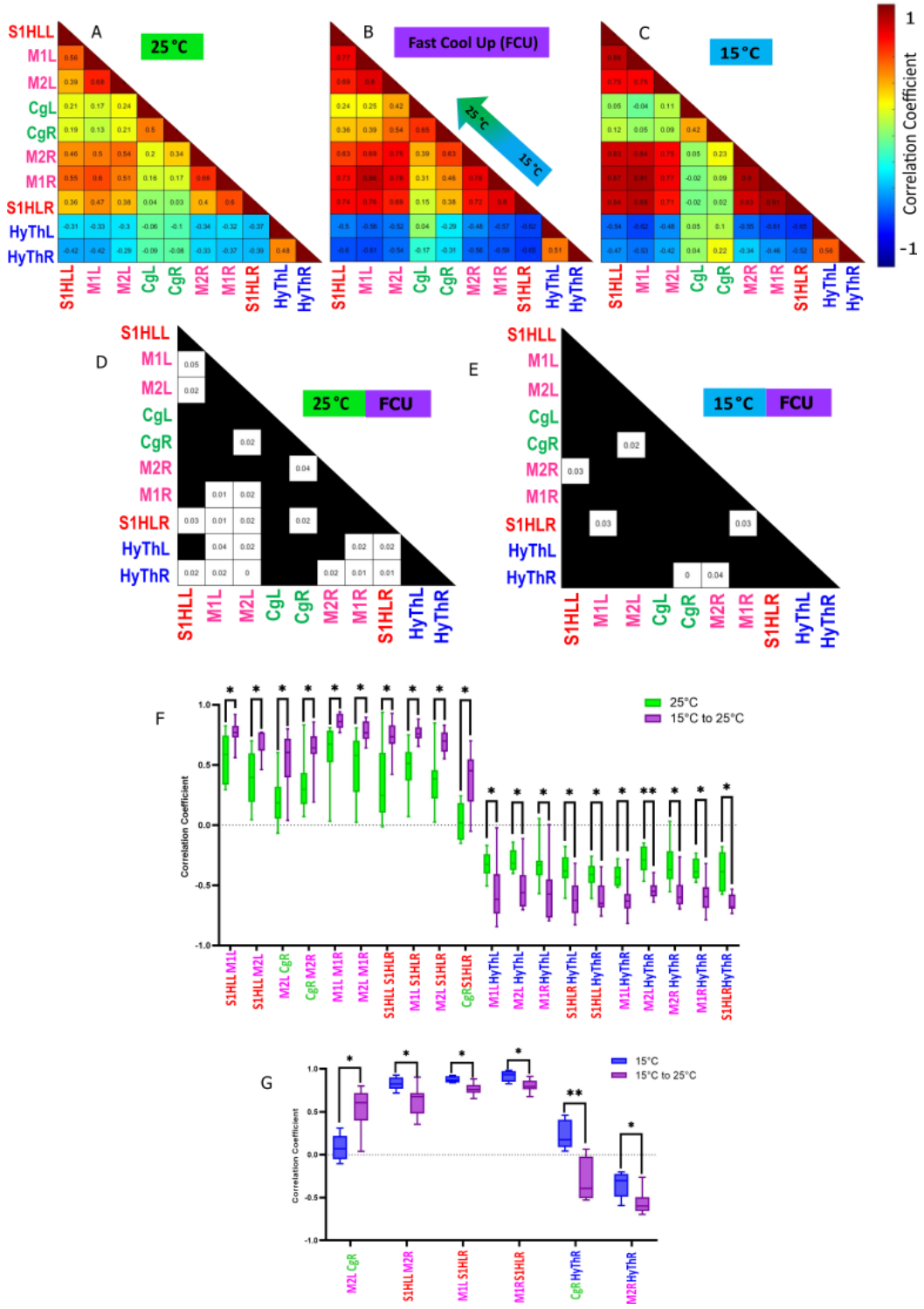

Figure 66: Functional connectivity comparison using correlation matrices of Fast Cool Up ramp (FCU) with 15°C and 25°C show strong differences *characterized by an increase in correlation in the somato-motor-cingulate ROI pairs and an anti-correlation in the hypothalamic ROI pairs during the FCU ramps. (A-C) Averaged Pearson correlation matrix of N=8 imaging sessions at 25°C, N=10 imaging sessions during FCD, and N=8 imaging sessions at 15°C respectively. (D, E) Matrix indicating the ROI pairs with significant differences between FCU Vs 25°C and FCU Vs 15°C respectively. The correlation coefficients of ROI pairs were Fisher transformed. In case of a normal distribution, a parametric Welsh test was performed and otherwise Wilcoxon rank-sum test was performed. Benjamini-Hochberg's correction for multiple comparisons was applied with a false discovery rate of 0.05. Pairs of ROIs with significant alterations between any two groups is indicated by the white squares with its corresponding p-values. (F,G) Boxplot representation of each ROI pair with a significant FC alteration between the groups between FCU (purple) Vs 25°C (green) and FCD Vs 15°C (blue). *p < 0.05, **p < 0.01 and ***p < 0.001*

b. Alterations in FC during slow rate of change of temperature

In order to investigate the effect of a slow pace of temperature change on FC, we compared the slow cold ramps, Slow Cool Down (25°C to 15 °C decreasing at 0.5°C per minute) and Slow Cool Up (15°C to 25 °C increasing at 0.5°C per minute) to their corresponding counterparts 25°C and 15°C in the stationary FC analysis. The average Pearson correlation matrices were compared to find the significant FC alterations *Figure 67* (A-E). As anticipated, they revealed striking differences from the fast cold ramps. Much to our surprise, both the Slow Cool Down and Slow Cool Up ramps had only statistically significant FC alterations only when compared to 25°C and not with 15°C.

Slow Cool Down when compared to 25°C, disclosed 15 ROI pairs – 7 somato-motor regions and 8 hypothalamus- somato-motor pair of regions *Figure 67* (F). There is an increased FC in the somato-motor regions during the Slow Cool Down ramp than at 25°C. Although the hypothalamus-somato-motor regions are anti-correlated at 25°C, they are much more strongly anti-correlated during the ramps. These results fall in the same pattern as the fast cold ramps but with a much lesser number of ROI pairs. There are far more significant hypothalamic regions in this comparison than the other comparisons.

Slow Cool Up when compared to 25°C, showed 21 ROI pairs with significant differences *Figure 67* (G). Among them 12 were within the somato-motor and 9 were among hypothalamus and somato-motor. Similar to the results from Slow Cool Down, the FC was increasingly strengthened in the somato-motor regions during the ramp. The anti-correlation among the hypothalamus-somato-motor was also stronger during the ramp.

Taken together, rate of change of temperature is a key component that drives central mechanisms. The lack of difference between 15°C and the slow cold ramps suggests that interplay between brain regions during slow changes in the temperature in the cold range is similar to that of a fixed cold temperature. It is also safe to assume that this very interplay is different during fast cold ramps.

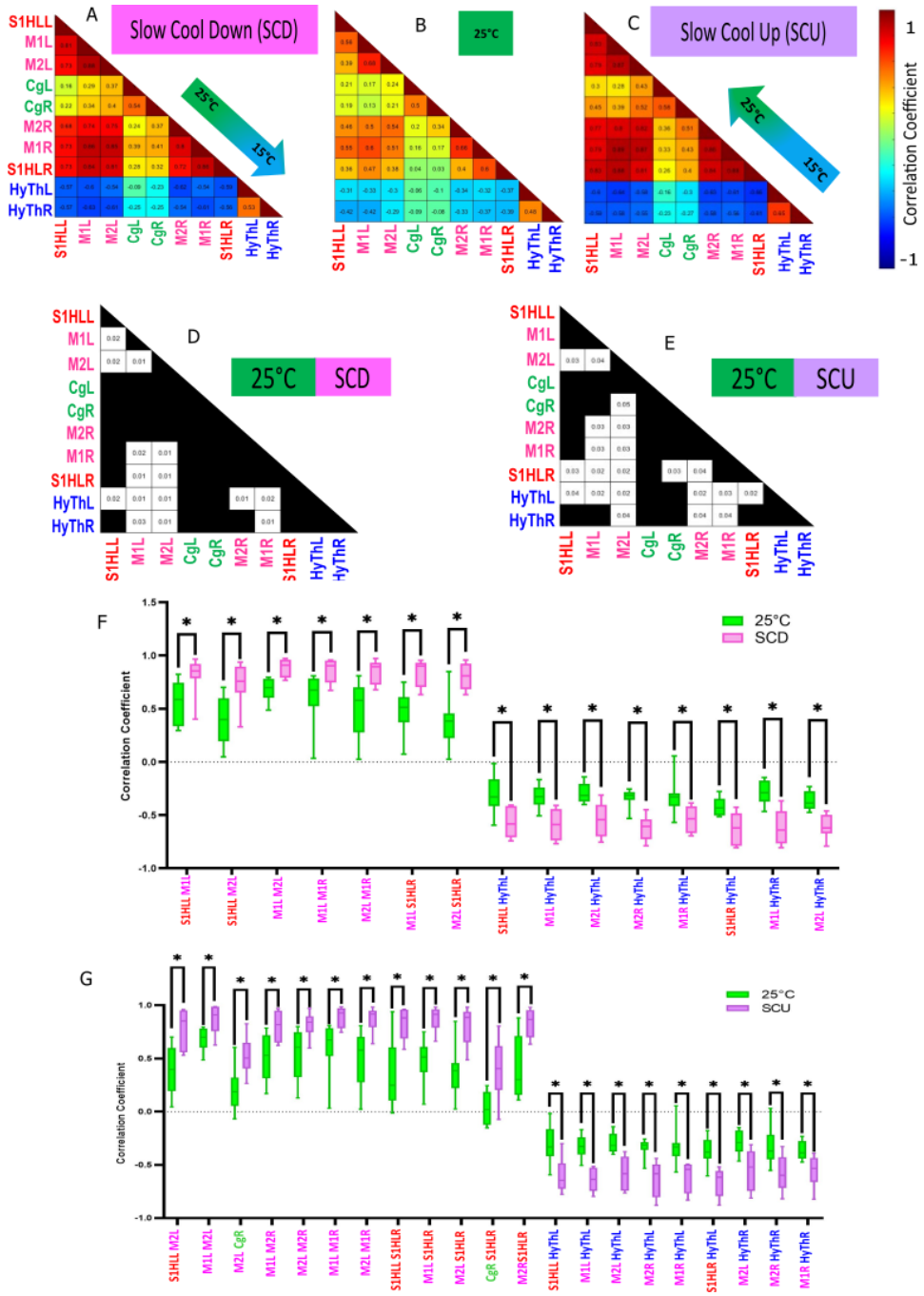

Figure 67: Functional connectivity comparison using correlation matrices of Slow Cool Down and Slow Cool Up show strong differences *only with 25°C characterized by an increase in correlation in the somato-motor-cingulate ROI pairs and anti-correlation in the hypothalamic ROI pairs during the SCD and SCU ramps. (A, B, C) Averaged Pearson correlation matrix of N=8 SCD , N=8 25°C and N=6 SCU imaging sessions respectively. (D, E) Matrix indicating the ROI pairs with significant differences between SCD Vs 25°C and SCU Vs 25°C respectively. The correlation coefficients of ROI pairs were Fisher transformed. In case of a normal distribution, a parametric Welsh test was performed and otherwise Wilcoxon rank-sum test was performed. Benjamini-Hochberg's correction for multiple comparisons was applied with a false discovery rate of 0.05. Pairs of ROIs with significant alterations between any two groups is indicated by the white squares with its corresponding p-values. (F, G) Boxplot representation of each ROI pair with a significant FC alteration between the groups between SCD Vs 25°C and SCU Vs 25°C. *p < 0.05, **p < 0.01 and ***p < 0.001*

4.1.3. Warm Ramps Vs Fixed Warm And Neutral Temperature

Similar to the analysis of cold ramps, Warm Up and Warm Down ramps in the fast and slow pace were compared to their corresponding counterparts 25°C and 35°C in the stationary FC analysis. The average Pearson Correlation matrices were compared to find the ROI pairs with significant FC alterations *Figure 68* (A-H).

The same experimental paradigms of fast and slow ramps in the warm range did not produce as many significant results, as the cold. The Slow Warm Up and Slow Warm Down showed minimal differences in FC, when compared to 25°C. Noticeably they showed no significant difference in FC, when compared to 35°C, suggesting that the interactions between brain regions during warm ramps are not that different than at fixed temperature 35°C (*Figure 68*).

Even more strikingly, none of the comparisons among Fast Heat Up and Fast Heat Down and 25°C and 35°C, produced significant results (*Figure 69*). This is in contrast to the strong effects observed during the Fast Cool Down and Fast Cool Up.

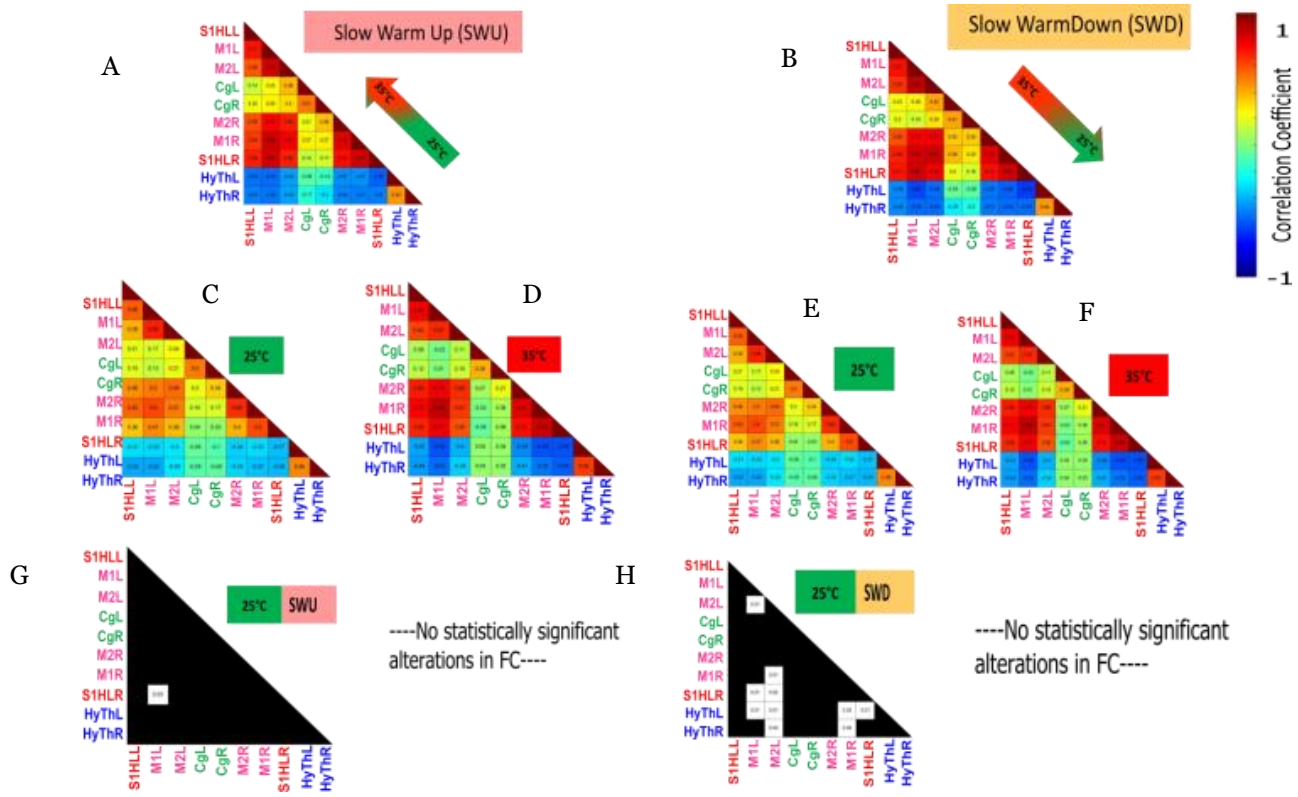

Figure 68: Functional connectivity comparison using correlation matrices of Slow Warm Up and Slow Warm Down with 35°C and 25°C *show very mild changes only when compared with 25°C. (A, B) Averaged Pearson correlation matrix of N=8 and N=8 imaging sessions during SWU and*

*SWD. (C, E) Averaged Pearson correlation matrix of N=8 imaging sessions at 25°C. (D, F). Averaged Pearson correlation matrix of N=8 imaging sessions at 35°C. (G, H) Matrix indicating the ROI pairs with significant differences between SWU Vs 25°C and SWD Vs 25°C respectively. The correlation coefficients of ROI pairs were Fisher transformed. In case of a normal distribution, a parametric Welsh test was performed and otherwise Wilcoxon rank-sum test was performed. Benjamini-Hochberg's correction for multiple comparisons was applied with a false discovery rate of 0.05. Pairs of ROIs with significant alterations between any two groups is indicated by the white squares with its corresponding p-values. *p < 0.05, **p < 0.01 and ***p < 0.001*

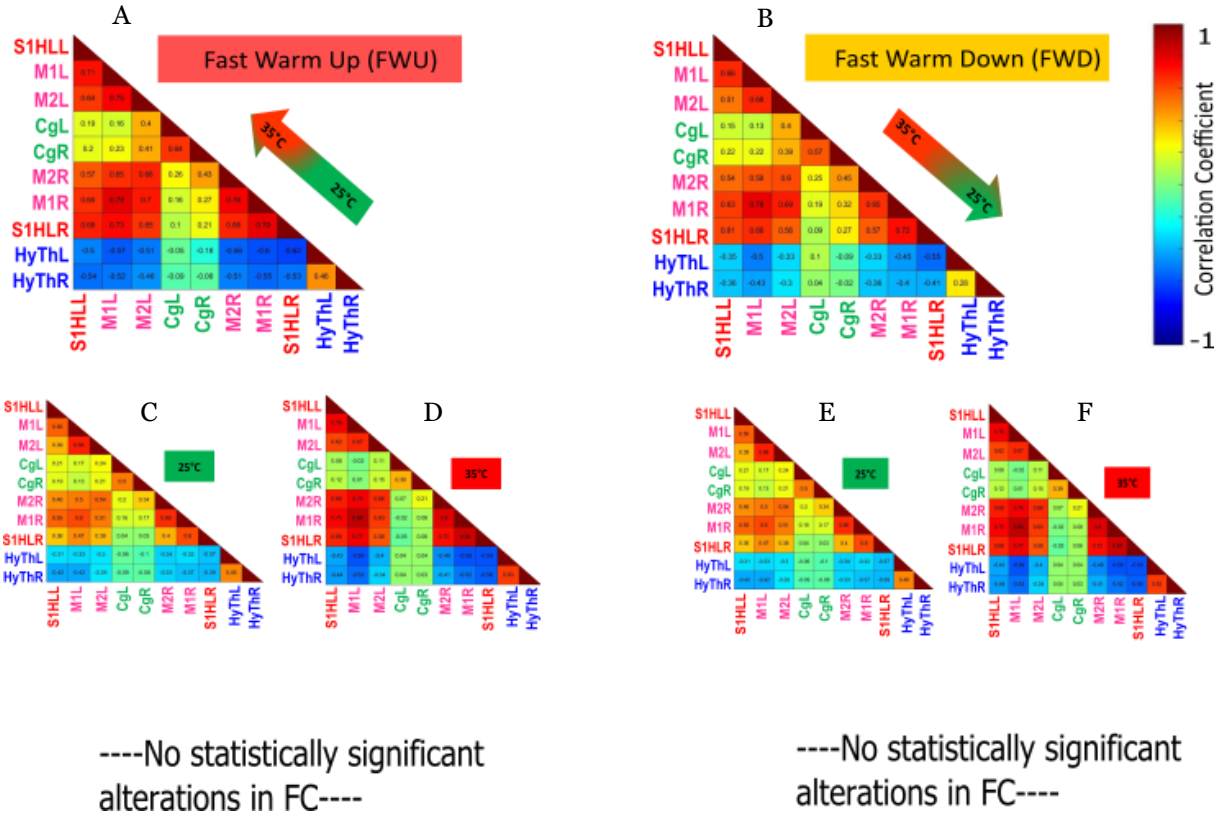

Figure 69: Functional connectivity comparison using correlation matrices of Fast Warm Up and Fast Warm Down with 35°C and 25°C show NO statistical changes of the FC alterations. *(A, B) Averaged Pearson correlation matrix of N=8 and N=8 imaging sessions during FWU and FWD. (C, E). Averaged Pearson correlation matrix of N=8 imaging sessions at 25°C. (D, F). Averaged Pearson correlation matrix of N=8 imaging sessions at 35°C. No statistically significant alterations changes of FC was observed.*

4.2. DYNAMIC FC ANALYSIS

4.2.1. K-means Clustering Analysis

While the classical averaged correlation analysis confirmed that there are FC connectivity alterations that are specific to temperature, we predicted that the intrinsic dynamic characteristics during thermal coding might be even stronger.

An unsupervised k-means clustering analysis of all the thermal conditions: Fixed temperatures: 25°C, 15°C, 35°C, warm and cold ramps at fast and slow pace was performed. The time series data from all the 92 acquisitions were concatenated together to form one single time series (10x 84499, where 10 is the number of ROIs and 84499 is the number of time points). To obtain a time resolved correlation matrix, Pearson correlation was computed at each timepoint between any two ROIs. The time resolved matrices was subjected to k-means clustering. It was performed for k=, 5, 6, and 7 clusters and was proved to be very robust and consistent. For instance, clustering for k=5 resulted in 5 brain state matrices. The probability of occurrence of each of the brain state matrix was calculated for cold and warm conditions.

Decomposition into 7 brain states are shown in *Figure 70*. The brain state matrices are ordered from highest correlation to lowest correlation and denoted by a number (1-7) i.e., 1 being the strongly correlated and 7 being the weakly correlated. The number of cooccurrences (n) and p-value (p) are also noted below each brain state matrix. The probability of occurrence was calculated for the 7 brain state matrices in the cold and warm conditions. In agreement with the stationary FC analysis, the dynamic FC analysis only have significant results in the cold conditions and not in the warm.

Noticeably, Brain states 1 and 7 showed significant differences in the occurrence rate between the cold conditions. Brain State 1 was more frequent in the cold ramps (FCD, FCU, SCU) than 25°C and 15°C (*Figure 70*). On the other hand, brain state 7 was more frequent in 25°C than 15°C, FCD and SCU (*Figure 70*). It can be concluded that the strongly correlated/decorrelated state (brain state #1) is more common in the cold ramps and the weakly correlated state (brain state #7) is mostly associated to the 25°C. It is also worthwhile to notice that the weakly correlated brain state 7 has the highest number of occurrences (50% of

total occurrences) and its probability to occur in all conditions are is higher than any other states.

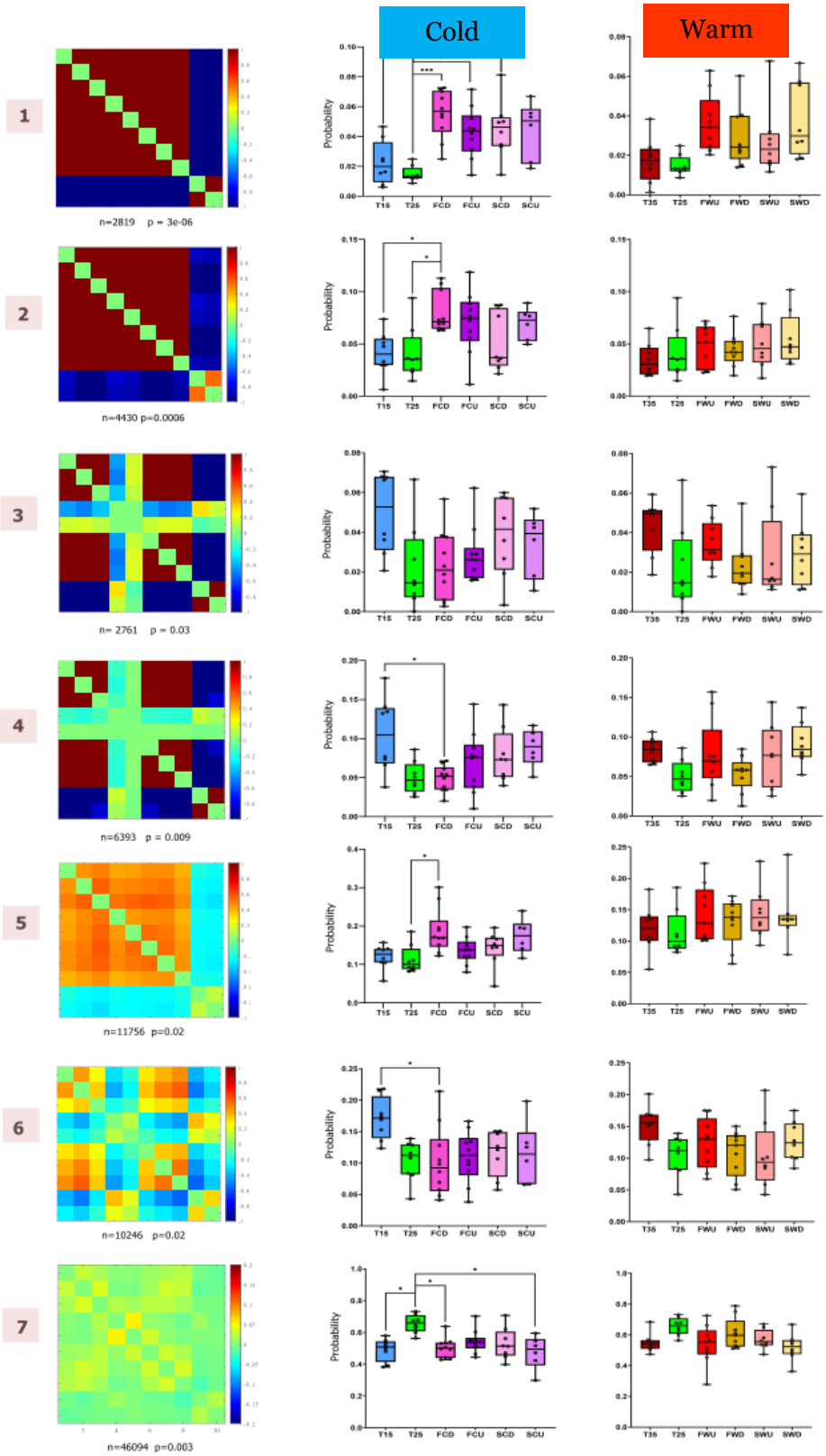

Figure 70: Dynamic functional connectivity analysis of thermal coding using k-means clustering for 7 states*. The clustering resulted in 7 brain state matrices which are ordered from 1-7 in the order of descending level of connectivity. The probability of occurrence was calculated for each brain state for all thermal conditions and the cold and warm conditions were compared separately. The p-value at the bottom of the brain*

states show that the probability of occurrence is altered for Brain States #1, #2, #4,# 5, #6, #7 in the cold conditions and not in the warm conditions. Brain State #1 is more frequent in the cold ramps rather than 25°C and 15°C. Brain state #2 occurs more in FCD than 25°C and 15°C. Brain State 4 and 6 occurs more frequently at 15°C, than FCD. Brain State #5 appears more frequently in FCD, than 25°C. Brain State #7, the weakly connected brain state, occurs more frequently at 25°C than 15°C, or FCD and SCU.

The same analysis was done for k=6 and k=5 states. When decomposed into 6 states, the states are reorganized from the previous analysis for 7 states (*Figure 71*). While most of the brain states are retained from the k=7 analysis, states #4 and #6 are most likely pooled together along with some others states (See the numbering on the left side of each brain state). Notice that the number of occurrences is different and since the number of states is reduced to 6 from 7. Even then, the results are consistent considering the significant results in the cold and lack of changes in the warm conditions. Brain states (BS) #1 and #7 follow the same pattern as previously observed. The brain state that is highly correlated and anticorrelates: BS #1 has a high probability of occurring in the cold condition, whereas the low connectivity BS #7 is more occurrence at 25°C. Decomposition of the data into 5 clusters also yield the same pattern of results, again proving the robustness of the analysis (*Figure 72*).

The dynamic functional connectivity patterns show that strong connectivity in the somato-motor network and the strong decrease in connectivity of hypothalamus-somato-motor network is more of a characteristic in the cold condition. On the contrary, the weak connectivity between somato-motor-cingulate-hypothalamus is the most frequently occurring pattern but is significantly more in the 25°C.

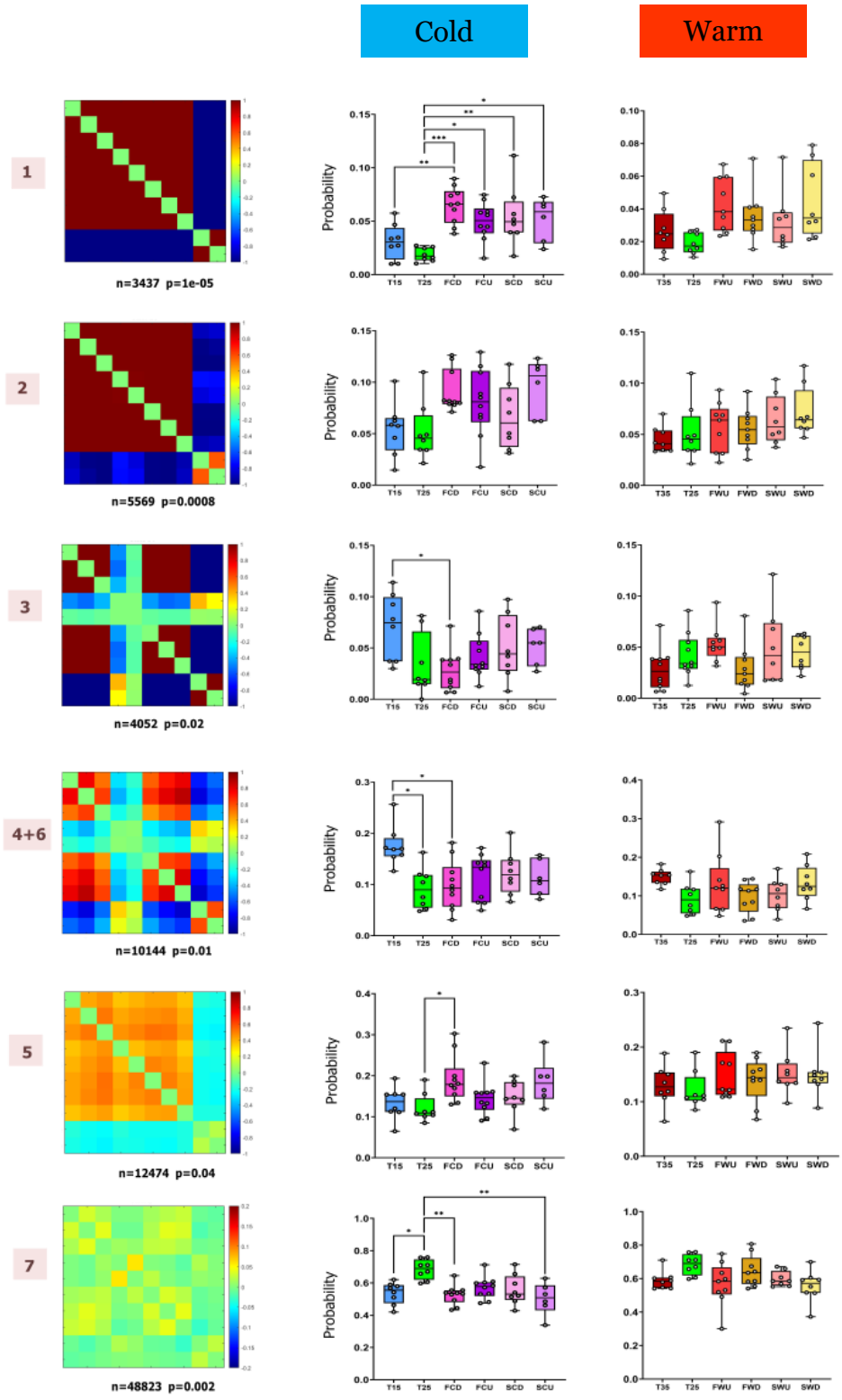

Figure 71: Dynamic functional connectivity analysis of thermal coding using k-means clustering for 6 states. *Notice the number next to the brain state refers to the original numbering (1-7). It means that brain states (BS) #1,# 2, #3, #5, #7 are retained with changes in the number of occurrences (n). BS #4 and #6 have pooled together, but also redistributed in other groups. The clustering resulted in 6 brain state matrices ordered from highest to lowest connectivity. The probability of occurrence was calculated for each brain state for all thermal conditions and the cold and warm conditions were compared separately. The p-value at the bottom of the brain states show that the probability of occurrence is altered for BS #1, #3, #4+6, #5, #7 in the cold conditions. BS #1 is more frequent in the cold ramps rather than 25°C and 15°C. BS #3 occurs more in 15°C than FCD. BS #4+6 occurs more in 15°C than FCD and 25°C . BS #5 appear more frequently in FCD than 25°C. Finally, BS #7, the weakly connected brain state, occurs frequently during 25°C than 15°C, FCD and SCU.*

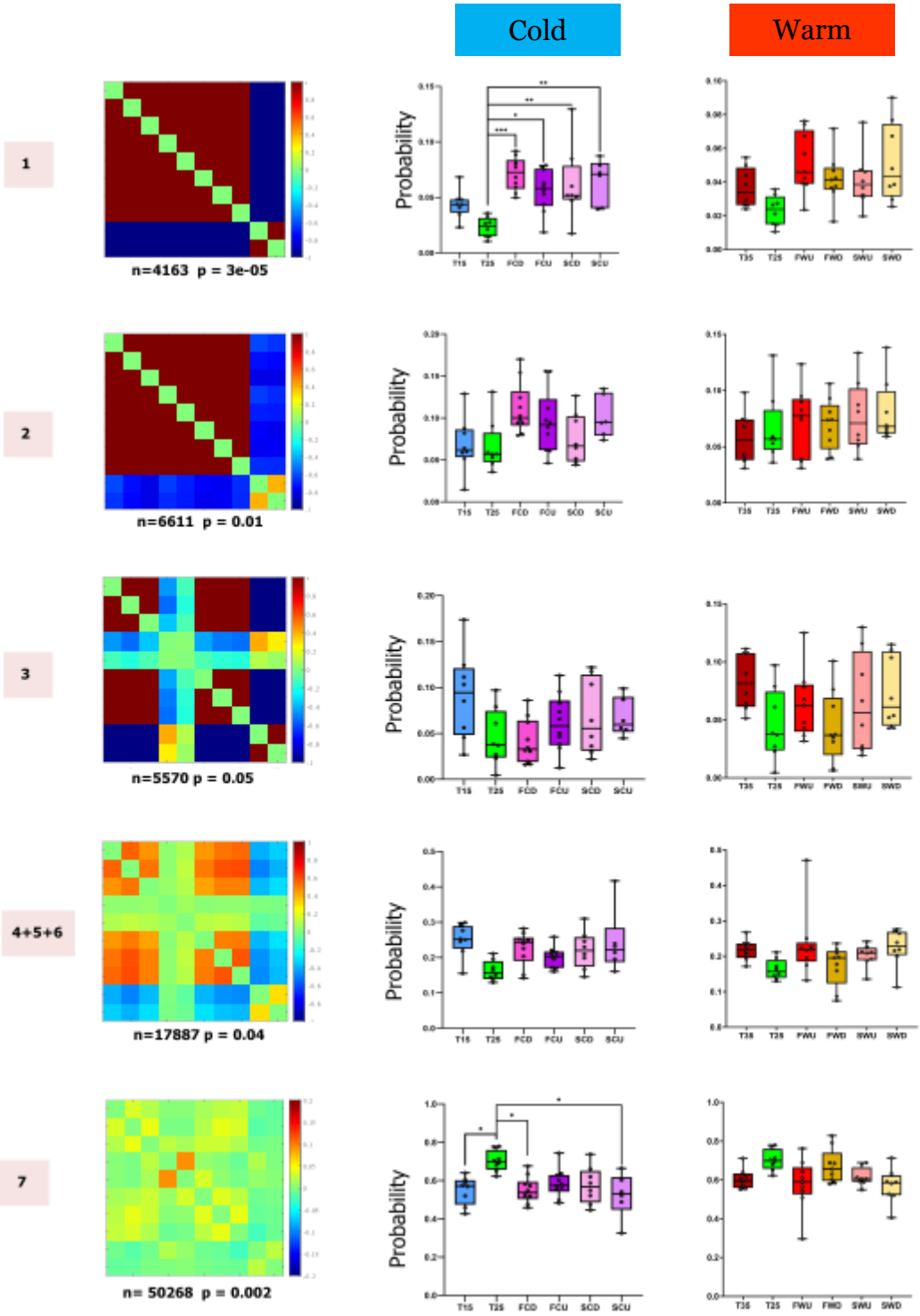

Figure 72: Dynamic functional connectivity analysis of thermal coding using k-means clustering for 5 states. *Notice the number next to the brain state refers to the original numbering (1-7). It means that BS #1, #2, #3, #7 are retained with changes in the number of occurrences (n). BS #4+6 and 5 have pooled together but also redistributed in other groups. The clustering resulted in 5 brain state matrices ordered from highest to lowest connectivity. The probability of occurrence was calculated for each brain state for all thermal conditions and the cold and warm conditions were compared separately. The p-value at the bottom of the brain states show that the probability of occurrence is altered for BS #1 and #7 in the cold conditions. Brain State 1 is more frequent in the cold ramps rather than 25°C. BS #7, the weakly connected brain state, occurs frequently during 25°C than 15°C, FCD and SCU.*

5. DISCUSSION

Researchers have always been curious about the peripheral and central mechanisms that integrate the thermal information to form thermal perception. Our early knowledge about thermosensation is deduced from psychophysical studies, electrophysiological studies, thermal behavior experiments, molecular characterizations and calcium imaging. With the advent of fMRI and PET studies in humans, we were able to expand our knowledge of the supraspinal areas.

Our study aimed at discovering how different brain regions are involved in innocuous thermal coding in mice, using a versatile neuroimaging technique: functional ultrasound. fUS imaging in awake mice poses several challenges. The habituation and handling procedure, minimizing stress and motion artefacts in the ultrasound signal from the free movement are a few. Although insular cortex is an unavoidable part of the thermosensory circuit, we are unable to image it due to technical difficulties. Instead, we focused on imaging the somato-motor, cingulate and hypothalamus regions. Keeping in mind, the transcranial imaging approach and longitudinal nature of the study, the best way forward was to reimage a single plane (Bregma -0.34mm) in multiple thermal conditions. The temperature range in the study was limited to 15-35°C as it was the optimal range which caused minimal discomfort and less motion-artefacts.

Although there are other imaging techniques such as intrinsic optical imaging, calcium imaging, head-fixed imaging that has been used in rodent thermal studies (Paricio-Montesinos et al., 2020; Ran et al., 2016; Wang et al., 2018), fUS imaging is capable of recording the innate awake responses. Complete movement restriction of the head is essential for techniques such as two-photon imaging and electrophysiological recordings. Compared to this highly controlled approach, awake fUS imaging measures brain activity in the most natural setting possible.

In this study, we put forward a thorough stationary and dynamic functional connectivity study of the interplay between brain regions during innocuous thermal sensation.

5.1. FC-A Strong Marker Of Strength Of Interaction Between Brain Regions

Studying the low frequency fluctuations in brain activity has given rise to findings that revolutionized neuroscience research. The default mode network (DMN) which is activated during rest is a major resting-state neuronal network and has been widely studied (Fox et al., 2005; Fox and Raichle, 2007; Raichle, 2015, 2011, 2010). DMN is shown to have alterations in many neuro-psychiatric illnesses (Buckner et al., 2008b; Dennis and Thompson, 2014b; Mohan et al., 2016). However, task or behavior related functional connectivity studies using fMRI also has been increasing in numbers in the recent years (Barch et al., 2013; Cole et al., 2021, 2014; Di and Biswal, 2019; Kieliba et al., 2019). Recently (Ferrier et al., 2020) showed resting state FC and task FC in mice using fUS imaging. It was also shown that, using fUS imaging, FC can be measured anesthetized rats (Osmanski et al., 2014) and in pharmacological studies (Rabut et al., 2020).

Unlike the conventional time averaged analysis of FC, there has been tremendous advancements in studying the dynamic nature of FC (Hutchison et al., 2013; Preti et al., 2017). The temporal evolution of FC can reveal how FC reshapes according to the physiological or behavioral changes, at rest or task or in case of neurodegenerative or neuro-psychiatric illnesses (Barttfeld et al., 2015; Demertzi et al., 2019b; Gonzalez-Castillo and Bandettini, 2018; Gu et al., 2020; Tian et al., 2018; Zou and Yang, 2019).

In this study, we used fUS imaging to study both stationary (time-averaged) and dynamic functional connectivity (unsupervised k-means clustering) between somato-motor, cingulate and hypothalamic regions during thermal stimulations. Even though, the mice are not subjected to a task in our study, they are physiologically and behaviorally responding to the thermal stimulation which is either cold, warm or neutral. Our study shows that stationary and dynamic functional connectivity vary significantly in cold, but not warm sensing.

5.3. Absence Of Fc Alterations In Warm Temperatures

The stationary FC analysis between warm, cold and neutral fixed temperatures revealed that FC during cold substantially varied from warm.

The intriguing absence of any impact in functional connectivity during fixed 35°C and the Warm Up (25°C to 35°C) and Warm Down (35°C to 25°C) ramps in both slow and fast pace can be primarily attributed to the molecular mechanisms associated with heat sensing. Thermal psychophysics studies have shown that when the skin is adapted to temperature values ranging from ~30 to ~34◦C, neither warm nor cool sensations are experienced (Filingeri, 2016). Therefore, 35◦C could not have evoked any response. Furthermore, the transition from ambient to warm temperature between 32-39°C and 26-34°C activates TRPV3 and TRPV4 channels respectively (Huang et al., 2011). TRPM2 channel is activated at approximately at 35°C by sensing environmental temperatures (Tan and McNaughton, 2016) (Song et al., 2016).

The spinal cord is the first hub that integrates the thermal cues transmitted from the periphery and it still lacks the depth of knowledge that we have at the afferent level. (Ran et al., 2016) studied the response of dorsal horn neurons to heat and shows only 15% of heat sensitive neurons are activated when heated from 32°C to 37°C. The percentage of heat responsive neurons increases with the increase in temperature, reinstating that the stronger responses were evoked by higher absolute temperatures and not higher heating rates. This is consistent with the finding that, heat predominantly follows graded coding (Wang et al., 2018). Simply put, as we increase the heat, more heat-sensitive neurons are recruited and the individual neurons are much strongly activated.

However, this lack of changes in FC suggests that mice perceived the neutral and warm in the same manner and corroborates the psychophysical studies and molecular mechanisms. The central mechanism that drives the connectivity patterns between the brain regions is still unclear, but it is certain that there are multiple mechanisms that lead to the integration of warm or ambient thermal information in the brain.

5.3. Strong Fc Alterations in The Cold Temperatures

Cold, in clear contrast to the heat, exhibits strong alterations in functional connectivity. At the molecular level, the cool mediating TRPM8 sensor is activated below 27°C (Peier et al., 2002), (McKemy et al., 2002). Interestingly, the cold ramps in our study falls in the innocuous to beginning of noxious range for mice and therefore could have activated both noxious and innocuous cold sensors on the skin.

We know that in the spinal cord circuitry, lowering the temperature activated cool sensitive neurons, but each responding neuron is turned on at a particular temperature as illustrated in (Ran et al., 2016). They also show that the rate of cooling did not significantly affect the percentage of responsive neurons. But a majority of the neurons were found to be activated during temperature change and not at stable temperatures, indicating that cold-sensitive neurons respond to temperature changes (ΔT).

In our study, the cold ramps displayed noticeable alterations of the functional connectivity, when compared to the fixed temperatures. It is safe to assume that, at each point in the cold ramps there is a combination of cold-sensitive neurons that detect the temperature changes and are activated. (Wang et al., 2018) ha d showed that the encoding of cold temperatures is done in a combinatory fashion. The combinations of individually activated cold-sensitive neurons enable this.

Psychophysical aspects of thermal sensing, mostly studied in humans, could also be a driving factor in the strong effects in the cold temperature (Filingeri, 2016). The ramps began at 25°C which is lower than the initial adaptive skin temperature: 30-34°C. The faster ramps have much more significant changes than the slow ramp. This could be because, faster the rate of change, even a small change can induce a thermal sensation. Interestingly in humans, face and head are more sensitive to warmth, while torso is sensitive to cold (Filingeri, 2016). It is safe to assume that the proximity of the torso to the metal floor of the Bioseb led to a much stronger cold sensation. Unfortunately, this could not be verified because the primary somatosensory cortex of the trunk region (S1Tr) is not available in our chosen plane.

The central nervous system integrates the physiological and psychophysical aspects to form a thermal perception. Spinothalamic neurons are projecting to thalamic nuclei such as the VPL, VPM and the PoT (Bokiniec et al., 2018) which is then sent to the primary (S1) and secondary (S2) somatosensory and insular cortices. At the supraspinal level, early fMRI studies in humans have found the involvement of thalamic and cortical (insula, S2) activations to heat and cold stimuli (Davis et al., 1998). In a recent study, (Milenkovic et al., 2014), it was found that primary sensory cortical neurons play a major role in cool perception. Other fMRI studies has shown the role of numerous brain regions such as cingulate, somatosensory, motor cortices, thalamus, basal ganglia and insula during noxious heat and cold stimulations (Tracey et al., 2000). (Craig et al., 2000) advocates that insular cortex is as important, as S1 in forming thermal perception of cutaneous temperatures. The hedonic component which decides the pleasantness or comfort is mainly associated with the cingulate cortex, which is widely studied for its involvement in the processing pain and emotion. (Aizawa et al., 2019; Hua et al., 2005; Kwan et al., 2000b). The thermoregulatory role of hypothalamus, especially the preoptic area (POA) (Berner and Heller, 1998; Wang et al., 2019b; Westerman et al., 2010) and lateral parabrachial nucleus (LPB) (Yahiro et al., 2017b) in behavioral thermoregulation also contributes to the global thermal perceptive process.

In our study, we imaged the somatosensory cortex of hind limb, primary and secondary motor cortex, cingulate cortex and hypothalamus. By measuring the CBV changes in these brain regions using fUS imaging in awake and freely moving mice, we were able to measure the functional connectivity between these regions during the thermal conditions. Our results show that fast cold ramps have higher somato-motor connectivity and a stronger decrease in hypothalamic connectivity. As we know somatosensory and motor regions are the crucial for thermosensation, the high coherence between somato-motor regions was anticipated. The alterations in FC in somato-motor-cingulate ROI pairs during the fast cold ramps may be due to the unpleasantness or discomfort experienced. We postulate that this hub handles the hedonic or emotional component of thermosensation. The anti-correlation of hypothalamus with all the other regions lead us to the hypothesis that it is part of a secondary thermoregulatory network. This anti-correlation could also mean that there is a time lag between the temporal CBV signals from these regions. Taken together, we identified that the somato-motor, somato-motor-cingulate, and

somato-motor-hypothalamus networks have their own roles to play in thermosensation. Unmasking the underlying phenomenon that unify these hubs needs further investigations.

5.4. Dynamic Patterns Of Connectivity In Thermal Sensations

In majority of the classical functional connectivity studies, the temporal resting-state signals from regions of interest are averaged and Pearson correlation is used to measure the strength of their coherence or incoherence. In short, these studies assume temporal stationarity. (Chang and Glover, 2010) suggested that resting-state activity is more dynamic and can change in a matter of seconds. Later on dynamic functional connectivity (dFC) expanded as separate body of research (See Reviews Cohen, 2018; Hutchison et al., 2013; Park and Friston, 2013; Preti et al., 2017). dFC is found to be altered in autism (Li et al., 2020), schizophrenia (Zou and Yang, 2019), Alzheimer's disease (Gu et al., 2020) aging (Tian et al., 2018) and in task related approaches (Gonzalez-Castillo and Bandettini, 2018; Kieliba et al., 2019). Although the brain is structurally defined like any other organ in our body, its functional versatility is perplexing and challenging at the same time.

In our study, we did a dFC analysis to understand the intrinsic connectivity patterns that occurs during different thermal conditions. By measuring the temporal fluctuations in the time series, we obtained time-resolved correlation matrices. The dFC states or brain states were then obtained by an unsupervised k-means clustering approach.

Initially we performed the k-means clustering of time-resolved correlation matrices for k=7. This revealed 7 patterns of varying connectivity strengths. Later this analysis was done for 6 and 5 states. The results were very robust and the showed statistically significant differences between the cold conditions, similar to the stationary FC analysis.

Brain state #1 and #7 were particularly prominent. Brain state #1 was characterized by high somato-motor-cingulate connectivity and strong decrease in connectivity with hypothalamus. This essentially supports our hypothesis in stationary FC that

these regions are hubs for thermal perception and thermal regulation. On the contrary, Brain state #7 showed overall weak connectivity and was the most frequent state in all conditions, occurring over 50% of the total occurrences. It is particularly frequent during the neutral temperature 25°C. fMRI studies in monkeys (Barttfeld et al., 2015) and humans (Demertzi et al., 2019b) have shown that the low strength / low coupling of connections is a marker for lack of consciousness. (Gu et al., 2020) shows that elderly people spent more time in a weakly connected brain state. (Barttfeld et al., 2015) also points out that the weakly connected state in their analysis resembles the structural matrix. We postulate that temperature sensation and regulation in different thermosensory circuits takes place in short bouts during the strongly connected-disconnected states, like Brain state #1. As low connectivity brain states such as Brain state #7 is associated to low cognitive functionality and the finding that it is more frequent in the neutral temperature, it is safe to conclude that it is associated to minimal responsiveness to temperature. In other words, it could be a characteristic of neutral or adaptive state.

6. CONCLUSION

At the moment, we believe that our study is the first to investigate thermal coding at the supraspinal level in awake animals. Limitations in imaging techniques such as fMRI, PET etc. to image rodents in their awake state is always a challenge. Head-fixed awake imaging might induce stress related to restrictive movements. fUS imaging with awake mice, was not only minimally invasive but also recorded the most innate thermal responses. Stationary and dynamic analysis of FC revealed that cold temperature (fixed and ramps) elicited the most noticeable changes. Dynamic analysis showed that repetitive patterns occur during different levels of thermosensation ranging from a high connectivity state to a weakly connected state.

Due to technical limitations, we were unable to capture the insula which is crucial in thermal processing. With the current probe, imaging the laterally positioned insular cortex is challenging but with the development of new probes, this could be possible.

CHAPTER 5:

CONCLUSION AND PERSPECTIVES

The long quest to decrypt thermal coding is still ongoing. In this thesis, we investigated the regions that are involved in thermal processing and studied the interplay between some of the brain regions in encoding thermal information. Functional ultrasound imaging technique is an emerging neuroimaging modality that facilitated the execution of this thesis at the Physics for Medicine Laboratory. Using this technique, we were able to conduct innocuous and noxious thermal experiments in anesthetized and awake conditions.

The first study aimed at functionally mapping the regions that are involved in thermal processing in anesthetized rats. To this goal, we studied the localized CBV increases in areas that are already been shown to be part of the thermosensory circuit such as thalamus, somatosensory and motor cortex, insular cortex, cingulate cortex and hypothalamus. It was concluded that isoflurane is better suited for thermal experiments using fUS imaging. However, we also learnt that the arterial blood pressure changes can influence the CBV responses and therefore we identified how much of this response is due to the increased blood pressure. It was concluded that S1 and mid cingulate exhibited strong activation in response to noxious stimulation, which is in line with previous studies.

The second study on awake mice aimed at studying the connectivity patterns between the regions that are involved with thermal coding. The plane that we chose contained somato-motor, cingulate and hypothalamus brain regions. Stationary and dynamic connectivity analysis showed that cold temperature induced a strong contrast in the connectivity patterns: strongly connected somato-motor regions and strongly disconnected hypothalamic-somato-motor regions (Figure 73). A weakly connected brain state was prominent during the neutral temperatures.

Inability to study noxious temperatures in awake condition is a limiting factor in the awake study. During the initial phase, we observed that noxious temperature induced discomfort and averseness and even escape behavior in some cases and the imaging session ended up being excluded. For this reason, we had to use a more comfortable but restricted temperature range (15-35°C). Another challenge was the technical difficulty in imaging a major brain region implicated in thermal coding: insular cortex. Placement of the probe in a lateral position in awake mice is an obstacle. With new advancements in probe design, it could be possible to incorporate this idea.

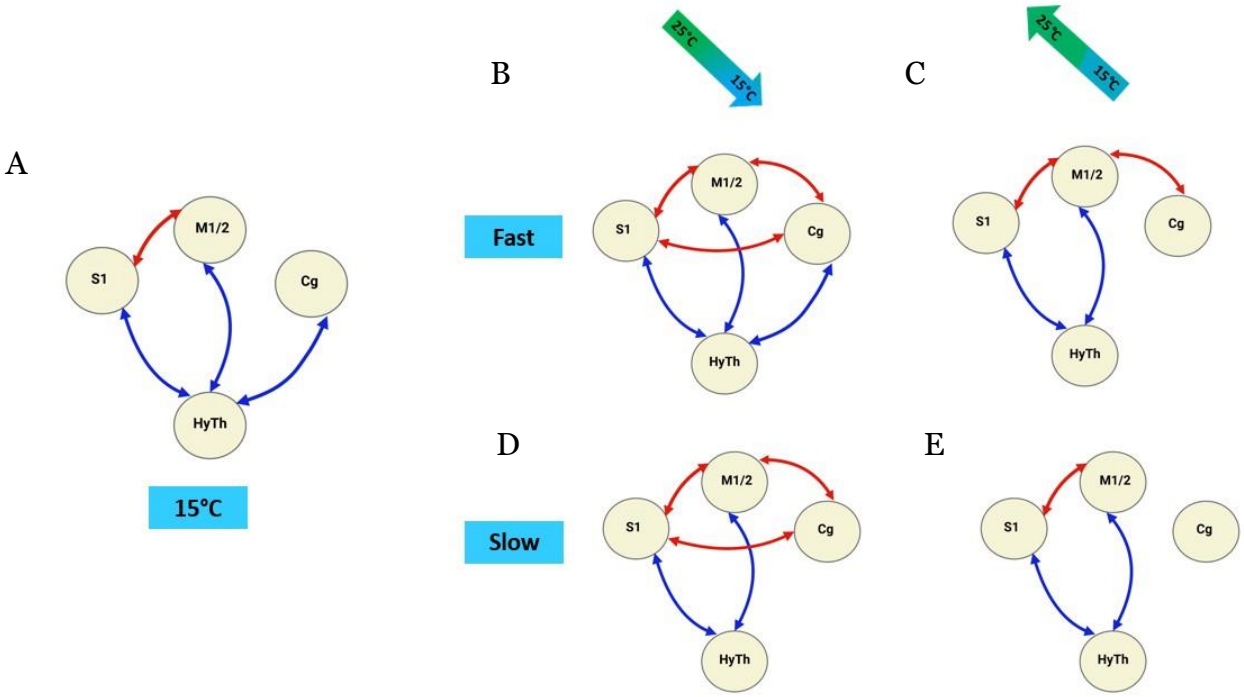

Figure 73: Graphical summary illustrating the connectivity alterations (red for correlation and blue for anti-correlation) between somatomotor, cingulate and hypothalamus regions when comparing cold conditions with neutral temperature 25°C. *(A) Constant application of 15°C shows increased somatomotor connectivity. Somatomotor and cingulate are anti-correlated with hypothalamus. (B) Fast cold down shows highly correlated hub of somatomotor-cingulate and an anti-correlated hub of somatomotor-cingulate with hypothalamus. (C) Fast cold up shows increased somatomotor and motor-cingulate connectivity while somato-motor is anti-correlated with hypothalamus. (D) Slow cold down shows a highly correlated hub of somatomotor-cingulate and an anti-correlated hub of somatomotor with hypothalamus similar to fast cold down. (E) Slow cold up also shows highly correlated somato-motor and anti-correlated somato-motor-hypothalamus.*

The study of thermal psychophysics in humans reveal that absolute temperature, rate of change of temperature, surface area of thermal contact and the region of the body plays significant role in the perceptional variations. Humans are capable of complex assessments of environmental thermal cues that will induce biophysical changes that takes form of a thermal perception. In awake study in mice, there is no way of knowing these psychophysical mechanisms. Moreover, there are a lot of studies that study thermal behaviors such as paw withdrawal latencies, dwell times, and avoidance behavior and associate the results to thermoception. Another aspect of the awake study that could be explored further is coupling fUS and thermal behavioral experiments. Behavioral experiments as a stand-alone technique might not be able to answer how temperature is sensed and perceived. By combining it with fUS, we could study the organization of thermal circuits and can image discriminative and affective components of thermal sensation.

Taken together, thermal information is perceived after complex integration of peripheral and central mechanisms and extensive study is still required to understand fully the mechanisms underlying thermosensation. By using fUS imaging (alone or in combination with another techniques), we could now capture the most authentic brain responses in behaving animals, with high sensitivity and resolution, to thermal stimulations and this work is only a first step in that direction.

List of Abbreviations

BOLD	Blood-Oxygen-Level Dependent
CBV	Cerebral Blood Volume
DMN	Default Mode Network
DRG	Dorsal Root Ganglion
EEG	Electroencephalography
fUS	Functional Ultrasound
NMDA	N-methyl-D-aspartate
ROI	Region of Interest
SVD	Singular Value Decomposition
TRP	Transient Receptor Potential
S1	Primary Somatosensory Cortex
HL	Hind Limb
FL	Fore Limb
Tr	Trunk
S2	Secondary Somatosensory Cortex
M1	Primary Motor Cortex
Cg	Cingulate Cortex
CPu	Caudate Putamen
GP	Globus Pallidus
ACC	Anterior Cingulate Cortex
MCC	Mid Cingulate Cortex
PCC	Posterior Cingulate Cortex
LPtA	Lateral Parietal Association Cortex
V2ML	Secondary Visual Cortex Mediolateral Area
VPM	Ventral Posteromedial Thalamic Nucleus
VPL	Ventral Posterolateral Thalamic Nucleus
RSD	Retrosplenial Dysgranular Cortex
RSG	Retrosplenial Granular Cortex

BIBLIOGRAPHY

Aaslid, R., Markwalder, T.-M., Nornes, H., 1982. Noninvasive transcranial Doppler ultrasound recording of flow velocity in basal cerebral arteries. J. Neurosurg. 57, 769–774. https://doi.org/10.3171/jns.1982.57.6.0769

Aizawa, Y., Harada, T., Nakata, H., Tsunakawa, M., Sadato, N., Nagashima, K., 2019. Assessment of brain mechanisms involved in the processes of thermal sensation, pleasantness/unpleasantness, and evaluation. IBRO Rep. 6, 54–63. https://doi.org/10.1016/j.ibror.2019.01.003

Aldrich, J.E., 2007. Basic physics of ultrasound imaging: Crit. Care Med. 35, S131–S137. https://doi.org/10.1097/01.CCM.0000260624.99430.22

Andrew, D., Craig, A.D., 2001. Spinothalamic lamina I neurones selectively responsive to cutaneous warming in cats. J. Physiol. 537, 489–495. https://doi.org/10.1111/j.1469-7793.2001.00489.x

Auen, E.L., Poulos, D.A., Hirata, H., Molt, J.T., 1980. Location and organization of thalamic thermosensitive neurons responding to cooling the cat oral-facial regions. Brain Res. 191, 260–264. https://doi.org/10.1016/0006-8993(80)90330-3

Baliki, M.N., Geha, P.Y., Apkarian, A.V., Chialvo, D.R., 2008. Beyond Feeling: Chronic Pain Hurts the Brain, Disrupting the Default-Mode Network Dynamics. J. Neurosci. 28, 1398–1403. https://doi.org/10.1523/JNEUROSCI.4123-07.2008

Bandell, M., Story, G.M., Hwang, S.W., Viswanath, V., Eid, S.R., Petrus, M.J., Earley, T.J., Patapoutian, A., 2004. Noxious Cold Ion Channel TRPA1 Is Activated by Pungent Compounds and Bradykinin. Neuron 41, 849–857. https://doi.org/10.1016/S0896-6273(04)00150-3

Baranger, J., Demene, C., Frerot, A., Faure, F., Delanoë, C., Serroune, H., Houdouin, A., Mairesse, J., Biran, V., Baud, O., Tanter, M., 2021. Bedside functional monitoring of the dynamic brain connectivity in human neonates. Nat. Commun. 12, 1080. https://doi.org/10.1038/s41467-021-21387-x

Barch, D.M., Burgess, G.C., Harms, M.P., Petersen, S.E., Schlaggar, B.L., Corbetta, M., Glasser, M.F., Curtiss, S., Dixit, S., Feldt, C., Nolan, D., Bryant, E., Hartley, T., Footer, O., Bjork, J.M., Poldrack, R., Smith, S., Johansen-Berg, H., Snyder, A.Z., Van Essen, D.C., 2013. Function in the human connectome: Task-fMRI and individual differences in behavior. NeuroImage 80, 169–189. https://doi.org/10.1016/j.neuroimage.2013.05.033

Barthas, F., Sellmeijer, J., Hugel, S., Waltisperger, E., Barrot, M., Yalcin, I., 2015. The Anterior Cingulate Cortex Is a Critical Hub for Pain-Induced Depression. Biol. Psychiatry 77, 236–245. https://doi.org/10.1016/j.biopsych.2014.08.004

Barttfeld, P., Uhrig, L., Sitt, J.D., Sigman, M., Jarraya, B., Dehaene, S., 2015. Signature of consciousness in the dynamics of resting-state brain activity. Proc. Natl. Acad. Sci. 112, 887–892. https://doi.org/10.1073/pnas.1418031112

Bathelt, J., Geurts, H.M., 2021. Difference in default mode network subsystems in autism across childhood and adolescence. Autism 25, 556–565. https://doi.org/10.1177/1362361320969258

Bautista, D.M., Jordt, S.-E., Nikai, T., Tsuruda, P.R., Read, A.J., Poblete, J., Yamoah, E.N., Basbaum, A.I., Julius, D., 2006. TRPA1 Mediates the Inflammatory Actions of Environmental Irritants and Proalgesic Agents. Cell 124, 1269–1282. https://doi.org/10.1016/j.cell.2006.02.023

Bautista, D.M., Siemens, J., Glazer, J.M., Tsuruda, P.R., Basbaum, A.I., Stucky, C.L., Jordt, S.-E., Julius, D., 2007. The menthol receptor TRPM8 is the principal

detector of environmental cold. Nature 448, 204–208. https://doi.org/10.1038/nature05910

Becerra, L., Chang, P.C., Bishop, J., Borsook, D., 2011. CNS activation maps in awake rats exposed to thermal stimuli to the dorsum of the hindpaw. NeuroImage 54, 1355–1366. https://doi.org/10.1016/j.neuroimage.2010.08.056

Becerra, L.R., Breiter, H.C., Stojanovic, M., Fishman, S., Edwards, A., Comite, A.R., Gonzalez, R.G., Borsook, D., 1999. Human brain activation under controlled thermal stimulation and habituation to noxious heat: An fMRI study. Magn. Reson. Med. 41, 1044–1057. https://doi.org/10.1002/(SICI)1522-2594(199905)41:5<1044::AID-MRM25>3.0.CO;2-M

Bennett, G.J., 2000. Update on the Neurophysiology of Pain Transmission and Modulation: Focus on the NMDA-Receptor 19, 5.

Bercoff, J., 2011. Ultrafast Ultrasound Imaging, in: Ultrasound Imaging. p. 25.

Bercoff, J., Montaldo, G., Loupas, T., Savery, D., Mézière, F., Fink, M., Tanter, M., 2011. Ultrafast compound doppler imaging: providing full blood flow characterization. IEEE Trans. Ultrason. Ferroelectr. Freq. Control 58, 134–147. https://doi.org/10.1109/TUFFC.2011.1780

Bergel, A., Tiran, E., Deffieux, T., Demené, C., Tanter, M., Cohen, I., 2020. Adaptive modulation of brain hemodynamics across stereotyped running episodes. Nat. Commun. 11, 6193. https://doi.org/10.1038/s41467-020-19948-7

Berk, M.L., Finkelstein, J.A., 1981. Afferent projections to the preoptic area and hypothalamic regions in the rat brain. Neuroscience 6, 1601–1624. https://doi.org/10.1016/0306-4522(81)90227-X

Berner, N.J., Heller, H.C., 1998. Does the preoptic anterior hypothalamus receive thermoafferent information? Am. J. Physiol.-Regul. Integr. Comp. Physiol. 274, R9–R18. https://doi.org/10.1152/ajpregu.1998.274.1.R9

Bertolo, A., Nouhoum, M., Cazzanelli, S., Ferrier, J., Mariani, J.-C., Kliewer, A., Belliard, B., Osmanski, B.-F., Deffieux, T., Pezet, S., Lenkei, Z., Tanter, M., 2021. Whole-Brain 3D Activation and Functional Connectivity Mapping in Mice using Transcranial Functional Ultrasound Imaging. J. Vis. Exp. 62267. https://doi.org/10.3791/62267

Bessou, P., Perl, E.R., 1969. Response of cutaneous sensory units with unmyelinated fibers to noxious stimuli. J. Neurophysiol. 32, 1025–1043. https://doi.org/10.1152/jn.1969.32.6.1025

Bimbard, C., Demene, C., Girard, C., Radtke-Schuller, S., Shamma, S., Tanter, M., Boubenec, Y., 2018. Multi-scale mapping along the auditory hierarchy using high-resolution functional UltraSound in the awake ferret. eLife 7, e35028. https://doi.org/10.7554/eLife.35028

Birklein, F., Rolke, R., Müller-Forell, W., 2005. Isolated insular infarction eliminates contralateral cold, cold pain, and pinprick perception 7.

Biswal, B., Zerrin Yetkin, F., Haughton, V.M., Hyde, J.S., 1995. Functional connectivity in the motor cortex of resting human brain using echo-planar mri. Magn. Reson. Med. 34, 537–541. https://doi.org/10.1002/mrm.1910340409

Biswal, B.B., Kylen, J.V., Hyde, J.S., 1997. Simultaneous assessment of flow and BOLD signals in resting-state functional connectivity maps. NMR Biomed. 10, 165–170. https://doi.org/10.1002/(SICI)1099-1492(199706/08)10:4/5<165::AID-NBM454>3.0.CO;2-7

Biswal, B.B., Mennes, M., Zuo, X.-N., Gohel, S., Kelly, C., Smith, S.M., Beckmann, C.F., Adelstein, J.S., Buckner, R.L., Colcombe, S., Dogonowski, A.-M., Ernst, M., Fair, D., Hampson, M., Hoptman, M.J., Hyde, J.S., Kiviniemi, V.J., Kotter, R., Li, S.-J., Lin, C.-P., Lowe, M.J., Mackay, C., Madden, D.J., Madsen, K.H., Margulies, D.S., Mayberg, H.S., McMahon, K., Monk, C.S., Mostofsky, S.H., Nagel, B.J.,

Pekar, J.J., Peltier, S.J., Petersen, S.E., Riedl, V., Rombouts, S.A.R.B., Rypma, B., Schlaggar, B.L., Schmidt, S., Seidler, R.D., Siegle, G.J., Sorg, C., Teng, G.-J., Veijola, J., Villringer, A., Walter, M., Wang, L., Weng, X.-C., Whitfield-Gabrieli, S., Williamson, P., Windischberger, C., Zang, Y.-F., Zhang, H.-Y., Castellanos, F.X., Milham, M.P., 2010. Toward discovery science of human brain function. Proc. Natl. Acad. Sci. 107, 4734–4739. https://doi.org/10.1073/pnas.0911855107

Blatteis, C.M., Banet, M., 1986. Autonomic thermoregulation after separation of the preoptic area from the hypothalamus in rats. Pfl�gers Arch. Eur. J. Physiol. 406, 480–484. https://doi.org/10.1007/BF00583370

Boido, D., Rungta, R.L., Osmanski, B.-F., Roche, M., Tsurugizawa, T., Le Bihan, D., Ciobanu, L., Charpak, S., 2019. Mesoscopic and microscopic imaging of sensory responses in the same animal. Nat. Commun. 10, 1110. https://doi.org/10.1038/s41467-019-09082-4

Bokiniec, P., Zampieri, N., Lewin, G.R., Poulet, J.F., 2018. The neural circuits of thermal perception. Curr. Opin. Neurobiol. 52, 98–106. https://doi.org/10.1016/j.conb.2018.04.006

Bowsher, D., 1961. The termination of secondary somatosensory neurons within the thalamus ofMacaca mulatta: An Experimental Degeneration Study. J. Comp. Neurol. 117, 213–227. https://doi.org/10.1002/cne.901170207

Brooks, J.C.W., Nurmikko, T.J., Bimson, W.E., Singh, K.D., Roberts, N., 2002. fMRI of Thermal Pain: Effects of Stimulus Laterality and Attention. NeuroImage 15, 293–301. https://doi.org/10.1006/nimg.2001.0974

Brown, A.G., Iggo, A., 1967. A quantitative study of cutaneous receptors and afferent fibres in the cat and rabbit. J. Physiol. 193, 707–733. https://doi.org/10.1113/jphysiol.1967.sp008390

Büchel, C., Bornhövd, K., Quante, M., Glauche, V., Bromm, B., Weiller, C., 2002. Dissociable Neural Responses Related to Pain Intensity, Stimulus Intensity, and Stimulus Awareness within the Anterior Cingulate Cortex: A Parametric Single-Trial Laser Functional Magnetic Resonance Imaging Study. J. Neurosci. 22, 970–976. https://doi.org/10.1523/JNEUROSCI.22-03-00970.2002

Buckner, R.L., Andrews-Hanna, J.R., Schacter, D.L., 2008a. The Brain's Default Network: Anatomy, Function, and Relevance to Disease. Ann. N. Y. Acad. Sci. 1124, 1–38. https://doi.org/10.1196/annals.1440.011

Buckner, R.L., Andrews-Hanna, J.R., Schacter, D.L., 2008b. *The Brain's Default Network*: *Anatomy, Function, and Relevance to Disease*. Ann. N. Y. Acad. Sci. 1124, 1–38. https://doi.org/10.1196/annals.1440.011

Burton, H., Forbes, D.J., Benjamin, R.M., 1970. Thalamic neurons responsive to temperature changes of glabrous hand and foot skin in squirrel monkey. Brain Res. 24, 179–190. https://doi.org/10.1016/0006-8993(70)90099-5

Bushnell, M.C., Duncan, G.H., Tremblay, N., 1993. Thalamic VPM nucleus in the behaving monkey. I. Multimodal and discriminative properties of thermosensitive neurons. J. Neurophysiol. 69, 739–752. https://doi.org/10.1152/jn.1993.69.3.739

C. Stevens Kenneth K. Choo, J., 1998. Temperature sensitivity of the body surface over the life span. Somatosens. Mot. Res. 15, 13–28. https://doi.org/10.1080/08990229870925

Campbell, S., 2013. A Short History of Sonography in Obstetrics and Gynaecology 17.

Campero, M., Baumann, T.K., Bostock, H., Ochoa, J.L., 2009. Human cutaneous C fibres activated by cooling, heating and menthol: Unmyelinated hot-burning fibres in man. J. Physiol. 587, 5633–5652. https://doi.org/10.1113/jphysiol.2009.176040

Campero, M., Serra, J., Bostock, H., Ochoa, J.L., 2001a. Slowly conducting afferents activated by innocuous low temperature in human skin. J. Physiol. 535, 855–865. https://doi.org/10.1111/j.1469-7793.2001.t01-1-00855.x

Campero, M., Serra, J., Bostock, H., Ochoa, J.L., 2001b. Slowly conducting afferents activated by innocuous low temperature in human skin. J. Physiol. 535, 855–865. https://doi.org/10.1111/j.1469-7793.2001.t01-1-00855.x

Campero, M., Serra, J., Ochoa, J.L., 1996. C-polymodal nociceptors activated by noxious low temperature in human skin. J. Physiol. 497, 565–572. https://doi.org/10.1113/jphysiol.1996.sp021789

Caterina, M.J., Schumacher, M.A., Tominaga, M., Rosen, T.A., Levine, J.D., Julius, D., 1997. The capsaicin receptor: a heat-activated ion channel in the pain pathway. Nature 389, 816–824. https://doi.org/10.1038/39807

Cauli, B., 2010. Revisiting the role of neurons in neurovascular coupling. Front. Neuroenergetics 2. https://doi.org/10.3389/fnene.2010.00009

Chang, C., Glover, G.H., 2010. Time–frequency dynamics of resting-state brain connectivity measured with fMRI. NeuroImage 50, 81–98. https://doi.org/10.1016/j.neuroimage.2009.12.011

Chatt, A.B., Kenshalo, D.R., 1977. Cerebral evoked responses to skin warming recorded from human scalp. Exp. Brain Res. 28. https://doi.org/10.1007/BF00236469

Clapham, D.E., Miller, C., 2011. A thermodynamic framework for understanding temperature sensing by transient receptor potential (TRP) channels. Proc. Natl. Acad. Sci. 108, 19492–19497. https://doi.org/10.1073/pnas.1117485108

Coghill, R.C., Sang, C.N., Maisog, J.Ma., Iadarola, M.J., 1999. Pain Intensity Processing Within the Human Brain: A Bilateral, Distributed Mechanism. J. Neurophysiol. 82, 1934–1943. https://doi.org/10.1152/jn.1999.82.4.1934

Cohen, J.R., 2018. The behavioral and cognitive relevance of time-varying, dynamic changes in functional connectivity. NeuroImage 180, 515–525. https://doi.org/10.1016/j.neuroimage.2017.09.036

Cole, M.W., Bassett, D.S., Power, J.D., Braver, T.S., Petersen, S.E., 2014. Intrinsic and Task-Evoked Network Architectures of the Human Brain. Neuron 83, 238–251. https://doi.org/10.1016/j.neuron.2014.05.014

Cole, M.W., Ito, T., Cocuzza, C., Sanchez-Romero, R., 2021. The Functional Relevance of Task-State Functional Connectivity. J. Neurosci. 41, 2684–2702. https://doi.org/10.1523/JNEUROSCI.1713-20.2021

Cordes, D., Haughton, V.M., Arfanakis, K., Wendt, G.J., Turski, P.A., Moritz, C.H., Quigley, M.A., Meyerand, M.E., 2000. Mapping Functionally Related Regions of Brain with Functional Connectivity MR Imaging 9.

Corradi-Dell'Acqua, C., Hofstetter, C., Vuilleumier, P., 2011. Felt and Seen Pain Evoke the Same Local Patterns of Cortical Activity in Insular and Cingulate Cortex. J. Neurosci. 31, 17996–18006. https://doi.org/10.1523/JNEUROSCI.2686-11.2011

Craig, A.D., 2002. How do you feel? Interoception: the sense of the physiological condition of the body. Nat. Rev. Neurosci. 3, 655–666. https://doi.org/10.1038/nrn894

Craig, A.D., Bushnell, M.C., 1994. The Thermal Grill Illusion: Unmasking the Burn of Cold Pain. Science 265, 252–255. https://doi.org/10.1126/science.8023144

Craig, A.D., Bushnell, M.C., Zhang, E.-T., Blomqvist, A., 1994a. A thalamic nucleus specific for pain and temperature sensation. Nature 372, 770–773. https://doi.org/10.1038/372770a0

Craig, A.D., Bushnell, M.C., Zhang, E.-T., Blomqvist, A., 1994b. A thalamic nucleus specific for pain and temperature sensation. Nature 372, 770–773. https://doi.org/10.1038/372770a0

Craig, A.D., Chen, K., Bandy, D., Reiman, E.M., 2000. Thermosensory activation of insular cortex. Nat. Neurosci. 3, 184–190. https://doi.org/10.1038/72131

Craig, A.D., Krout, K., Andrew, D., 2001. Quantitative Response Characteristics of Thermoreceptive and Nociceptive Lamina I Spinothalamic Neurons in the Cat. J. Neurophysiol. 86, 1459–1480. https://doi.org/10.1152/jn.2001.86.3.1459

Craig, A.D., Reiman, E.M., Evans, A., Bushnell, M.C., 1996. Functional imaging of an illusion of pain. Nature 384, 258–260. https://doi.org/10.1038/384258a0

Damoiseaux, J.S., Rombouts, S.A.R.B., Barkhof, F., Scheltens, P., Stam, C.J., Smith, S.M., Beckmann, C.F., 2006. Consistent resting-state networks across healthy subjects. Proc. Natl. Acad. Sci. 103, 13848–13853. https://doi.org/10.1073/pnas.0601417103

Darian-Smith, I., Johnson, K.O., Dykes, R., 1973. "Cold" fiber population innervating palmar and digital skin of the monkey: responses to cooling pulses. J. Neurophysiol. 36, 325–346. https://doi.org/10.1152/jn.1973.36.2.325

Davis, K.D., Kwan, C.L., Crawley, A.P., Mikulis, D.J., 1998. Functional MRI Study of Thalamic and Cortical Activations Evoked by Cutaneous Heat, Cold, and Tactile Stimuli. J. Neurophysiol. 80, 1533–1546. https://doi.org/10.1152/jn.1998.80.3.1533

Davis, K.D., Lozano, A.M., Manduch, M., Tasker, R.R., Kiss, Z.H.T., Dostrovsky, J.O., 1999a. Thalamic Relay Site for Cold Perception in Humans. J. Neurophysiol. 81, 1970–1973. https://doi.org/10.1152/jn.1999.81.4.1970

Davis, K.D., Lozano, A.M., Manduch, M., Tasker, R.R., Kiss, Z.H.T., Dostrovsky, J.O., 1999b. Thalamic Relay Site for Cold Perception in Humans. J. Neurophysiol. 81, 1970–1973. https://doi.org/10.1152/jn.1999.81.4.1970

De Luca, M., Smith, S., De Stefano, N., Federico, A., Matthews, P.M., 2005. Blood oxygenation level dependent contrast resting state networks are relevant to functional activity in the neocortical sensorimotor system. Exp. Brain Res. 167, 587–594. https://doi.org/10.1007/s00221-005-0059-1

Deffieux, T., Demene, C., Pernot, M., Tanter, M., 2018. Functional ultrasound neuroimaging: a review of the preclinical and clinical state of the art. Curr. Opin. Neurobiol. 50, 128–135. https://doi.org/10.1016/j.conb.2018.02.001

Deffieux, T., Demené, C., Tanter, M., 2021. Functional Ultrasound Imaging: A New Imaging Modality for Neuroscience. Neuroscience 474, 110–121. https://doi.org/10.1016/j.neuroscience.2021.03.005

Defrin, R., Ohry, A., Blumen, N., Urca, G., 2002. Sensory determinants of thermal pain. Brain 125, 501–510. https://doi.org/10.1093/brain/awf055

Demene, C., Baranger, J., Bernal, M., Delanoe, C., Auvin, S., Biran, V., Alison, M., Mairesse, J., Harribaud, E., Pernot, M., Tanter, M., Baud, O., 2017. Functional ultrasound imaging of brain activity in human newborns. Sci. Transl. Med. 9, eaah6756. https://doi.org/10.1126/scitranslmed.aah6756

Demene, C., Deffieux, T., Pernot, M., Osmanski, B.-F., Biran, V., Gennisson, J.-L., Sieu, L.-A., Bergel, A., Franqui, S., Correas, J.-M., Cohen, I., Baud, O., Tanter, M., 2015. Spatiotemporal Clutter Filtering of Ultrafast Ultrasound Data Highly Increases Doppler and fUltrasound Sensitivity. IEEE Trans. Med. Imaging 34, 2271–2285. https://doi.org/10.1109/TMI.2015.2428634

Demertzi, A., Tagliazucchi, E., Dehaene, S., Deco, G., Barttfeld, P., Raimondo, F., Martial, C., Fernández-Espejo, D., Rohaut, B., Voss, H.U., Schiff, N.D., Owen,

A.M., Laureys, S., Naccache, L., Sitt, J.D., 2019a. Human consciousness is supported by dynamic complex patterns of brain signal coordination. Sci. Adv. 5, eaat7603. https://doi.org/10.1126/sciadv.aat7603

Demertzi, A., Tagliazucchi, E., Dehaene, S., Deco, G., Barttfeld, P., Raimondo, F., Martial, C., Fernández-Espejo, D., Rohaut, B., Voss, H.U., Schiff, N.D., Owen, A.M., Laureys, S., Naccache, L., Sitt, J.D., 2019b. Human consciousness is supported by dynamic complex patterns of brain signal coordination. Sci. Adv. 5, eaat7603. https://doi.org/10.1126/sciadv.aat7603

Dennis, E.L., Thompson, P.M., 2014a. Functional Brain Connectivity Using fMRI in Aging and Alzheimer's Disease. Neuropsychol. Rev. 24, 49–62. https://doi.org/10.1007/s11065-014-9249-6

Dennis, E.L., Thompson, P.M., 2014b. Functional Brain Connectivity Using fMRI in Aging and Alzheimer's Disease. Neuropsychol. Rev. 24, 49–62. https://doi.org/10.1007/s11065-014-9249-6

Derbyshire, S.W.G., Jones, A.K.P., Creed, F., Starz, T., Meltzer, C.C., Townsend, D.W., Peterson, A.M., Firestone, L., 2002. Cerebral Responses to Noxious Thermal Stimulation in Chronic Low Back Pain Patients and Normal Controls. NeuroImage 16, 158–168. https://doi.org/10.1006/nimg.2002.1066

Derbyshire, S.W.G., Jones, A.K.P., Gyulai, F., Clark, S., Townsend, D., Firestone, L.L., 1997. Pain processing during three levels of noxious stimulation produces differential patterns of central activity. Pain 73, 431–445. https://doi.org/10.1016/S0304-3959(97)00138-3

Devinsky, O., Morrell, M.J., Vogt, B.A., 1995. Contributions of anterior cingulate cortex to behaviour. Brain 118, 279–306. https://doi.org/10.1093/brain/118.1.279

Dhaka, A., Murray, A.N., Mathur, J., Earley, T.J., Petrus, M.J., Patapoutian, A., 2007. TRPM8 Is Required for Cold Sensation in Mice. Neuron 54, 371–378. https://doi.org/10.1016/j.neuron.2007.02.024

Di, X., Biswal, B.B., 2019. Toward Task Connectomics: Examining Whole-Brain Task Modulated Connectivity in Different Task Domains. Cereb. Cortex 29, 1572–1583. https://doi.org/10.1093/cercor/bhy055

DiMicco, J.A., Zaretsky, D.V., 2007. The dorsomedial hypothalamus: a new player in thermoregulation. Am. J. Physiol.-Regul. Integr. Comp. Physiol. 292, R47–R63. https://doi.org/10.1152/ajpregu.00498.2006

Donahue, R.R., LaGraize, S.C., Fuchs, P.N., 2001. Electrolytic lesion of the anterior cingulate cortex decreases inflammatory, but not neuropathic nociceptive behavior in rats. Brain Res. 897, 131–138. https://doi.org/10.1016/S0006-8993(01)02103-5

Donaldson, H.H., 1885. On the Temperature-Sense 19.

Downer, J., Zubek, J.P., 1954. Role of the cerebral cortex in temperature discrimination in the rat. J. Comp. Physiol. Psychol. 47, 199–203. https://doi.org/10.1037/h0053911

Duclaux, R., Kenshalo, D.R., 1972a. The temperature sensitivity of the Type I slowly adapting mechanoreceptors in cats and monkeys. J. Physiol. 224, 647–664. https://doi.org/10.1113/jphysiol.1972.sp009917

Duclaux, R., Kenshalo, D.R., 1972b. The temperature sensitivity of the Type I slowly adapting mechanoreceptors in cats and monkeys. J. Physiol. 224, 647–664. https://doi.org/10.1113/jphysiol.1972.sp009917

Duncan, G.H., Bushnell, M.C., Oliveras, J.L., Bastrash, N., Tremblay, N., 1993. Thalamic VPM nucleus in the behaving monkey. III. Effects of reversible

inactivation by lidocaine on thermal and mechanical discrimination. J. Neurophysiol. 70, 2086–2096. https://doi.org/10.1152/jn.1993.70.5.2086

Egan, G.F., Johnson, J., Farrell, M., McAllen, R., Zamarripa, F., McKinley, M.J., Lancaster, J., Denton, D., Fox, P.T., 2005. Cortical, thalamic, and hypothalamic responses to cooling and warming the skin in awake humans: A positron-emission tomography study. Proc. Natl. Acad. Sci. 102, 5262–5267. https://doi.org/10.1073/pnas.0409753102

Errico, C., Osmanski, B.-F., Pezet, S., Couture, O., Lenkei, Z., Tanter, M., 2016. Transcranial functional ultrasound imaging of the brain using microbubble-enhanced ultrasensitive Doppler. NeuroImage 124, 752–761. https://doi.org/10.1016/j.neuroimage.2015.09.037

Ferrier, J., Tiran, E., Deffieux, T., Tanter, M., Lenkei, Z., 2020. Functional imaging evidence for task-induced deactivation and disconnection of a major default mode network hub in the mouse brain. Proc. Natl. Acad. Sci. 117, 15270–15280. https://doi.org/10.1073/pnas.1920475117

Filingeri, D., 2016. Neurophysiology of Skin Thermal Sensations. Comprehensive Physiology 6, 1429–1491. https://doi.org/10.1002/cphy.c150040

Finger, S., Frommer, G.P., 1970. Effects of cortical and thalamic lesions on temperature discrimination and responsiveness to foot shock in the rat. Brain Res. 24, 69–89. https://doi.org/10.1016/0006-8993(70)90274-X

Finger, S., Scheff, S., Warshaw, I., Cohen, K., 1970. Retention and acquisition of fine temperature discriminations following somatosensory cortical lesions in the rat. Exp. Brain Res. 10, 340–346. https://doi.org/10.1007/BF02324763

Fox, M.D., Raichle, M.E., 2007. Spontaneous fluctuations in brain activity observed with functional magnetic resonance imaging. Nat. Rev. Neurosci. 8, 700–711. https://doi.org/10.1038/nrn2201

Fox, M.D., Snyder, A.Z., Vincent, J.L., Corbetta, M., Raichle, M.E., 2005. The human brain is intrinsically organized into dynamic, anticorrelated functional networks 6.

Franceschini, M.A., Radhakrishnan, H., Thakur, K., Wu, W., Ruvinskaya, S., Carp, S., Boas, D.A., 2010. The effect of different anesthetics on neurovascular coupling. NeuroImage 51, 1367–1377. https://doi.org/10.1016/j.neuroimage.2010.03.060

Franks, N.P., Lieb, W.R., 1994. Molecular and cellular mechanisms of general anaesthesia. Nature 367, 607–614. https://doi.org/10.1038/367607a0

Fuchs, P.N., Peng, Y.B., Boyette-Davis, J.A., Uhelski, M.L., 2014. The anterior cingulate cortex and pain processing. Front. Integr. Neurosci. 8. https://doi.org/10.3389/fnint.2014.00035

Gagge, A.P., Gonzalez, R.R., 1996. Mechanisms of Heat Exchange: Biophysics and Physiology, in: Terjung, R. (Ed.), Comprehensive Physiology. Wiley, pp. 45–84. https://doi.org/10.1002/cphy.cp040104

Gagge, A.P., Nishi, Y., 1977. Heat Exchange Between Human Skin Surface and Thermal Environment, in: Terjung, R. (Ed.), Comprehensive Physiology. Wiley, pp. 69–92. https://doi.org/10.1002/cphy.cp090105

Garrity, A.G., Pearlson, G.D., McKiernan, K., Lloyd, D., Kiehl, K.A., Calhoun, V.D., 2007. Aberrant “Default Mode” Functional Connectivity in Schizophrenia. Am J Psychiatry 8.

Gasquoine, P.G., 2013. Localization of function in anterior cingulate cortex: From psychosurgery to functional neuroimaging. Neurosci. Biobehav. Rev. 37, 340–348. https://doi.org/10.1016/j.neubiorev.2013.01.002

Gauriau, C., Bernard, J.-F., 2004. A comparative reappraisal of projections from the superficial laminae of the dorsal horn in the rat: The forebrain. J. Comp. Neurol. 468, 24–56. https://doi.org/10.1002/cne.10873

Gebhart, G.F., Schmidt, R.F. (Eds.), 2013. Primary Afferents/Neurons, in: Encyclopedia of Pain. Springer Berlin Heidelberg, Berlin, Heidelberg, pp. 3173–3174. https://doi.org/10.1007/978-3-642-28753-4_201762

Gelnar, P.A., Krauss, B.R., Sheehe, P.R., Szeverenyi, N.M., Apkarian, A.V., 1999. A Comparative fMRI Study of Cortical Representations for Thermal Painful, Vibrotactile, and Motor Performance Tasks. NeuroImage 10, 460–482. https://doi.org/10.1006/nimg.1999.0482

Gerrett, N., Ouzzahra, Y., Coleby, S., Hobbs, S., Redortier, B., Voelcker, T., Havenith, G., 2014. Thermal sensitivity to warmth during rest and exercise: a sex comparison. Eur. J. Appl. Physiol. 114, 1451–1462. https://doi.org/10.1007/s00421-014-2875-0

Gesnik, M., Blaize, K., Deffieux, T., Gennisson, J.-L., Sahel, J.-A., Fink, M., Picaud, S., Tanter, M., 2017. 3D functional ultrasound imaging of the cerebral visual system in rodents. NeuroImage 149, 267–274. https://doi.org/10.1016/j.neuroimage.2017.01.071

Gloor, P., 1969. Hans Berger and the discovery of the electroencephalogram. Electroencephalogr. Clin. Neurophysiol. Suppl 28:1-36.

Gogolla, N., Takesian, A.E., Feng, G., Fagiolini, M., Hensch, T.K., 2014. Sensory Integration in Mouse Insular Cortex Reflects GABA Circuit Maturation. Neuron 83, 894–905. https://doi.org/10.1016/j.neuron.2014.06.033

Gonen, O.M., Kwan, P., O'Brien, T.J., Lui, E., Desmond, P.M., 2020. Resting-state functional MRI of the default mode network in epilepsy. Epilepsy Behav. 111, 107308. https://doi.org/10.1016/j.yebeh.2020.107308

Gong, J., Liu, Jinzhi, Ronan, E.A., He, F., Cai, W., Fatima, M., Zhang, W., Lee, H., Li, Z., Kim, G.-H., Pipe, K.P., Duan, B., Liu, Jianfeng, Xu, X.Z.S., 2019. A Cold-Sensing Receptor Encoded by a Glutamate Receptor Gene. Cell 178, 1375-1386.e11. https://doi.org/10.1016/j.cell.2019.07.034

Gonzalez-Castillo, J., Bandettini, P.A., 2018. Task-based dynamic functional connectivity: Recent findings and open questions. NeuroImage 180, 526–533. https://doi.org/10.1016/j.neuroimage.2017.08.006

Gracheva, E.O., Bagriantsev, S.N., 2015. Evolutionary adaptation to thermosensation. Curr. Opin. Neurobiol. 34, 67–73. https://doi.org/10.1016/j.conb.2015.01.021

Grandjean, J., Canella, C., Anckaerts, C., Ayrancı, G., Bougacha, S., Bienert, T., Buehlmann, D., Coletta, L., Gallino, D., Gass, N., Garin, C.M., Nadkarni, N.A., Hübner, N.S., Karatas, M., Komaki, Y., Kreitz, S., Mandino, F., Mechling, A.E., Sato, C., Sauer, K., Shah, D., Strobelt, S., Takata, N., Wank, I., Wu, T., Yahata, N., Yeow, L.Y., Yee, Y., Aoki, I., Chakravarty, M.M., Chang, W.-T., Dhenain, M., von Elverfeldt, D., Harsan, L.-A., Hess, A., Jiang, T., Keliris, G.A., Lerch, J.P., Meyer-Lindenberg, A., Okano, H., Rudin, M., Sartorius, A., Van der Linden, A., Verhoye, M., Weber-Fahr, W., Wenderoth, N., Zerbi, V., Gozzi, A., 2020. Common functional networks in the mouse brain revealed by multi-centre resting-state fMRI analysis. NeuroImage 205, 116278. https://doi.org/10.1016/j.neuroimage.2019.116278

Green, B.G., 2004. Temperature perception and nociception. J. Neurobiol. 61, 13–29. https://doi.org/10.1002/neu.20081

Greenspan, J.D., Lee, R.R., Lenz, F.A., 1999. Pain sensitivity alterations as a function of lesion location in the parasylvian cortex. Pain 81, 273–282. https://doi.org/10.1016/S0304-3959(99)00021-4

Greicius, M.D., Krasnow, B., Reiss, A.L., Menon, V., 2003. Functional connectivity in the resting brain: A network analysis of the default mode hypothesis. Proc. Natl. Acad. Sci. 100, 253–258. https://doi.org/10.1073/pnas.0135058100

Greicius, M.D., Srivastava, G., Reiss, A.L., Menon, V., 2004. Default-mode network activity distinguishes Alzheimer's disease from healthy aging: Evidence from functional MRI. Proc. Natl. Acad. Sci. 101, 4637–4642. https://doi.org/10.1073/pnas.0308627101

Gu, Y., Lin, Y., Huang, L., Ma, J., Zhang, J., Xiao, Y., Dai, Z., Alzheimer's Disease Neuroimaging Initiative, 2020. Abnormal dynamic functional connectivity in Alzheimer's disease. CNS Neurosci. Ther. 26, 962–971. https://doi.org/10.1111/cns.13387

Haraguchi, K., Kawamoto, A., Isami, K., Maeda, S., Kusano, A., Asakura, K., Shirakawa, H., Mori, Y., Nakagawa, T., Kaneko, S., 2012. TRPM2 Contributes to Inflammatory and Neuropathic Pain through the Aggravation of Pronociceptive Inflammatory Responses in Mice. J. Neurosci. 32, 3931–3941. https://doi.org/10.1523/JNEUROSCI.4703-11.2012

He, J.-W., Liu, H., Peng, Y., 2015. Hemodynamic and Light-Scattering Changes of Rat Spinal Cord and Primary Somatosensory Cortex in Response to Innocuous and Noxious Stimuli. Brain Sci. 5, 400–418. https://doi.org/10.3390/brainsci5040400

Hellon, R.F., Misra, N.K., 1973. Neurones in the dorsal horn of the rat responding to scrotal skin temperature changes. J Physiol 14.

Hellon, R.F., Misra, N.K., Provins, K.A., 1973a. Neurones in the somatosensory cortex of the rat responding to scrotal skin temperature changes. J. Physiol. 232, 401–411. https://doi.org/10.1113/jphysiol.1973.sp010277

Hellon, R.F., Misra, N.K., Provins, K.A., 1973b. Neurones in the somatosensory cortex of the rat responding to scrotal skin temperature changes. J. Physiol. 232, 401–411. https://doi.org/10.1113/jphysiol.1973.sp010277

Hensel, H., Boman, K.K.A., 1960. AFFERENT IMPULSES IN CUTANEOUS SENSORY NERVES IN HUMAN SUBJECTS. J. Neurophysiol. 23, 564–578. https://doi.org/10.1152/jn.1960.23.5.564

Hille, B., 2001. Ion Channels of Excitable Membranes, Third. ed.

Hoffman, H.G., Richards, T.L., Coda, B., Bills, A.R., Blough, D., Richards, A.L., Sharar, S.R., 2004. Modulation of thermal pain-related brain activity with virtual reality: evidence from fMRI: NeuroReport 15, 1245–1248. https://doi.org/10.1097/01.wnr.0000127826.73576.91

Hoffstaetter, L.J., Bagriantsev, S.N., Gracheva, E.O., 2018. TRPs et al.: a molecular toolkit for thermosensory adaptations. Pflüg. Arch. - Eur. J. Physiol. 470, 745–759. https://doi.org/10.1007/s00424-018-2120-5

Hua, L.H., Strigo, I.A., Baxter, L.C., Johnson, S.C., Craig, A.D. (Bud), 2005. Anteroposterior somatotopy of innocuous cooling activation focus in human dorsal posterior insular cortex. Am. J. Physiol.-Regul. Integr. Comp. Physiol. 289, R319–R325. https://doi.org/10.1152/ajpregu.00123.2005

Huang, S.M., Li, X., Yu, Y., Wang, J., Caterina, M.J., 2011. TRPV3 and TRPV4 Ion Channels are Not Major Contributors to Mouse Heat Sensation. Mol. Pain 7, 1744-8069-7–37. https://doi.org/10.1186/1744-8069-7-37

Hutchison, R.M., Womelsdorf, T., Allen, E.A., Bandettini, P.A., Calhoun, V.D., Corbetta, M., Della Penna, S., Duyn, J.H., Glover, G.H., Gonzalez-Castillo, J., Handwerker, D.A., Keilholz, S., Kiviniemi, V., Leopold, D.A., de Pasquale, F., Sporns, O., Walter, M., Chang, C., 2013. Dynamic functional connectivity:

Promise, issues, and interpretations. NeuroImage 80, 360–378. https://doi.org/10.1016/j.neuroimage.2013.05.079

Hutchison, W.D., Davis, K.D., Lozano, A.M., Tasker, R.R., Dostrovsky, J.O., 1999. Pain-related neurons in the human cingulate cortex. Nat. Neurosci. 2, 403–405. https://doi.org/10.1038/8065

Iggo, A., 1959. CUTANEOUS HEAT AND COLD RECEPTORS WITH SLOWLY CONDUCTING (C) AFFERENT FIBRES. Q. J. Exp. Physiol. Cogn. Med. Sci. 44, 362–370. https://doi.org/10.1113/expphysiol.1959.sp001417

Imbault, M., Chauvet, D., Gennisson, J.-L., Capelle, L., Tanter, M., 2017. Intraoperative Functional Ultrasound Imaging of Human Brain Activity. Sci. Rep. 7, 7304. https://doi.org/10.1038/s41598-017-06474-8

İnce, R., Adanır, S.S., Sevmez, F., 2021. The inventor of electroencephalography (EEG): Hans Berger (1873–1941). Childs Nerv. Syst. 37, 2723–2724. https://doi.org/10.1007/s00381-020-04564-z

Ishiwata, T., Hasegawa, H., Yazawa, T., Otokawa, M., Aihara, Y., 2002. Functional role of the preoptic area and anterior hypothalamus in thermoregulation in freely moving rats. Neurosci. Lett. 325, 167–170. https://doi.org/10.1016/S0304-3940(02)00266-5

Iwata, K., Kamo, H., Ogawa, A., Tsuboi, Y., Noma, N., Mitsuhashi, Y., Taira, M., Koshikawa, N., Kitagawa, J., 2005. Anterior Cingulate Cortical Neuronal Activity During Perception of Noxious Thermal Stimuli in Monkeys. J. Neurophysiol. 94, 1980–1991. https://doi.org/10.1152/jn.00190.2005

Jeffrey-Gauthier, R., Guillemot, J.-P., Piché, M., 2013. Neurovascular coupling during nociceptive processing in the primary somatosensory cortex of the rat. Pain 154, 1434–1441. https://doi.org/10.1016/j.pain.2013.04.042

Jenkins, A.C., 2019. Rethinking Cognitive Load: A Default-Mode Network Perspective. Trends Cogn. Sci. 23, 531–533. https://doi.org/10.1016/j.tics.2019.04.008

Jensen, J.A., 2007. Medical ultrasound imaging. Prog. Biophys. Mol. Biol. 93, 153–165. https://doi.org/10.1016/j.pbiomolbio.2006.07.025

Jones, L.A., Berris, M., 2002. The psychophysics of temperature perception and thermal-interface design, in: Proceedings 10th Symposium on Haptic Interfaces for Virtual Environment and Teleoperator Systems. HAPTICS 2002. Presented at the 10th Symposium on Haptic Interfaces for Virtual Environment and Teleoperator Systems. HAPTICS 2002, IEEE Comput. Soc, Orlando, FL, USA, pp. 137–142. https://doi.org/10.1109/HAPTIC.2002.998951

Julius, D., 2013. TRP Channels and Pain. Annu. Rev. Cell Dev. Biol. 29, 355–384. https://doi.org/10.1146/annurev-cellbio-101011-155833

Kenshalo, D.R., Decker, T., Hamilton, A., 1967. Spatial summation on the forehead, forearm, and back produced by radiant and conducted heat. J. Comp. Physiol. Psychol. 63, 510–515. https://doi.org/10.1037/h0024610

Kenshalo, D.R., Duclaux, R., 1977. Response characteristics of cutaneous cold receptors in the monkey. J. Neurophysiol. 40, 319–332. https://doi.org/10.1152/jn.1977.40.2.319

Kenshalo, D.R., Holmes, C.E., Wood, P.B., 1968. Warm and cool thresholds as a function of rate of stimulus temperature change. Percept. Psychophys. 3, 81–84. https://doi.org/10.3758/BF03212769

Kieliba, P., Madugula, S., Filippini, N., Duff, E.P., Makin, T.R., 2019. Large-scale intrinsic connectivity is consistent across varying task demands. PLOS ONE 14, e0213861. https://doi.org/10.1371/journal.pone.0213861

Knowlton, W.M., Palkar, R., Lippoldt, E.K., McCoy, D.D., Baluch, F., Chen, J., McKemy, D.D., 2013. A Sensory-Labeled Line for Cold: TRPM8-Expressing

Sensory Neurons Define the Cellular Basis for Cold, Cold Pain, and Cooling-Mediated Analgesia. J. Neurosci. 33, 2837–2848. https://doi.org/10.1523/JNEUROSCI.1943-12.2013

Kwan, C.L., Crawley, A.P., Mikulis, D.J., Davis, K.D., 2000a. An fMRI study of the anterior cingulate cortex and surrounding medial wall activations evoked by noxious cutaneous heat and cold stimuli. Pain 85, 359–374. https://doi.org/10.1016/S0304-3959(99)00287-0

Kwan, C.L., Crawley, A.P., Mikulis, D.J., Davis, K.D., 2000b. An fMRI study of the anterior cingulate cortex and surrounding medial wall activations evoked by noxious cutaneous heat and cold stimuli. Pain 85, 359–374. https://doi.org/10.1016/S0304-3959(99)00287-0

Kwan, K.Y., Allchorne, A.J., Vollrath, M.A., Christensen, A.P., Zhang, D.-S., Woolf, C.J., Corey, D.P., 2006. TRPA1 Contributes to Cold, Mechanical, and Chemical Nociception but Is Not Essential for Hair-Cell Transduction. Neuron 50, 277–289. https://doi.org/10.1016/j.neuron.2006.03.042

Lahti, K.M., Ferris, C.F., Li, F., Sotak, C.H., King, J.A., 1999. Comparison of evoked cortical activity in conscious and propofol-anesthetized rats using functional MRI. Magn. Reson. Med. 41, 412–416. https://doi.org/10.1002/(SICI)1522-2594(199902)41:2<412::AID-MRM28>3.0.CO;2-3

Landgren, S., 1960. Thalamic Neurones Responding to Cooling of the Cat's Tongue. Acta Physiol. Scand. 48, 255–267. https://doi.org/10.1111/j.1748-1716.1960.tb01860.x

Landgren, S., 1957a. Cortical Reception of Cold Impulses from the Tongue of the Cat. Acta Physiol. Scand. 40, 202–209. https://doi.org/10.1111/j.1748-1716.1957.tb01489.x

Landgren, S., 1957b. Cortical Reception of Cold Impulses from the Tongue of the Cat. Acta Physiol. Scand. 40, 202–209. https://doi.org/10.1111/j.1748-1716.1957.tb01489.x

Li, F., Lu, L., Shang, S., Chen, H., Wang, P., Muthaiah, V.P., Yin, X., Chen, Y.-C., 2021. Altered static and dynamic functional network connectivity in post-traumatic headache. J. Headache Pain 22, 137. https://doi.org/10.1186/s10194-021-01348-x

Li, Y., Zhu, Y., Nguchu, B.A., Wang, Y., Wang, H., Qiu, B., Wang, X., 2020. Dynamic Functional Connectivity Reveals Abnormal Variability and Hyper-connected Pattern in Autism Spectrum Disorder. Autism Res. 13, 230–243. https://doi.org/10.1002/aur.2212

Lu, C., Yang, T., Zhao, H., Zhang, M., Meng, F., Fu, H., Xie, Y., Xu, H., 2016. Insular Cortex is Critical for the Perception, Modulation, and Chronification of Pain. Neurosci. Bull. 32, 191–201. https://doi.org/10.1007/s12264-016-0016-y

Ma, Q., 2010. Labeled lines meet and talk: population coding of somatic sensations. J. Clin. Invest. 120, 3773–3778. https://doi.org/10.1172/JCI43426

Macé, E., Montaldo, G., Cohen, I., Baulac, M., Fink, M., Tanter, M., 2011. Functional ultrasound imaging of the brain. Nat. Methods 8, 662–664. https://doi.org/10.1038/nmeth.1641

Mace, E., Montaldo, G., Osmanski, B.-F., Cohen, I., Fink, M., Tanter, M., 2013. Functional ultrasound imaging of the brain: theory and basic principles. IEEE Trans. Ultrason. Ferroelectr. Freq. Control 60, 492–506. https://doi.org/10.1109/TUFFC.2013.2592

Macé, É., Montaldo, G., Trenholm, S., Cowan, C., Brignall, A., Urban, A., Roska, B., 2018. Whole-Brain Functional Ultrasound Imaging Reveals Brain Modules for

Visuomotor Integration. Neuron 100, 1241-1251.e7. https://doi.org/10.1016/j.neuron.2018.11.031

Margulies, D.S., Kelly, A.M.C., Uddin, L.Q., Biswal, B.B., Castellanos, F.X., Milham, M.P., 2007. Mapping the functional connectivity of anterior cingulate cortex. NeuroImage 37, 579–588. https://doi.org/10.1016/j.neuroimage.2007.05.019

Masamoto, K., Kanno, I., 2012. Anesthesia and the Quantitative Evaluation of Neurovascular Coupling. J. Cereb. Blood Flow Metab. 32, 1233–1247. https://doi.org/10.1038/jcbfm.2012.50

Matta, J.A., Ahern, G.P., 2007. Voltage is a partial activator of rat thermosensitive TRP channels: Voltage-independent gating of TRPV1 and TRPM8. J. Physiol. 585, 469–482. https://doi.org/10.1113/jphysiol.2007.144287

McKemy, D.D., Neuhausser, W.M., Julius, D., 2002. Identification of a cold receptor reveals a general role for TRP channels in thermosensation. Nature 416, 52–58. https://doi.org/10.1038/nature719

Milenkovic, N., Zhao, W.-J., Walcher, J., Albert, T., Siemens, J., Lewin, G.R., Poulet, J.F.A., 2014. A somatosensory circuit for cooling perception in mice. Nat. Neurosci. 17, 1560–1566. https://doi.org/10.1038/nn.3828

Mishra, S.K., Hoon, M.A., 2010. Ablation of TrpV1 neurons reveals their selective role in thermal pain sensation. Mol. Cell. Neurosci. 43, 157–163. https://doi.org/10.1016/j.mcn.2009.10.006

Mohan, Akansha, Roberto, A.J., Mohan, Abhishek, Lorenzo, A., Jones, K., Carney, M.J., Liogier-Weyback, L., Hwang, S., Lapidus, K.A.B., 2016. The Significance of the Default Mode Network (DMN) in Neurological and Neuropsychiatric Disorders: A Review 9.

Mohan, Akansha, Roberto, A.J., Mohan, Abhishek, Lorenzo, A., Jones, K., Carney, M.J., Liogier-Weyback, L., Hwang, S., Lapidus, K.A.B., n.d. The Significance of

the Default Mode Network (DMN) in Neurological and Neuropsychiatric Disorders: A Review 9.

Montaldo, G., Tanter, M., Bercoff, J., Benech, N., Fink, M., 2009. Coherent plane-wave compounding for very high frame rate ultrasonography and transient elastography. IEEE Trans. Ultrason. Ferroelectr. Freq. Control 56, 489–506. https://doi.org/10.1109/TUFFC.2009.1067

Moulton, E.A., Pendse, G., Becerra, L.R., Borsook, D., 2012. BOLD Responses in Somatosensory Cortices Better Reflect Heat Sensation than Pain. J. Neurosci. 32, 6024–6031. https://doi.org/10.1523/JNEUROSCI.0006-12.2012

Nagashima, K., Tokizawa, K., Marui, S., 2018. Thermal comfort, in: Handbook of Clinical Neurology. Elsevier, pp. 249–260. https://doi.org/10.1016/B978-0-444-63912-7.00015-1

Nandakumar, B., Blumenthal, G.H., Pauzin, F.P., Moxon, K.A., 2021. Hindlimb Somatosensory Information Influences Trunk Sensory and Motor Cortices to Support Trunk Stabilization. Cereb. Cortex 31, 5165–5187. https://doi.org/10.1093/cercor/bhab150

Nevian, T., 2017. The cingulate cortex: divided in pain. Nat. Neurosci. 20, 1515–1517. https://doi.org/10.1038/nn.4664

Norrsell, U., Craig, A.D., 1999. Behavioral Thermosensitivity After Lesions of Thalamic Target Areas of a Thermosensory Spinothalamic Pathway in the Cat. J. Neurophysiol. 82, 611–625. https://doi.org/10.1152/jn.1999.82.2.611

Norrsell, U., Finger, S., Lajonchere, C., 1999. Cutaneous sensory spots and the “law of specific nerve energies”: history and development of ideas. Brain Res. Bull. 48, 457–465. https://doi.org/10.1016/S0361-9230(98)00067-7

Olausson, H., Charron, J., Marchand, S., Villemure, C., Strigo, I.A., Bushnell, M.C., 2005. Feelings of warmth correlate with neural activity in right anterior insular cortex. Neurosci. Lett. 389, 1–5. https://doi.org/10.1016/j.neulet.2005.06.065

Osmanski, B.-F., Pezet, S., Ricobaraza, A., Lenkei, Z., Tanter, M., 2014. Functional ultrasound imaging of intrinsic connectivity in the living rat brain with high spatiotemporal resolution. Nat. Commun. 5, 5023. https://doi.org/10.1038/ncomms6023

Pais-Roldán, P., Mateo, C., Pan, W.-J., Acland, B., Kleinfeld, D., Snyder, L.H., Yu, X., Keilholz, S., 2021. Contribution of animal models toward understanding resting state functional connectivity. NeuroImage 245, 118630. https://doi.org/10.1016/j.neuroimage.2021.118630

Paquette, T., Leblond, H., Piché, M., 2019a. Isoflurane anesthesia does not affect spinal cord neurovascular coupling: evidence from decerebrated rats. J. Physiol. Sci. 69, 13–21. https://doi.org/10.1007/s12576-018-0607-7

Paquette, T., Tokunaga, R., Touj, S., Leblond, H., Piché, M., 2019b. Regulation of cortical blood flow responses by the nucleus basalis of Meynert during nociceptive processing. Neurosci. Res. 149, 22–28. https://doi.org/10.1016/j.neures.2019.01.008

Paricio-Montesinos, R., Schwaller, F., Udhayachandran, A., Rau, F., Walcher, J., Evangelista, R., Vriens, J., Voets, T., Poulet, J.F.A., Lewin, G.R., 2020. The Sensory Coding of Warm Perception. Neuron 106, 830-841.e3. https://doi.org/10.1016/j.neuron.2020.02.035

Park, H.-J., Friston, K., 2013. Structural and Functional Brain Networks: From Connections to Cognition. Science 342, 1238411. https://doi.org/10.1126/science.1238411

Parsons, N., Bowden, S.C., Vogrin, S., D'Souza, W.J., 2020. Default mode network dysfunction in idiopathic generalised epilepsy. Epilepsy Res. 159, 106254. https://doi.org/10.1016/j.eplepsyres.2019.106254

Patapoutian, A., Peier, A.M., Story, G.M., Viswanath, V., 2003. ThermoTRP channels and beyond: mechanisms of temperature sensation. Nat. Rev. Neurosci. 4, 529–539. https://doi.org/10.1038/nrn1141

Paxinos, G., Franklin, K.B., 2011. Paxinos and Franklin's the mouse brain in stereotaxic coordinates.

Paxinos, G., Watson, C., 1997. The Rat Brain in Stereotaxic Coordinates.

Peier, A.M., Moqrich, A., Hergarden, A.C., Reeve, A.J., Andersson, D.A., Story, G.M., Earley, T.J., Dragoni, I., McIntyre, P., Bevan, S., Patapoutian, A., 2002. A TRP Channel that Senses Cold Stimuli and Menthol. Cell 108, 705–715. https://doi.org/10.1016/S0092-8674(02)00652-9

Peltz, E., Seifert, F., DeCol, R., Dörfler, A., Schwab, S., Maihöfner, C., 2011. Functional connectivity of the human insular cortex during noxious and innocuous thermal stimulation. NeuroImage 54, 1324–1335. https://doi.org/10.1016/j.neuroimage.2010.09.012

Penfield, W., Faulk, M.E., 1955. THE INSULA: FURTHER OBSERVATIONS ON ITS FUNCTION. Brain 78, 445–470. https://doi.org/10.1093/brain/78.4.445

Petrenko, A.B., Yamakura, T., Baba, H., Shimoji, K., 2003. The Role of N-Methyl-d-Aspartate (NMDA) Receptors in Pain: A Review: Anesth. Analg. 1108–1116. https://doi.org/10.1213/01.ANE.0000081061.12235.55

Piché, M., Paquette, T., Leblond, H., 2017. Tight neurovascular coupling in the spinal cord during nociceptive stimulation in intact and spinal rats. Neuroscience 355, 1–8. https://doi.org/10.1016/j.neuroscience.2017.04.038

Ploner, M., Gross, J., Timmermann, L., Schnitzler, A., 2002. Cortical representation of first and second pain sensation in humans. Proc. Natl. Acad. Sci. 99, 12444–12448. https://doi.org/10.1073/pnas.182272899

Porter, L.H., Hecht, G.S., Sheaffer, R., 1993. Disturbances in the performance of thermal discrimination tasks following cortical ablations in rats. Brain Res. 621, 319–330. https://doi.org/10.1016/0006-8993(93)90122-4

Poulos, D.A., Benjamin, R.M., 1968. Response of thalamic neurons to thermal stimulation of the tongue. J. Neurophysiol. 31, 28–43. https://doi.org/10.1152/jn.1968.31.1.28

Powles, A.EJ., Martin, D.J., Wells, I.TP., Goodwin, C.R., 2018. Physics of ultrasound. Anaesth. Intensive Care Med. 19, 202–205. https://doi.org/10.1016/j.mpaic.2018.01.005

Prescott, S.A., Ma, Q., De Koninck, Y., 2014. Normal and abnormal coding of somatosensory stimuli causing pain. Nat. Neurosci. 17, 183–191. https://doi.org/10.1038/nn.3629

Prescott, S.A., Ratté, S., 2012. Pain processing by spinal microcircuits: afferent combinatorics. Curr. Opin. Neurobiol. 22, 631–639. https://doi.org/10.1016/j.conb.2012.02.010

Preti, M.G., Bolton, T.A., Van De Ville, D., 2017. The dynamic functional connectome: State-of-the-art and perspectives. NeuroImage 160, 41–54. https://doi.org/10.1016/j.neuroimage.2016.12.061

Rabut, C., Ferrier, J., Bertolo, A., Osmanski, B., Mousset, X., Pezet, S., Deffieux, T., Lenkei, Z., Tanter, M., 2020. Pharmaco-fUS: Quantification of pharmacologically-induced dynamic changes in brain perfusion and connectivity by functional ultrasound imaging in awake mice. NeuroImage 222, 117231. https://doi.org/10.1016/j.neuroimage.2020.117231

Rahal, L., Thibaut, M., Rivals, I., Claron, J., Lenkei, Z., Sitt, J.D., Tanter, M., Pezet, S., 2020. Ultrafast ultrasound imaging pattern analysis reveals distinctive dynamic brain states and potent sub-network alterations in arthritic animals. Sci. Rep. 10, 10485. https://doi.org/10.1038/s41598-020-66967-x

Raichle, M.E., 2015. The Brain's Default Mode Network. Annu. Rev. Neurosci. 38, 433–447. https://doi.org/10.1146/annurev-neuro-071013-014030

Raichle, M.E., 2011. The Restless Brain. Brain Connect. 1, 3–12. https://doi.org/10.1089/brain.2011.0019

Raichle, M.E., 2010. Two views of brain function. Trends Cogn. Sci. 14, 180–190. https://doi.org/10.1016/j.tics.2010.01.008

Raichle, M.E., MacLeod, A.M., Snyder, A.Z., Powers, W.J., Gusnard, D.A., Shulman, G.L., 2001. A default mode of brain function. Proc. Natl. Acad. Sci. 98, 676–682. https://doi.org/10.1073/pnas.98.2.676

Raichle, M.E., Snyder, A.Z., 2007. A default mode of brain function: A brief history of an evolving idea. NeuroImage 37, 1083–1090. https://doi.org/10.1016/j.neuroimage.2007.02.041

Ran, C., Chen, X., 2019. Probing the coding logic of thermosensation using spinal cord calcium imaging. Exp. Neurol. 318, 42–49. https://doi.org/10.1016/j.expneurol.2019.04.009

Ran, C., Hoon, M.A., Chen, X., 2016. The coding of cutaneous temperature in the spinal cord. Nat. Neurosci. 19, 1201–1209. https://doi.org/10.1038/nn.4350

Rodgers, K.M., Benison, A.M., Klein, A., Barth, D.S., 2008. Auditory, Somatosensory, and Multisensory Insular Cortex in the Rat. Cereb. Cortex 18, 2941–2951. https://doi.org/10.1093/cercor/bhn054

Rothhaas, R., Chung, S., 2021. Role of the Preoptic Area in Sleep and Thermoregulation. Front. Neurosci. 15, 664781. https://doi.org/10.3389/fnins.2021.664781

Rungta, R.L., Osmanski, B.-F., Boido, D., Tanter, M., Charpak, S., 2017. Light controls cerebral blood flow in naive animals. Nat. Commun. 8, 14191. https://doi.org/10.1038/ncomms14191

Satpute, A.B., Lindquist, K.A., 2019. The Default Mode Network's Role in Discrete Emotion. Trends Cogn. Sci. 23, 851–864. https://doi.org/10.1016/j.tics.2019.07.003

Scheinost, D., Sinha, R., Cross, S.N., Kwon, S.H., Sze, G., Constable, R.T., Ment, L.R., 2017. Does prenatal stress alter the developing connectome? Pediatr. Res. 81, 214–226. https://doi.org/10.1038/pr.2016.197

Schepers, R.J., Ringkamp, M., 2010. Thermoreceptors and thermosensitive afferents. Neurosci. Biobehav. Rev. 8.

Schingnitz, G., Werner, J., 1980. Responses of thalamic neurons to thermal stimulation of the limbs, scrotum and tongue in the rat. J. Therm. Biol. 5, 53–61. https://doi.org/10.1016/0306-4565(80)90040-6

Sieu, L.-A., Bergel, A., Tiran, E., Deffieux, T., Pernot, M., Gennisson, J.-L., Tanter, M., Cohen, I., 2015. EEG and functional ultrasound imaging in mobile rats. Nat. Methods 12, 831–834. https://doi.org/10.1038/nmeth.3506

Simone, D.A., Kajander, K.C., 1997. Responses of Cutaneous A-Fiber Nociceptors to Noxious Cold. J. Neurophysiol. 77, 2049–2060. https://doi.org/10.1152/jn.1997.77.4.2049

Singh, A., Patel, D., Li, A., Hu, L., Zhang, Q., Liu, Y., Guo, X., Robinson, E., Martinez, E., Doan, L., Rudy, B., Chen, Z.S., Wang, J., 2020. Mapping Cortical Integration

of Sensory and Affective Pain Pathways. Curr. Biol. 30, 1703-1715.e5. https://doi.org/10.1016/j.cub.2020.02.091

Sleigh, J., 2014. Ketamine - More mechanisms of action than just NMDA blockade. Trends Anaesth. Crit. Care 6.

Smith, S.M., Fox, P.T., Miller, K.L., Glahn, D.C., Fox, P.M., Mackay, C.E., Filippini, N., Watkins, K.E., Toro, R., Laird, A.R., Beckmann, C.F., 2009. Correspondence of the brain's functional architecture during activation and rest. Proc. Natl. Acad. Sci. 106, 13040–13045. https://doi.org/10.1073/pnas.0905267106

Soloukey, S., Vincent, A.J.P.E., Satoer, D.D., Mastik, F., Smits, M., Dirven, C.M.F., Strydis, C., Bosch, J.G., van der Steen, A.F.W., De Zeeuw, C.I., Koekkoek, S.K.E., Kruizinga, P., 2020. Functional Ultrasound (fUS) During Awake Brain Surgery: The Clinical Potential of Intra-Operative Functional and Vascular Brain Mapping. Front. Neurosci. 13, 1384. https://doi.org/10.3389/fnins.2019.01384

Song, K., Wang, H., Kamm, G.B., Pohle, J., Reis, F. d. C., Heppenstall, P., Wende, H., Siemens, J., 2016. The TRPM2 channel is a hypothalamic heat sensor that limits fever and can drive hypothermia. Science 353, 1393–1398. https://doi.org/10.1126/science.aaf7537

Story, G.M., Peier, A.M., Reeve, A.J., Eid, S.R., Mosbacher, J., Hricik, T.R., Earley, T.J., Hergarden, A.C., Andersson, D.A., Hwang, S.W., McIntyre, P., Jegla, T., Bevan, S., Patapoutian, A., 2003. ANKTM1, a TRP-like Channel Expressed in Nociceptive Neurons, Is Activated by Cold Temperatures. Cell 112, 819–829. https://doi.org/10.1016/S0092-8674(03)00158-2

Tan, C.-H., McNaughton, P.A., 2018. TRPM2 and warmth sensation. Pflüg. Arch. - Eur. J. Physiol. 470, 787–798. https://doi.org/10.1007/s00424-018-2139-7

Tan, C.-H., McNaughton, P.A., 2016. The TRPM2 ion channel is required for sensitivity to warmth. Nature 536, 460–463. https://doi.org/10.1038/nature19074

Tanter, M., Bercoff, J., Sandrin, L., Fink, M., 2002. Ultrafast compound imaging for 2-D motion vector estimation: application to transient elastography. IEEE Trans. Ultrason. Ferroelectr. Freq. Control 49, 1363–1374. https://doi.org/10.1109/TUFFC.2002.1041078

Tanter, M., Fink, M., 2014. Ultrafast imaging in biomedical ultrasound. IEEE Trans. Ultrason. Ferroelectr. Freq. Control 61, 102–119. https://doi.org/10.1109/TUFFC.2014.2882

Tian, L., Li, Q., Wang, C., Yu, J., 2018. Changes in dynamic functional connections with aging. NeuroImage 172, 31–39. https://doi.org/10.1016/j.neuroimage.2018.01.040

Tiran, E., Deffieux, T., Correia, M., Maresca, D., Osmanski, B.-F., Sieu, L.-A., Bergel, A., Cohen, I., Pernot, M., Tanter, M., 2015. Multiplane wave imaging increases signal-to-noise ratio in ultrafast ultrasound imaging. Phys. Med. Biol. 60, 8549–8566. https://doi.org/10.1088/0031-9155/60/21/8549

Tiran, E., Ferrier, J., Deffieux, T., Gennisson, J.-L., Pezet, S., Lenkei, Z., Tanter, M., 2017. Transcranial Functional Ultrasound Imaging in Freely Moving Awake Mice and Anesthetized Young Rats without Contrast Agent. Ultrasound Med. Biol. 43, 1679–1689. https://doi.org/10.1016/j.ultrasmedbio.2017.03.011

Tracey, I., Becerra, L., Chang, I., Breiter, H., Jenkins, L., Borsook, D., González, R.G., 2000. Noxious hot and cold stimulation produce common patterns of brain activation in humans: a functional magnetic resonance imaging study. Neurosci. Lett. 288, 159–162. https://doi.org/10.1016/S0304-3940(00)01224-6

Tsuboi, Y., Iwata, K., Muramatsu, H., Yagi, J., Inomata, Y., Sumino, R., 1993. Response properties of primary somatosensory cortical neurons responsive to cold

stimulation of the facial skin and oral mucous membrane. Brain Res. 613, 193–202. https://doi.org/10.1016/0006-8993(93)90899-X

Urban, A., Mace, E., Brunner, C., Heidmann, M., Rossier, J., Montaldo, G., 2014. Chronic assessment of cerebral hemodynamics during rat forepaw electrical stimulation using functional ultrasound imaging. NeuroImage 101, 138–149. https://doi.org/10.1016/j.neuroimage.2014.06.063

Van Tienhoven, A., Scott, N.R., Hillman, P.E., 1979. The Hypothalamus and Thermoregulation: A Review. Poult. Sci. 58, 1633–1639. https://doi.org/10.3382/ps.0581633

Vandewauw, I., De Clercq, K., Mulier, M., Held, K., Pinto, S., Van Ranst, N., Segal, A., Voet, T., Vennekens, R., Zimmermann, K., Vriens, J., Voets, T., 2018. A TRP channel trio mediates acute noxious heat sensing. Nature 555, 662–666. https://doi.org/10.1038/nature26137

Veldhuijzen, D.S., Greenspan, J.D., Kim, J.H., Lenz, F.A., 2010a. Altered pain and thermal sensation in subjects with isolated parietal and insular cortical lesions. Eur. J. Pain 14, 535.e1-535.e11. https://doi.org/10.1016/j.ejpain.2009.10.002

Veldhuijzen, D.S., Greenspan, J.D., Kim, J.H., Lenz, F.A., 2010b. Altered pain and thermal sensation in subjects with isolated parietal and insular cortical lesions. Eur. J. Pain 14, 535.e1-535.e11. https://doi.org/10.1016/j.ejpain.2009.10.002

Venkatachalam, K., Montell, C., 2007. TRP Channels. Annu. Rev. Biochem. 76, 387–417. https://doi.org/10.1146/annurev.biochem.75.103004.142819

Vilar, B., Tan, C.-H., McNaughton, P.A., 2020. Heat detection by the TRPM2 ion channel. Nature 584, E5–E12. https://doi.org/10.1038/s41586-020-2510-7

Viswarupan, N., 2017. K-Means Data Clustering.

Voets, T., Droogmans, G., Wissenbach, U., Janssens, A., Flockerzi, V., Nilius, B., 2004. The principle of temperature-dependent gating in cold- and heat-sensitive TRP channels. Nature 430, 748–754. https://doi.org/10.1038/nature02732

Vogt, B.A., 2005. Pain and emotion interactions in subregions of the cingulate gyrus. Nat. Rev. Neurosci. 6, 533–544. https://doi.org/10.1038/nrn1704

Vogt, B.A., n.d. Structural Organization of Cingulate Cortex: Areas, Neurons, and Somatodendritic Transmitter Receptors 52.

Vogt, B.A., Derbyshire, S., Jones, A.K.P., 1996. Pain Processing in Four Regions of Human Cingulate Cortex Localized with Co-registered PET and MR Imaging. Eur. J. Neurosci. 8, 1461–1473. https://doi.org/10.1111/j.1460-9568.1996.tb01608.x

Vogt, B.A., Sikes, R.W., Vogt, L.J., 1993. Anterior Cingulate Cortex and the Medial Pain System 32.

VOOSEN, P., 2019. A 500-million-year survey of Earth's climate reveals dire warning for humanity. Science.

Vriens, J., Nilius, B., Voets, T., 2014. Peripheral thermosensation in mammals. Nat. Rev. Neurosci. 15, 573–589. https://doi.org/10.1038/nrn3784

Wager, T.D., Atlas, L.Y., Lindquist, M.A., Roy, M., Woo, C.-W., Kross, E., 2013. An fMRI-Based Neurologic Signature of Physical Pain. N. Engl. J. Med. 368, 1388–1397. https://doi.org/10.1056/NEJMoa1204471

Wang, F., Bélanger, E., Côté, S.L., Desrosiers, P., Prescott, S.A., Côté, D.C., De Koninck, Y., 2018. Sensory Afferents Use Different Coding Strategies for Heat and Cold. Cell Rep. 23, 2001–2013. https://doi.org/10.1016/j.celrep.2018.04.065

Wang, T.A., Teo, C.F., Åkerblom, M., Chen, C., Tynan-La Fontaine, M., Greiner, V.J., Diaz, A., McManus, M.T., Jan, Y.N., Jan, L.Y., 2019a. Thermoregulation via

Temperature-Dependent PGD2 Production in Mouse Preoptic Area. Neuron 103, 309-322.e7. https://doi.org/10.1016/j.neuron.2019.04.035

Wang, T.A., Teo, C.F., Åkerblom, M., Chen, C., Tynan-La Fontaine, M., Greiner, V.J., Diaz, A., McManus, M.T., Jan, Y.N., Jan, L.Y., 2019b. Thermoregulation via Temperature-Dependent PGD2 Production in Mouse Preoptic Area. Neuron 103, 309-322.e7. https://doi.org/10.1016/j.neuron.2019.04.035

Westerman, A.T., Roma, P.G., Price, R.C., Dominguez, J.M., 2010. Assessing the role of the medial preoptic area in ethanol-induced hypothermia. Neurosci. Lett. 475, 25–28. https://doi.org/10.1016/j.neulet.2010.03.034

Xiao, R., Xu, X.Z.S., 2021. Temperature Sensation: From Molecular Thermosensors to Neural Circuits and Coding Principles. Annu. Rev. Physiol. 83, 205–230. https://doi.org/10.1146/annurev-physiol-031220-095215

Xiao, X., Ding, M., Zhang, Y.-Q., 2021. Role of the Anterior Cingulate Cortex in Translational Pain Research. Neurosci. Bull. 37, 405–422. https://doi.org/10.1007/s12264-020-00615-2

Xiao, X., Zhang, Y.-Q., 2018. A new perspective on the anterior cingulate cortex and affective pain. Neurosci. Biobehav. Rev. 90, 200–211. https://doi.org/10.1016/j.neubiorev.2018.03.022

Yahiro, T., Kataoka, N., Nakamura, Y., Nakamura, K., 2017a. The lateral parabrachial nucleus, but not the thalamus, mediates thermosensory pathways for behavioural thermoregulation. Sci. Rep. 7, 5031. https://doi.org/10.1038/s41598-017-05327-8

Yahiro, T., Kataoka, N., Nakamura, Y., Nakamura, K., 2017b. The lateral parabrachial nucleus, but not the thalamus, mediates thermosensory pathways for behavioural thermoregulation. Sci. Rep. 7, 5031. https://doi.org/10.1038/s41598-017-05327-8

Yamamoto, T., Yaksh, T.L., 1992. Spinal pharmacology of thermal hyperesthesia induced by constriction injury of sciatic nerve. Excitatory amino acid antagonists. Pain 49, 121–128. https://doi.org/10.1016/0304-3959(92)90198-K

Yarnitsky, D., Zaslanky, R., Hemli, J.A., Sprecher, E., 1994. Heat pain thresholds: normative d and repeatability. Pain 4. https://doi.org/10.1016/0304-3959(94)00132-x

You, T., Im, G.H., Kim, S.-G., 2021. Characterization of brain-wide somatosensory BOLD fMRI in mice under dexmedetomidine/isoflurane and ketamine/xylazine. Sci. Rep. 11, 13110. https://doi.org/10.1038/s41598-021-92582-5

Yue, L., Xu, H., 2021. TRP channels in health and disease at a glance. J. Cell Sci. 134, jcs258372. https://doi.org/10.1242/jcs.258372

Zhang, X., 2006. Thermally Identified Subgroups of Marginal Zone Neurons Project to Distinct Regions of the Ventral Posterior Lateral Nucleus in Rats. J. Neurosci. 26, 5215–5223. https://doi.org/10.1523/JNEUROSCI.0701-06.2006

Zhao, X.-H., Wang, P.-J., Li, C.-B., Hu, Z.-H., Xi, Q., Wu, W.-Y., Tang, X.-W., 2007. Altered default mode network activity in patient with anxiety disorders: An fMRI study. Eur. J. Radiol. 63, 373–378. https://doi.org/10.1016/j.ejrad.2007.02.006

Zou, H., Yang, J., 2019. Dynamic thresholding networks for schizophrenia diagnosis. Artif. Intell. Med. 96, 25–32. https://doi.org/10.1016/j.artmed.2019.03.007

RÉSUMÉ

Les mécanismes centraux du codage thermique sont très complexes et impliquent principalement le thalamus, le cortex somatosensoriel, le cortex insulaire, le cortex cingulaire et l'hypothalamus. L'objectif de ce travail de thèse était d'étudier le rôle des circuits supra-spinaux dans le codage thermique chez les rongeurs, grâce à l'imagerie fonctionnelle ultrasonore (fUS). L'imagerie fUS est basée sur le couplage neurovasculaire, phénomène physiologique qui lie l'activité neuronale et les changements du volume sanguin cérébral (CBV).

Notre première étude visait à cartographier la matrice des zones activées par des stimulations thermiques cutanées nociceptives ou non chez le rat anesthésié. Le résultat de cette étude a malheureusement été essentiellement négatif. Nous avons conclu que les stimuli non douloureux n'induisaient aucun changement du CBV. A l'inverse, les stimulations thermiques nociceptives induisaient une augmentation locale du CBV, mais de manière non reproductible, en raison de facteurs physiologiques tels que l'augmentation de la pression artérielle qui entraîne de fortes fluctuations du CBV.

La deuxième étude visait à déchiffrer l'interaction entre les régions somato-motrices, cingulaires et hypothalamus dans le traitement de la sensation thermique. Nous avons choisi d'aborder cette question en utilisant l'imagerie fUS sur des souris éveillées et libres de leurs mouvements. L'imagerie fUS transcrânienne fut réalisée pendant que les souris étaient exposées à une température fixe (neutre 25°C, chaude 35°C et froide 15°C) ou à une température variable à un rythme rapide et lent. L'étude de la connectivité fonctionnelle, une mesure indirecte de la fonction et de la force des réseaux cérébraux, a révélé une dichotomie de fonction entre le réseau somato-moteur (SM)-cingulaire et le réseau SM-hypothalamique dans la détection du froid. L'étude des états dynamiques du cerveau a révélé i) des modes spécifiques pour cette dichotomie, ii) un mode dans lequel, pendant l'exposition statique à une température froide (15°C), où le cortex cingulaire était connecté différemment aux autres réseaux et enfin iii) un mode "état de repos", qui est le plus fréquent de tous et est significativement plus présent à la température de repos.

Ces résultats apportent des informations clef sur la dynamique des réseaux impliqués dans la sensibilité au froid.

MOTS CLÉS

échographie fonctionnelle, neuroimagerie, connectivité fonctionnelle, plasticité

ABSTRACT

The underlying central mechanisms of thermal coding are very complex and involves mainly the thalamus, somatosensory cortex, insular cortex, cingulate cortex and hypothalamus. The functional dependency of these brain regions in thermal sensation, thermal perception and thermal regulation has been of interest for researchers for decades. The aim of the thesis was to investigate the role of supraspinal circuitry in thermal coding in rodents using a new imaging modality named, functional ultrasound (fUS) imaging. fUS imaging is based on neurovascular coupling i.e., the phenomenon that links neural activity and changes in cerebral blood volume (CBV).

Our first study aimed at mapping the matrix of areas activated by innocuous and noxious thermal skin stimulations in anesthetized rats. The outcome of this study was mostly negative. We concluded that innocuous stimuli did not induce any change of CBV. On the contrary, noxious thermal stimulations induced local increase of CBV, but in a non-reproducible manner, due to the physiological factors such as increased arterial blood pressure that leads to high fluctuations in CBV.

The second study aimed at deciphering the interplay between the somato-motor, cingulate and hypothalamus regions in thermal processing. We chose to address this question, using fUS imaging on awake and freely moving mice, which allows recording of natural and innate brain responses without the bias of anesthesia. Transcranial fUS imaging was performed while the mice were exposed to either a fixed temperature (neutral 25°C, warm 35°Cand cold 15°C) or varying temperature at a fast and slow pace. Study of the functional connectivity, an indirect measure of brain network's function and strength, revealed a dichotomy of function between the somato-motor (SM)-cingulate network and the SM-hypothalamic network in cold sensing. Study of the dynamic brain states revealed: i) specific modes for this dichotomy, ii) a mode in which, during static exposure to cold temperature (15°C) the cingulate cortices is differently connected to the other networks studies and finally iii) a 'resting state' mode, which is the most frequent of all as is more frequently present at the resting temperature. These results provide key information on the dynamic of networks in cold sensing.

KEYWORDS

Neuroimaging, functional connectivity, functional ultrasound, plasticity